Carbon Fibre Reinforced Plastic Prestressing and Shear Reinforcements for Concrete Highway Bridges

by

Amir Z. Fam

A Thesis

presented to the University of Manitoba

in partial fulfilment of the

Requirements for the Degree of

Master of Science

Structural Engineering Division
Department of Civil & Geological Engineering
University of Manitoba
Winnipeg, Manitoba

ISBN 0-612-13115-7

Canada

Name Amir Zakaria Y. M. Fam

Dissertation Abstracts International is arranged by broad, general subject categories. Please select the one subject which most nearly describes the content of your dissertation. Enter the corresponding four-digit code in the spaces provided.

Civil

SUBJECT TERM

0543 U·M·I

SUBJECT CODE

Subject Categories

THE HUMANITIES AND SOCIAL SCIENCES

COMMUNICATIONS AND THE ARTS

Architecture 0729
Art History 0377
Cinema 0900
Dance 0378
Fine Arts 0357
Information Science 0723
Journalism 0391
Library Science 0399
Mass Communications 0708
Music 0413
Speech Communication 0459
Theater 0465

EDUCATION

General 0515
Administration 0514
Adult and Continuing 0516
Agricultural 0517
Art 0273
Bilingual and Multicultural 0282
Business 0688
Community College 0275
Curriculum and Instruction 0727
Early Childhood 0518
Elementary 0524
Finance 0277
Guidance and Counseling 0519
Health 0680
Higher 0745
History of 0520
Home Economics 0278
Industrial 0521
Language and Literature 0279
Mathematics 0280
Music 0522
Philosophy of 0998
Physical 0523
Psychology 0525
Reading 0535
Religious 0527
Sciences 0714
Secondary 0533
Social Sciences 0534
Sociology of 0340
Special 0529
Teacher Training 0530
Technology 0710
Tests and Measurements 0288
Vocational 0747

LANGUAGE, LITERATURE AND LINGUISTICS

Language
- General 0679
- Ancient 0289
- Linguistics 0290
- Modern 0291

Literature
- General 0401
- Classical 0294
- Comparative 0295
- Medieval 0297
- Modern 0298
- African 0316
- American 0591
- Asian 0305
- Canadian (English) 0352
- Canadian (French) 0355
- English 0593
- Germanic 0311
- Latin American 0312
- Middle Eastern 0315
- Romance 0313
- Slavic and East European 0314

PHILOSOPHY, RELIGION AND THEOLOGY

Philosophy 0422
Religion
- General 0318
- Biblical Studies 0321
- Clergy 0319
- History of 0320
- Philosophy of 0322

Theology 0469

SOCIAL SCIENCES

American Studies 0323
Anthropology
- Archaeology 0324
- Cultural 0326
- Physical 0327

Business Administration
- General 0310
- Accounting 0272
- Banking 0770
- Management 0454
- Marketing 0338

Canadian Studies 0385
Economics
- General 0501
- Agricultural 0503
- Commerce-Business 0505
- Finance 0508
- History 0509
- Labor 0510
- Theory 0511

Folklore 0358
Geography 0366
Gerontology 0351
History
- General 0578
- Ancient 0579
- Medieval 0581
- Modern 0582
- Black 0328
- African 0331
- Asia, Australia and Oceania 0332
- Canadian 0334
- European 0335
- Latin American 0336
- Middle Eastern 0333
- United States 0337

History of Science 0585
Law 0398
Political Science
- General 0615
- International Law and Relations 0616
- Public Administration 0617

Recreation 0814
Social Work 0452
Sociology
- General 0626
- Criminology and Penology 0627
- Demography 0938
- Ethnic and Racial Studies 0631
- Individual and Family Studies 0628
- Industrial and Labor Relations 0629
- Public and Social Welfare 0630
- Social Structure and Development 0700
- Theory and Methods 0344

Transportation 0709
Urban and Regional Planning 0999
Women's Studies 0453

THE SCIENCES AND ENGINEERING

BIOLOGICAL SCIENCES

Agriculture
- General 0473
- Agronomy 0285
- Animal Culture and Nutrition 0475
- Animal Pathology 0476
- Food Science and Technology 0359
- Forestry and Wildlife 0478
- Plant Culture 0479
- Plant Pathology 0480
- Plant Physiology 0817
- Range Management 0777
- Wood Technology 0746

Biology
- General 0306
- Anatomy 0287
- Biostatistics 0308
- Botany 0309
- Cell 0379
- Ecology 0329
- Entomology 0353
- Genetics 0369
- Limnology 0793
- Microbiology 0410
- Molecular 0307
- Neuroscience 0317
- Oceanography 0416
- Physiology 0433
- Radiation 0821
- Veterinary Science 0778
- Zoology 0472

Biophysics
- General 0786
- Medical 0760

EARTH SCIENCES

Biogeochemistry 0425
Geochemistry 0996
Geodesy 0370
Geology 0372
Geophysics 0373
Hydrology 0388
Mineralogy 0411
Paleobotany 0345
Paleoecology 0426
Paleontology 0418
Paleozoology 0985
Palynology 0427
Physical Geography 0368
Physical Oceanography 0415

HEALTH AND ENVIRONMENTAL SCIENCES

Environmental Sciences 0768
Health Sciences
- General 0566
- Audiology 0300
- Chemotherapy 0992
- Dentistry 0567
- Education 0350
- Hospital Management 0769
- Human Development 0758
- Immunology 0982
- Medicine and Surgery 0564
- Mental Health 0347
- Nursing 0569
- Nutrition 0570
- Obstetrics and Gynecology 0380
- Occupational Health and Therapy 0354
- Ophthalmology 0381
- Pathology 0571
- Pharmacology 0419
- Pharmacy 0572
- Physical Therapy 0382
- Public Health 0573
- Radiology 0574
- Recreation 0575
- Speech Pathology 0460
- Toxicology 0383

Home Economics 0386

PHYSICAL SCIENCES

Pure Sciences

Chemistry
- General 0485
- Agricultural 0749
- Analytical 0486
- Biochemistry 0487
- Inorganic 0488
- Nuclear 0738
- Organic 0490
- Pharmaceutical 0491
- Physical 0494
- Polymer 0495
- Radiation 0754

Mathematics 0405
Physics
- General 0605
- Acoustics 0986
- Astronomy and Astrophysics 0606
- Atmospheric Science 0608
- Atomic 0748
- Electronics and Electricity 0607
- Elementary Particles and High Energy 0798
- Fluid and Plasma 0759
- Molecular 0609
- Nuclear 0610
- Optics 0752
- Radiation 0756
- Solid State 0611

Statistics 0463

Applied Sciences

Applied Mechanics 0346
Computer Science 0984
Engineering
- General 0537
- Aerospace 0538
- Agricultural 0539
- Automotive 0540
- Biomedical 0541
- Chemical 0542
- Civil 0543
- Electronics and Electrical 0544
- Heat and Thermodynamics 0348
- Hydraulic 0545
- Industrial 0546
- Marine 0547
- Materials Science 0794
- Mechanical 0548
- Metallurgy 0743
- Mining 0551
- Nuclear 0552
- Packaging 0549
- Petroleum 0765
- Sanitary and Municipal 0554
- System Science 0790

Geotechnology 0428
Operations Research 0796
Plastics Technology 0795
Textile Technology 0994

PSYCHOLOGY

General 0621
Behavioral 0384
Clinical 0622
Developmental 0620
Experimental 0623
Industrial 0624
Personality 0625
Physiological 0989
Psychobiology 0349
Psychometrics 0632
Social 0451

Nom _____

Dissertation Abstracts International est organisé en catégories de sujets. Veuillez s.v.p. choisir le sujet qui décrit le mieux votre thèse et inscrivez le code numérique approprié dans l'espace réservé ci-dessous.

_____ ☐☐☐ U·M·I

SUJET — CODE DE SUJET

Catégories par sujets

HUMANITÉS ET SCIENCES SOCIALES

COMMUNICATIONS ET LES ARTS
Architecture 0729
Beaux-arts 0357
Bibliothéconomie 0399
Cinéma 0900
Communication verbale 0459
Communications 0708
Danse 0378
Histoire de l'art 0377
Journalisme 0391
Musique 0413
Sciences de l'information 0723
Théâtre 0465

ÉDUCATION
Généralités 515
Administration 0514
Art 0273
Collèges communautaires 0275
Commerce 0688
Économie domestique 0278
Éducation permanente 0516
Éducation préscolaire 0518
Éducation sanitaire 0680
Enseignement agricole 0517
Enseignement bilingue et multiculturel 0282
Enseignement industriel 0521
Enseignement primaire. 0524
Enseignement professionnel 0747
Enseignement religieux 0527
Enseignement secondaire 0533
Enseignement spécial 0529
Enseignement supérieur 0745
Évaluation 0288
Finances 0277
Formation des enseignants 0530
Histoire de l'éducation 0520
Langues et littérature 0279
Lecture 0535
Mathématiques 0280
Musique 0522
Orientation et consultation 0519
Philosophie de l'éducation 0998
Physique 0523
Programmes d'études et enseignement 0727
Psychologie 0525
Sciences 0714
Sciences sociales 0534
Sociologie de l'éducation 0340
Technologie 0710

LANGUE, LITTÉRATURE ET LINGUISTIQUE
Langues
- Généralités 0679
- Anciennes 0289
- Linguistique 0290
- Modernes 0291

Littérature
- Généralités 0401
- Anciennes 0294
- Comparée 0295
- Médiévale 0297
- Moderne 0298
- Africaine 0316
- Américaine 0591
- Anglaise 0593
- Asiatique 0305
- Canadienne (Anglaise) 0352
- Canadienne (Française) 0355
- Germanique 0311
- Latino-américaine 0312
- Moyen-orientale 0315
- Romane 0313
- Slave et est-européenne 0314

PHILOSOPHIE, RELIGION ET THÉOLOGIE
Philosophie 0422
Religion
- Généralités 0318
- Clergé 0319
- Études bibliques 0321
- Histoire des religions 0320
- Philosophie de la religion 0322

Théologie 0469

SCIENCES SOCIALES
Anthropologie
- Archéologie 0324
- Culturelle 0326
- Physique 0327

Droit 0398
Économie
- Généralités 0501
- Commerce-Affaires 0505
- Économie agricole 0503
- Économie du travail 0510
- Finances 0508
- Histoire 0509
- Théorie 0511

Études américaines 0323
Études canadiennes 0385
Études féministes 0453
Folklore 0358
Géographie 0366
Gérontologie 0351
Gestion des affaires
- Généralités 0310
- Administration 0454
- Banques 0770
- Comptabilité 0272
- Marketing 0338

Histoire
- Histoire générale 0578
- Ancienne 0579
- Médiévale 0581
- Moderne 0582
- Histoire des noirs 0328
- Africaine 0331
- Canadienne 0334
- États-Unis 0337
- Européenne 0335
- Moyen-orientale 0333
- Latino-américaine 0336
- Asie, Australie et Océanie 0332

Histoire des sciences 0585
Loisirs 0814
Planification urbaine et régionale 0999
Science politique
- Généralités 0615
- Administration publique 0617
- Droit et relations internationales 0616

Sociologie
- Généralités 0626
- Aide et bien-être social 0630
- Criminologie et établissements pénitentiaires 0627
- Démographie 0938
- Études de l' individu et de la famille 0628
- Études des relations interethniques et des relations raciales 0631
- Structure et développement social 0700
- Théorie et méthodes. 0344
- Travail et relations industrielles 0629

Transports 0709
Travail social 0452

SCIENCES ET INGÉNIERIE

SCIENCES BIOLOGIQUES
Agriculture
- Généralités 0473
- Agronomie. 0285
- Alimentation et technologie alimentaire 0359
- Culture 0479
- Élevage et alimentation 0475
- Exploitation des pâturages 0777
- Pathologie animale 0476
- Pathologie végétale 0480
- Physiologie végétale 0817
- Sylviculture et faune 0478
- Technologie du bois 0746

Biologie
- Généralités 0306
- Anatomie 0287
- Biologie (Statistiques) 0308
- Biologie moléculaire 0307
- Botanique 0309
- Cellule 0379
- Écologie 0329
- Entomologie 0353
- Génétique 0369
- Limnologie 0793
- Microbiologie 0410
- Neurologie 0317
- Océanographie 0416
- Physiologie 0433
- Radiation 0821
- Science vétérinaire 0778
- Zoologie 0472

Biophysique
- Généralités 0786
- Medicale 0760

SCIENCES DE LA TERRE
Biogéochimie 0425
Géochimie 0996
Géodésie 0370
Géographie physique 0368
Géologie 0372
Géophysique 0373
Hydrologie 0388
Minéralogie 0411
Océanographie physique 0415
Paléobotanique 0345
Paléoécologie 0426
Paléontologie 0418
Paléozoologie 0985
Palynologie 0427

SCIENCES DE LA SANTÉ ET DE L'ENVIRONNEMENT
Économie domestique 0386
Sciences de l'environnement 0768
Sciences de la santé
- Généralités 0566
- Administration des hôpitaux 0769
- Alimentation et nutrition 0570
- Audiologie 0300
- Chimiothérapie 0992
- Dentisterie 0567
- Développement humain 0758
- Enseignement 0350
- Immunologie 0982
- Loisirs 0575
- Médecine du travail et thérapie 0354
- Médecine et chirurgie 0564
- Obstétrique et gynécologie 0380
- Ophtalmologie 0381
- Orthophonie 0460
- Pathologie 0571
- Pharmacie 0572
- Pharmacologie 0419
- Physiothérapie 0382
- Radiologie 0574
- Santé mentale 0347
- Santé publique 0573
- Soins infirmiers 0569
- Toxicologie 0383

SCIENCES PHYSIQUES
Sciences Pures
Chimie
- Généralités 0485
- Biochimie 487
- Chimie agricole 0749
- Chimie analytique 0486
- Chimie minérale 0488
- Chimie nucléaire 0738
- Chimie organique 0490
- Chimie pharmaceutique 0491
- Physique 0494
- PolymÈres 0495
- Radiation 0754

Mathématiques 0405
Physique
- Généralités 0605
- Acoustique 0986
- Astronomie et astrophysique 0606
- Électronique et électricité 0607
- Fluides et plasma 0759
- Météorologie 0608
- Optique 0752
- Particules (Physique nucléaire) 0798
- Physique atomique 0748
- Physique de l'état solide 0611
- Physique moléculaire 0609
- Physique nucléaire 0610
- Radiation 0756

Statistiques 0463

Sciences Appliqués Et Technologie
Informatique 0984
Ingénierie
- Généralités 0537
- Agricole 0539
- Automobile 0540
- Biomédicale 0541
- Chaleur et thermodynamique 0348
- Conditionnement (Emballage) 0549
- Génie aérospatial 0538
- Génie chimique 0542
- Génie civil 0543
- Génie électronique et électrique 0544
- Génie industriel 0546
- Génie mécanique 0548
- Génie nucléaire 0552
- Ingénierie des systèmes 0790
- Mécanique navale 0547
- Métallurgie 0743
- Science des matériaux 0794
- Technique du pétrole 0765
- Technique minière 0551
- Techniques sanitaires et municipales 0554
- Technologie hydraulique 0545

Mécanique appliquée 0346
Géotechnologie 0428
Matières plastiques (Technologie) 0795
Recherche opérationnelle 0796
Textiles et tissus (Technologie) 0794

PSYCHOLOGIE
Généralités 0621
Personnalité 0625
Psychobiologie 0349
Psychologie clinique 0622
Psychologie du comportement 0384
Psychologie du développement 0620
Psychologie expérimentale 0623
Psychologie industrielle 0624
Psychologie physiologique 0989
Psychologie sociale 0451
Psychométrie 0632

CARBON FIBRE REINFORCED PLASTIC PRESTRESSING AND SHEAR REINFORCEMENTS FOR CONCRETE HIGHWAY BRIDGES

BY

AMIR Z. FAM

A Thesis submitted to the Faculty of Graduate Studies of the University of Manitoba in partial fulfillment of the requirements of the degree of

MASTER OF SCIENCE

ABSTRACT

Bridges in Canada are exposed to harsh environments characterized by a wide range of temperature changes and use of salt for de-icing in addition to the typical effects of cyclic and impact loads of traffic. The Province of Manitoba is undertaking the challenge to construct the first concrete bridge in the world of a 32.5 meters span consisting of prestressed girders and deck slabs totally reinforced by Carbon Fibre Reinforced Plastic, CFRP, reinforcements. Since the characteristics of the CFRP reinforcements are highly dependant on the direction of the fibres [12], they may affect the shear cracks behaviour which are inclined with the stirrups.

This thesis presents the experimental program undertaken at the Structural Engineering and Construction R&D Facility of the University of Manitoba to test a total of six beams with one third scale of the bridge girders. The beams had an I-shape cross section, with same span-to-depth ratio and prestressed level of the bridge girders. All beams were 9.3 meters long and 0.5 meter in depth. A 50 mm thick top slab was cast after a minimum age of seven days for each beam to act in composite action with the beam similar to the prototype bridge girder [18]. The CFRP stirrups were projected from the beams into the slabs to provide the dowel action and transfer the horizontal shear stresses. Three beams were prestressed by Carbon Fibre Composite Cables, CFCC tendons and reinforced by three different sizes of CFCC stirrups, Two beams prestressed by Leadline rods and reinforced by two different configurations of Leadline stirrups, and one beam prestressed by conventional steel strands and reinforced by steel stirrups used as control specimen. All beams were tested under static loading conditions to failure to examine the various limit states behaviours, the

shear mechanism using different

types, sizes, and materials for the stirrups, and the feasibility of draping the CFRP prestressing tendons with an angle of four degrees, which is typically used for these types of bridge girders to achieve uniform and allowable stresses at the ends of the beams.

The measured deflection, flexural cracks, and diagonal cracks are evaluated according to the type of prestressing and shear reinforcements provided, including the dowel action between the precast beam and the top slab. Two beams prestressed by CFCC cables and reinforced by two different sizes of CFCC stirrups failed in flexure by rupture of the lower draped cable at the draping point, the third one of the same type of reinforcement failed in flexure by rupture of the bottom straight cables within the middle zone at about the same load level of the other two. One beam prestressed by Leadline rods and reinforced by double legged Leadline stirrups showed a premature failure at the high shear stresses sections. the stirrups stretched at the bend between the web and the bottom flange causing spalling of the concrete cover and collapse of the beam, however, the other beam with the same type of reinforcement but with single legged stirrups failed at higher load level in flexure by rupture of the bottom Leadline rods in the middle part. The sixth beam totally reinforced for shear and prestressing by steel failed in flexure by yielding of the bottom strands followed by crushing the concrete at the top surface. In all the beams, no slip was observed between the girder and the top slab. Results will be used to provide design guidelines for the prototype bridge expected to be constructed in the fall of 1995.

ACKNOWLEDGMENTS

The author would like to express his sincere thanks to Dr. Sami Rizkalla for providing excellent guidance, assistance, and advice during the research program.

The technical assistance given by Messrs. Ed. Lemke, Moray McVey, and Scott Sparrow during the experimental work is greatly appreciated. Special thanks go to Mr. Haney Louka and all the graduate students for their assistance during construction and testing of test specimens.

The financial assistance provided by the Highway and Transportation, Bridges and Structures Department, Province of Manitoba, is greatly acknowledged.

Appreciation is also extended to Con-Force Structures Company Ltd., Winnipeg, Manitoba, for their significant contribution and cooperation during fabrication of test beams.

Finally, the author wishes to express his deeply-felt gratitude to his parents who made all this possible. The support and patience of my father Zakaria Y. Fam cannot be praised enough; to him this thesis is dedicated.

TABLE OF CONTENTS

ABSTRACT.....i

ACKNOWLEDGMENTS.....iii

TABLE OF CONTENTS.....iv

LIST OF TABLES.....x

LIST OF FIGURES.....xi

NOTATION.....xvi

CHAPTER 1. INTRODUCTION

1.1 GENERAL.....1

1.2 OBJECTIVES.....1

1.3 SCOPE.....2

CHAPTER 2. BACK GROUND AND LITERATURE REVIEW

2.1 GENERAL.....4

2.2 FIBRE REINFORCED PLASTIC REINFORCEMENTS, FRP.....4

2.2.1 Carbon fibre reinforced plastic, CFRP.....4

2.2.1.1 Tokyo Rope.....5

2.2.1.2 Mitsubishi Kasei.....6

2.2.2 General applications of FRP.....6

2.2.3 Examples of prestressed concrete bridges using FRP tendons.....8

2.2.3.1 Bridges prestressed by carbon reinforced tendons.....8

2.2.3.2 Bridges prestressed by glass-reinforced tendons.....8

2.2.3.3 Bridges prestressed by aramid reinforced tendons.....9

2.3 SHEAR STRENGTH OF CONCRETE BEAMS 9

2.3.1 General.....9

2.3.1.1 Basic mechanisms of shear transfer.....10

2.3.1.2 Possible failure modes due to shear in beam with web reinforcement.....11

2.3.2 Analytical and design approaches.....11

2.3.2.1 45 degrees truss model.....12

2.3.2.2 ACI approach.....13

2.3.2.3 CSA simplified method.....15

2.3.2.4 Variable angle truss model.....17

2.3.2.5 Compression field theory.....19

2.3.2.6 Modified compression field theory.....21

2.3.2.7 The CSA general method.....24

2.4 PREVIOUS STUDIES ON FRP AS SHEAR REINFORCEMENTS.....27

2.4.1 Diagonal tensile characteristics of FRP rods.....27

2.4.2 Tensile strength characteristics of FRP bent bars.....28

CHAPTER 3. EXPERIMENTAL WORK

3.1 GENERAL.....33

3.2 BRIDGE OUTLINE.....33

3.3 TEST SPECIMENS....34
3.3.1 Design of the specimens....34
3.3.2 Longitudinal reinforcement....36
3.3.3 Shear reinforcement....37
3.3.3.1 CFCC stirrups....38
3.3.3.2 Leadline stirrups....38
3.3.3.3 Steel stirrups....38
3.4 MATERIAL PROPERTIES....39
3.4.1 Concrete....39
3.4.2 Longitudinal prestressing....39
3.4.3 Shear reinforcement....39
3.5 FABRICATION OF THE SPECIMENS....40
3.5.1 Preparation of the form....40
3.5.2 Stressing of the tendons....40
3.5.2.1 Steel couplers....40
3.5.2.2 Hold-down system....42
3.5.2.3 Hold-up system....43
3.5.2.4 Special considerations for stressing the Leadline rods....43
3.5.2.5 Jacking process....44
3.5.3 Preparation for casting....44
3.5.4 Concrete casting and curing....45
3.5.5 Release of prestressing....45

3.5.6 Casting of top slab....46

3.6 INSTRUMENTATION....46

3.6.1 Electrical strain gauges....46

3.6.2 Concrete strain measurements....48

3.6.3 Deflection measurements....49

3.6.4 Crack-width measurements....49

3.6.5 Other measurements....50

3.6.6 Data acquisition system....50

3.7 TESTING PROCEDURE....50

3.7.1 Test setup....50

3.7.2 Preparation for testing....52

3.7.3 Testing....53

CHAPTER 4. TEST RESULTS

4.1 INTRODUCTION....79

4.2 SAMPLE DATA - BEAM TR-1-7.5/7....79

4.3 OBSERVED BEHAVIOUR....80

4.3.1 Beam TR-1-7.5/7....81

4.3.2 Beam TR-2-5/1....82

4.3.3 Beam TR-3-5/7....83

4.3.4 Beam LL-4-2B....84

4.3.5 Beam LL-5-1B....86

4.3.6 Beam ST-6-C....87

CHAPTER 5. DISCUSSION OF TEST RESULTS

5.1 INTRODUCTION....107

5.2 BEHAVIOUR OF TEST BEAMS....107

5.3 FLEXURAL BEHAVIOUR OF TEST BEAMS....108

5.3.1 Stiffness of test beams....108

5.3.2 Flexural cracks....109

5.3.3 Flexural modes of failure....109

5.3.4 Analytical model....111

5.4 SHEAR BEHAVIOUR OF TEST BEAMS....114

5.4.1 Effect of web reinforcement ratio....116

5.4.2 Effect of elastic modulus....118

5.4.3 Failure mode of beam LL-4-2B....119

5.5 ANALYTICAL MODELS FOR SHEAR BEHAVIOUR....120

5.5.1 Modified Compression Field Theory....120

5.5.1.1 Input file....120

5.5.1.2 Performing analysis....124

5.5.1.3 Refining of the output....125

5.5.1.4 Effect of draping....126

5.5.1.5 Effect of releasing post-tensioned strands....126

5.5.1.6 Comparison of results....127

5.5.2 ACI approach....128

5.5.2.1 Shear cracking load....128

5.5.2.2 Behaviour after diagonal cracking....129

5.5.3 CSA simplified method of 1984, and 1994 codes....130

5.5.3.1 Shear cracking load....130

5.5.3.2 Behaviour after diagonal cracking....131

5.5.4 Evaluation of the code prediction....131

CHAPTER 6. SUMMARY AND CONCLUSIONS

6.1 SUMMARY....156

6.2 CONCLUSIONS....156

6.3 RECOMMENDATIONS FOR FUTURE WORK....158

REFERENCES....160

APPENDIX A. EXPERIMENTAL RESULTS OF PRESTRESSED CONCRETE BEAMS FULLY REINFORCED BY CFRP REINFORCEMENTS....164

APPENDIX B. RELATIVE LOCATION OF DEMEC STATIONS WITH RESPECT TO THE CRACK PATTERNS....205

APPENDIX C. INPUT FILE OF PROGRAM " RESPONSE" FOR BEAM TR-1-7.5/7 AT SECTION # 1....209

List of Tables

Table

3.1 Description of test results.....54

3.2 Measured concrete properties of the test specimens at different stages.....55

4.1 Summary of flexural and shear cracking loads, ultimate load, and modes of failure of test beams.....89

4.2 Measured strains of prestressing strands from jacking up to testing using electrical strain gauges for beam TR-1-7.5/7.....90

5.1 Stiffness of test beams at different stages.....132

A.2 Measured strains of prestressing tendons from jacking up to testing using electrical strain gauges for the other test beams TR-2-5/1, TR-3-5/7, LL-4-2B, LL-5-1B, and ST-6-c.....166, 174, 182, 190, 198

List of Figures

Figure

2.1 Equilibrium considerations for 45 degrees truss model....29

2.2 Equilibrium considerations for variable angle truss model....29

2.3 Compatibility conditions for cracked web element....29

2.4 Compressive stress-strain relationship for cracked concrete....30

2.5 Equilibrium conditions of modified compression field theory....30

2.6 Transmitting forces across the diagonal cracks....31

2.7 Tensile stress-strain relationship of cracked concrete in tension....31

2.8 Test specimen used to determine the diagonal tensile characteristics of FRP rods....32

3.1 General layout of bridge girders....56

3.2 Beam-slab composite section details for all test beams....57

3.3 Prestressing and reinforcing details of test beams....58, 59

3.4 End block reinforcement at anchorage zone of external prestressing....60

3.5 Different configurations of stirrups....61

3.6 Material properties of prestressing tendons....62

3.7 Material properties of stirrups....63

3.8 General view of the casting bed showing the sides of the form and the abutments at the jacking end....64

3.9 General layout of jacking system....64

3.10 Components of the steel coupler....65

3.11 Tokyo Rope strands connected to steel strands through the couplers....65

3.12 Components of the Leadline anchorage....66

3.13 Leadline bars connected to steel strands through the couplers....66

3.14 Hold-down system consists of steel pins supported by the sides of the form....67

3.15 Hold-up system and the draped tendons....67

3.16 Yoke used to prevent couplers of draped Leadline bars from rotating during jacking....68

3.17 Aluminum spacers used to reduce the spacing between each two draped Leadline bars....68

3.18 Reinforcing cage after assembling. Only the straight tendons are jacked....69

3.19 Reinforcement at end block....69

3.20 Supporting the girder downward at pin locations before releasing the form....70

3.21 External post-tensioning of the I-girder....70

3.22 Test beam before and after casting top slab....71

3.23 Layout of strain gauges locations along the prestressing tendons....72

3.24 Layout of demec stations at the maximum moment zone....73

3.25 Layout of "Rosette" demec stations at maximum shear stresses zone....74

3.26 Deflection measurements using LMTs system....75

3.27 Arrangement of dial gauges at ends of the beam....75

3.28 General view of test setup....76, 77

3.29 Spreader beams system used to apply the load....77

3.30 Steel frame jacked to the floor used to enhance the safety at failure stage....78

4.1 Measured load-deflection at mid-span....91

4.2 Measured concrete strain at top surface at six demec stations.....92

4.3 Average of measured concrete strain at top surface.....92

4.4 Measured strains at bottom strands level at three demec stations.....93

4.5 Measured strains at the bottom strands during testing using strain gauges.....93

4.6 Total strains in strands including effective pre-strains and strains during testing.....94

4.7 Measured crack width at maximum moment zone based on microscope readings.....94

4.8 Measured strain on concrete surface in direction of stirrups at five demec stations based on 200 mm gauge length.....95

4.9 Measured strain on concrete surface in direction of stirrups at five demec stations based on 50.8 mm gauge length.....95

4.10 Measured strain on concrete surface in the horizontal direction at five demec stations based on 200 mm gauge length.....96

4.11 Measured strain on concrete surface in the diagonal direction at five demec stations based on 200 mm gauge length.....96

4.12 Flexural crack patterns of beams prestressed by Tokyo Rope strands, (top), Leadline bars, (middle), and steel strands, (bottom).....97

4.13 Diagonal crack patterns of test beams.....98, 99, 100

4.14 Failure mode of test beams.....101, 102, 103, 104, 105, 106

5.1 Measured load-deflection for six test beams.....133

5.2 Modified Ramberg-Osgood function for the material of prestressing tendons.....133

5.3 Stress-strain curves of prestressing tendons as used in program "RESPONSE".....134

5.4 Different sections analyzed using program "RESPONSE".....135

5.5 Typical moment-curvature curve as obtained from program "RESPONSE" at any section of the beams prestressed by CFRP tendons.....135

5.6 Moment-curvature response of beams prestressed by CFCC strands.....136

5.7 Measured and predicted load-deflection diagrams for test beams.....137, 138, 139

5.8 Diagonal cracks covering the entire span of beams prestressed by Leadline bars.....140

5.9 Locations of critical zones in shear.....140

5.10 Effect of web reinforcement ratio on stirrups strain.....141

5.11 Effect of web reinforcement ratio on the diagonal crack width.....142

5.12 Effect of elastic modulus on the stirrups strain.....143

5.13 Effect of elastic modulus on the diagonal crack width.....143

5.14 Stress-strain curves of stirrups as used in program "RESPONSE".....144

5.15 Shear-stirrups strain response as obtained from program "RESPONSE".....145

5.16 Structural model used to predict the effect of releasing post-tensioned strands.....145

5.17 Modified compression field theory prediction.....146, 147, 148

5.18 ACI code prediction.....149, 150, 151

5.19 Prediction using simplified method of 84 and 94 CSA code.....152, 153, 154

5.20 Proposed reduction in concrete contribution in shear.....155

A.1 Measured load-deflection at mid span for the other test beams.....167, 175, 183, 191, 199

A.2 Measured concrete strain at top surface at six demec stations for the other test beams.....168, 176, 184, 192, 200

A.3 Average of measured concrete strain at top surface for the other test

beams.....168, 176, 184, 192, 200

A.4 Measured strains at bottom strands level at three demec stations for the other test beams.....169, 177, 185, 193, 201

A.5 Measured strains at the bottom strands during testing using strain gauges for the other test beams.....169, 177, 185, 193, 201

A.6 Total strains in strands including effective pre-strains and strains during testing for the other test beams.....170, 178, 186, 194, 202

A.7 Measured crack width at the maximum moment zone based on microscope readings for the other test beam.....170, 178, 186, 194, 202

A.8 Measured strain on concrete surface in direction of stirrups at five demec stations for based on 200 mm gauge length for the other test beams.....171, 179, 187, 195, 203

A.9 Measured strain on concrete surface in direction of stirrups at five demec stations based on 50.8 mm gauge length for the other test beams.....171, 179, 187, 195, 203

A.10 Measured strain on concrete surface in the horizontal direction at five demec stations based on 200 mm gauge length for the other test beams.....172, 180, 188, 196, 204

A.11 Measured strain on concrete surface in the diagonal direction at five demec stations based on 200 mm gauge length for the other test beams.....172, 180, 188, 196, 204

NOTATION

A_p = area of prestressed reinforcement

A_{px} = area of prestressed reinforcement in x-direction

A_s = Area of non-prestressed tension reinforcement

A_{sx} = Area of non-prestressed tension reinforcement in x-direction

A_v = Area of shear reinforcement

a = aggregate size

b_w = web width

b_v = web width

C_v = half distance between the two branches of stirrups

C_x = distance between the centroid axis of the section and the upper longitudinal reinforcement

d = distance from extreme compression fibre to the centroid of tension reinforcement

d_p = distance from extreme compression fibre to the centroid of pre-stressed reinforcement

d_{px} = diameter of prestressing tendons

d_{pv} = diameter of stirrups branch

d_v = effective shear depth taken as flexural lever arm, ≥ 0.9 d

E_c = modulus of elasticity of concrete

E_p = modulus of elasticity of prestressed reinforcement

E_s = modulus of elasticity of reinforcing steel

f_1 = maximum principal stress

f_2 = minimum principal stress

f_{2max} = ultimate compressive stress of the diagonally cracked concrete

f_c' = specified compressive stress of concrete

f_{cr} = cracking strength of concrete in tension

f_d = stress due to unfactored dead load, at extreme fibre of section where tensile stress is caused by externally applied load

f_l = stress in the tension reinforcement in x-direction

f_p = stress in the tension prestressed reinforcement in x-direction

f_{pc} = compressive stress in concrete after allowance for all prestress losses at centroid of cross section resisting externally applied loads, or at junction of web and flange when the centroid lies within the flange. In composite members, f_{pc} is resultant compressive stress at centroid of composite section, due to both prestress and moments resisted by precast member acting alone

f_{pe} = compressive stress in concrete due to effective prestress forces only after allowance for all prestress losses at extreme fibre of section where tensile stress is caused by externally applied loads

f_{po} = stress in the prestressing tendons when the stress in the surrounding concrete is zero, may be taken as 1.1 times the effective stress, f_{pe}

f_{pu} = specified tensile strength of prestressing tendons

f_{sx} = tensile stress in the reinforcing steel in x-direction

f_v = stress in the web reinforcement

f_{vy} = stress in the web reinforcement at crack location when it yields

f_u = actual tensile strength of the FRP rods

f_{u0} = reduced tensile strength of FRP rods when the load is applied at an angle θ with respect to the bar

f_y = yielding strength of the steel stirrups

I = moment of inertia

I_g = moment of inertia of gross concrete section

j_d = distance between the centroid of compression and the centroid of tension

K = reduction factor for tensile strength of FRP rods to account for the direction of loading

K_1 = factor to account for bond characteristics of the reinforcement taken as 0.4 for deformed bars and 0.8 for plain bars or bonded tendons

M_{cr} = cracking moment

M_d = moment due to specified dead load

M_f = moment due to factored loads

M_{max} = maximum factored moment at section due to externally applied loads

M_u = factored moment at section

N_f = factored axial load normal to the cross section occurring simultaneously with V_f, taken as positive for tension and negative for compression

N_v = additional normal force acting on the section due to shear

S = spacing of stirrups

S_{mv} = average crack spacing that would result if the member was subjected to a transverse

tension

S_{mx} = average crack spacing that would result if the member was subjected to longitudinal tension

$S_{m\theta}$ = spacing of diagonal cracks

S_x = horizontal spacing of tendons

V = shear load

V_c = nominal shear strength provided by concrete

V_{cg} = factored shear strength attributed to the concrete

V_{ci} = nominal shear strength provided by concrete when diagonal cracking results from combined shear and moment

V_{cr} = diagonal cracking shear load

V_{cw} = nominal shear strength provided by concrete when diagonal cracking results from excessive principal tensile stress in web

V_d = shear force at section due to unfactored dead load

V_f = factored shear force

V_i = factored shear force at section due to externally applied loads occurring simultaneously with M_{max}

V_n = nominal shear strength

V_p = vertical component of effective prestress force at a section

V_r = factored shear resistance

V_{rg} = factored shear resistance

V_s = nominal shear strength provided by shear reinforcement

V_{sg} = factored shear resistance provided by shear reinforcement

V_u = factored shear force at section

v_{ci} = local shear stress on the crack surface

w = crack width

y_t = distance from centroid of gross section to extreme fibre in tension

α_1 = factor accounts for bond characteristics of concrete

α_2 = factor accounts for the type of loading

β = factor accounting for the shear resistance of cracked concrete

$\Delta\epsilon_p$ = difference in strain between the concrete and prestressing tendons

ϵ_1 = maximum principal tensile strain

ϵ_2 = minimum principal tensile strain

ϵ_c' = strain of concrete corresponding to the ultimate compressive strength

ϵ_{cr} = cracking strain of concrete

ϵ_p = strain in prestressed reinforcement

ϵ_{pu} = ultimate strain of prestressed reinforcement

ϵ_{sh} = strain at the end of yielding plateau and beginning of hardening of reinforcing steel

ϵ_t = strain of stirrups

ϵ_u = ultimate strain of the reinforcement

ϵ_x = longitudinal strain of the concrete element

ϵ_y = yielding strain of the reinforcement

θ = angle of the diagonal compressive stresses in a cracked web of concrete beam

λ = correction factor related to the unit mass of the concrete

ρ_v = web reinforcement ratio

ρ_x = longitudinal reinforcement ratio

ϕ_c = resistance factor for concrete

ϕ_p = resistance factor for prestressing tendons

ϕ_s = resistance factor for reinforcing steel

CHAPTER 1

INTRODUCTION

1.1 GENERAL

Service life and serviceability of concrete bridges are significantly affected by deterioration of concrete due to corrosion of steel reinforcement. Carbon Fibre Reinforced Plastics, CFRP, tendons and reinforcements are suitable for prestressed concrete bridges exposed to tough environment effects due to their high strength to weight ratio, light weight, non-magnetic, and non-corrosion characteristics [13], [20]. This study is focused on two types of CFRP reinforcements, Carbon Fibre Composite Cables, CFCC, produced by Tokyo Rope, Japan, and Leadline rods produced by Mitsubishi Kasei, Japan.

Due to lack of information in the literature on the performance of CFRP as shear reinforcement, various stirrup sizes were used to study their effects on the shear and flexural behaviour of prestressed concrete girders.

1.2 OBJECTIVES

The main objective of this research program was to investigate the behaviour of prestressed concrete I-girders totally reinforced by CFRP for shear and prestressing reinforcements in terms of flexural cracks, deflections, and ultimate resistance. The study was also focused on the effect of web reinforcement ratio and the elastic modulus on the shear resistance of the beams in terms of the strain level in stirrups, diagonal crack width, crack distribution, and the dowel action. The beams were also tested to examine the efficiency of the draped prestressed CFRP reinforcements with an angle of four degrees, which is typically

used for the bridge, to achieve uniform and allowable stress distribution at the ends of the girders.

1.3 SCOPE

A total of six beams, 1:3.658 scale of the prototype of the bridge girders were fabricated and tested up to failure in this experimental program. All the test beams were pre-tensioned prestressed concrete beams with an I-shape cross section. A concrete slab was casted after a minimum age of seven days of the beams to simulate the effect of the deck slab of the bridge. All the stirrups were exposed from the girders into the slabs to provide the dowel action needed to simulate the composite behaviour. The test beams were designed to have same span-to-depth ratio and same induced stress in the section due to prestressing as the bridge girders. All test beams were tested to failure under the same static loading conditions using a loading system that simulates an equivalent truck loading condition. The different types of shear reinforcements included double legged CFCC stirrups of three different sizes for beams pre-tensioned by CFCC tendons, two different configurations of Leadline stirrups, single and double legged stirrups for beams pre-tensioned by Leadline rods, and double legged steel stirrups for one beam pre-tensioned by conventional steel strands.

A brief review of shear in prestressed concrete beams is given in chapter 2. The characteristics of CFRP and its applications is also mentioned in the same chapter.

The entire experimental program is detailed in chapter 3, including design and fabrication of test beams, material properties, test setup, instrumentation, and test procedure.

Chapter 4 summarizes the observed behaviour and measured data of all the beams during the entire period from casting to testing. Sample data is presented to describe the behaviour of one of the beams. The complete data is presented in Appendix A.

Discussion of the test results is given in chapter 5 including the behaviour of the beams as well as the analytical models.

The last chapter, chapter 6, includes the conclusions and recommendations based on this experimental program.

CHAPTER 2

BACK GROUND AND LITERATURE REVIEW

2.1 GENERAL

In this chapter the back ground and major applications of the advanced composite materials are presented. The behaviour of concrete beams in shear is reviewed including relevant design procedures and analytical methods. Very few studies have been done in the field of shear using fibre reinforced plastic reinforcements, summary of the major findings of these studies is provided.

2.2 FIBRE REINFORCED PLASTIC REINFORCEMENTS, FRP

A great deal of attention is focused on the research and development of fibre materials including carbon fibres, aramid fibres, and glass fibres as alternatives to the steel used in the reinforced and prestressed concrete. Despite their low specific gravity as compared to steel, they posses high tensile strength and many of them provide excellent resistance to the elements of weather and chemical attacks. When used as reinforcing materials, the fibres are usually bonded together with the help of binding agents as resins and cement, resulting in widely different appearances and compositions. The discussion is focused on the carbon fibres reinforced plastic materials since it is used in this project.

2.2.1 Carbon fibre reinforced plastic, CFRP

There are many manufacturers of carbon fibres in Japan, U.S.A., and Europe. Two types of CFRP were used in this experimental program, one is produced by Tokyo Rope,

Japan, and the other is produced by Mitsubisi kasei, Japan. The products of both are discussed below:

2.2.1.1 Tokyo Rope [15], [20] Unidirectional, carbon fibre composite cables, are produced by Tokyo Rope under the trade name, CFCC, using carbon fibres of poly-acrylonitrile (PAN) type, supplied by Toho Rayon, Japan, and called prepregs. These prepregs consists of 12,000 filaments impregnated with resin. The CFCC manufacturing process involves the layer process, where the multiple prepregs are stranded to make a primary composite strand. The surface of the strand is wrapped with special material to make a composite linear body or single strand. This coating protects the core from ultraviolet radiation, mechanical damage, and enhances the bonding characteristics to concrete. Ropes are made from either single, seven, nineteen, or thirty seven strands. Multiple strand ropes are twisted to allow better redistribution of the stresses through the cross section. Heat curing is used for the hardening process of the resin matrix. The sizes range from 3 mm diameter, single strands, to 40 mm diameter ropes. The maximum length of CFCC, currently produced, is 600 meters, with future plans to produce lengths up to 3000 meters. The ropes are flexible enough to be coiled in drums for transportation. Prior to heat curing, CFCC can be shaped into rectangular and circular spirals for stirrups and confining reinforcements.

The weight of CFCC is only one fifth of the weight of steel strand. Impact and fatigue testing of CFCC have indicated no significant deficiencies of the cables. However, heat resistance is low, due to the thermal setting matrix, and shearing strength is poor. The creep and relaxation are only about half of those of steel strands.

The main use of CFCC is as prestressing tendons and reinforcements for concrete elements. Die cast wedge anchors have been developed for the CFCC. It is envisaged that CFCC may in future be used as supporting cables of cable-stayed and suspended bridges.

2.2.1.2 Mitsubishi Kasei [13], [15] Mitsubishi Kasei uses a coal tar pitch-based continuous carbon fibre, name brand DIALEAD, to produce Leadline rods, unidirectional tape (UD), and winding strands. Leadline is a carbon fibre reinforced plastic (CFRP) rods, pultruded using DIALEAD and an epoxy resin. The Leadline rods have one fifth the weight of steel tendons, good durability, good corrosion resistance, and are non-magnetic. Round bars and deformed bars are available. Available diameters are 1 to 17 mm for round bars and 5 to 7 mm for deformed bars. Since Leadline bars have all fibres linearly oriented, they are stronger than twisted carbon fibre cables of the same diameter.

The (UD) tape is produced from unidirectional continuous carbon fibres impregnated with epoxy resin. The (UD) tape in conjunction with continuous carbon fibre winding strands, are currently being used to improve the resistance of structures against earth quakes, retrofitting of tall concrete chimneys, and they also introduce an excellent potential for petrofitting concrete columns supporting large spaces and bridge piers.

2.2.2 General applications of FRP

FRP may be used in the form of laminates, structural sections using pultrusion process, in addition to the unidirectional applications such as prestressing tendons. A leading characteristic of FRP is being non-corrosive material which is considered to be a major

advantage over conventional steel structural elements resulting in longer life time of the structure. A second leading characteristic of FRP is the high strength-to-weight ratio ranging from 3 to 5 times higher than the prestressing steel which makes handling and installation much easier.

The use of FRP is already introduced in structural applications through different avenues such as short span bridges, pedestrian bridges, and long span bridges where the FRP structural sections can be utilized in the construction of bridge girders or the unidirectional FRP tendons can be used for prestressing or reinforcing the girders. Repair of structures is also one of the applications that makes use of the light weight characteristic of FRP. A number of chimneys have been strengthened with CFRP products to protect them against earth quake damage using the unidirectional carbon fibre tape (UD) and carbon fibre winding strands. Repair was also extended to old high way bridges where the increase of the weight of trucks in addition to the corrosion problems resulted in deterioration of those bridges. In this case strengthening is done by bonding carbon fibre reinforced epoxy laminates to the exterior surface of the deteriorated steel or concrete elements. FRP grids can also be used in tunnel lining to reinforce shotcrete. Its flexibility makes it suitable for curved surfaces while its excellent alkali, acid, and chemical resisting properties makes it the most suitable material to reinforce concrete elements placed into soil and conduct different chemical fluids. Glass FRP has been used for long time in marine applications where about 95 percent of the boats are constructed from fibre glass. Fibre glass pre-tensioned concrete piles can also be used in marine environments.

2.2.3 Examples of prestressed concrete bridges using FRP tendons

2.2.3.1 Bridges prestressed by carbon reinforced tendons [9] A very representative structure of this type was recently built in Canada. The Calgary Beddington Trail Bridge, the first concrete high way bridge prestressed by carbon fibre cables in this country, was opened to traffic on November 5, 1993. The two spans continuous skew bridge consists of 13 bulb-tee section precast prestressed concrete girders in each of the 22.83 and 19.23 meters spans. Two types of CFRP tendons imported from japan were used to pretension six precast concrete girders. The structural design of the girders was based on strain compatibility and the material properties of CFRP and concrete. According to preliminary testing conducted at the University of Manitoba on 1:3.3 scale model beams, the CFRP pre-tensioned girders should provide identical behaviour to the other girders pre-tensioned by steel strands under service conditions [1]. Construction of this bridge in Calgary allowed Canadian construction companies to gain first-hand experience in the handling of new materials, and to propose new solutions to problems encountered with these materials such as using coupling system to apply prestressing force to the CFRP tendons.

2.2.3.2 Bridges prestressed by glass-reinforced tendons [9], [16] Most efforts in this area were developed in Germany. One of the earliest applications of prestressed concrete structures with glass-reinforced composite tendons and the first of its type in Europe was the pedestrian Lünen'sche Gasse Bridge, built in Düsseldorf in 1980. The single span slab bridge, with span of 6.55 meters, contains one hundred GFRP bars of 7.5 mm diameter, grouped into twelve, 7 meters long, unbonded prestressing tendons.

Also in Düsseldorf, the Ulenbergstrasse Bridge was the first road bridge using GFRP prestressing tendons. Completed in 1986, the bridge has two continuous spans of 21.3 and 25.6 meters, respectively. The slab in which the tendons are embedded is 1.5 meters thick. Prestressing is provided by 59 GFRP tendons, each one composed of 19 rods of 7.5 mm diameter.

2.2.3.3 Bridges prestressed by aramid reinforced tendons [9] The Sumitomo Construction Company constructed a demonstration bridge at its Oyama research facility in Japan. The structure consists of two parallel bridges. The first one is 25 meters long and 3.59 meters wide single box-girder, post-tensioned using ten AFRP internal tendons in the webs, and six external AFRP tendons located in the bottom invert of the box girder. The second bridge has a 12.5 meters long span with three pre-tensioned box-girders spaced at 1.695 meters at centre, each 1.3 meters high and 0.6 meter wide. Each girder contains sixteen prestressing AFRP tendons and stirrups built from AFRP rods.

2.3 SHEAR STRENGTH OF CONCRETE BEAMS

2.3.1 General

In the design of a concrete element, flexure is usually considered first, leading to the size of the section and the arrangement of reinforcement to provide the necessary moment resistance. Limits are placed on the amount of flexural reinforcement to ensure enough ductility before failure. Because shear failure is frequently sudden and brittle, the design for shear must ensure that the shear strength equals or exceeds the flexural strength at all points

in the beam. A considerable amount of research work has been conducted to investigate the shear behaviour of both, reinforced and prestressed beams. Due to the complexity of the problem and the large number of variables affecting the behaviour, researchers have not been able to develop a unified approach to predict accurately the response of beams in shear. Most of the experimental work has led to the identification of the many mechanisms influencing the shear behaviour of the concrete members.

2.3.1.1 Basic mechanisms of shear transfer [11] Before diagonal cracking occurs, the shear stress transfer can easily be understood based on the elastic beam theory and mohr's circle of stresses, where the shear is resisted by diagonal tensile, and diagonal compressive stresses acting at 45 degrees if no other normal stresses exist, or at any other angle according to the magnitude and direction of the normal stress. However, after cracking, the mechanism is totally different and becomes more complicated. The main modes of shear transfer at a cracked section can be summarized as follow:

a. Shear stress in the uncracked part of the concrete section.

b. Interface shear transfer or aggregate interlock within the cracked portion of the section.

c. Dowel action in the longitudinal reinforcements.

d. Tension in the transverse reinforcements, stirrups.

e. Compression stresses through the arch action, only in short and deep beams.

f. Tension in the bent up bars or draped prestressing tendons.

2.3.1.2 Possible failure modes due to shear in beam with web reinforcement [11]

1. Failure due to yielding of the stirrups, which accelerates the widening and propagation of cracks and reduces both, the aggregate interlock resistance and the shear resistance in the uncracked part. However, beams reinforced by FRP stirrups do not face this mode of failure since the material is linear elastic under tension up to failure.
2. Shear failure initiated by failure of the stirrups anchorage which does not allow the stirrups to achieve its full strength. Generally the upper end of the inclined crack approaches very close to the compression face of the beam and for this reason the stirrups usually include hooks at the upper end totally embedded in the compression zone.
3. Shear failure due to crushing of the web usually occurs in thin-walled beams and beams including high web reinforcement ratio when the compressive strain in the web reaches its ultimate value. Since the cracked concrete in the web is usually weaker and softer due to the high tensile strain in the transverse direction, it fails at lower stresses compared to a concrete cylinder tested in compression. This mode of failure is sudden, very brittle, and destructive. For this reason the code limits the web reinforcement ratio to a maximum value in order to achieve yielding of the stirrups before the web crushes.
4. Shear failure initiated by failure of the tension chord, either by yielding of the longitudinal reinforcement or by slip at the support. Both modes of failure accelerate the shear failure because of the same reasons discussed before in the first mode of failure.

2.3.2 Analytical and design approaches

Although there is no unified rational model has yet been achieved for design for shear,

several models have been developed in the last few decades. This section summarizes most of these models including the 45 degrees truss model, ACI approach, CSA simplified method, variable angle truss model including the plasticity solutions, compression field theory, modified compression field theory, and the CSA general method.

Both the ACI code and the simplified method of the CSA code are based on the 45 degrees truss model. Both The compression field theory and the modified compression field theory are based on the variable angle truss model. The general method of 1984 CSA code is based on the compression field theory while the general method of the 1994 CSA code is based on the modified compression field theory.

2.3.2.1 <u>45 degrees truss model</u> [3], [11] In 1899 Ritter explained the flow of forces in a cracked reinforced concrete beam in terms of a truss model, where the diagonal compressive stresses in the concrete act as the diagonal members of the truss while the stirrups act as vertical tension members. The bottom longitudinal reinforcements in the beam represent the bottom chord while the flexural compression zone of the beam acts as the top chord. In 1902, Mörsch made it clear that rather than having individual diagonal struts, a continuous field of diagonal compression exists.

Since the model represents the beam only after diagonal cracking, it ignores the uncracked behaviour of the beam. It also neglects the tensile stresses in the diagonally cracked concrete. The model assumes a constant inclination of 45 degrees for the diagonal cracks and assumes that the diagonal stresses are constant over the area of the web.

The equilibrium conditions of this model are summarized in Figure 2.1, from which

the following equilibrium equations are driven:

$$f_2 = \frac{2\ V}{b_w\ jd} \qquad (2.1)$$

$$f_v = \frac{V\ s}{A_v\ jd} \qquad (2.2)$$

$$N_v = V \qquad (2.3)$$

From these equilibrium equations, the stresses in the diagonal struts, stirrups, and the bottom chord can be defined for a given shear level.

2.3.2.2 <u>ACI approach</u> [2] The early tests of concrete beams under shear demonstrated that the measured stirrups strains were considerably lower than those predicted by the 45 degrees truss model. In other words, the 45 degrees truss model predicts that a beam without stirrups would have zero shear strength, which is not true because the beam will carry load until diagonal cracks are formed. Later, the truss model was corrected by a semi-empirical term to account for what is commonly referred to as the "concrete contribution". This procedure formed the basis of many codes including the ACI and CSA codes.

The ACI assumes that the shear resistance of a beam, V_n, has two components, namely, the "concrete contribution", V_c, and "steel contribution", V_s.

$$V_n = V_c + V_s \qquad (2.4)$$

The concrete contribution, V_c, is taken as the shear at the initiation of diagonal cracking and

assumed to be the failure load of a beam without transverse reinforcements. The code provides different expressions for V_c for different cases including non-prestressed and prestressed beams. It also accounts for the applied normal forces to the member whether it is tension or compression, however, for all these cases the steel contribution, is calculated using the 45 degrees truss model. In this section only the equations for prestressed beams are given according to the 1989 code. For prestressed concrete member with an effective prestress force not less than 40 percent of the tensile strength of the flexural reinforcement, V_c is taken as the smaller of V_{ci} and V_{cw}, which represent the shear load at the initiation of flexural-shear cracks and web-shear cracks, respectively. These expressions are:

$$V_{ci} = \frac{\sqrt{f_c'}}{20} b_w d + V_d + \frac{V_i M_{cr}}{M_{max}} \qquad \geq \frac{\sqrt{f_c'}}{7} b_w d \qquad (2.5)$$

$$V_{cw} = 0.3 \left(\sqrt{f_c'} + f_{pc} \right) b_w d + V_p \qquad (2.6)$$

Where:

V_d = Shear force due to unfactored dead load acting on the part of the section carrying the dead loads acting prior to composite action, plus the unfactored superimposed dead load acting on the composite member.

$V_i = V_u - V_d$ and $M_{max} = M_u - M_d$, where V_u and M_u are the factored shear and moment due to total factored loads and M_d is the moment due to the unfactored dead load.

$M_{cr} = I/y_t \, (\sqrt{f_c'} / 2 + f_{pe} - f_d)$, flexural cracking moment.

I = moment of inertia of section resisting the externally applied factored loads.

y_t = distance from centroid axis of gross section, neglecting reinforcement, to the extreme fibre in tension.

f_{pc} = compressive stress in concrete due to effective prestress force at the extreme bottom fibre of the girder, not including top slab.

f_{cl} = stress due to unfactored dead load, at extreme bottom fibre of the girder only.

f_{pc} = compression stress in concrete (after allowance for all prestress losses) at the centroid of the composite section due to both, prestressing and moments resisted by precast member acting alone.

V_p = vertical component of effective prestress force at the section.

For a beam including stirrups perpendicular to its axis, the equation for V_s is:

$$V_s = \frac{A_v f_y d}{s} \qquad (2.7)$$

Where:

A_v = area of shear reinforcements within distance, s.

f_y = yield stress of the stirrups.

d = distance from extreme compression level to centroid of longitudinal reinforcements or 0.8 h, which ever is grater.

s = spacing of shear reinforcement.

2.3.2.3 <u>CSA simplified method</u> [7], [8] Similar to the ACI approach, the CSA simplified method considers the concrete contribution in a prestressed beam as the smaller of

flexural-shear cracking, V_c, and web-shear cracking resistance, V_{cw}, as follows:

- The 1984 code:

$$V_c = \left(0.06 \lambda \sqrt{f_c'} + 6 \frac{V_f d_p}{M_f} \right) \varphi_c b_w d_p \geq 0.2 \lambda \varphi_c \sqrt{f_c'} \quad (2.8)$$

$$V_{cw} = 0.4 \lambda \varphi_c \sqrt{f_c'} \sqrt{1 + \frac{f_{pc}}{0.4 \lambda \varphi_c \sqrt{f_c'}}} b_w d_p + \varphi_p V_p \quad (2.9)$$

- The 1994 code:

$$V_c = 0.06 \lambda \varphi_c \sqrt{f_c'} b_w d + \frac{V_f}{M_f} M_{cr} \geq 0.17 \lambda \varphi_c \sqrt{f_c'} b_w d \quad (2.10)$$

$$V_{cw} = 0.4 \lambda \varphi_c \sqrt{f_c'} \sqrt{1 + \frac{\varphi_p f_{cp}}{0.4 \lambda \varphi_c \sqrt{f_c'}}} b_w d + \varphi_p V_p \quad (2.11)$$

Where:

V_f and M_f = factored shear force and moment due to factored load.

d_p or d = distance from extreme compression fibre to centroid of longitudinal reinforcement, need not be taken less than 0.8 h.

λ = factor to account for density of concrete, taken one for normal weight concrete.

ϕ_c and ϕ_p = resistance factor for concrete and prestressing steel respectively.

$M_{cr} = I_g/y_t \, (0.6 \lambda \phi_c \sqrt{f_c'} + \phi_p f_{ce})$, flexural cracking moment.

I_g = moment of inertia of gross concrete section neglecting reinforcement.

y_t = distance from centroid of gross section to extreme fibre in tension.

f_{ce} = compressive stress in concrete due to effective prestress only after allowance for all prestress losses at extreme fibre of section where tensile stress is caused by externally applied loads.

f_{cp} = resultant compressive stress in concrete after allowance for all prestress loss at centroid of the composite section due to both prestress and moments being resisted by the precast member acting alone.

V_p = component of the force in the draped strands in direction of the applied shear.

The web reinforcement contribution in shear resistance is:

$$V_s = \frac{\varphi_s A_v f_y d}{s} \qquad (2.12)$$

Where:

ϕ_s = resistance factor for the steel of the stirrups.

Av, fy, d, and s are similar to Equation 2.7.

2.3.2.4 <u>Variable angle truss model</u> [3], [11] Mörsch's 45 degrees truss model can be made more accurate by accounting for the fact that θ is variable. Figure 2.2 summarizes the equilibrium conditions for the variable angle truss model at section subjected to pure shear. However, it should be noted that this model is only valid for a cracked concrete beam and it ignores the concrete contribution in tension after diagonal cracking. In other words the principal tensile stress, $f_1 = 0$. The following are the equilibrium equations:

$$f_2 = \frac{V}{b_w jd} (\tan\theta + \cot\theta) \qquad (2.13)$$

$$f_v = \frac{V\ s}{A_v\ jd} \tan\theta \qquad (2.14)$$

$$N_v = V \cot\theta \qquad (2.15)$$

For a given shear load, there are four unknowns, the principal compressive stress, f_2, tensile force in the longitudinal reinforcements, N_v, stress level in the stirrups, f_v, and the inclination of the principal compressive stresses, θ, but only three equilibrium equations are available. Different solutions were proposed including the plasticity methods which consider the failure mechanisms of the system as follow:

- Assuming that at failure stirrups will yield and $\theta = 45$ degrees, the failure shear can be calculated using Equation 2.14. Alternatively, for a given shear level the stress in the stirrups can be computed using the same equation.
- Assuming a maximum value of the principal compressive stress, f_2, (a value of 0.6 f_c' is frequently recommended), and solving the two simultaneous equations 2.13 and 2.14, the angle θ and the stress in the stirrups can be calculated for a given shear load.
- Assuming the longitudinal steel yields at failure in Equation 2.15, and solving Equations 2.14 and 2.15, the angle and the stress in stirrups can also be found for a given shear.

This model was introduced into the 1978 CEB-FIP code where θ ranges between 31 and 59 degrees.

2.3.2.5 Compression field theory [3], [4] The major problem in using the variable angle truss model is the value of the angle θ, which has to be assumed. The compression field theory can predict the angle and the full response of the section subjected to shear using equilibrium conditions, strain compatibility, and the appropriate material properties.

For a case of beam including longitudinal prestressed, non prestressed, and transverse reinforcements, the unknowns at a given shear level are: the stress in the stirrups, f_v, diagonal compressive stress in the concrete, f_2, inclination of the diagonal struts, θ, stress in the longitudinal prestressing reinforcement, f_p, and stress in the non-prestressed reinforcements, f_{sx}. To find these five unknowns, five equations are required. Three equilibrium equations are available from the variable angle truss model, Equations 2.13, 2.14, and 2.15. The other two equations can be obtained from the strain compatibility conditions. In a cracked web element, the average strains in the horizontal, vertical, and diagonal directions, ϵ_x, ϵ_t, ϵ_2, and ϵ_1 are linked to the inclination θ as shown in Figure 2.3, where ϵ_t is considered to be equivalent to the stirrups strain, ϵ_2 is the diagonal principal compressive strain in direction of the compression stresses field, and ϵ_1 is the principal tensile strain perpendicular to the compression field. Equation 2.16 (a) and (b) relates the different strains.

$$\tan^2\theta = \frac{\epsilon_x - \epsilon_2}{\epsilon_t - \epsilon_2} \qquad (2.16a)$$

$$\epsilon_x + \epsilon_t = \epsilon_1 + \epsilon_2 \qquad (2.16b)$$

The other compatibility equation of strains in the longitudinal direction:

$$\epsilon_p = \epsilon_x + \Delta\epsilon_P \qquad (2.17)$$

where $\Delta\epsilon_p$ is the difference in strain between the concrete and the prestressing tendons.

Using the three equilibrium equations and the two compatibility equations in addition to the appropriate stress-strain relationship of the diagonally cracked concrete, prestressed, and non-prestressed reinforcements, the load-deformation response of section loaded in shear could be predicted. The behaviour of the diagonally cracked concrete within the compression field is usually different from a regular case of a concrete cylinder loaded in compression. The pre-cracked concrete is usually softer due to the lateral tensile strain as shown in Figure 2.4. It is appropriate to consider that the ultimate compressive capacity of the diagonally cracked concrete, f_{2max}, is dependent on the transverse principal tensile strain, ϵ_1, as given in Equation 2.18. Equation 2.19 shows the stress-strain relationship of diagonally cracked concrete as a parabolic function. These findings were based on tests done by Vecchio and Collins [21] where reinforced concrete elements were tested under pure shear.

$$f_{2max} = \frac{f_c'}{0.8 + 170\ \epsilon_1} \qquad (2.18)$$

$$f_2 = f_{2max}\ [\ 2\ (\epsilon_2/\epsilon_c') - (\epsilon_2/\epsilon_c')^2\ ] \qquad (2.19)$$

Since the compression field theory neglects the behaviour before cracking and the contribution of tensile stresses in the cracked concrete, tension stiffening, it overestimates the deformations.

2.3.2.6 Modified compression field theory [3], [21] If a section of a beam is subjected to pure shear, before diagonal cracking occurs, the shear is carried equally by diagonal tensile and diagonal compressive stresses, f_1 and f_2, acting at 45 degrees. After diagonal cracks form,

the tensile stresses in the concrete are substantially reduced, however, it remains acting in between the diagonal cracks, which is referred to as the tension stiffening of concrete. There are two major differences between the compression field theory and the modified compression field theory, the first is based on the variable angle truss model which ignores the behaviour before cracking, while the other considers both the cracked and the uncracked behaviour. The first ignores the tensile stresses between cracks, while the other considers the tension stiffening after cracking.

The equilibrium equations of the modified compression field theory are introduced using a section subjected to pure shear as shown in Figure 2.5. From mohr's circle of stresses:

$$f_2 = (\tan\theta + \cot\theta)\ \frac{V}{b_w jd} - f_1 \qquad (2.20)$$

From the equilibrium in the vertical direction:

$$V = f_1 \, b_w \, jd \, \cot\theta + \frac{A_v f_v}{s} \, jd \, \cot\theta \qquad (2.21)$$

From the equilibrium in the horizontal direction:

$$A_{sx} f_l + A_{px} f_p = V \cot\theta - f_1 \, b_w \, jd \qquad (2.22)$$

In the treatment above , we have considered average stresses and average strains and have not dealt with local variations. At a crack the tensile stress in concrete, f_1, goes to zero, while the tensile stress in the reinforcement becomes larger. The shear capacity of the member may be limited by the ability of the member to transmit forces across the crack. At low shear values tension is transmitted across the crack by local increases in the reinforcement stresses. At a certain shear level, the reinforcement will yield at the crack location. At higher shear levels transmitting tension across the crack will require local shear stress, v_{ci}, on the crack surface as shown in Figure 2.6. The ability of the crack interface to transmit these shear stresses depends on the crack width, w, and the aggregate size, a. It is suggested that the limiting value of v_{ci} taken as:

$$v_{ci} = \frac{0.18 \sqrt{f'_c}}{0.3 + \frac{24 \, w}{a + 16}} \qquad MPa, \; mm \qquad (2.23)$$

The requirement that the two sets of stresses in Figure 2.6 produce same vertical force is:

$$f_1 = v_{ci} \tan\theta + \frac{A_v}{s \, b_w} (f_{vy} - f_y) \qquad (2.24)$$

The crack width, w, can be taken as:

$$w = \epsilon_1 \, s_{m\theta} \qquad (2.25)$$

Where $s_{m\theta}$ is the spacing of diagonal cracks and depends on the crack control characteristics in the horizontal and transverse directions and suggested to be as follows:

$$s_{m\theta} = 1 \; / \; (\frac{\sin\theta}{s_{mx}} + \frac{\cos\theta}{s_{mv}}) \qquad (2.26)$$

Where s_{mx} and s_{mv} are the crack spacing indicators of the crack control characteristics of the longitudinal and transverse reinforcements respectively and can be estimated from the CEB-FIP code. The expressions for s_{mx} and s_{mv} are given in details and used in section 5.5.1.1 of chapter 5.

Yielding of the longitudinal reinforcement at crack may also limit the magnitude of concrete tension that can be transmitted. The requirement that the two sets of stresses in Figure 2.6 produce the same horizontal force will be satisfied if:

$$A_{sx} f_y + A_{px} f_{ps} \geq A_{sx} f_{sx} + A_{px} f_{px} + f_1 \, b_w \, jd + [f_1 - \frac{A_v}{b_w \, s} (f_{vy} - f_v)] \, b_w \, jd \, \cot^2\theta \qquad (2.27)$$

The stress-strain relationship of the cracked concrete in compression is described before and given in Equations 2.18 and 2.19. Based on their tests of reinforced concrete panels in pure shear, Vecchio and Collins recommended the average tensile stress versus average tensile strain relationship illustrated in Figure 2.7 and given in Equations 2.28 and

2.29 as follow:

$$If\ \epsilon_1 \le \epsilon_{cr}: \qquad f_1 = E_c\ \epsilon_1 \qquad (2.28)$$

$$If\ \epsilon_1 > \epsilon_{cr}: \qquad f_1 = \frac{\alpha_1\ \alpha_2\ f_{cr}}{1 + \sqrt{500\ \epsilon_1}} \qquad (2.29)$$

Where α_1 and α_2 are factors to account for the bond characteristics of reinforcements and the type of loading.

All the relations needed to predict the response of a section of a beam loaded in shear are given above. Program "RESPONSE" [5] provides a solution technique using these equations for a general case including normal force, shear force, and bending moment.

2.3.2.7 The CSA general method [6], [8]

- The 1984 code: The general method of 1984 CSA code is based on the compression field theory. For a given applied factored shear, V_f:

1. Assume angle θ between 15 and 75 degrees and assume the amount of web reinforcement ratio, A_v and s.
2. Assume that stirrups yield at failure to insure a ductile failure, $f_v = f_y$.
3. Calculate the factored shear resistance of the section, V_r, to make sure it is $\ge V_f$:

$$V_r = \frac{\phi_s\ A_v\ f_y\ d_v}{s\ \tan\theta} + \phi_p\ V_p \qquad (2.30)$$

4. Check that the web will not crush, $f_2 < f_{2max}$

$$f_2 = \frac{V_f}{b_v\, d_v} (\tan\theta + \cot\theta) \qquad (2.31)$$

$$f_{2max} = \frac{\lambda\ \phi_c\ f_c'}{0.8 + 170\ \epsilon_1} \qquad (2.32)$$

Where ϵ_1 is calculated from Equation 2.31:

$$\epsilon_1 = \epsilon_x + \frac{\epsilon_x + 0.002}{\tan^2\theta} \qquad (2.33)$$

ϵ_x can be calculated at mid-hight of the section from plane section analysis or can be assumed 0.002. the principal compressive strain, ϵ_2 is already assumed -0.002 in the equation.

5. Calculate the additional tension force in the longitudinal reinforcement:

$$N_v = \frac{V_f}{\tan\theta} \qquad (2.34)$$

- The 1994 code: The general method of 1994 is based on the modified compression field theory where the concrete contribution in shear resistance is considered. The factored shear resistance is determined by:

$$V_{rg} = V_{cg} + V_{sg} + \phi_p\, V_p \quad \leq \quad 0.25\ \phi_c\, f_c'\, b_w\, d_v + \phi_p\, V_p \qquad (2.35)$$

1. The value of V_{cg} can be computed from:

$$V_{cg} = 1.3\ \lambda\ \phi_c\ \beta\ \sqrt{f_c'}\ b_w\ d_v \qquad (2.36)$$

Where β is a factor accounting for shear resistance of cracked concrete. For a given shear load the code provides tables and charts for β. The value of β is based on the longitudinal strain, ϵ_x, at the bottom reinforcement level. ϵ_x is calculated as follow:

$$\epsilon_x = \frac{0.5\ (N_f + V_f \cot\theta) + \dfrac{M_f}{d_v} - A_p f_{po}}{E_s A_s + E_p A_p} \leq 0.002 \qquad (2.37)$$

The decompression stress, f_{po}, may be taken as 1.1 times the effective prestress. Since ϵ_x is dependent on angle θ, trials have to be made by assuming different values of θ until the corresponding correct value of ϵ_x is obtained and the corresponding β can be used in Equation 2.34.

2. Determine V_{sg} as follow:

$$V_{sg} = \frac{\phi_s A_v f_y d_v \cot\theta}{s} \qquad (2.38)$$

3. Calculate is the effective vertical component of the force in the prestressed draped strands, V_p

The resistance of tension reinforcement should be grater than or equal to:

$$\frac{M_f}{d_v} + 0.5\ N_f + (V_f - 0.5\ V_{sg} - \phi_p\ V_p) \cot\theta \qquad (2.39)$$

2.4 PREVIOUS STUDIES ON FRP AS SHEAR REINFORCEMENTS

2.4.1 Diagonal tensile characteristics of FRP rods [12]

An experimental program was conducted in Japan to investigate the behaviour of FRP rods embedded in concrete specimens at various angles with respect to the longitudinal direction of tension. The specimens were subjected to tension to simulate stirrups under the effect of the diagonal principal stresses in a cracked beam as shown in Figure 2.8. Three types of FRP rods were tested: carbon, aramid, and glass bars of 5 and 6 mm diameter. Steel bars were also tested to compare the behaviour. The bars were located at angles of 0, 10, 20, and 30 degrees. No significant reduction was found in the strength of the steel bars when the angle was increased, however, the strength of the FRP bars was significantly reduced as a linear function of the arrangement angle. The following equation was suggested:

$$f_{u\theta} = f_u \left(1 - \frac{k}{100}\theta\right) \qquad (2.40)$$

Where: $f_{u\theta}$ = diagonal tensile strength of the FRP rods located at an angle θ with respect to the longitudinal direction of tension.

f_u = actual tensile strength of the rods, when θ = zero.

k = reduction factor, 0.1 for steel, 1.3 for glass, 1.9 for aramid, 1.9 for strand type carbon rods, and 2.3 for pultrusion type carbon rods.

θ = arrangement angle.

The diagonal tensile strength differed depending on the kind of fibres showing the largest reduction in carbon fibre, followed by aramid, and then glass. It was found that the diagonal tensile strength at a 30 degrees arrangement angle was about 30 percent of the actual

tensile strength in carbon rods, 45 percent in aramid rods, and 65 percent in glass rods.

2.4.2 Tensile strength characteristics of FRP bent bars [14]

This experimental program was conducted in Japan to investigate the tensile strength of FRP stirrups which believed to be reduced because of the bent at the corners. The tested FRP bars composed of continuous glass and high strength carbon fibres impregnated with resin. Two types of specimens were tested, bent FRP bars intersecting deformed steel bar at the corner representing the longitudinal reinforcement, and bent FRP bars intersecting FRP longitudinal bar. In the first type of specimens, the straight portion of the FRP bent bars was debonded and different curvatures were used for the bent including a radius of one to three times the diameter of the bent bars. In the second type of specimens, two types of bend were used, folded and curved with 20 mm radius. The test was performed by pulling the FRP bar out of the concrete, and after failure the concrete block was broken and the failure mode of the bar was observed. The following is a summary of the findings of this study:

1. When tension force was applied to FRP bent bars, large tensile strain was measured at the inside surface of the bend while compressive strain was measured at the out side surface. As the radius increases this compressive strains become tension.
2. As the radius decreases, the tensile capacity of the FRP bars reduces.
3. The fibres of FRP bent bars broke in sequence from the inside of the bend.
4. The tensile capacity of the FRP bent bars was lower when FRP bars were used as longitudinal reinforcement at the corner.

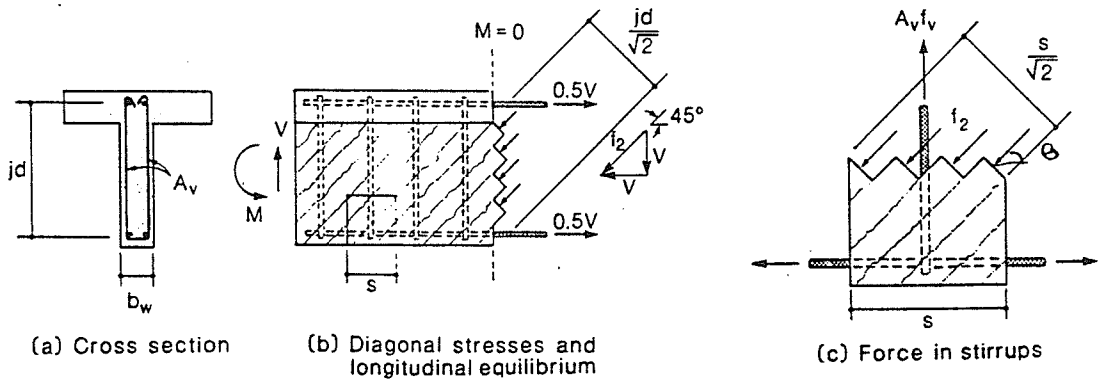

Figure 2.1 Equilibrium considerations for 45 degrees truss model

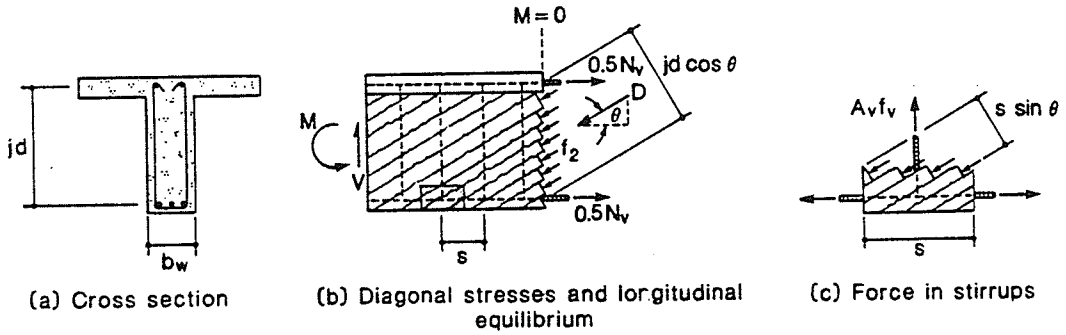

Figure 2.2 Equilibrium considerations for variable angle truss model

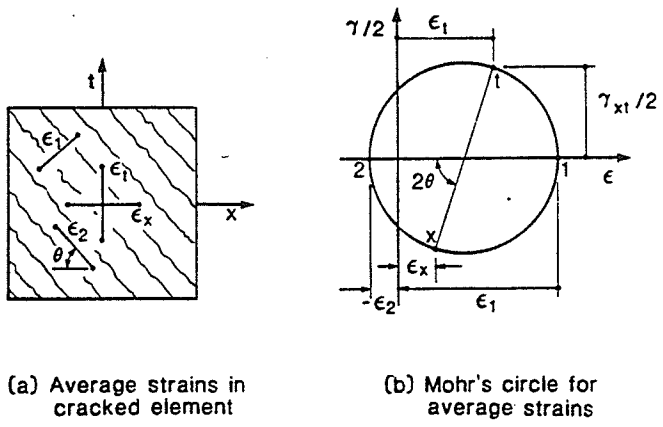

Figure 2.3 Compatibility conditions for cracked web element

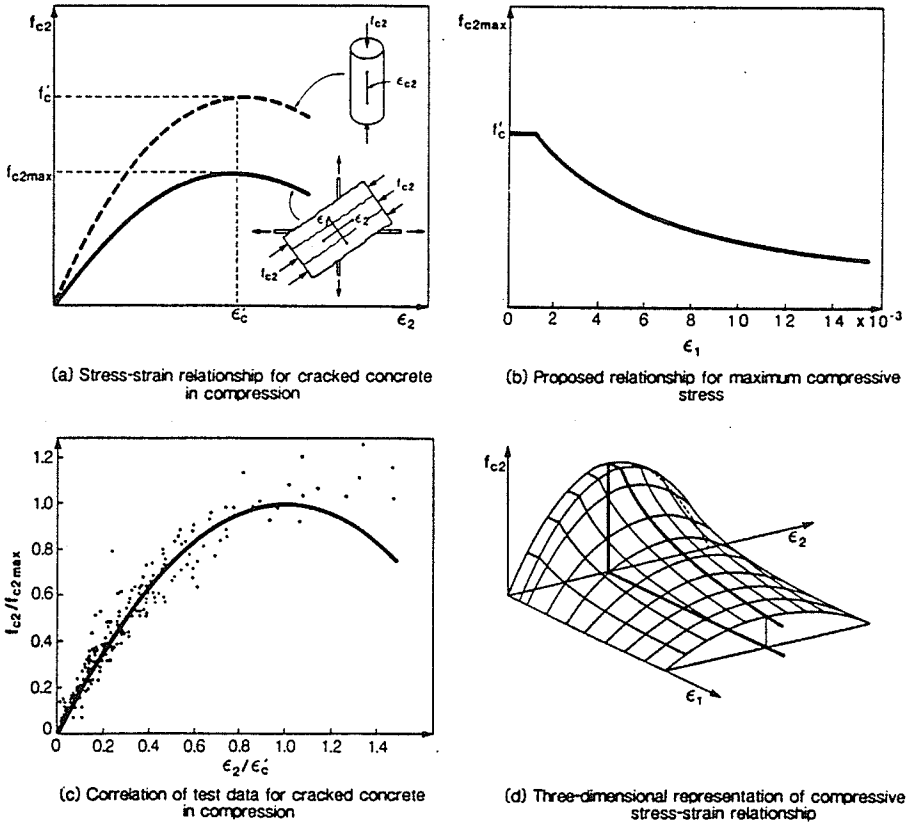

Figure 2.4 Compressive stress-strain relationship for cracked concrete

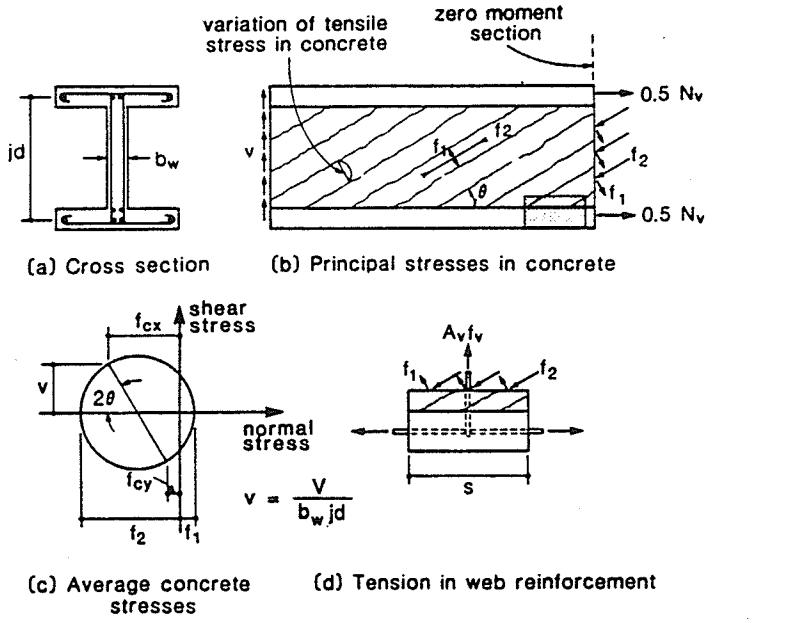

Figure 2.5 Equilibrium conditions of modified compression field theory

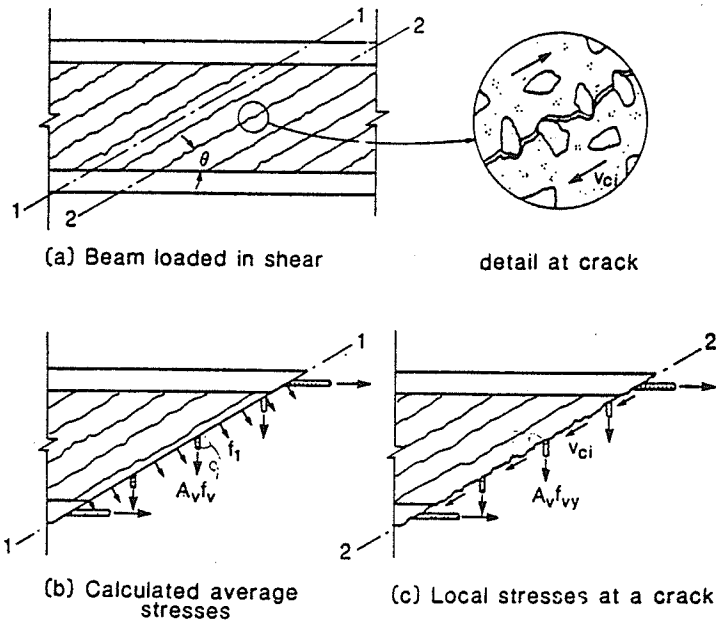

Figure 2.6 Transmitting forces across the diagonal cracks

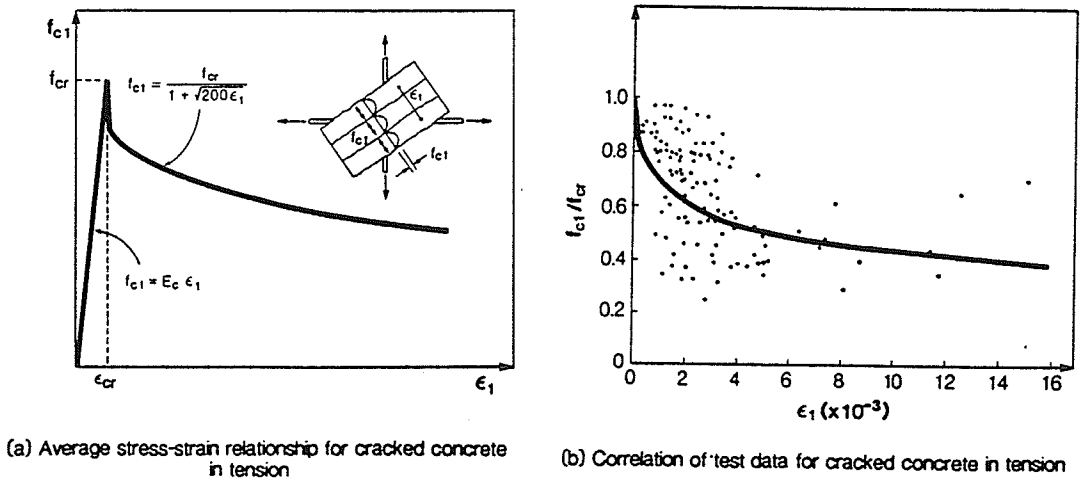

Figure 2.7 Tensile stress-strain relationship for cracked concrete in tension

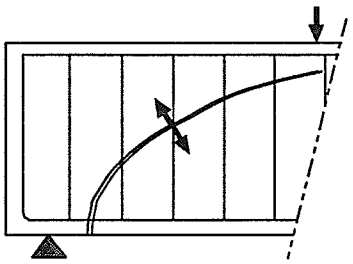

stirrups subjected to principal tensile stresses

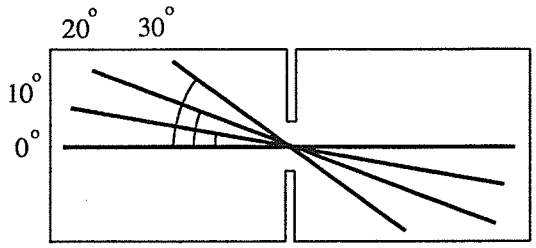

angle of embeded FRP rods

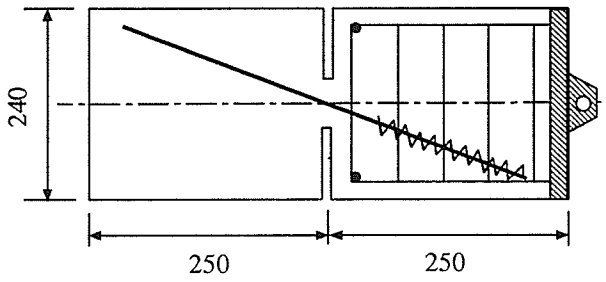

test specimen

Figure 2.8 Test specimen used to determine the diagonal tensile characteristics of FRP rods

CHAPTER 3

EXPERIMENTAL WORK

3.1 GENERAL

The experimental program was designed to evaluate the behaviour of pre-tensioned I-girders fully reinforced by Carbon Fibre Reinforced Plastic, CFRP, for prestressing and shear under static loading condition in comparison to conventional steel. Two types of CFRP were considered in this investigation, Carbon Fibre Composite Cables , CFCC, and Leadline rods. A total of six beams were tested, three fully reinforced by CFCC for prestressing and stirrups, two by Leadline rods for prestressing and stirrups, and the sixth beam by conventional steel for prestressing and stirrups. The main parameter considered in this investigation was the web reinforcement ratio in terms of stirrups size and stirrups configuration.

The performance of test beams was evaluated and compared according to :

- Flexural behaviour in terms of flexural cracking load, crack width, crack spacing, deflection, ultimate flexural strength, and mode of failure.
- Shear behaviour in terms of shear cracking load, shear cracks pattern, inclination of cracks, diagonal crack width, and stress levels in stirrups.

3.2 BRIDGE OUTLINE

The high way bridge is planned to be constructed over the Assiniboine river, Parish of Headingley, Winnipeg, Manitoba, Canada. The bridge consists of five spans, 32.5 meters each, covering a total length of 165.1 meters. All the forty girders of the bridge are precast pre-tensioned and simply supported. The girders have an I-shape cross section of AASHTO

type, transversely spaced at 1.8 meters, and supporting a 187 mm thick deck slab. Each girder has an overall length of 32.9 meters and a simply supported span of 32.5 meters. The depth of the girders is 1829 mm, top flange and bottom bulb have a width of 660 mm, and the thickness of the web is 178 mm. Each girder has two end blocks of 1370 mm long each.

The girders are designed using conventional steel strands and stirrups. Each girder is pre-tensioned by a total of 40 H.T.S seven wire strands of 13 mm diameter, 24 strands are straight and 16 are draped with an angles ranging between 3.1 and 5.1 degrees from both ends at distances equal to 12.875 meters from the ends of the beam. The girders were reinforced by M15 deformed steel stirrups spaced at 400 mm within the I-shape portion and at 150 mm within the end blocks. Figure 3.1 shows the general layout of the bridge girder.

3.3 TEST SPECIMENS

3.3.1 Design of the specimens

A total of six pre-tensioned concrete I-girders were tested in this program. All the girders had a top slab that was casted after a minimum age of seven days from the time of release. The stirrups were projected from the I-girders into the slabs to provide the dowel action. Three of the beams were prestressed by CFCC cables and reinforced by three different sizes of double legged CFCC stirrups, two beams were prestressed by Leadline rods and reinforced by two different configurations of Leadline stirrups, and the sixth beam was prestressed by conventional steel strands and reinforced by double legged steel stirrups.

The beams were designed to provide similar conditions in comparison to the prototype: same span-to-depth ratio of 17.8, same jacking stress for the tendons of 60

percent of the guaranteed strength, same stresses in the beam cross section due to prestressing, and same flexural mode of failure. The beams were designed with different web reinforcement ratios to induce different stress levels in the stirrups. A length scale of 1:3.6 was selected to model the bridge girder and part of the deck slab equivalent to the spacing between the girders. The number and layout of the tendons for each beam was obtained to satisfy the same induced stress level in the cross section after release as the bridge girders. In all the test beams, 40 percent of the prestressing tendons were draped with an angle of 4 degrees at distance equal to 40 percent of the span measured from the supports from both ends similar to the bridge girders. The rest of the tendons were kept straight. The beams had an I-shape cross section along the entire span except from both ends solid end blocks were provided to improve the bearing conditions and stress transfer after release similar to the bridge girders. The spacing of the stirrups was proportional to the spacing of the stirrups in the bridge girder through the same scale factor. The spacing was kept constant in all the beams within the I-shape portion at 110 mm spacing and reduced to 50 mm within the end blocks to improve the confinement at the end zone similar to the end blocks of the bridge girders.

Due to the small dimensions of the test beams, the resulting stresses in the beam cross section due to its own weight only were considerably less in comparison to the bridge girders, therefore combination of stresses due to prestressing and own weight induced tensile stresses at the top surface exceeding the tensile strength of the concrete [23]. Temporarily external post- tensioning was used to reduce the tensile stresses at top surface. At later stage, just before testing, the post tensioning was released as the testing machine was in full contact with

the test beam.

The notation used to identify the specimens was designed to reflect the following parameters: (a) Type of the prestressing and reinforcing materials, TR for CFCC (Tokyo Rope), LL for Leadline, and ST for steel. (b) Specimen number from 1 to 6. (c) Shear reinforcement, for CFCC reflects the (diameter / number of wires per cable), for Leadline reflects the (number of branches per stirrups), and for steel the notation C reflects that it is epoxy coated stirrups. Table 3.1 presents the above classification of the tested beams.

The beams were 9.28 meters long, simply supported over a span of 8.88 meters, and subjected to a symmetrical four - points loading. The loading system was designed to simulate an equivalent truck loading conditions. The four loads were spaced at 1.2 meters and the load was applied monotonically up to failure using stroke control. Figure 3.2 shows the general layout of the test beams.

3.3.2 Longitudinal reinforcement

Three beams were prestressed by five 15.2 mm CFCC seven wire cables each, the jacking force in the cables was 58 percent of the guaranteed strength of the material, resulting in a jacking force of 115 kN for each cable. Two beams were prestressed by ten 8 mm Leadline rods each, each two rods were used as one tendon with one anchorage head, the jacking force was 61.7 percent of the guaranteed strength, resulting in a jacking force of 115 kN per tendon. One beam was prestressed by five 13 mm conventional steel seven wire strands, the jacking force in the cables was 62 percent of the guaranteed strength, resulting in a jacking force of 115 kN per strand. For all the beams, 40 percent of the longitudinal

prestressing tendons was draped with an angle of four degrees and the remaining part was kept straight. Figure 3.3 shows the prestressing and reinforcing details of the beams.

The temporarily external post tensioning consisted of two 13 mm conventional steel seven wire strands, one each side of the web, located 50 mm beneath the flange of the I-girders, and anchored to the end blocks. The jacking force in the strands was 35 percent of the guaranteed strength, resulting in a jacking force of 64 kN per strand. A special reinforcement was designed to improve the confinement at the anchorage zone as shown in Figure 3.4.

The upper flange of the I-girder was reinforced by two steel rebars of 5.7 mm diameter each in order to support the stirrups. The top slab was reinforced by a WWF 102 x 102 welded wire mesh (4 mm diameter) for crack control due to shrinkage.

3.3.3 Shear reinforcement

Different sizes and configurations were used for shear reinforcements. All the stirrups were projected from the I-girders into the slabs to provide the dowel action required for the horizontal shear transfer. All the stirrups had rounded corners at the bends of radius equal to three times the diameter and a 17 mm concrete cover was provided. Anchorage of the stirrups at the top was provided by the inverted U-shape for the double legged stirrups or the 180 degrees hook for the single legged stirrups. At the bottom, anchorage was provided by the over lapped 90 degrees hook of the two branches. Double or single legged stirrups were used within the I-shape portion while rectangular stirrups were used within the end blocks. Figure 3.5 (a) shows different configurations of the used stirrups.

3.3.3.1 CFCC stirrups. The stirrups used within the I-shape portion consisted of two components each, a closed stirrup for the upper flange of the girder and an inverted U double branch stirrup with a bottom bulb for the web and the bottom flange. Three different sizes were used, 7.5 mm seven wire cable for beam TR-1-7.5/7, 5 mm solid cable for beam TR-2-5/1, and 5 mm seven wire cable for beam TR-3-5/7. Figure 3.5 (b) shows the CFCC stirrups.

3.3.3.2 Leadline stirrups. Similar to the CFCC stirrups, a closed stirrup was provided for the upper flange. Two different configurations were used for the web reinforcement, inverted U double legged stirrups with bottom bulb for beam LL-4-2B, and single legged stirrup with a bottom bulb and a 180 degree hook at the top for beam LL-5-1B. The two configurations were used to provide two different web reinforcement ratios using one size of Leadline bar, the bar was produced with a rounded corner rectangular cross section of an equivalent area of 7 mm diameter rods. The Leadline bar was covered by a deformed protective coating. Figure 3.5 (b) shows the Leadline stirrups.

3.3.3.3 Steel stirrups. The same configuration was used by providing closed stirrups for the top flange and double legged inverted U stirrups with bottom bulbs for the web and bottom flange. The stirrups were 6 mm diameter epoxy coated deformed steel for beam ST-6-C.

3.4 MATERIAL PROPERTIES

3.4.1 Concrete

The concrete used in the beams was designed for a nominal strength of 35 MPa at release and 40 MPa at 28 days. Normal portland cement was used. For each beam control cylinders were tested in compression at the day of release of the prestressing and six cylinders were tested in compression at the time of testing for each beam, three from the girder concrete and three from the slab concrete. Three beams were also tested in flexure to obtain the modulus of rupture for the concrete of each beam. The tests were conducted according to the ASTM specifications. Table 3.2 provides the measured concrete properties for the six beams as well as the age of the concrete beams at different stages.

3.4.2 Longitudinal prestressing

Several tension tests were done to investigate the stress - strain characteristics of the CFRP materials including Tokyo Rope strands and Leadline bars. Figure 3.6 summarizes the findings of these tests as reported by the manufacturers of both, Tokyo Rope strands, and Lead line bars in terms of the elastic modulus, guaranteed strength, ultimate strength, and strain at ultimate. The 1/2 inch (13 mm) steel strands used in this experimental program were also tested and the results are also shown in Figure 3.6 as reported by Con-force structures company Ltd.

3.4.3 Shear reinforcement

The material properties of Leadline and Tokyo Rope stirrups were also investigated

and summarized in Figure 3.7 as reported by the manufacturers. The steel stirrups were also tested and the stress - strain characteristics are summarized in Figure 3.7 as well.

3.5 FABRICATION OF THE SPECIMENS

3.5.1 Preparation of the form

The beams were fabricated by Con-force Structures Company Ltd, Winnipeg, Manitoba, Canada. A special form was constructed using steel and wooden sections to account for the shape and size of the beams. The form consisted of two individual sides and a bottom steel section. The form was cleaned and lubricated with pella oil before the reinforcements were placed. Figure 3.8 shows the casting bed and the side forms.

3.5.2 Stressing of the tendons

The abutments were fixed to the floor and spaced approximately at 24 meters. They also consisted of horizontal steel plates spaced in the vertical direction and tied together as shown in Figure 3.8. The system is normally used for jacking conventional steel strands. Figure 3.9 shows the general layout of the modified jacking system.

3.5.2.1 Steel couplers. [10] In order to minimize the coasts of CFRP and facilitate using the same system of abutments, special steel couplers were used to couple the CFCC tendons and the Leadline rods to conventional steel strands. Figure 3.10 shows the components of the steel couplers.

a. Anchorage of CFCC tendons: The CFCC cables are provided by ready made die-cast

ends and special steel chucks for anchorage. The die-cast consists of special alloy molten and die-molded on the end portion of the CFCC, a steel pipe is installed on to the die-cast portion and pressed to integrate the CFCC, the die-casting, and the steel pipe. Using this system the wedges can be installed through one-touch action. The chucks had a threaded surface that facilitate the connection to one end of the steel couplers while the other end is prepared to house regular steel chucks used for anchoring the conventional steel strands. Figure 3.11 shows the connection through the coupler.

Due to the fact that the spacing of the CFCC cables is only 50 mm and the couplers had a diameter of 82 mm, the couplers were staggered. For each beam three cables of 11.88 meters long and two cables of 13.88 meters long were ordered. The die-casts were located at the end of the cables, away from the heat and moisture which results during curing.

b. Anchorage of Leadline rods: Leadline rods were delivered in a form of rolls precut to the required lengths and steel anchorage components. A special technique recommended by the manufacturer was used to assemble the anchorage system. Every two rods were anchored together in one anchor-head. The Leadline rods were marked at 110 mm from the end, the two rods were placed through the narrow holes of the anchor-head, an aluminum pipe with four side slits was placed at the end of each rod, a tapered plastic film was placed around the wedges which consisted of two pieces for each rod, the wedges were placed about 10 mm from the end of the aluminum pipe, care was taken to overlap each two slits of the aluminum pipe with the gap between the wedges and to provide equal distance from both sides. The tapered plastic film was pulled back to wrap the wedges, the wedges were inserted into the anchor-head by pushing the anchor-head, a retainer plate was placed over the wedges

from the ends and fixed with four provided bolts, four tubular spacers were used between the retainer plate and the anchor-head to insure the proper fit of the wedges into the anchor-head. Care was taken to ensure equal lengths between anchorages to provide equal distribution of forces into the two bars. Figure 3.12 shows the components of the Leadline anchorage.

Once the setting of the rods was completed from both sides, the anchor-head was connected to the coupler through the threaded surface. Figure 3.13 shows the connection through the coupler.

c. Anchorage of steel strands: For the beam prestressed by steel strands, no couplers were used and the strands were jacked directly through the abutments.

3.5.2.2 Hold-down system. In order to allow draping of the strands, a hold-down system consisted of steel pins 32 mm diameter was used. The pins were supported by the steel sides of the form which were braced to the floor. At distance of 3.64 meters from both ends of the beam, two pins were installed and aligned vertically with a spacing of 50 mm and the bottom one was 66 mm from the bed level in order to support the two levels of the prestressing strands. The diameter of the pins were selected based on recommendation from the manufacturer of the materials taking in account the draping angle, and to insure enough strength to support the vertical reactions of the jacking forces.

A slight modification was added to the system by providing thin copper rotating sleaves around the pins in order to reduce the friction. Those sleaves were not used during jacking the steel strands of beam ST-6-C or the CFCC of beam TR-1-7.5/7 where slight localized damage of the protective external coating of the draped CFCC tendons was

observed, and the sleaves were used successfully for all beams. Figure 3.14 shows the hold-down system.

3.5.2.3 Hold-up system. A hold-up system consisted of a steel vertical arm supporting steel pins at different levels was used to provide the change in direction of the draped reinforcement to the horizontal position out side the beams for the jacking purpose at the abutment at each end. The steel arms were supported by steel cross reaction beams anchored to the side abutments. Rotating sleaves, covering the pins, were used to reduce the friction. Figure 3.15 shows the hold-up system.

3.5.2.4 Special considerations for stressing the Leadline rods. Each two Leadline rods were anchored into one anchor-head from each side which were coupled to the steel strands for the jacking purpose as mentioned before. Due to the nature of the steel seven wire strands, they tend to rotate (twist) during jacking process. Since there was a steel seven wire strand extension to the Leadline rods from each end, this action rotated the couplers into two different directions resulting in twisting the two Leadline rods. In case of the bottom straight rods the twisting was acceptable as long as the two rods were kept apart and parallel for an adequate distance from the face of the anchor-head by using plastic separators, however, for the draped rods, since they were supported by the pins, each two rods having the same anchorage were kept apart and parallel all the way from end to end. In order to achieve that, the couplers were prevented from rotating during jacking by using two flat sides for each coupler and holding it by a yoke fixed to the casting bed as shown in

Figure 3.16.

For beam LL-4-2B, the clear space between the two branches of the stirrups was about 30 mm, while the two draped Leadline rods were 33 mm apart out-to-out, accordingly the spacing between the two draped rods had to be reduced. Two aluminum spacers having two rounded edge holes each were machined and used to bring the two bars together. The holes were spaced at 25 mm for the first spacer, which was the original spacing between the rods at anchor-head, and the second spacer had holes spaced at 22 mm. The two separators were placed apart along the Leadline rods with a distance of about one meter in between to provide a gradual reduction in the spacing of the rods out side the beam region. Figure 3.17 shows the use of the aluminum spacers.

3.5.2.5 Jacking process. The tendons were anchored from one end and stressed from the other end by means of long -stroke hydraulic jack. Three different ways were used to check for the jacking force: the pressure of the hydraulic pump which was calibrated two month before, the elongation of the tendons, and finally the strains obtained from electrical strain gauges attached to the tendons surface. The tendons were jacked one at a time.

3.5.3 Preparation for casting

The two parts of each stirrup were assembled together and tied to the bottom strands in order to achieve the designed spacing. Two steel rebars were used at the top flange to support the stirrups. The form sides were assembled together in order to support the steel pins used to hold-down the draped strands. The reinforcement for the anchorage zone of the

post-tensioning was placed. Figure 3.18 shows the reinforcement cage and Figure 3.19 shows the reinforcement of the anchorage zone.

3.5.4 Concrete casting and curing

The concrete was supplied by a local concrete mixer in the factory. Electrical vibrators were attached to the steel sides of the form. The stirrups were exposed out of the upper surface of the concrete and the surface was prepared in a similar fashion typically used for bridge girders. Six standard size concrete cylinders and three concrete beams, 150X150X500, were casted for each girder. Additional cylinders were casted by the fabricators to check the strength at release and after 28 days. The girder, the cylinders, and the small beams were covered with plastic sheets and steam cured for one day. After a minimum age of seven days from casting of each girder, a form was prepared to cast the top slab. Three cylinders were casted with each slab.

3.5.5 Release of prestressing

Once the beam has achieved the specified strength at release, the following steps were used to insure that the induced stresses are within the allowable range:

a. The girder was supported downwards using wooden vertical posts supported by a steel reaction cross beam anchored to the sides of the abutments, as shown in Figure 3.20. The posts supported the top of the beam at the pins locations in order to allow removing the two sides of the form which were supporting the vertical reaction of the pins.

b. After the sides of the form were removed, the draped prestressing tendons were released.

c. The vertical wooden posts were released, and two external seven wire steel strands were inserted through ducts in the end blocks of the beam from both sides of the web and anchored from one side. The two strands located 50 mm beneath the upper flange.

d. The beam was supported laterally by horizontal wooden posts from both sides along the span and post-tensioning was applied using the two external strands. The first strand was prestressed to 50 percent of the total force followed by stressing the second strand to full force, and finally stressing the first strand to the full force. Figure 3.21 shows the post-tensioning of the external strands.

e. Finally the bottom straight prestressed strands were released. At that stage the girder was totally released and removed out of the casting bed as shown in Figure 3.22 (a).

f. The locations of the stirrups were marked down on the web from both sides and the initial camber was measured. A slight lateral curvature was observed. The girders were straightened up by means of lateral jacking before casting of the top slabs.

3.5.6 Casting of top slab

After a minimum age of about seven days from releasing the I-girders, a top slab was casted to simulate portion of the deck of the bridge in composite action. Figure 3.22 (b) shows a completed test beam.

3.6 INSTRUMENTATION

3.6.1 Electrical strain gauges

The strains were measured using electrical resistance strain gauges which were

attached to the prestressing reinforcements. The gauges were used to: (a) check for the jacking force during prestressing. (b) monitor the prestressing losses between the time of prestressing and the time of testing, and (c) measure the strains in the tendons during the tests. The locations of the strain gauges on the tendons were selected to cover the zone of constant moment and the critical location of shear. Figure 3.23 shows the typical layout of the strain gauges locations.

The type of gauges used was N11-FA-5-120-11 manufactured by SHOWA Measuring Instruments C0., Ltd, Japan. The gauge length was 5 mm and the resistance of the gauge was 120 ohms. The procedure of attaching the strain gauges comprised the following steps:

1. Surface preparation:

The surface was smoothed by the sand paper in case of the steel strands. For the Lead line rods, the surface was quite smooth and therefore didn't require special preparation, however for the Tokyo Rope strands, the protective transverse layer of fibres was removed carefully by a sharp blade to expose the main longitudinal fibres and sand paper was used gently to smoothen the surface. For all types of reinforcement the surface was thoroughly degreased with CSM-1 type, M-PREP conditioner A was applied with cotton tips and M-PREP Neutralizer 5A was applied after in the same way. The surface was wiped and dried.

2. Gauge installation:

The gauge was attached carefully to the prepared surface using a special tape. The bond-side of the gauge was wetted with the 200 Catalyst-B and one drop of the M-Bond 200 Adhesive was placed on the reinforcement surface at the location of the strain gauge. The gauge was placed carefully on the surface using a tape and uniform pressure was applied for

about 3 minutes.

For some of the strain gauges the M-Bond AE-10 and M-Bond GA-2 Adhesive were used instead of M-Bond 200 and the gauges were kept under pressure using rubber bads and clamps during the accelerated curing for one hour in temperature of 62 degrees using heat guns. The M-Bond AE-10 and M-Bond GA-2 system is more reliable because it lasts more at higher strain level compared to the M-Bond 200 system.

Electrical wires were attached to the Lead wires of the gauges using soldering station. M-Coat D (Acrylic coating) was applied on the gauge as well as the terminal connections and M-Coat B (Rubber coating) was applied through a length of 15 mm on the surface of the electrical wires to create a bondable surface. M-Coats, B and D were cured for 24 hours. Finally a butyl rubber sealant was applied for a relatively larger surface area to cover the M-Coats, B and D coats.

3.6.2 Concrete strain measurements

Demec points were attached to the surface of the concrete to measure the strains. Strain readings were recorded manually using two demec gauges of 200 mm and 50.8 mm gauge lengths. Six demec stations of the 200 mm gauge length were located at the top surface of the beam within the constant moment zone and three stations of the same gauge length were located on the side of the bottom flange at the level of the straight tendons within the constant moment zone. Figure 3.24 shows the arrangement of demec stations within the middle part of the beam.

Five demec stations were located on one side of the web at one end of the beam just

to the left of the first loading point to cover five stirrups location in the shear span. One station was located to the right of the same loading point, and another station was located on the web at the end of the beam just before the end block to measure possible web shear cracks. All the stations were located on the web at the stirrups locations at a hight of 265 mm from the bottom surface which is about half of the shear depth of the web. Each station typically consisted of 45 degrees strain rosette using gauge of 200 mm length, another three vertical stations of 50 mm length were added within the vertical gauge length of the rosette. Figure 3.25 shows the typical arrangement of the concrete strain measurements in shear.

3.6.3 Deflection measurements

Deflections were measured from both sides of the beam at mid span using two Linear Motion Transducers (LMTs). The LMTs were connected to steel rigid arms fixed to the columns of the testing machine from both sides of the beam and connected to the beam through steel loops projected from the slab surface as shown in Figure 3.26. The measurements were automatically recorded by the data acquisition system.

3.6.4 Crack-width measurements

Two different microscopes were used to measure crack width, a hand-held microscope with an accuracy of 0.1 mm and another microscope of an accuracy of 0.02 mm with a supporting frame.

3.6.5 Other measurements

A dial-gauge was fixed to the girder relative to the top slab from both ends of the beam to measure the movement of the girder with respect to the slab. Dial gauges were also fixed to the ends of the girders from both ends to monitor any possible slip of the tendons. Figure 3.27 shows the arrangement of the dial gauges.

3.6.6 Data acquisition system

A P-3500 strain indicator was used to monitor the strain gauges readings during fabrication. Just before testing the same strain indicator was used to monitor the effective pre-strain and the total losses. During testing, a Data Scan 7000 system was used to store and view all the measured data through the computer program LABTECH NOTEBOOK using HP 286 computer, the applied load, displacement of the actuator, readings of strain gauges, reading of LMTs, and the time were stored and viewed graphically during the tests.

3.7 TESTING PROCEDURE

3.7.1 Test setup

Each specimen was set on two solid 650 x 650 x 700 mm concrete blocks. The blocks were jacked to the floor through two dywidag bars each. The beams were supported by a steel roller support from each side consisted of two plates, each had a curved grove, and a steel pin in between. The plates and the pin were connected by a tie from each side to keep them together. The bottom plate of the roller was bolted to a steel block which was also bolted to a steel plate jacked with the concrete block to the floor. The upper plate of the

roller was supporting the end blocks of the test beams through a steel shoe welded to the upper plate of the roller from each end. A ± 1.2 million pounds MTS testing machine was used to apply the load using deflection control mode through a spreader beam system with four loading points. A load cell of 1000 kN capacity was placed between the actuator and the loading spherical head. The spreader beam was connected to the actuator through four threaded bars two be supported when the testing is not in progress but once the spreader beam was loading and the spherical loading head was in full contact with the spreader beam, the nuts the tied the threaded bars to the spreader beams were all loosed to allow free rotation of the loading points. Figure 3.28 shows a schematic and photo of the test setup.

The spreader beam system was designed to simulate a truck loading condition by applying four loads spaced at 1.2 meter. the system consisted of a large steel spreader beam to distribute the load to another two smaller spreader beams through hinged joints, the two spreader beams applied the load at each end to the upper surface of the test beams through four short steel beams transversally spaced at 1.2 meters and hanged through steel hinges. Stiffeners were provided to increase the stiffness of the rigidity of the system. Figure 3.29 shows the spreader beams system.

Lateral supports were provided at four points along the span from each side of the beam. Two points were provided at the locations of the two inner loading points at both sides using vertical steel sections braced laterally with an x-shape braces, as shown in Figure 3.29. The other two points were provided at the end of the beam using vertical steel sections fixed to the concrete blocks from each side as shown in Figure 3.29.

At the last three tests, four steel hollow columns of the H.S.S type were used two at

each side of the beam jacked to the floor to support steel screens in order to enhance the safety at the failure stage as shown in Figure 3.30.

For proper alignment of the beams, the supports, and the spreader beams loading system with respect to the centre line of the MTS testing machine, plumb bobs, level bars, and squares were used.

3.7.2 Preparation for testing

After the beam was properly aligned and levelled, strain gauges and LMTs wires were connected to the data acquisition system and checked through dry runs. A white wash was applied to the beam surface to identify small cracks and quick-set plaster bags were used in between the loading beams and the concrete surface to provide proper contact. The external post-tensioned steel strands were released before testing after application of approximately 3 kN in addition to the weight of the spreader beams which was 9 kN to insure the full contact between the beam and the loading system. Two oxyacetylene flames were used at the same time from each side of the web at one end to release the seven wire strands. The lateral eccentricity was prevented by the four lateral supports.

Initial demec readings at the constant moment zone were taken before the release, while for the rosettes, the initial demec readings were taken after the release. The load level at that stage was still way bellow the cracking shear load level and no significant strains were obtained before the shear cracking load. The existence of post tensioned steel strands which located very close to the web surface made it difficult to take initial readings before release.

3.7.3 Testing

The beams were subjected to static loading under deflection control mode. The load was applied through 1 mm / minute rate of loading up to post-cracking stage and than increased to 2 mm / minute up to the end of the test due to the reduction of the beam stiffness. In case of beams LL-5-1B and ST-6-C, the rate of loading was increased to 3 mm / minute near the end of the test. The load was applied in small increments near the expected flexural cracking load and once the first crack developed, the crack width measurements were taken at the bottom fibre level of the concrete. The cracks were marked down with the load stages with black felt pen. Photographs were taken at the initiation of shear cracks and after failure for both the critical sections in shear and the constant moment zone. All dial-gauges were continiousely monitored to check any possible slip.

Load, deflection, and strain gauges readings were monitored automatically to the end of the test by the data acquisition system. The demec readings were measured during the test up to about 90 to 95 percent of the ultimate load except for beams TR-3-5/7 and LL-5-1B demec readings were taken only up to 66 and 54 percent of the ultimate load respectively due to the brittle nature of the failure occurred for beam LL-4-2B.

Beam	Flexural prestressing	$\rho=A_s/A_c$	Shear reinforcement	$\rho_w=A_v/A_w$
TR-1-7.5/7	Identical flexural reinforcement, five 15.2 mm Φ, Tokyo Rope tendons, TR.	1.03 %	7.5 mm Φ seven wires stirrups, 7.5/7	0.789 %
TR-2-5/1			5 mm Φ single wire stirrups, 5/1	0.395 %
TR-3-5/7			5 mm Φ seven wire stirrups, 5/7	0.262 %
LL-4-2B	Identical flexural reinforcement, Ten 8 mm Φ Leadline rods, LL.	0.858 %	Double legged stirrups with rectangular cross section of the same area as 7 mm Φ rods, 2B	1.0 %
LL-5-1B			Same as in beam LL-4-2B but single legged stirrups, 1B	0.5 %
ST-6-C	five 13 mm Φ steel strands, ST	0.898 %	6 mm Φ epoxy coated deformed steel stirrups	0.737 %

"ρ" is flexural reinforcement ratio. "ρ_w" is web reinforcement ratio.

Table 3.1 Description of test beams.

Concrete properties:

Beam	Girder concrete properties							Slab concrete properties				
	slump (mm)	f_{ci}' at release (MPa)	f_c' at 28 days (MPa)	At testing time of beams				slump (mm)	f_c' at 28 days (MPa)	At testing time of beams		
				f_c' (MPa)	ϵ_c' (ms)	E_c * (MPa)	f_r ** (MPa)			f_c' (MPa)	ϵ_c' (ms)	E_c * (MPa)
TR-1-7.5/7	120	36.5	48	50.5	2.03	31334	5.83	120	60.3	61.1	2.47	33754
TR-2-5/1	70	35.1	51.8	60	2.54	34093	6.147	80	53.8	58.5	2.48	28638
TR-3-5/7	120	42.7	60.3	61.1	2.47	33754	6.253	100	58.7	60.6	2.23	36436
LL-4-2B	100	45	58.7	60.6	2.23	36436	6.398	150	53.8	65.5	2.22	35473
LL-5-1B	150	43	53.8	65.5	2.22	35473	6.909	-	59.5	61.1	2.12	35631
ST-6-C	120	34.3	51.1	51	-	-	6.397	120	48	50.5	2.03	31334

Age of concrete:

Beam	At release (days)	At casting slab (days)	At testing (days)
TR-1-7.5/7	2	9	126
TR-2-5/1	2	9	128
TR-3-5/7	3	13	160
LL-4-2B	4	7	118
LL-5-1B	4	6	145
ST-6-C	2	8	192

* Elastic modulus of concrete was the secant modulus at 0.45 f_c'

** Modulus of rupture of concrete was based on beam tests according to ASTM

Table 3.2 Measured concrete properties of the test specimens at different stages.

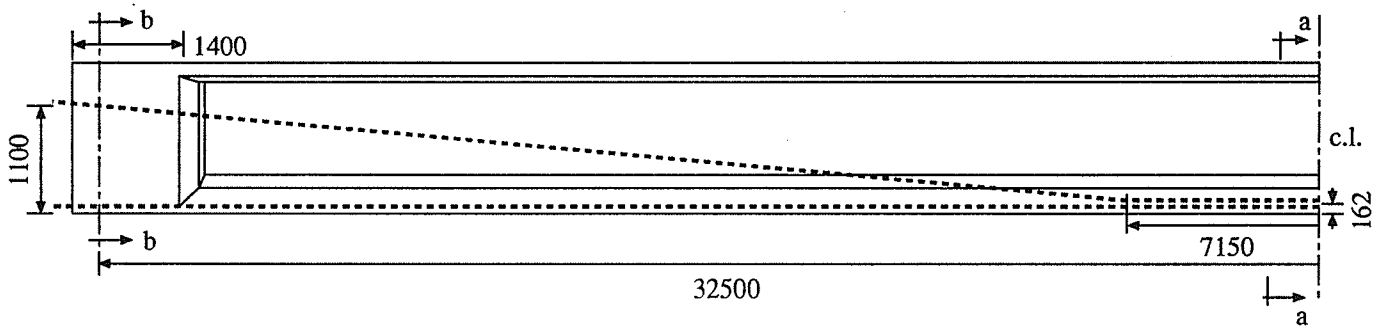

Half elevation of bridge girder

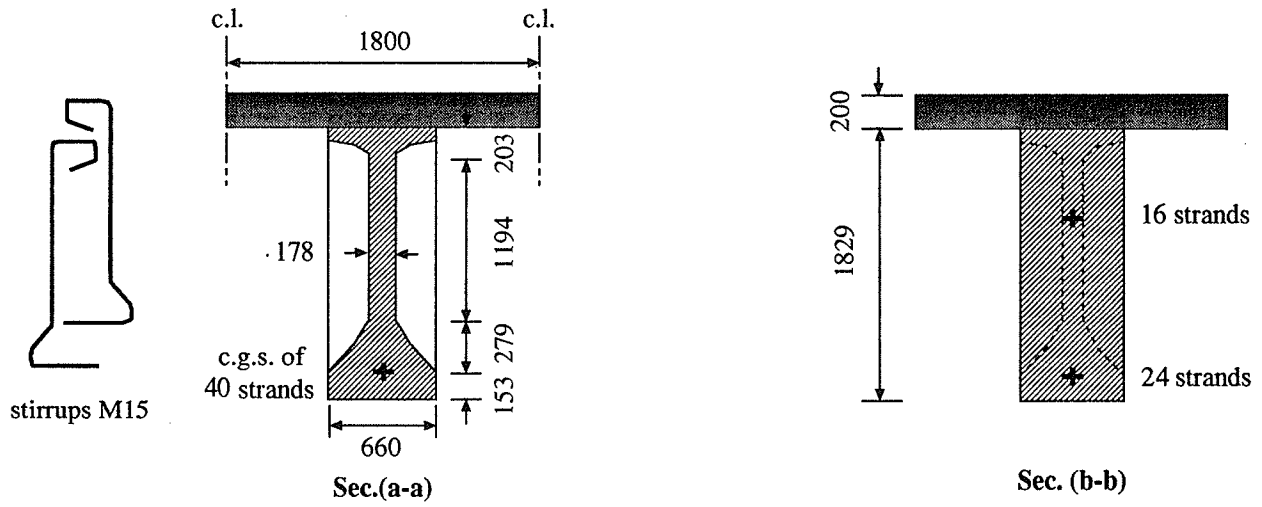

Sec.(a-a)

Sec. (b-b)

Figure 3.1 General layout of bridge girder

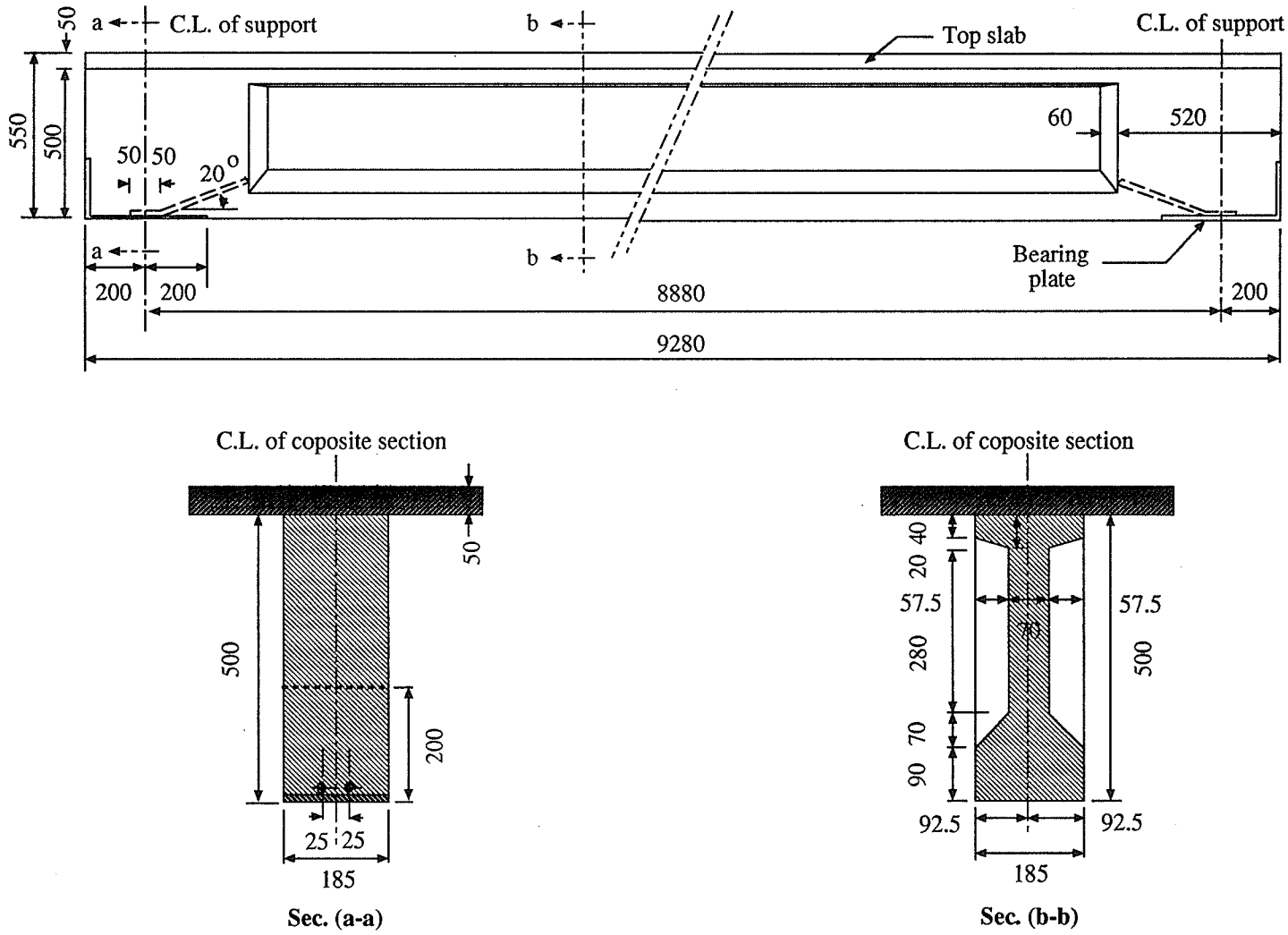

Figure 3.2 Beam - slab composite section details for all test beams

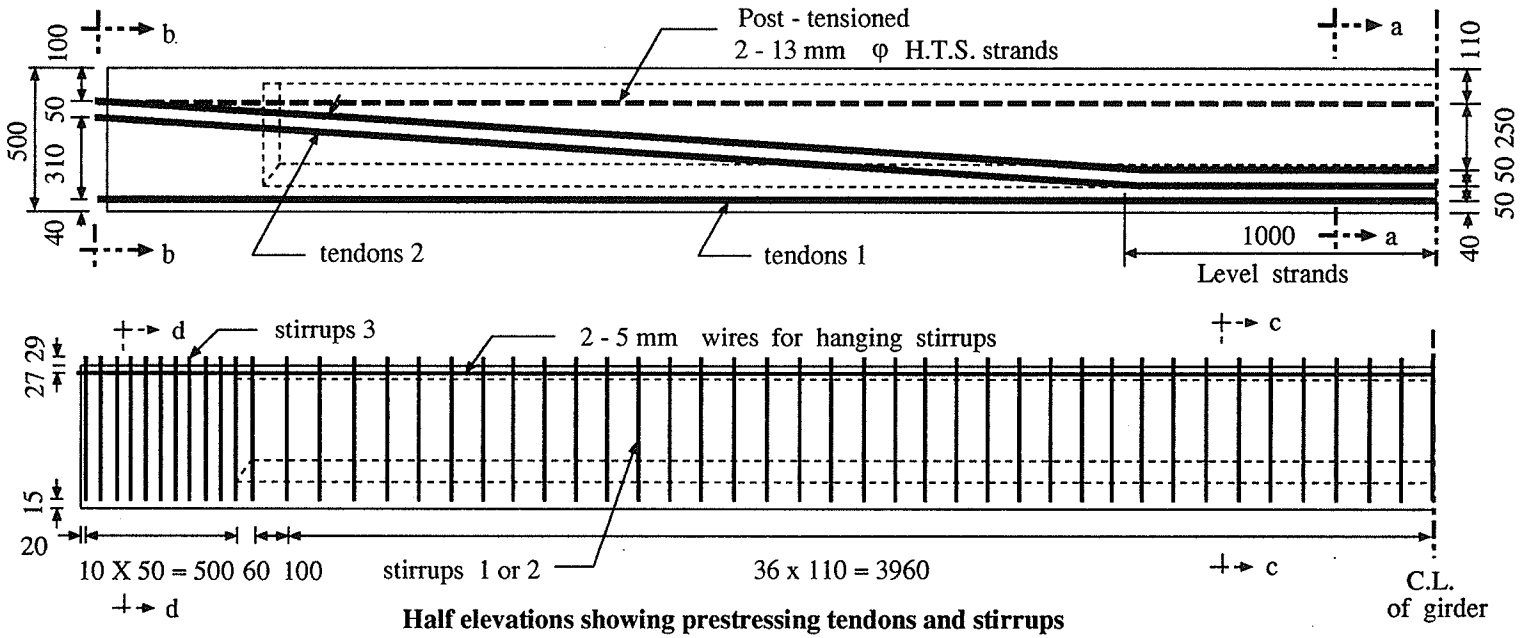

Half elevations showing prestressing tendons and stirrups

Beam	tendons 1	tendons 2	stirrups 1 (double legged)	stirrups 2 (single legged)	stirrups 3 (rectangular)
TR-1-7.5/7	3 - 15.2 mm φ (1X7)* CFCC tendons	2 - 15.2 mm φ (1X7) CFCC tendons	7.5 mm φ (1x7) CFCC		same size as stirrups 1 or 2 but rectangular
TR-2-5/1			5 mm φ (1) CFCC		
TR-3-5/7			5 mm φ (1x7) CFCC		
LL-4-2B	6 - 8 mm φ (1)** Leadline rods	4 - 8 mm φ Leadline rods	rounded corner rectangular section with an equivalent area as 7 mm φ rods		
LL-5-1B				same size used in LL-4-2B	
ST-6-C	3 - 13 mm φ H.T.S strands	2 - 13 mm φ H.T.S strands	6 mm φ epoxy coated deformed steel		

* seven wires cable ** solid cable or rod

Figure 3.3 Prestressing and reinforcing details of test beams

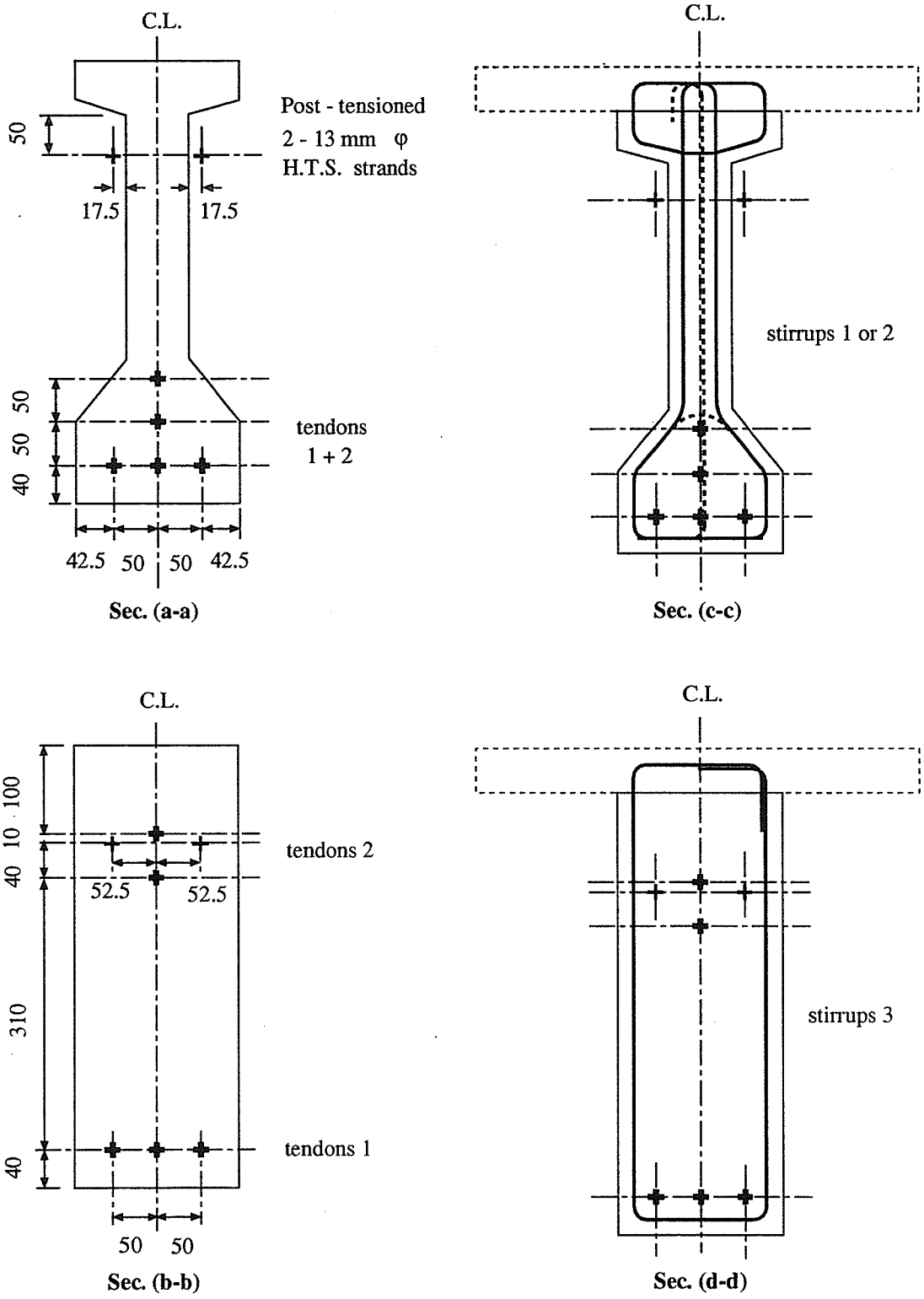

Figure 3.3 (Cont.) Prestressing and reinforcing details of test beams

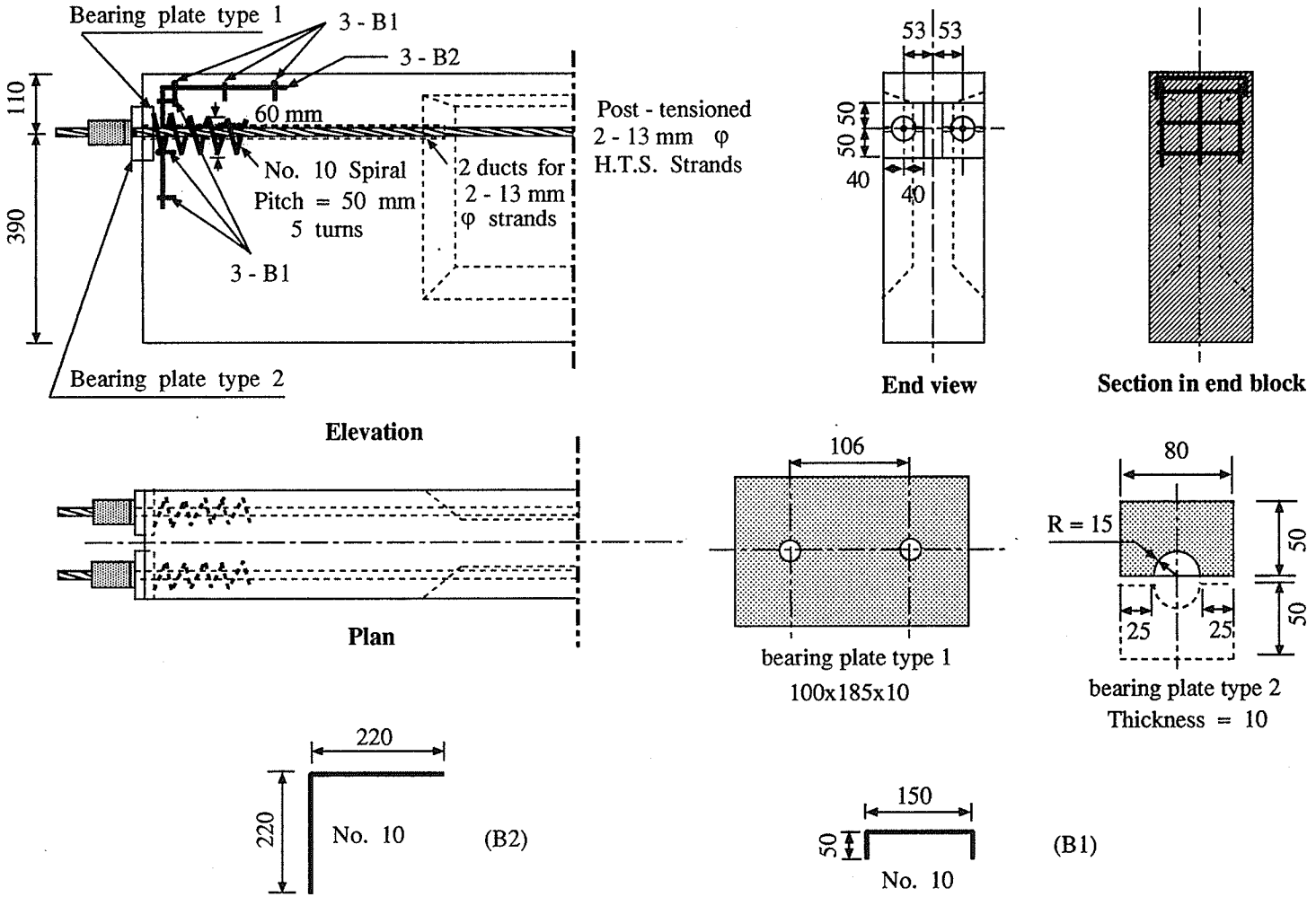

Figure 3.4 End block reinforcement at anchorage zone of external prestressing

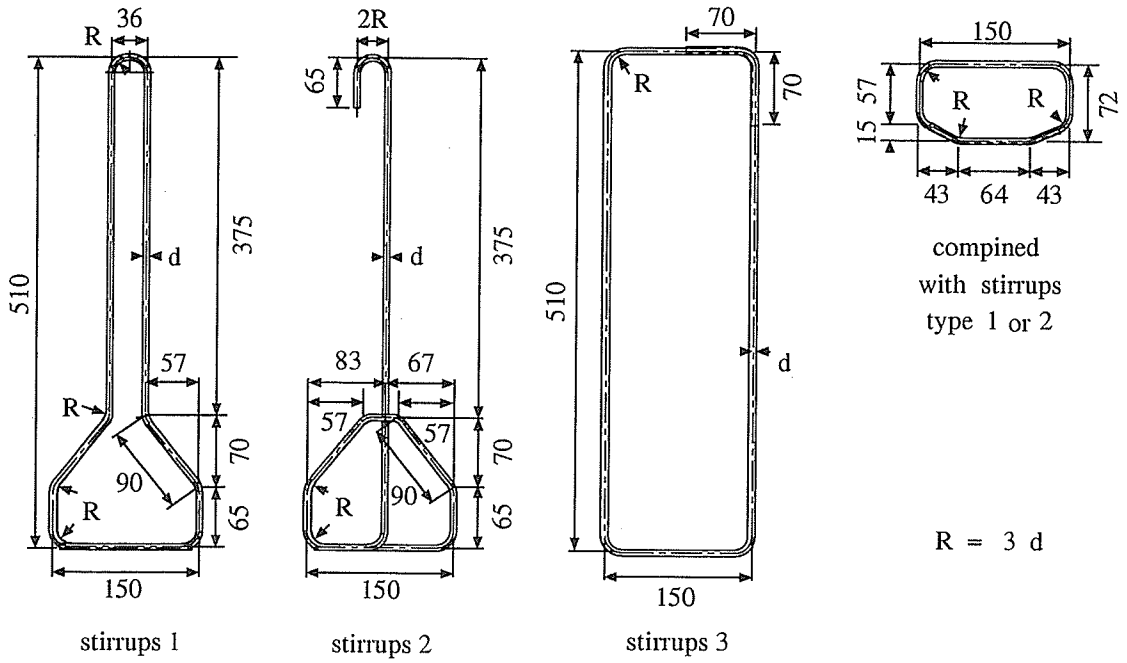

(a)

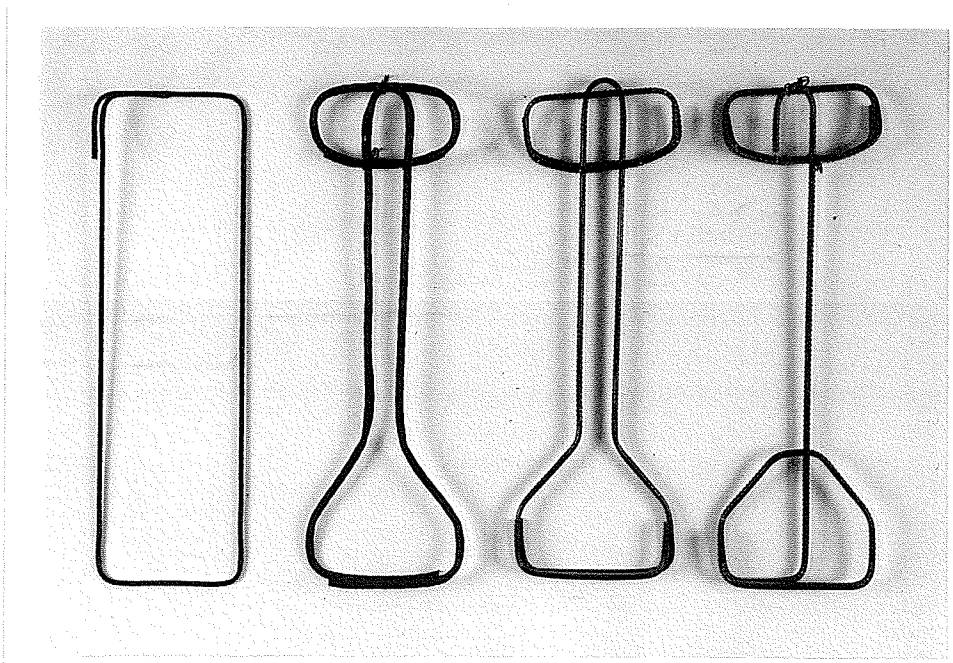

CFCC Leadline

(b)

Figure 3.5 Different configurations of stirrups

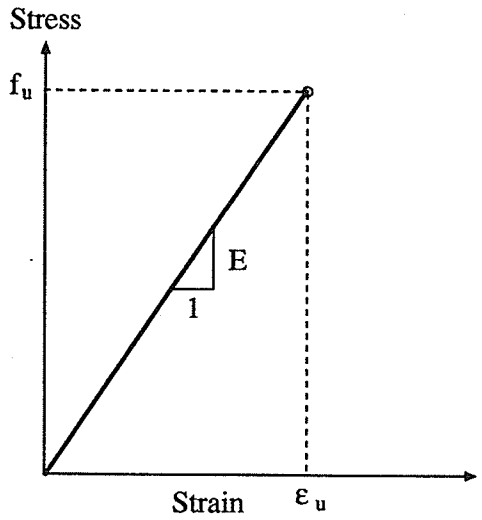

(a) CFRP

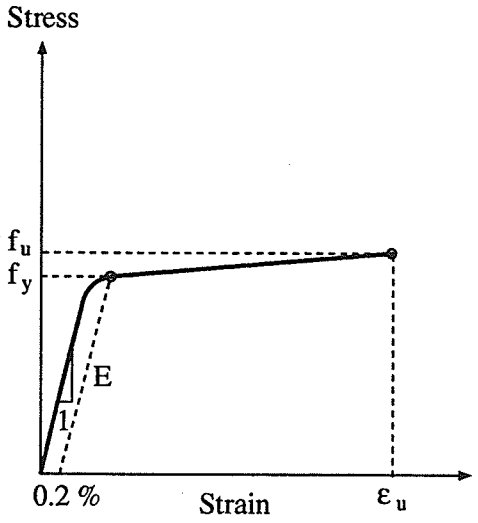

(b) Steel

Type	Φ (mm)	Area (mm^2)	See figure	f_y (MPa)	f_u (MPa)	ϵ_u (ms)	E (GPa)	Guranteed strength (MPa)	% Age (Jacking/ guranteed)
CFCC	15.2	113.6	(a)	-	2150	16	137	1750	58 %
Leadline	8	47.3	(a)	-	2950	20	147	1970	61 %
Steel	13	98.7	(b)	1752	1888	67	205.5	1860	62 %

Figure 3.6 Material properties of prestressing tendons

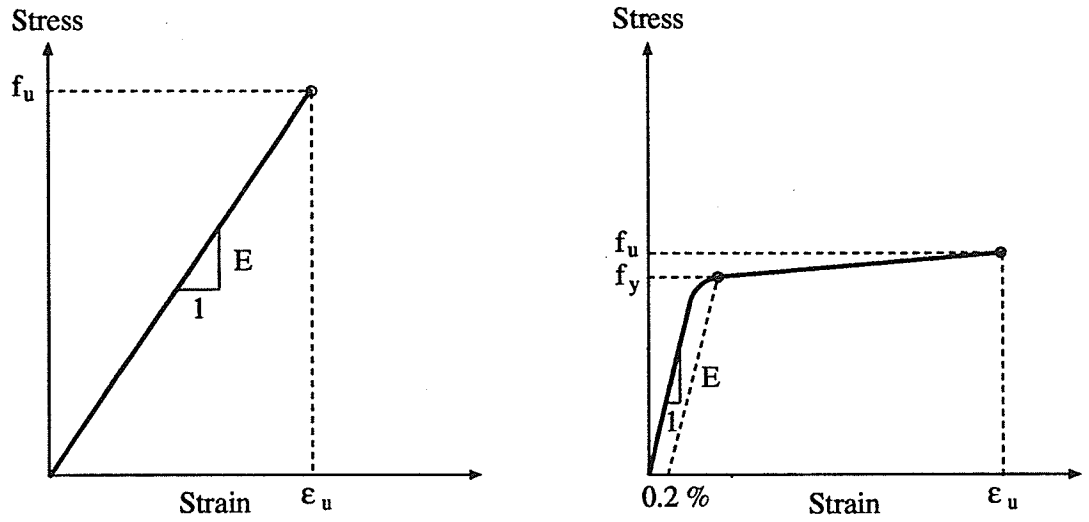

(a) CFRP (b) Steel

Type	Φ (mm)	Area of one branch (mm^2)	See figure	f_y (MPa)	f_u (MPa)	ϵ_u (ms)	E (GPa)
CFCC	7.5 (seven wires) 5.0 (single wire) 5.0 (seven wires)	30.4 15.2 10.1	(a)	-	1880 1840 1780	13.7 13.0 13.4	137 137 137
Leadline	7.0 (equivalent)	38.5	(a)	-	1886	13.0	140
Steel	6.0 (deformed)	28.8	(b)	600	650	16.0	205

Figure 3.7 Material properties of stirrups

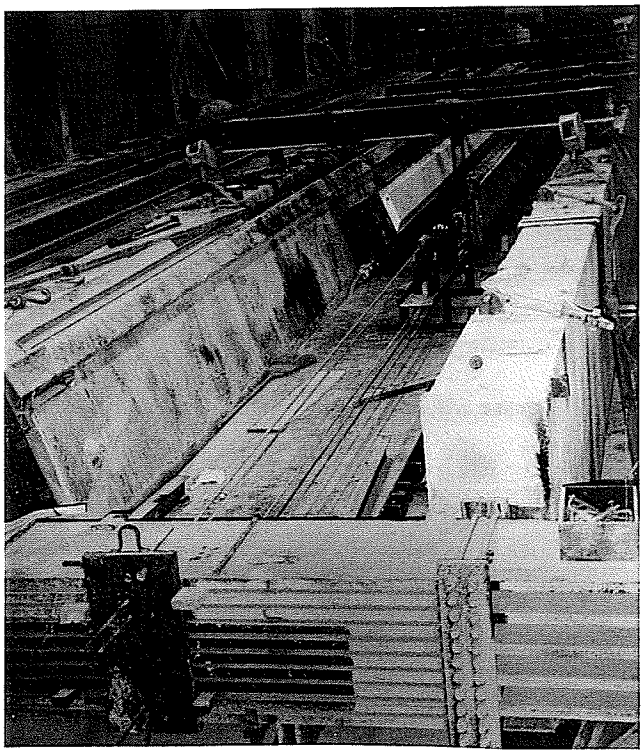

Figure 3.8 General view of the casting bed showing the sides of the form and the abutments at the jacking end

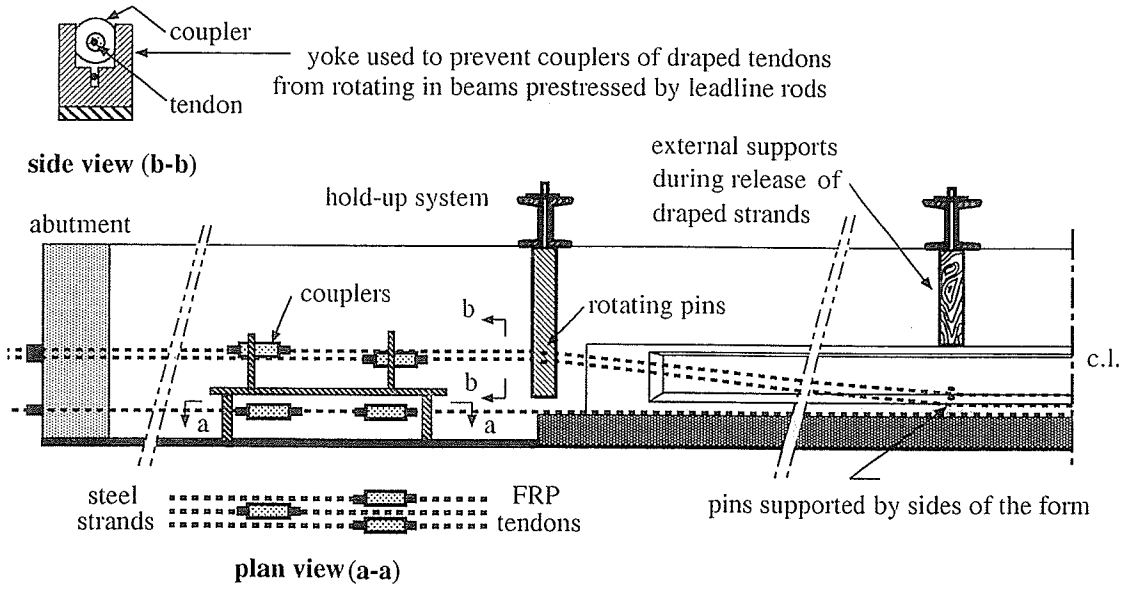

Figure 3.9 General layout of jacking system

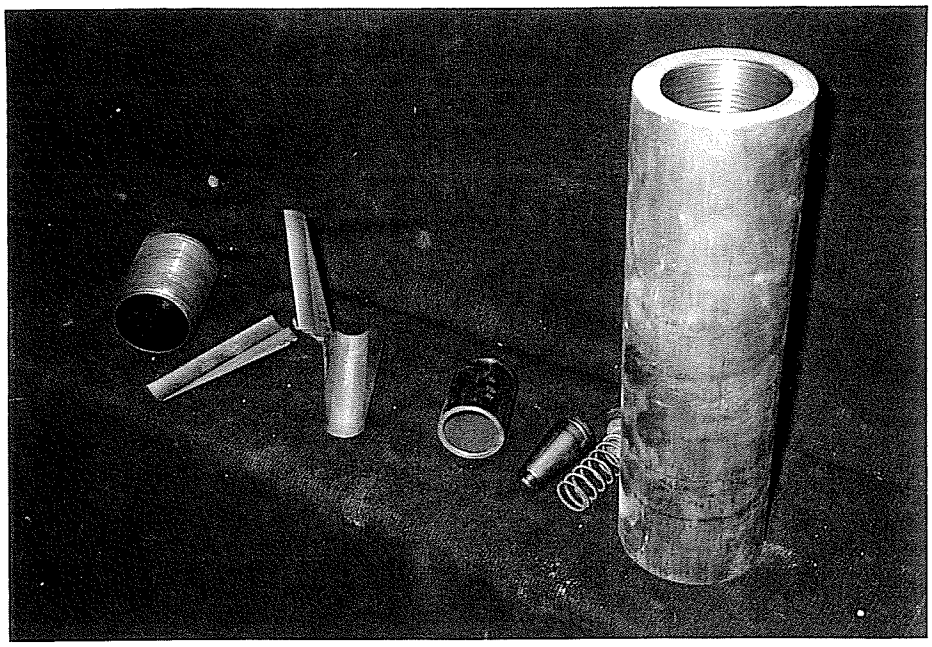

Figure 3.10 Components of the steel coupler

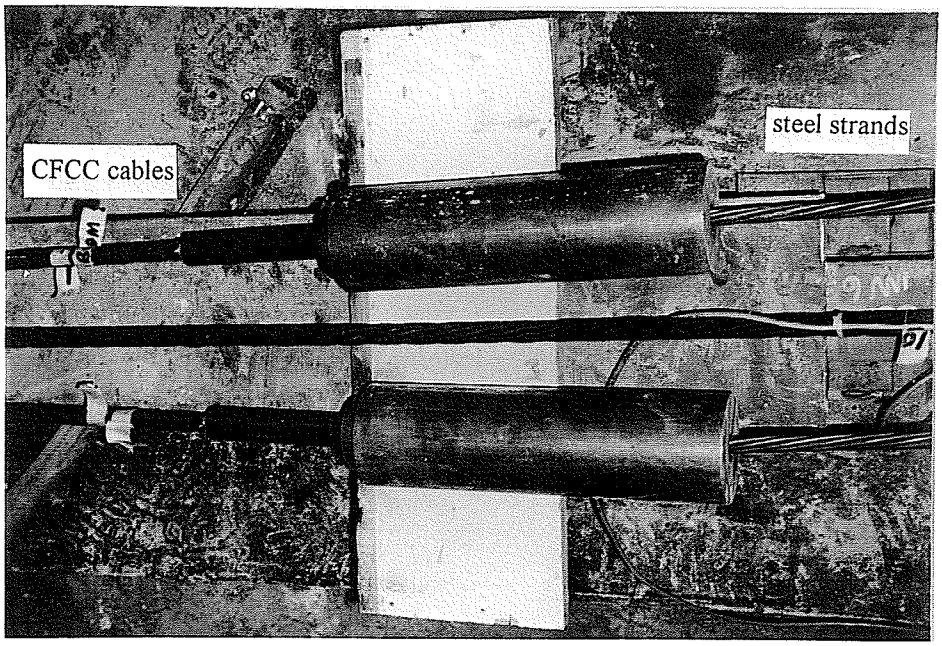

Figure 3.11 Tokyo Rope strands connected to steel strands through the couplers

Figure 3.12 Components of the Leadline anchorage

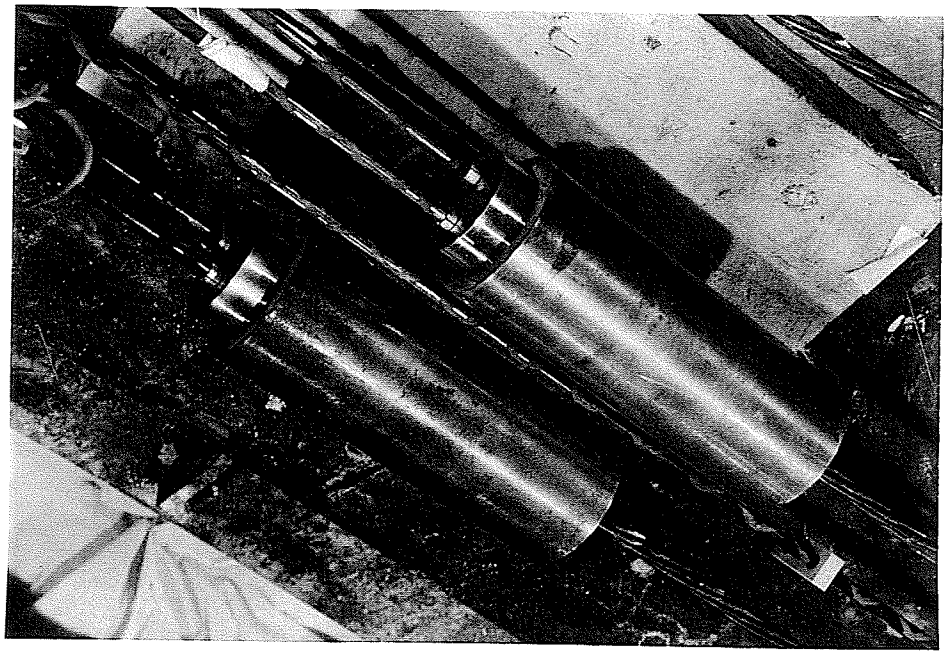

Figure 3.13 Leadline bars connected to steel strands through the couplers

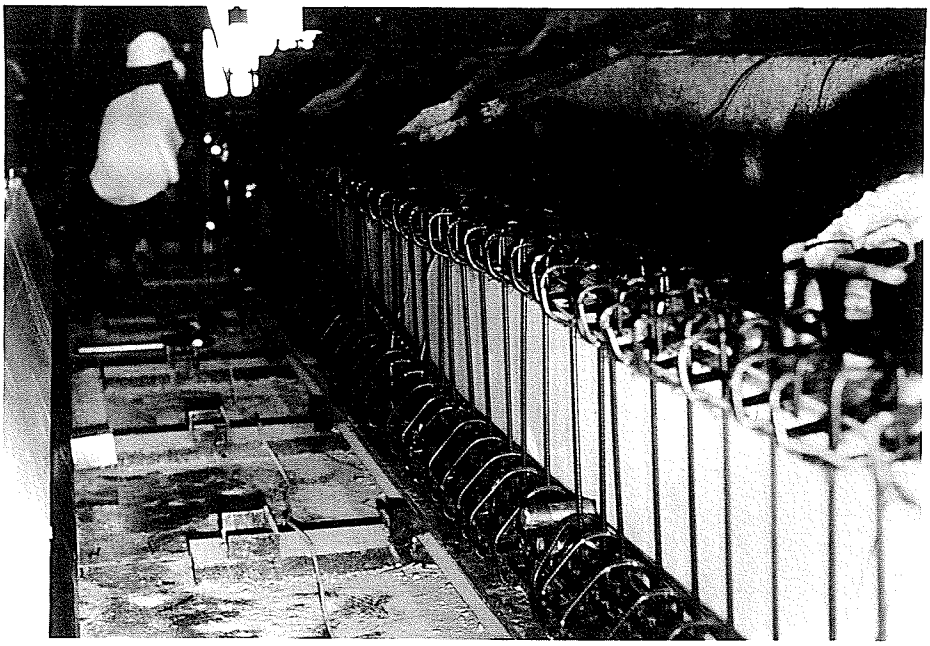

Figure 3.14 Hold-down system consists of steel pins supported by the sides of the form

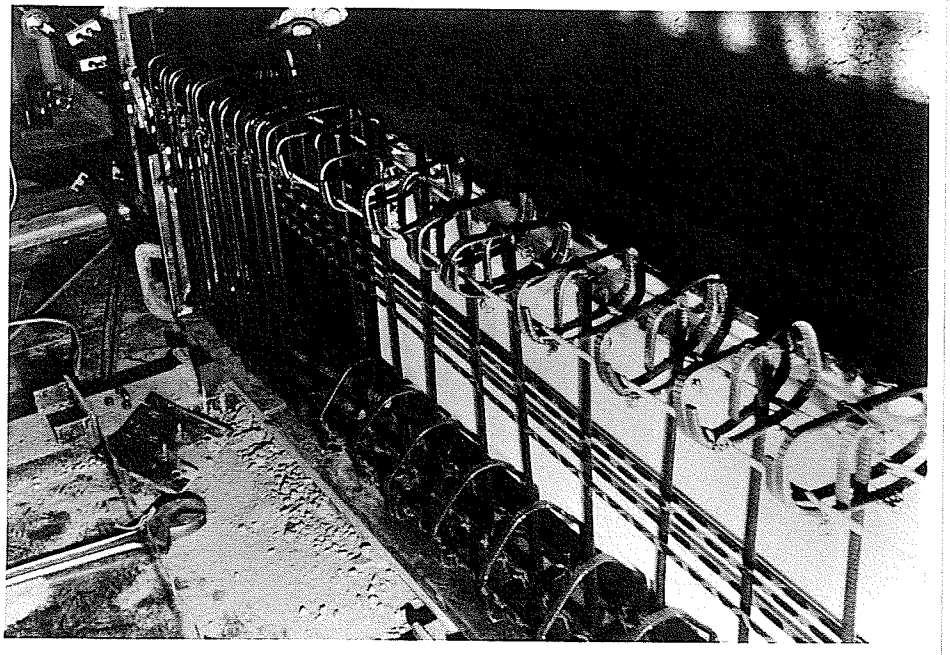

Figure 3.15 Hold-up system and the draped tendons

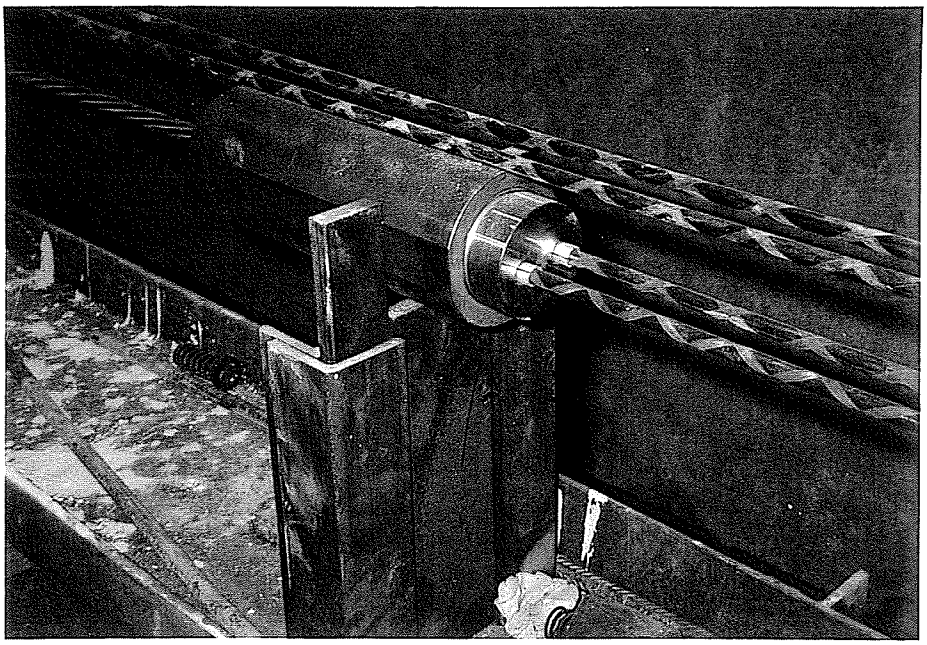

Figure 3.16 Yoke used to prevent couplers of draped Leadline bars from rotating during jacking

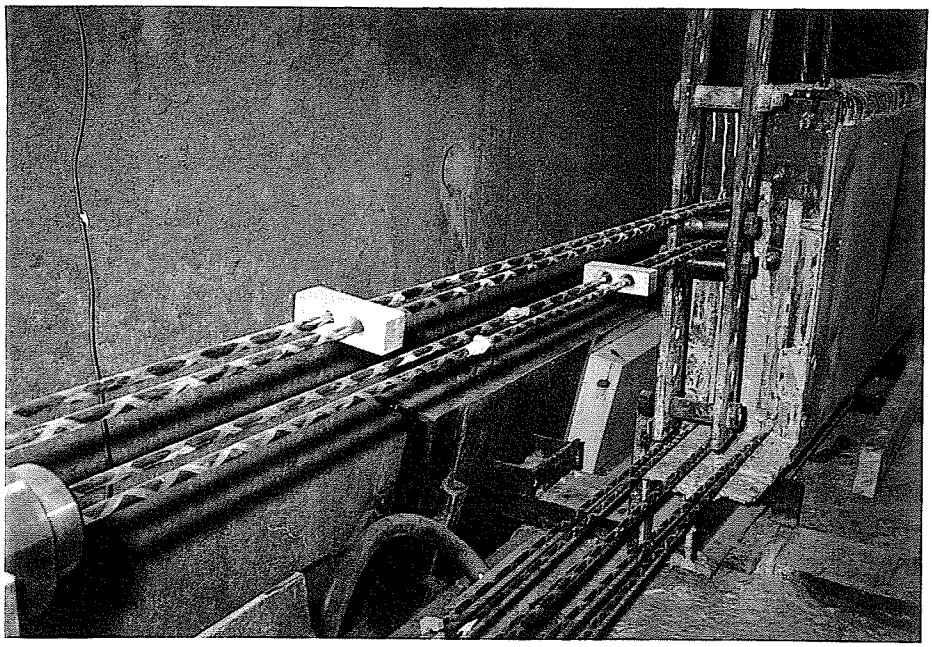

Figure 3.17 Aluminum spacers used to reduce the spacing between each two draped Leadline bars

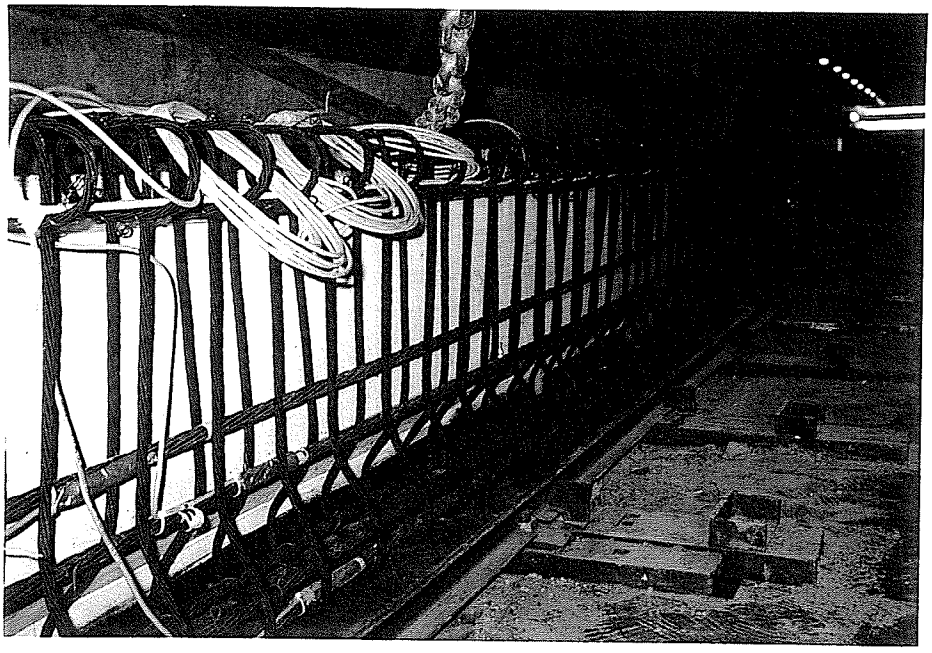

Figure 3.18 Reinforcing cage after assembling. Only the straight tendons are jacked.

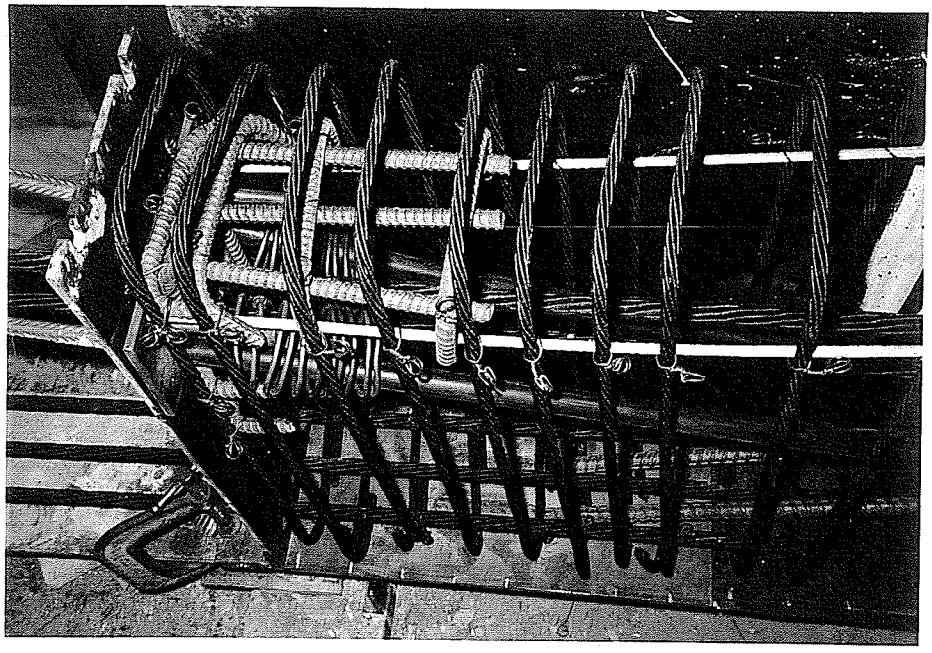

Figure 3.19 Reinforcement at end block

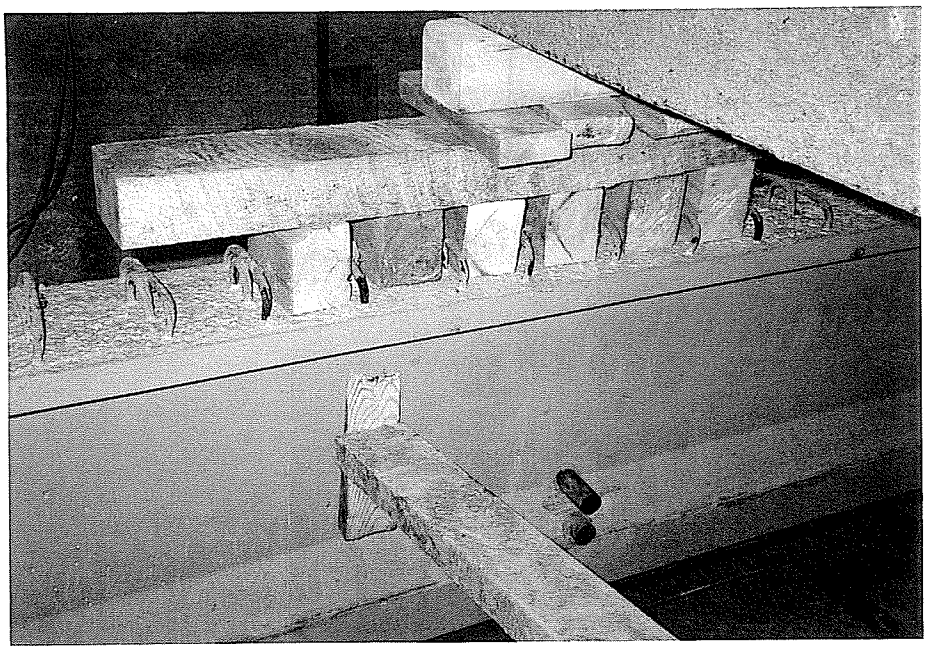

Figure 3.20 Supporting the girder downward at pin locations before releasing the form

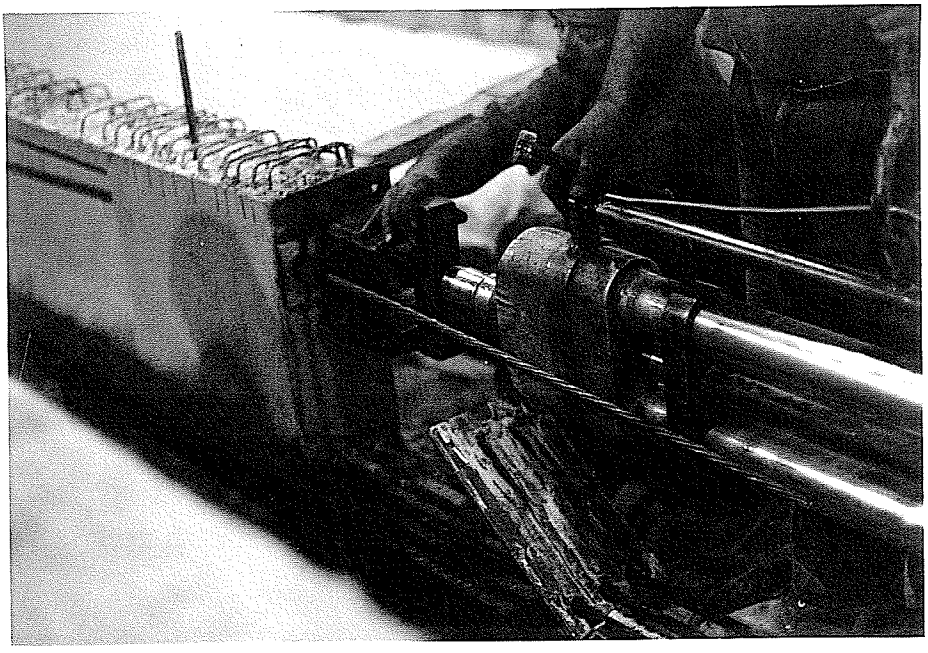

Figure 3.21 External post-tensioning of the I-girder

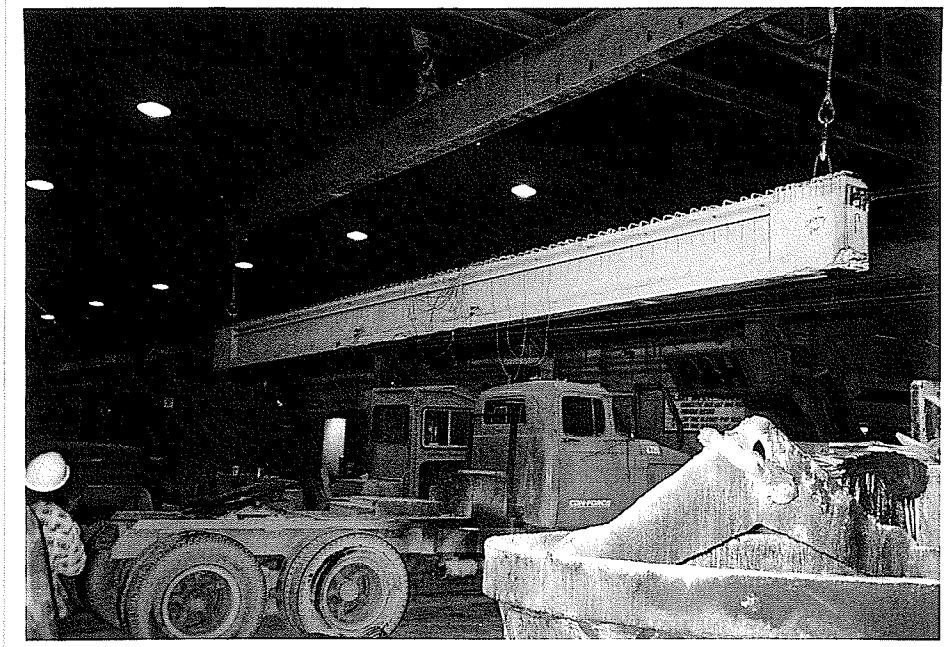

(a)

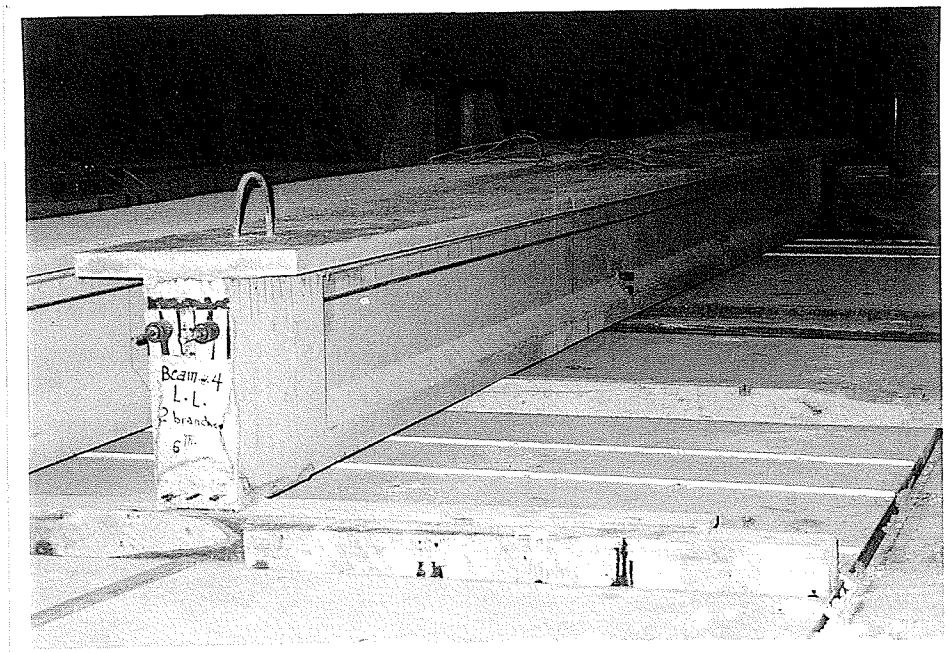

(b)

Figure 3.22 Test beam before and after casting top slab

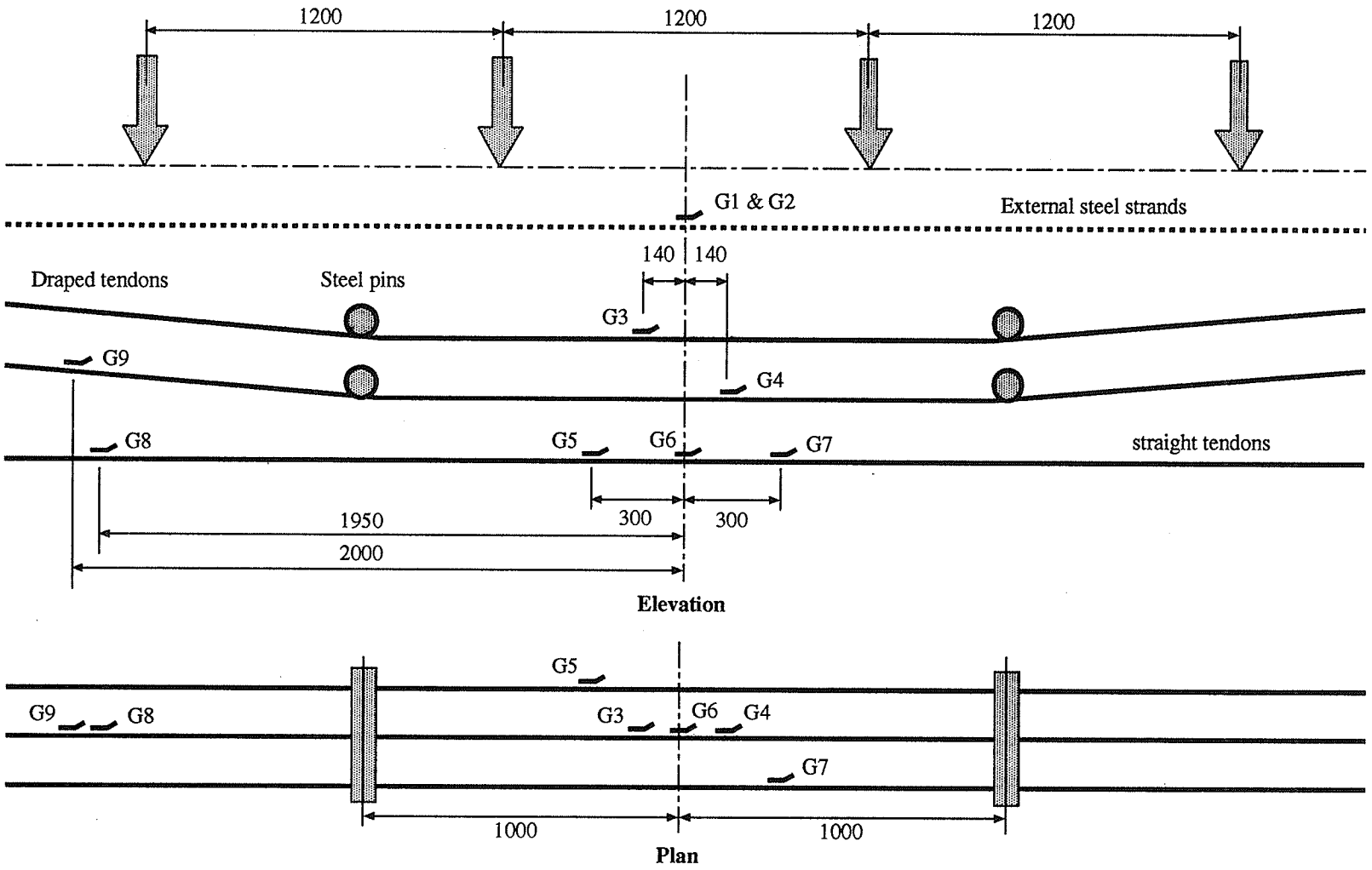

Figure 3.23 Layout of strain gauges locations along the prestressing tendons

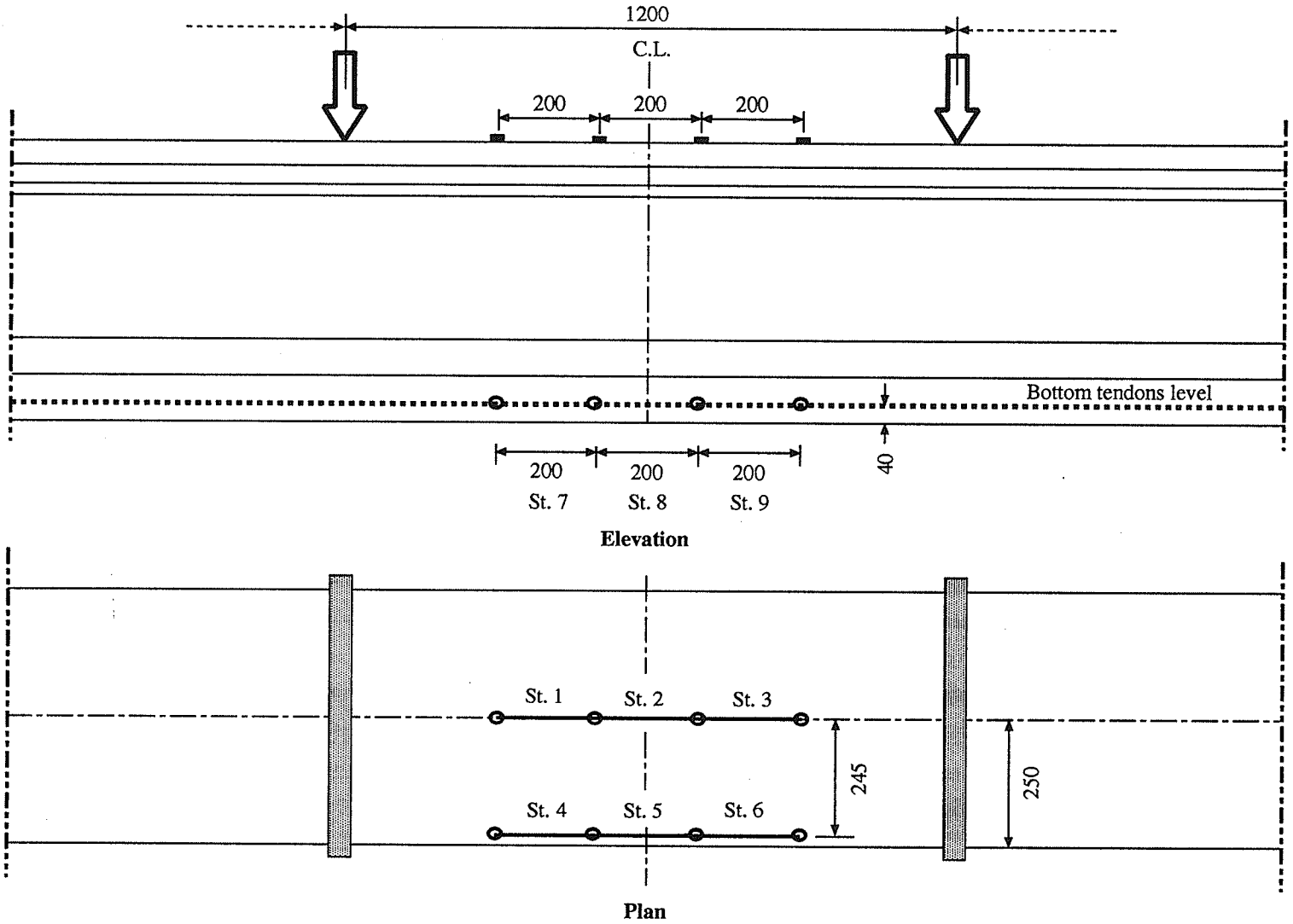

Figure 3.24 Layout of demec stations at the maximum moment zone

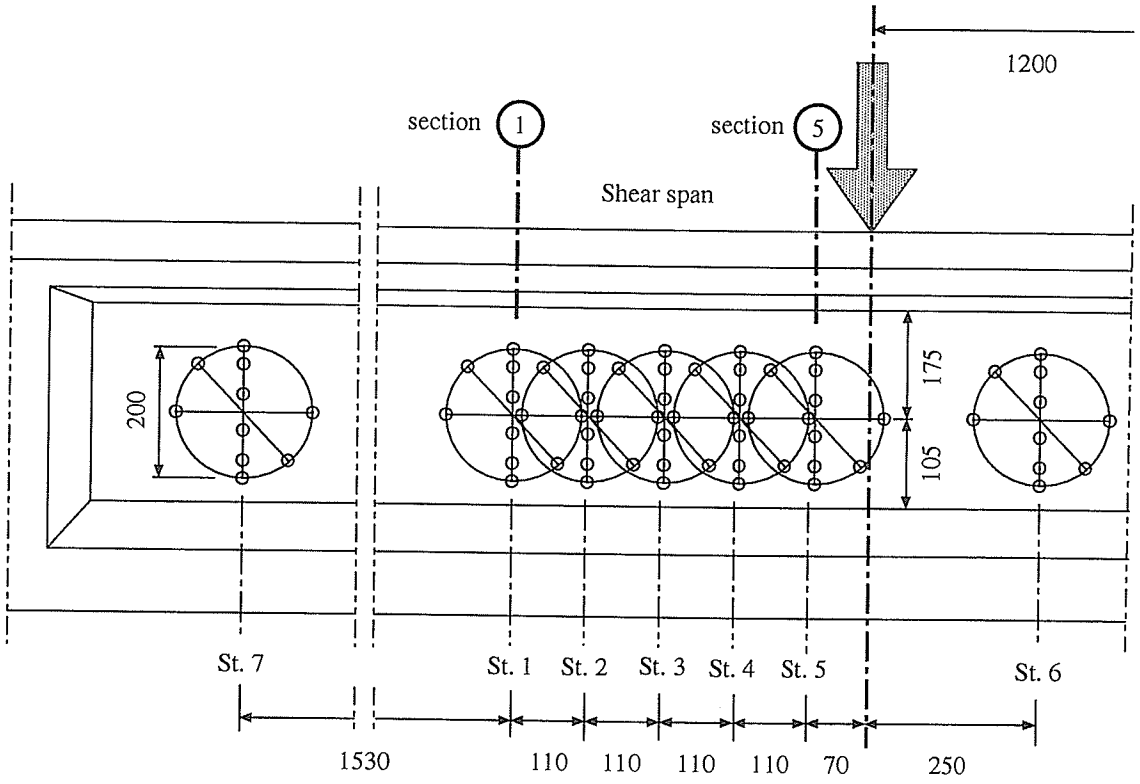

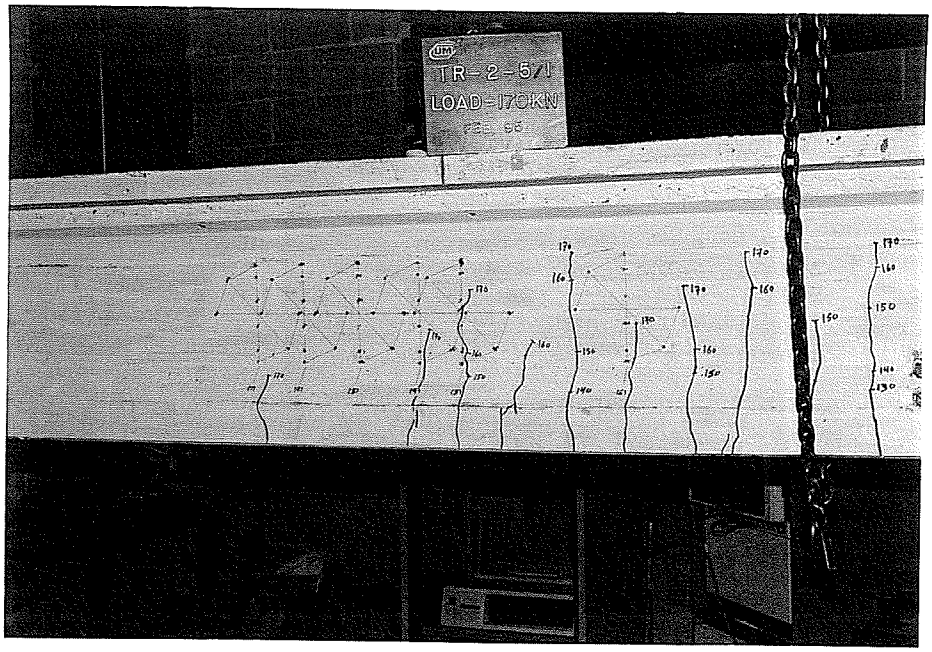

Figure 3.25 Lay out of " Rosette" demec stations at maximum shear stresses zone

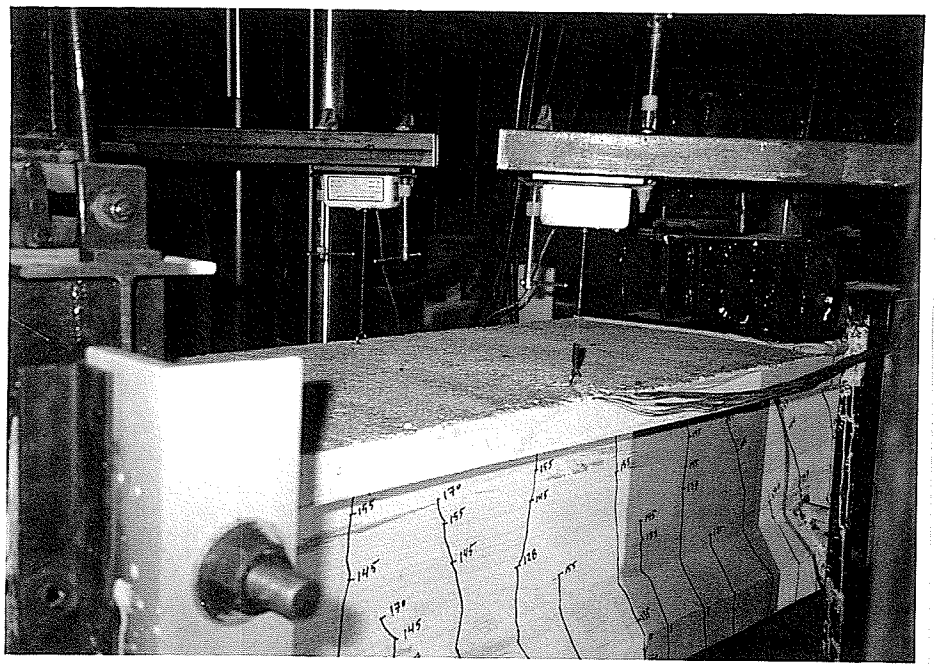

Figure 3.26 Deflection measurements using LMTs system

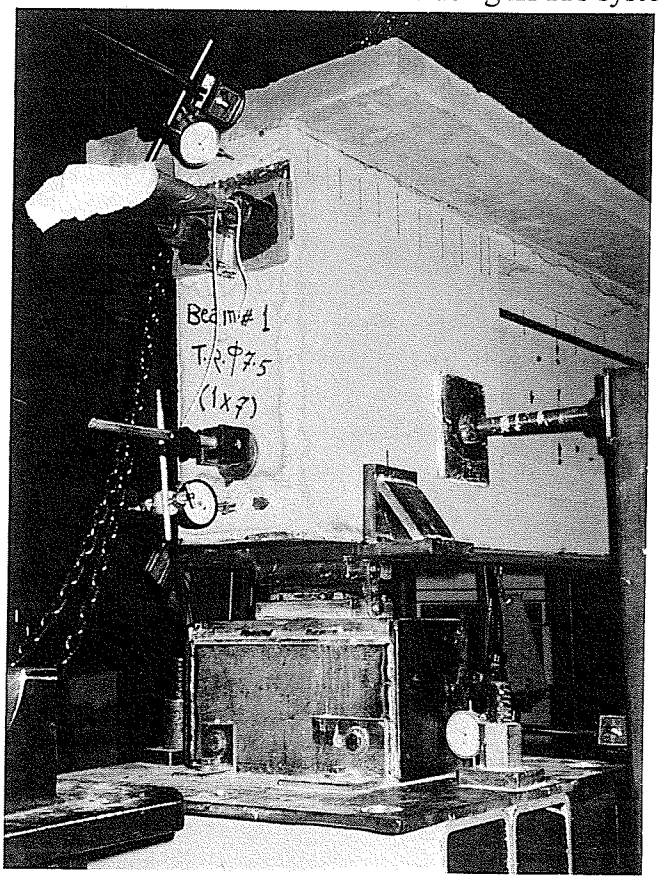

Figure 3.27 Arrangement of dial gauges at ends of the beam

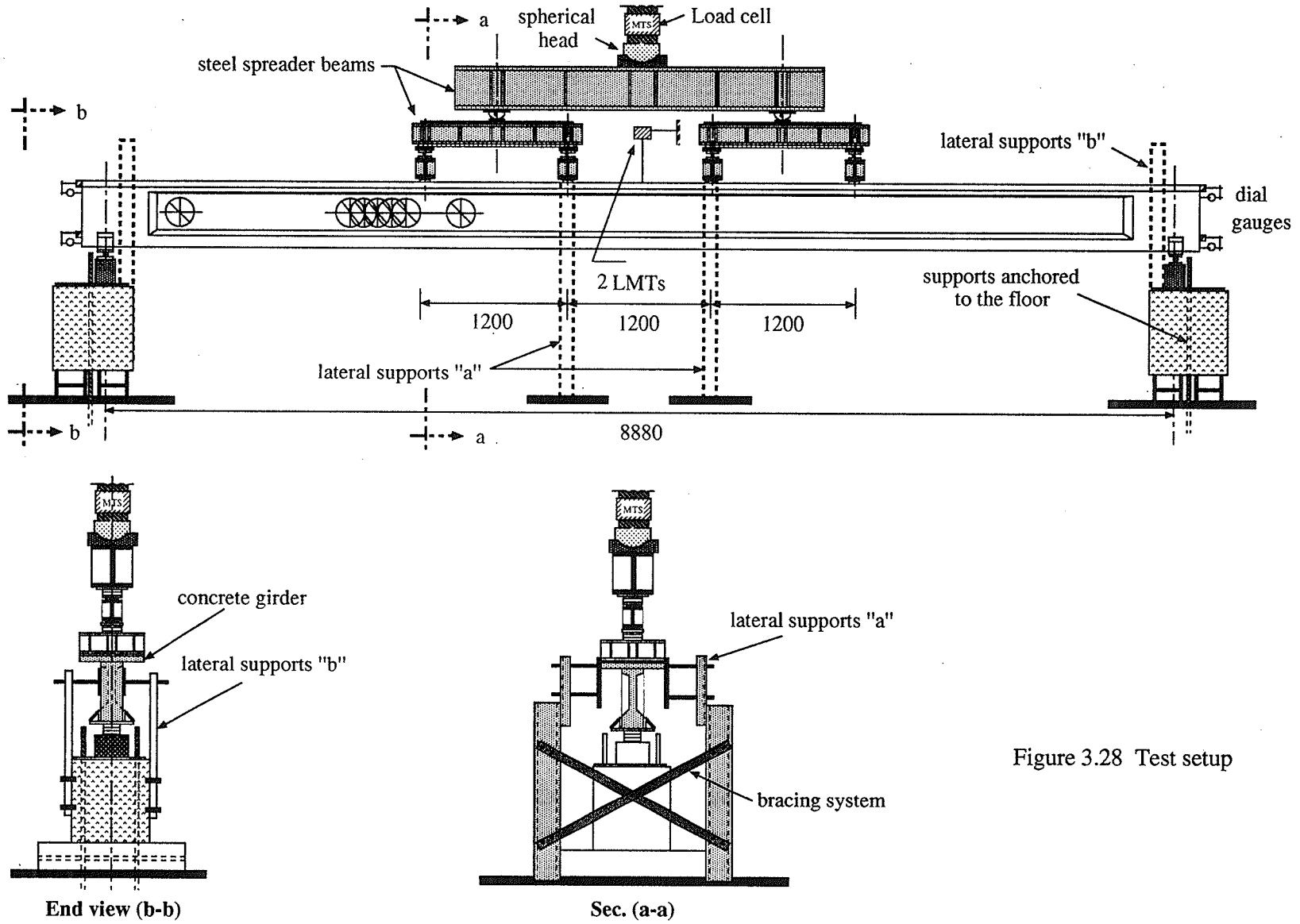

Figure 3.28 Test setup

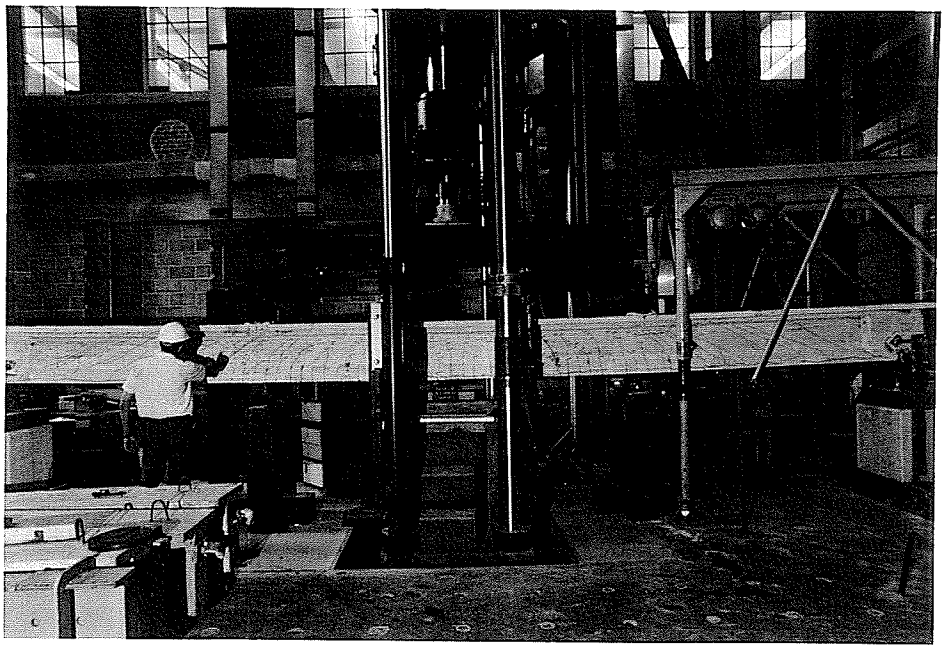

Figure 3.28 (cont.) General view of test setup

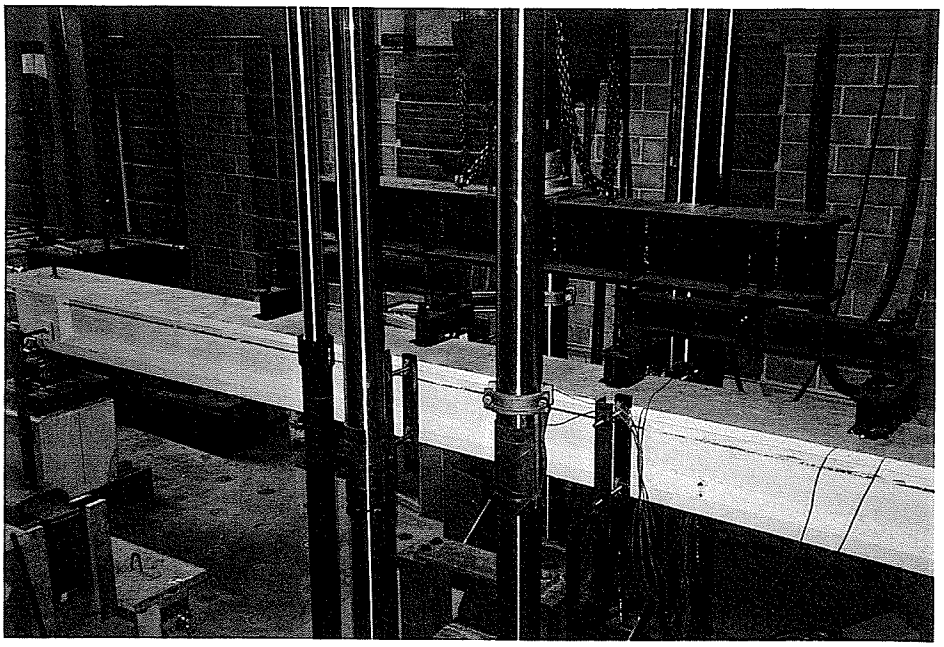

Figure 3.29 Spreader beams system used to apply the load

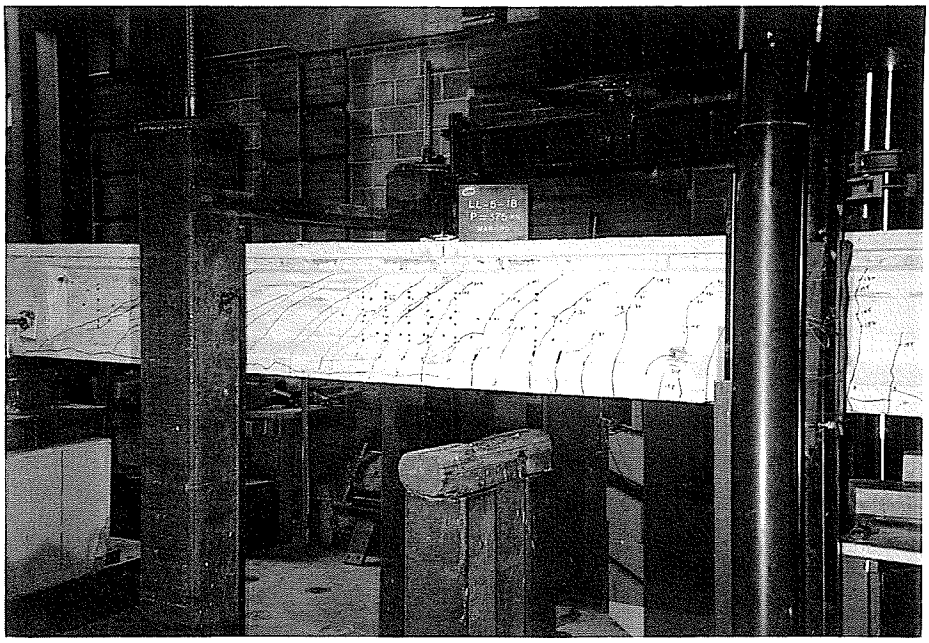

Figure 3.30 Steel frame jacked to the floor used to enhance the safety at failure stage

CHAPTER 4

TEST RESULTS

4.1 INTRODUCTION

Test results for all the specimens tested in this experimental program are presented in Appendix A. These results include all measurements taken at the critical sections such as load, deflections, strains in the prestressing reinforcements, concrete strains measurements by mechanical demec gauge, and crack width measured by the magnified microscope. The results also include measurements taken at the critical sections in shear such as strains measured in three different directions using mechanical dial gauge.

In this chapter, all the measured data for beam prestressed by Tokyo Rope and reinforced by 7.5 mm - 7 wire stirrups, TR-1-7.5/7, is all given in details in the same sequence presented in Appendix A. For other beams, tables and graphs are arranged similarly to the beam shown in this chapter. A comparison between the test results in terms of flexural cracking load, shear cracking load, ultimate load, and mode of failure are summarized in Table 4.1. The observed behaviour of all the tested beams is also discussed in this chapter.

4.2 SAMPLE DATA - BEAM TR-1-7.5/7

The measured strains of the tendons from jacking up to testing using electrical strain gauges with the layout shown in Figure 3.23, are presented in Table 4.2 including the total losses. The load - mid span deflection response based on the load cell and LMTs readings is shown in Figure 4.1. The load - concrete strain behaviour at top surface of the beam within the constant moment zone based on demec gauge readings at demec stations 1 to 6, shown

in Figure 3.24, are presented in Figure 4.2, the average of the readings at these stations versus the load is shown in Figure 4.3. The load - concrete strain behaviour at the lowest level of prestressing tendons within the constant moment zone based on demec gauge readings at stations 7, 8, and 9, shown in Figure 3.24, are shown in Figure 4.4. The load - strain behaviour of the prestressing tendons during the test based on the readings of electrical strain gauges 5, 6 and 7, shown in Figure 3.23 and located at the same level of demec stations 7,8, and 9 within the constant moment zone are shown in Figure 4.5. The total strains including the effective pre-strains and the induced strains during testing for gauges 3 to 7 are shown in Figure 4.6. The load - crack width behaviour within the constant moment zone based on microscope readings is shown in Figure 4.7.

At the location where maximum shear stresses were induced , the strains in the horizontal, vertical, and diagonal directions were measured on the web at five demec stations, shown in Figure 3.25. Figure 4.8 shows the variation of strains in the vertical direction with respect to the load at the five demec stations based on gauge length of 200 mm. Within the vertical measurements of the 200 mm, another three vertical measurements were taken using 50.8 mm demec gauge. The strains from the one that showed maximum values were plotted versus the load at each station as shown in Figure 4.9. Figures 4.10 and 4.11 show the variation of strains in the horizontal and diagonal directions at the five demec stations respectively using 200 mm gauge length.

4.3 OBSERVED BEHAVIOUR

This section highlights the most important aspects observed during the testing of the

specimens. The effect of the spreader beams was taken in account by adding the self weight of 9 kN and the corresponding deflection of about 1 mm to the observed load - deflection response and the total response is shown in Figure 4.1. Figure 4.12 shows the flexural crack patterns of three beams prestressed by three different types of tendons, Tokyo Rope strands, TR-2-5/1, Leadline bars, LL-4-2B, and steel strands, ST-6-C. Figure 4.13 shows the diagonal crack patterns of the six tested beams at failure.

Since the beams were tested under deflection control, a sudden increase of about 5 kN in the load was observed in all the tests when the temporarily external post-tensioned steel was released after applying 12 kN to the girders including weight of spreader beams.

4.3.1 Beam TR-1-7.5/7

a. Flexural cracks initiated at an applied load of about 130 kN within the centre span.

b. At a load of about 154 kN, eleven major flexural cracks were initiated within the constant moment zone.

c. Flexural shear cracks initiated at the pins locations at about 154 kN.

d. The first flexural shear crack initiated within the maximum shear span immediately out side the loading zone at about 172 kN.

e. At a load of about 224 kN, six major flexural shear cracks and another four minor ones were initiated within the measurement zone at the shear span.

f. At loads 179 kN, 224 kN, and 239 kN, additional three minor flexural cracks were observed within the constant moment zone.

g. At loads 239 kN, 259 kN, and 269 kN, another four flexural shear cracks with flatter slope

initiated at the maximum shear span out side the measurement zone extending to about one meter from the support.

h. Propagation of cracks through the web was limited beneath the top flange of the I-girder at about 240 kN.

i. Flexural failure occurred suddenly at a load level of 318 kN at the left side pins located 400 mm out side the constant moment zone. The lower draped strand was ruptured at the draping point followed by rupture of the three bottom straight strands and finally rupture of the top draped strand. The top slab reinforcements were sheared and the beam was snapped into two separate pieces. Rupture of the strands was accompanied by horizontal cracks and spalling of the concrete cover along the tendons level within the middle zone. Ten cracks were also observed after failure on the top surface through out the full width of the flange. Failure mode is shown in Figure 14 (a).

4.3.2 Beam TR-2-5/1

a. Flexural cracks at the centre span initiated at an approximate applied load of 130 kN.

b. At a load of about 159 kN, eleven major flexural cracks were initiated within the constant moment zone.

c. Flexural shear cracks initiated at one of the pins at about 139 kN and at the other pins at about 149 kN.

d. The first flexural shear crack initiated within the maximum shear span just outside the loading zone at a load of 174 kN.

e. At a load of about 249 kN, nine major flexural shear cracks and about six minor ones were

already initiated within the measurement zone at the maximum shear span.

f. At loads 194 kN, 249 kN, and 299 kN, six minor flexural cracks were observed within the constant moment zone.

g. At loads 270 kN to 290 kN another three flexural shear cracks with flatter slope were initiated within the maximum shear span outside the measurement zone extending to about one meter from the support.

h. Propagation of cracks through the web was limited up to a load of 250 kN beneath the top flange of the I-girder.

i. Flexural failure took place suddenly at 315 kN at one of the pins located 400 mm outside the constant moment zone. the lower draped strand was ruptured at the draping point followed by rupture of the three bottom straight strands and finally rupture of the upper draped strand. The top slab reinforcements were sheared and the beam snapped into two separate pieces as shown in Figure 4.14 (b). Rupture of the strands was accompanied by horizontal cracks and spalling of the concrete cover along the tendons level within the middle part. Thirteen cracks were also observed after failure on the top surface of the beam throughout the full width of the flange.

4.3.3 Beam TR-3-5/7

a. Flexural cracks at the centre span initiated at an applied load of about 127 kN.

b. At a load of about 159 kN, twelve major flexural cracks were already initiated within the constant moment zone.

c. Flexural shear cracks initiated at one of the pins at the right pins at about 125 kN and were

already developed to half depth of the web at left pins at about 159 kN.

d. The first flexural shear crack initiated at the maximum shear span just out side the loading zone at about 166 kN.

e. Because of the nature of the brittle failure that could happen, demec readings and cracks observation were stopped at load of 210 kN.

f. At load 210 kN, five flexural shear cracks were developed within the measurement zone at the maximum shear span. After the end of the test, three more cracks were observed within the same zone.

g. Flexural failure took place at 303 kN at the middle zone of the beam. The three bottom straight cables were all ruptured, two of them failed within the constant moment zone about 100 mm from the loading point and the third one failed at 300 mm out side the constant moment zone from the right side as shown in Figure 4.14 (c). The test was stopped at this stage to keep the beam as one unit. Rupture of the bottom straight strands was accompanied by horizontal cracks and spalling of the concrete cover along the tendons level within the middle zone. About fourteen cracks were observed after failure on the top surface of the beam throughout the full width of the flange.

h. After the end of the test, three additional minor flexural cracks were observed within the constant moment zone and another three flexural shear cracks were observed at the maximum shear span outside measurement zone and extending to about one meter from the supports.

4.3.4 Beam LL-4-2B

a. Flexural cracks at the centre span initiated at an applied load of about 138 kN.

b. At a load of about 159 kN, ten major flexural cracks were initiated within the constant moment zone.

c. Flexural shear cracks initiated at one of the pins at about 148 kN.

d. The first flexural shear crack initiated at the maximum shear span just outside the loading zone at about 183 kN.

e. At load of about 239 kN, four major flexural shear cracks were already initiated within the measurement zone at the maximum shear span.

f. At loads of about 260 kN, 280 kN, and 330 kN, three major flexural shear cracks were observed out side the measurement zone, extending to about one meter from the supports.

g. At load of about 330 kN, six web shear cracks with flatter slope initiated in the web close to the support.

h. Propagation of cracks through the web was limited at about 280 kN within the top flange of the I-girders.

i. At load of 359 kN, spalling of concrete cover was observed at the bend of the stirrup located at the rosette demec station number 1, Figure 3.25, at the maximum shear span from the web to the bottom flange and a dramatic failure occurred suddenly due to shear failure at the same zone. The beam was snapped into two pieces at that section. one piece of the beam, about 2.6 meters was lifted up about two meters above the beam level, snapped to another two pieces, and fell down as shown in Figure 4.14 (d). Large part of the concrete of the web was crushed and about eleven stirrups were ruptured at this zone. Both the straight and draped prestressing Leadline rods were all ruptured. Figure 4.14 (d) also shows the beam after assembling different parts.

4.3.5 Beam LL-5-1B

a. Flexural cracks at the centre span initiated at an applied load level of about 138 kN.

b. At load of 164 kN, eleven major flexural cracks and a minor one were initiated within the constant moment zone and one more crack initiated later at 179 kN.

c. Flexural shear cracks initiated at one of the pin location at 146 kN and at 164 kN at the other pin.

d. The first flexural shear crack initiated within the maximum shear span just out side the loading zone at about 194 kN.

e. Because of the nature of the brittle failure of the previous beam, demec readings and crack observation were not recorded after a load level of 210 kN. Extensive bracing system including steel screen was added for safety reasons.

f. At load of 210 kN, four flexural shear cracks were developed within the measurement zone at the maximum shear span. After the end of the test, two major cracks and another two minor ones, initiated at higher load level were found within the same zone.

g. After the end of the test, five major flexural shear cracks were found out side the measurement zone extending to about one meter from the support followed by five web shear cracks with flatter slope extending to the support.

h. Flexural failure took place at 381 kN at the constant moment zone which is significantly higher than the beam with double legged stirrups. The bottom straight tendons were ruptured and the load dropped to about 140 kN. At this stage the test was stopped to keep the beam as one unit since the draped tendons were not ruptured. Rupture of the bottoms straight tendons was accompanied by horizontal crack along the tendons level throughout the

full span of the beam. No cracks were observed on the top surface of the beam after failure. Failure mode is shown in Figure 4.14 (e).

4.3.6 Beam ST-6-C

a. Flexural cracks at the centre span initiated at an applied load of about 125 kN.

b. At a load of 154 kN, eleven major flexural cracks within the constant moment zone were already initiated.

c. Flexural shear cracks initiated at one of the pin locations at about 140 kN from both ends.

d. The first flexural shear crack initiated at the maximum shear span just out side the loading zone at about 160 kN.

e. At load of about 204 kN, five major flexural shear cracks and two minor ones were already initiated within the measurement zone at the maximum shear span.

f. At loads of 200 kN and 230 kN, two minor flexural cracks initiated within the constant moment zone.

g. At 229 kN, a major flexural shear crack initiated just outside the measurement zone in the maximum shear span.

h. Yielding of the bottom prestressing steel strands was observed at 230 kN.

i. Once the beam yielded at the middle span, propagation and opening of flexural shear cracks at the maximum shear span was limited.

j. Flexural failure took place at 261 kN within the constant moment zone by crushing of the concrete at the top slab to the right of the loading point, immediately followed by crushing the upper part of the web at the same zone as shown in Figure 4.15 (f). No horizontal cracks

were observed at the level of prestressing steel strands. Four cracks were observed in the top flange through out the full width of the slab after the end of the test.

Beam	Flexural cracking load (kN)	Shear cracking load (kN)	Ultimate load (kN)	Mode of failure
TR-1-7.5/7	130	172	318	Rupture of the bottom draped strand at pin location.
TR-2-5/1	130	174	315	Rupture of the bottom draped strand at pin location.
TR-3-5/7	127	163	303	Rupture of the straight strands within the middle portion.
LL-4-2B	138	183	359	Premature failure after spalling of concrete cover due to stretching of stirrups at maximum shear stresses zone.
LL-5-1B	138	194	381	Rupture of the straight rods within the middle portion.
ST-6-C	125	160	261	Yielding of steel strands followed by crushing of concrete at top surface.

Table 4.1 Summary of flexural and shear cracking loads, ultimate load, and modes of failure of test beams.

Beam TR-1-7.5/7

Time (days)	Case	Gauge number								
		1	2	3	4	5	6	7	8	9
0	Initial readings before jacking	1195	1432	-509	463	-39	-640	-138	562	24
0	After jacking bottom straight tendons					6575	6754	8003	8508	
1	After jacking draped tendons			6715	8911	6686	6797	8292	8707	7029
1	After casting concrete of the girder			6701	8924	6670	6805	8303	8701	6994
2	Before releasing form			6436	9464	6710	6596	8727	9060	6393
3	After releasing form			6388	9347	6582	6507	8582	8914	6309
3	After releasing draped tendons			6238	9168	6407	6350	8412	8783	6196
3	After applying post-tensioning	4553	4622	6178	9108	6350	6302	8363	8749	6132
3	After releasing bottom straight tendons	4511	4562	5805	8626	5882	5847	7821	8227	5782
127	Right before testing	3988	3989	4910	7618	4880	4962	6917	7218	4919
	Total losses (% Age)	16.8	19.8	24.9	15.3	25.6	24.2	13.3	16.2	30.1

Notes: - See Figure 3.23 for strain gauges layout.
- Strain = (reading at any stage) - (initial reading).
- All readings in micro strain.

Table 4.2 Measured strains of prestressing strands from jacking up to testing using electrical strain gauges

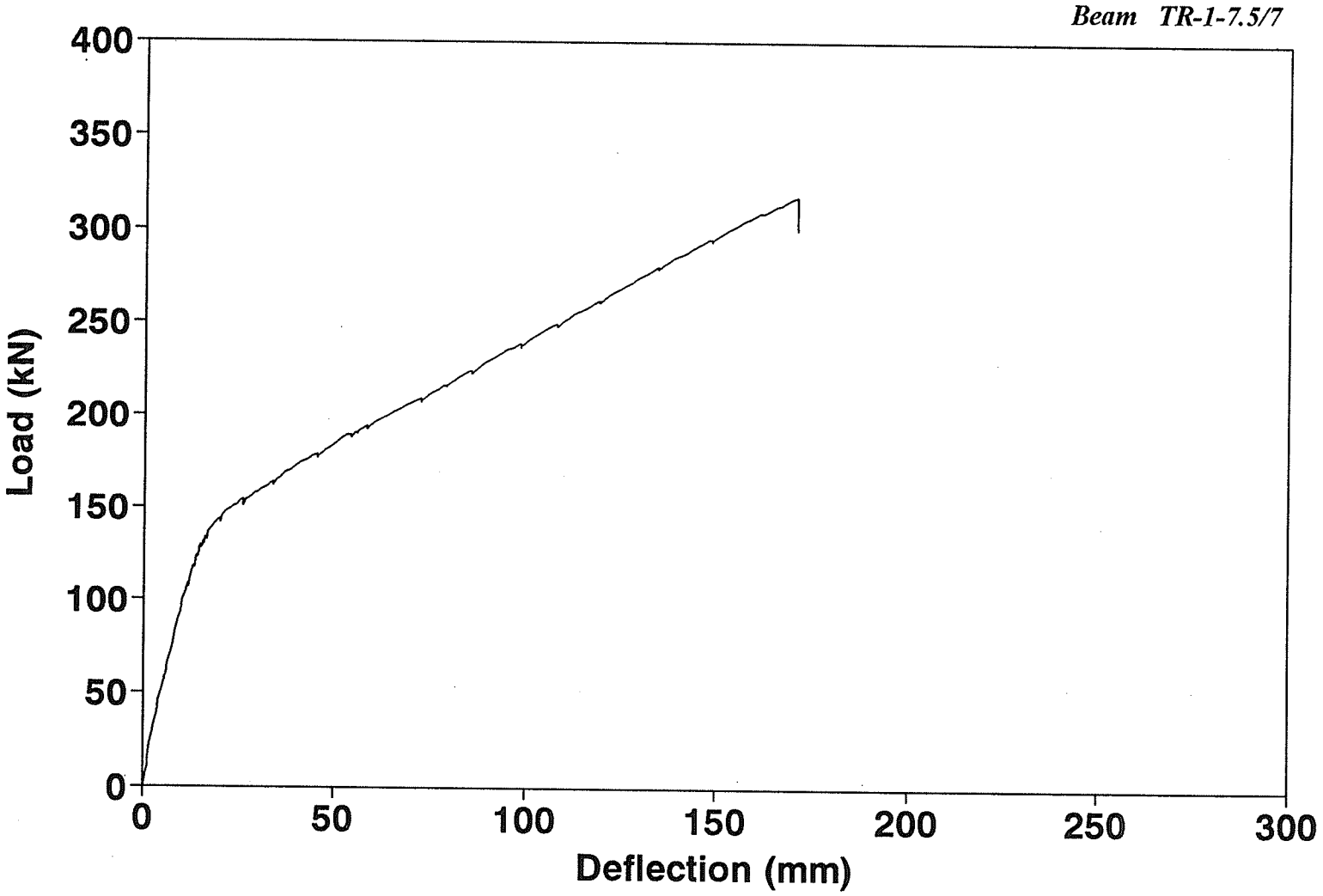

Figure 4.1 Measured Load - deflection at mid span

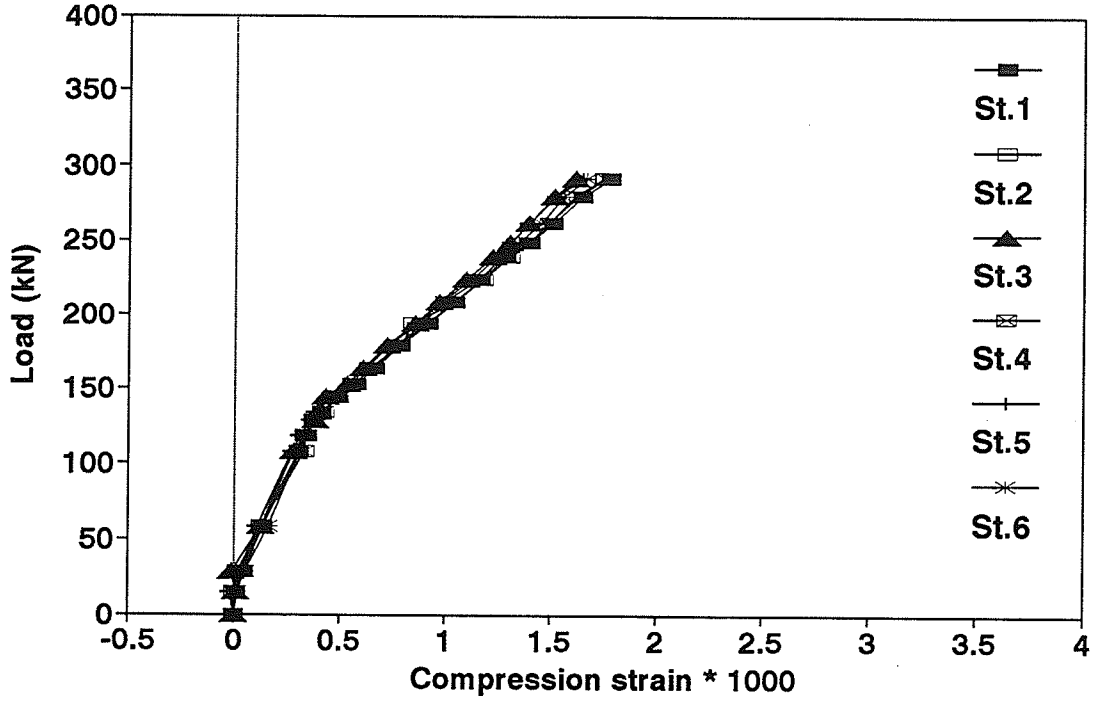

Figure 4.2 Measured concrete strain at top surface at six demec stations

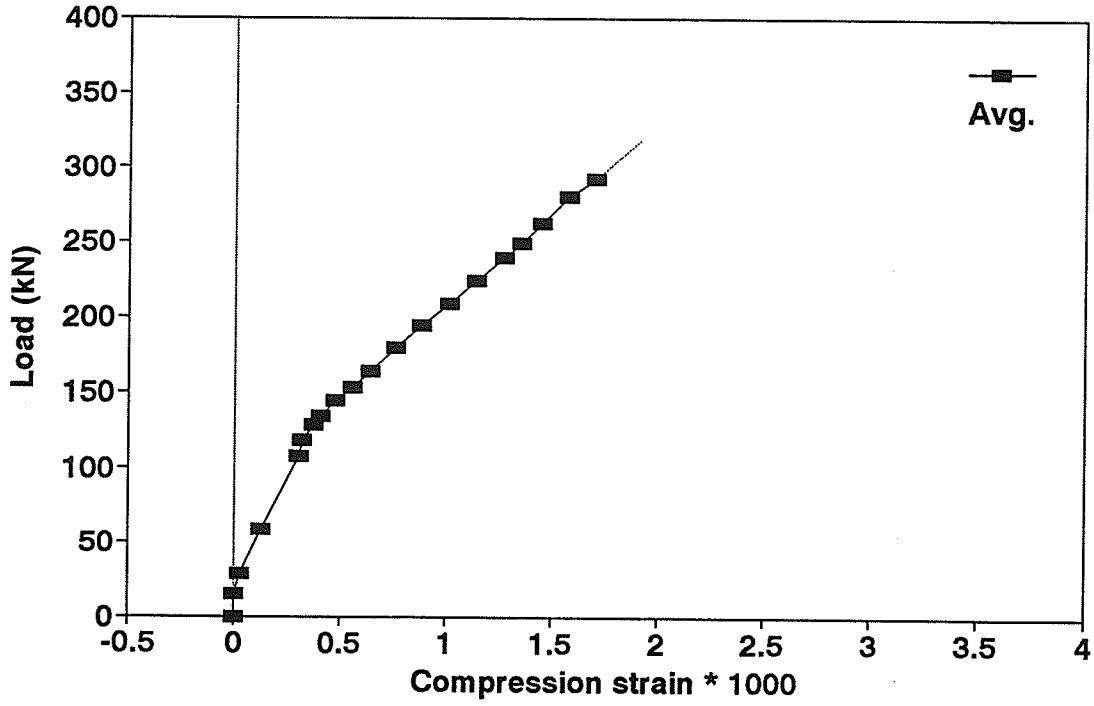

Figure 4.3 Average of measured concrete strain at top surface

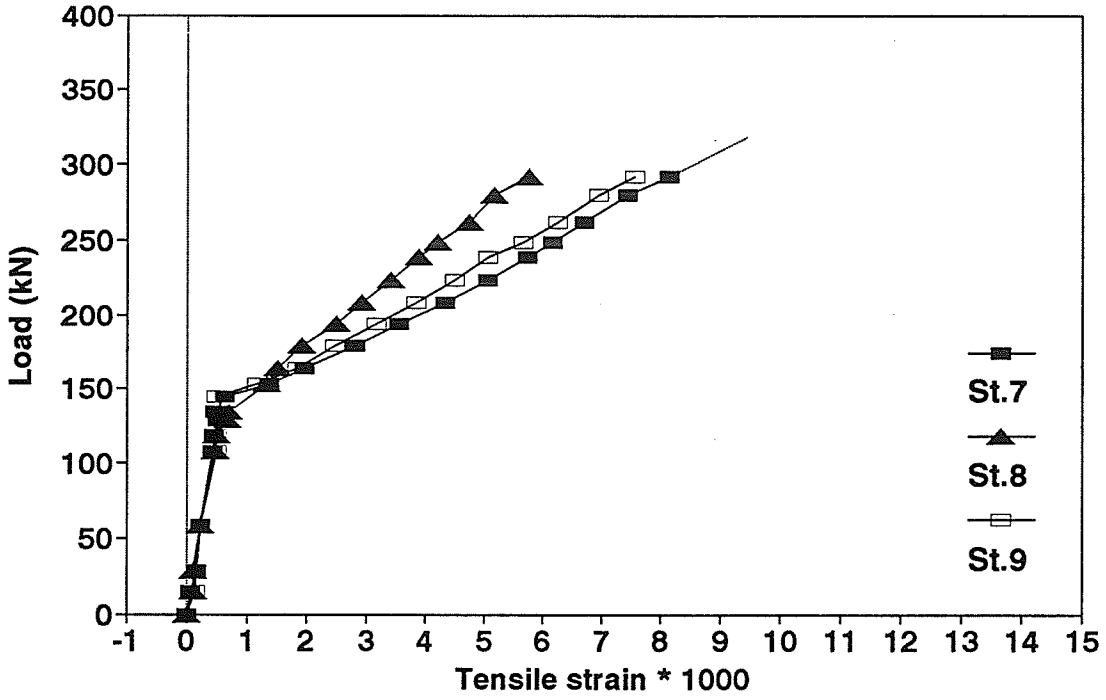

Figure 4.4 Measured strains at bottom strands level at three demec stations

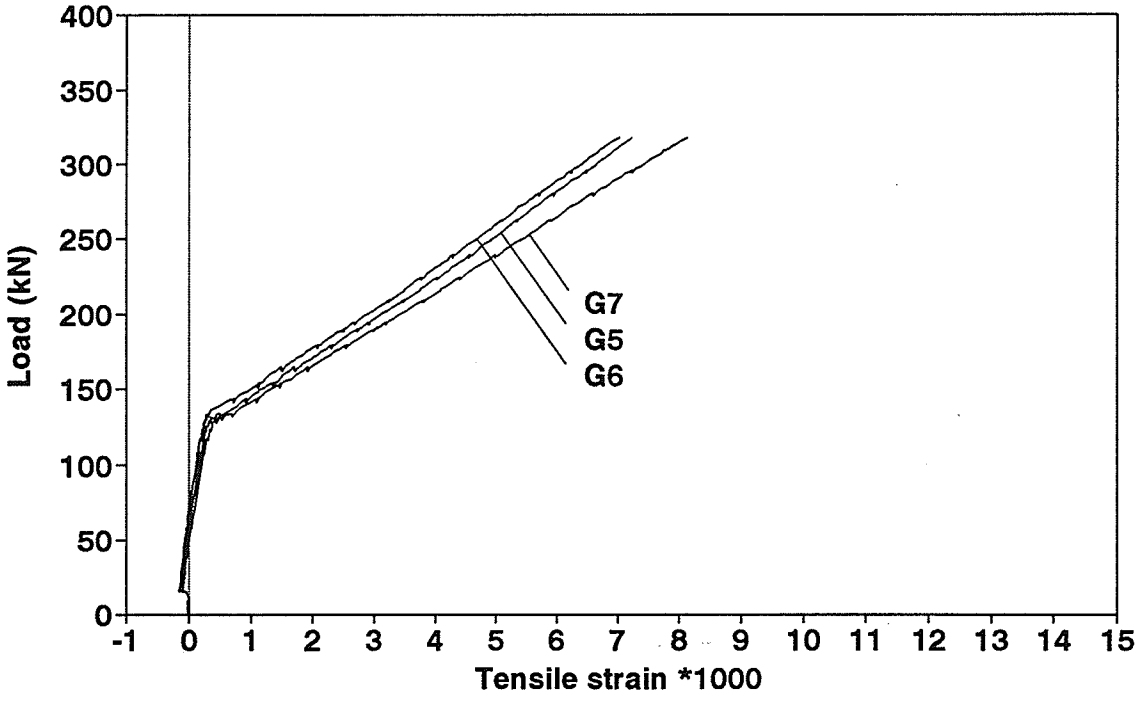

Figure 4.5 Measured strains on the bottom strands during testing using strain gauges

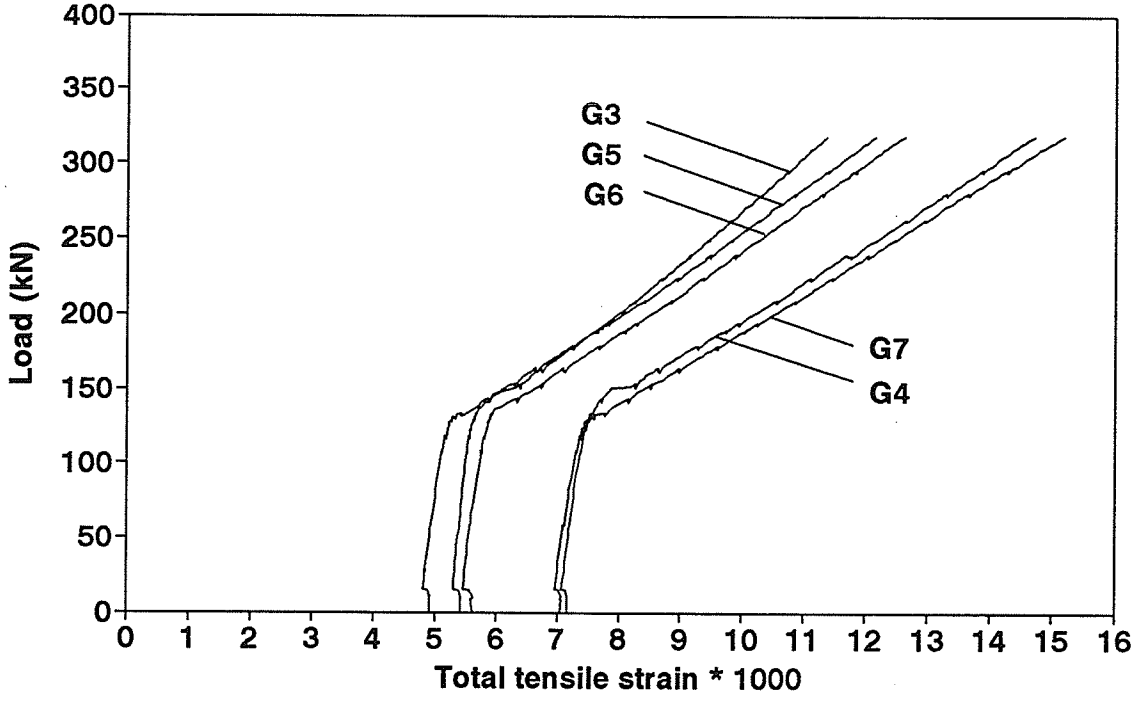

Figure 4.6 Total strains in strands including effective pre-strains and strains during testing

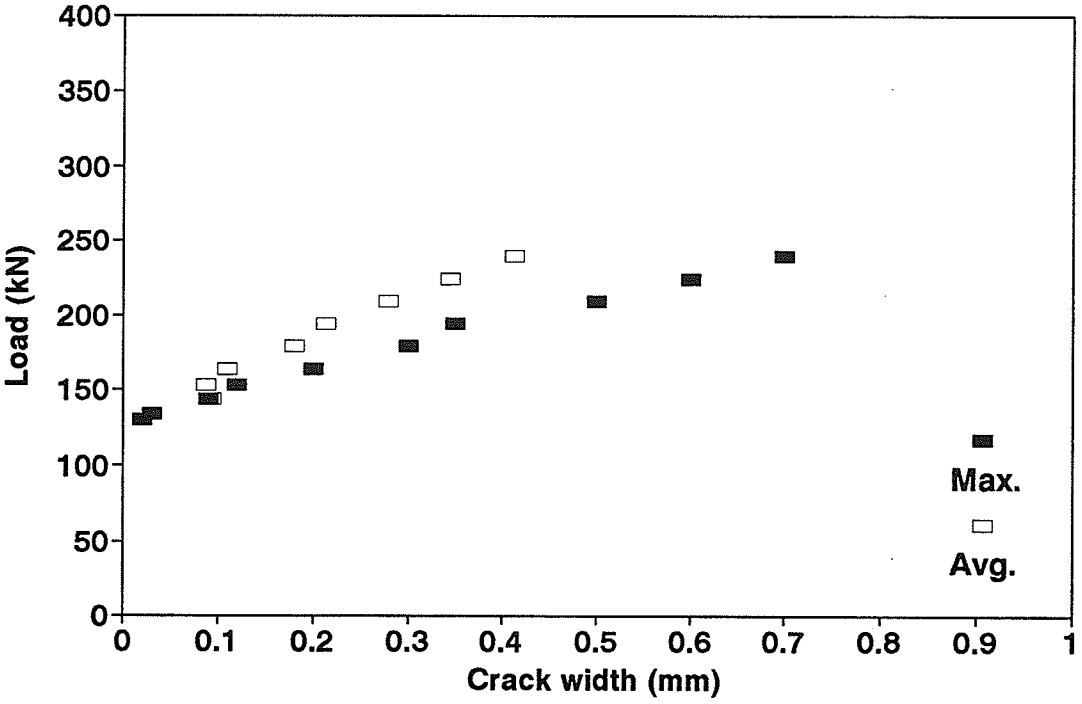

Figure 4.7 Measured crack width at the maximum moment zone based on microscope readings

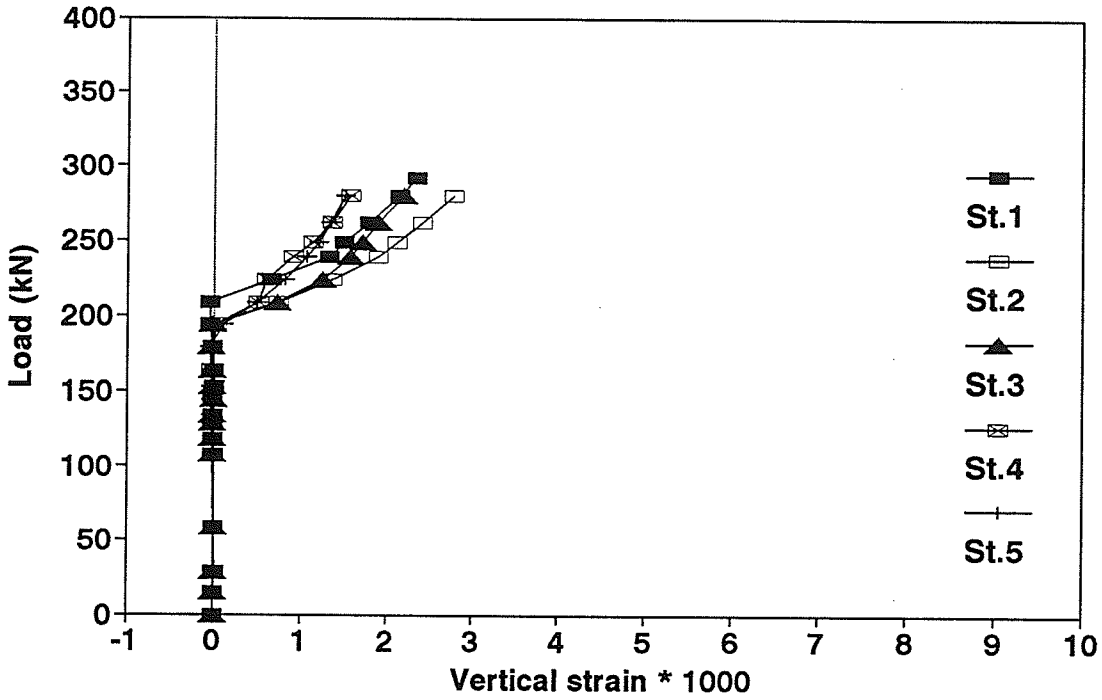

Figure 4.8 Measured strain on concrete surface in direction of stirrups at five demec stations based on 200 mm gauge length

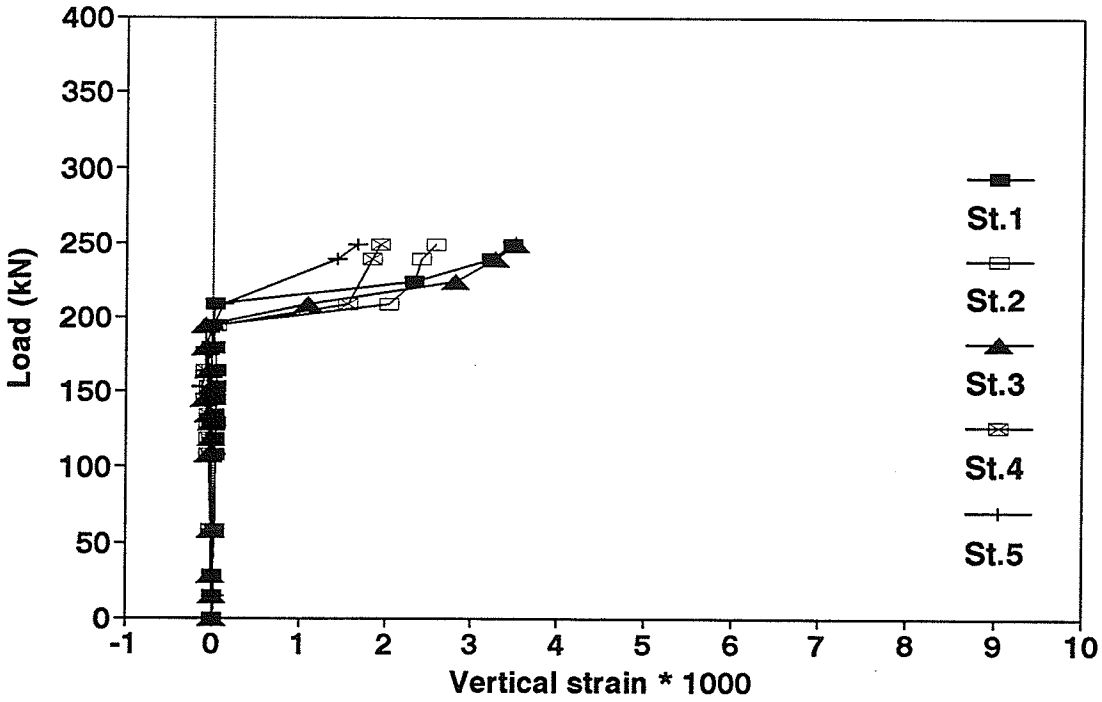

Figure 4.9 Measured strain on concrete surface in direction of stirrups at five demec stations based on 50.8 mm gauge length

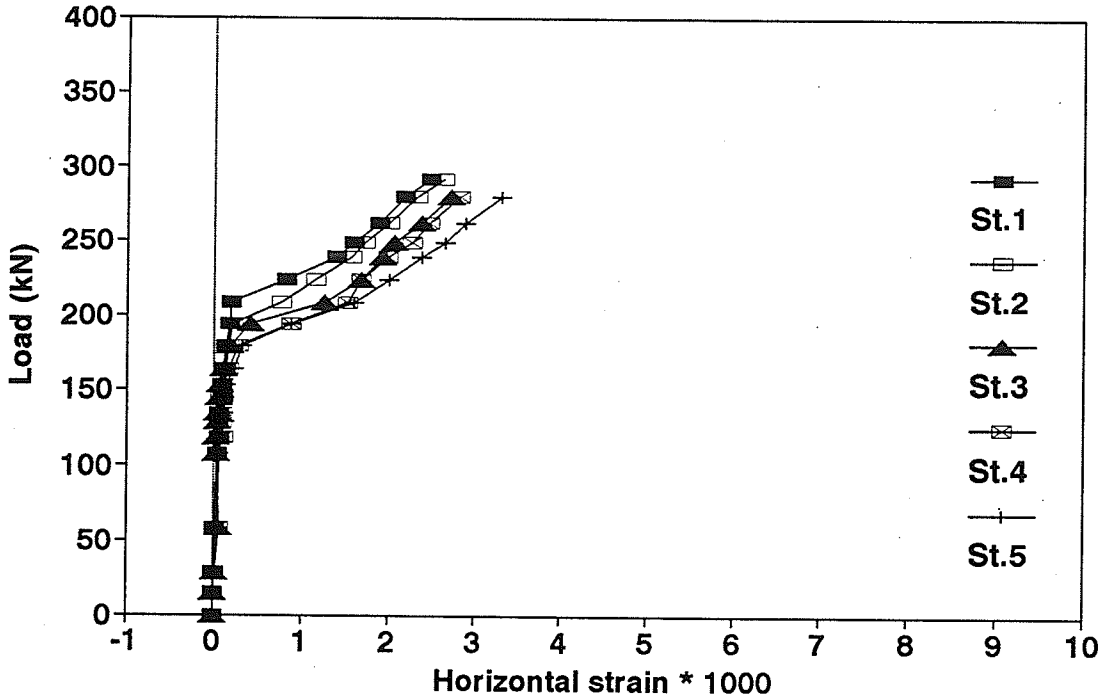

Figure A.10 Measured strain on concrete surface in the horizontal direction at five demec tations based on 200 mm gauge length

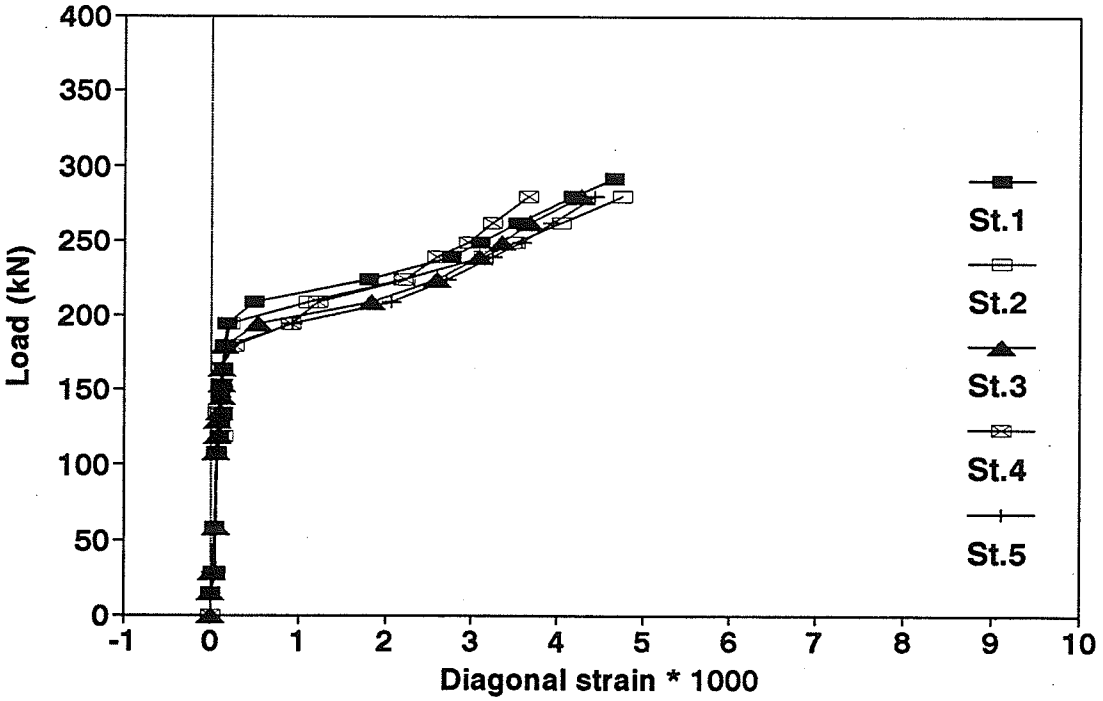

Figure A.11 Measured strain on concrete surface in the diagonal direction at five demec stations based on 200 mm gauge length

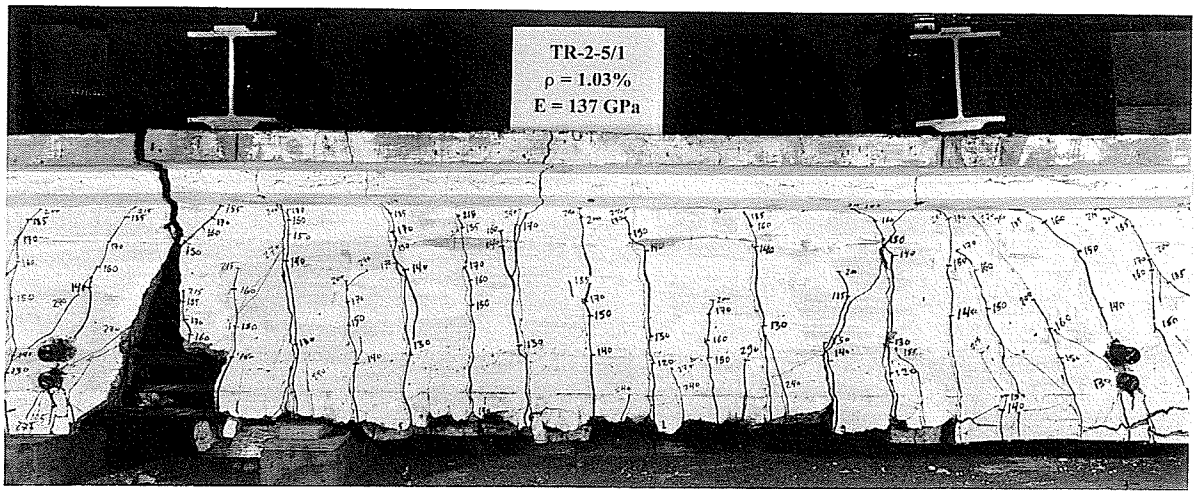

Beam TR-2-5/1

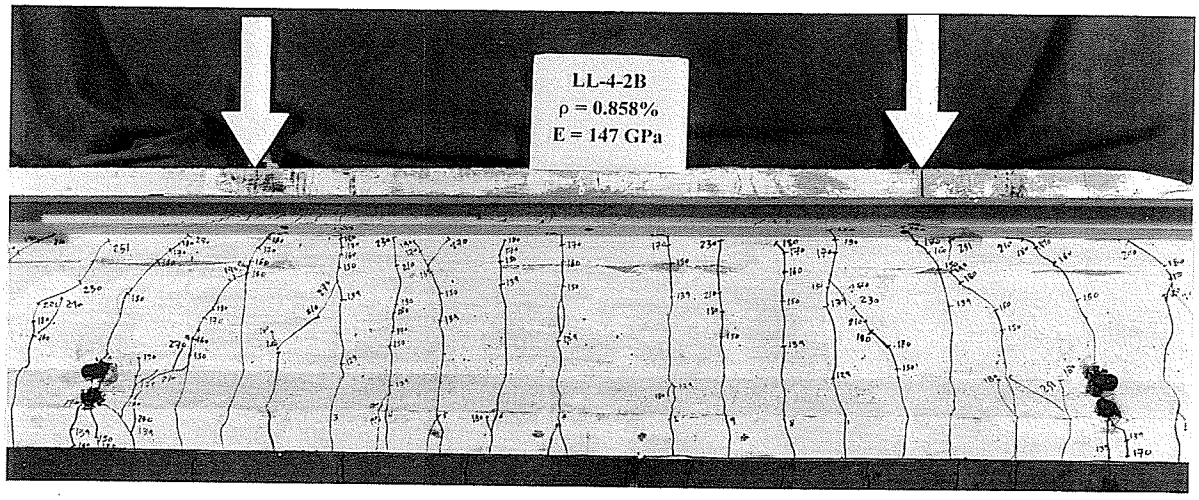

Beam LL-4-2B

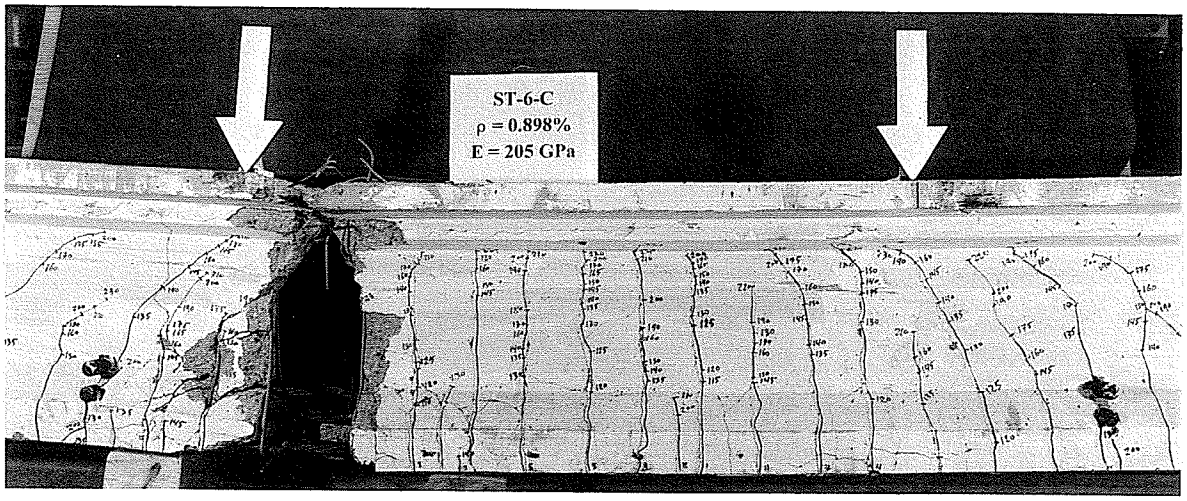

Beam ST-6-C

Figure 4.12 Flexural crack patterns of beams prestressed by Tokyo Rope strands, (top), Leadline bars, (middle), and steel strands, (bottom)

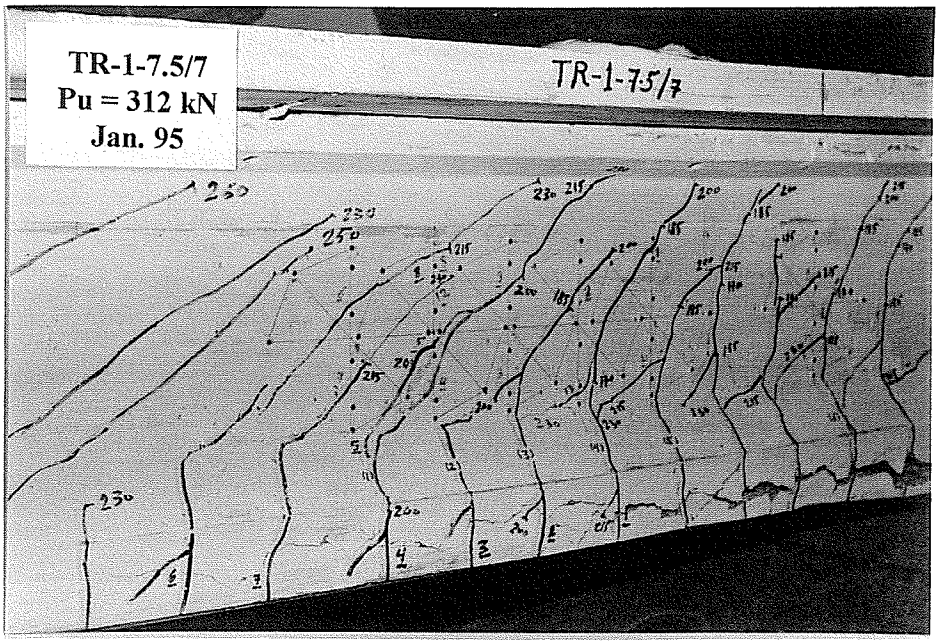

Figure 4.13 (a) Diagonal crack pattern of beam TR-1-7.5/7

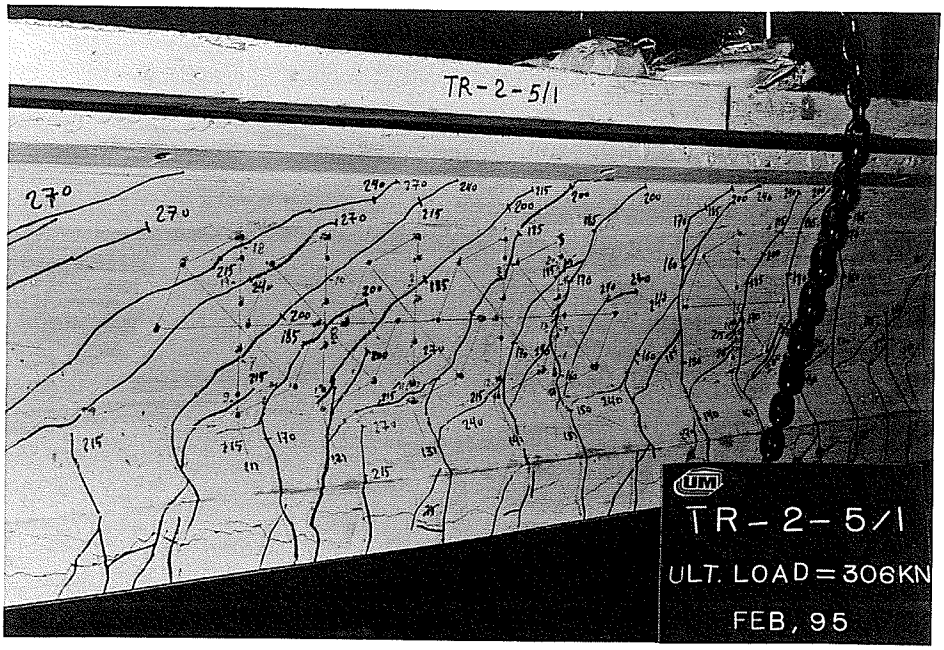

Figure 4.13 (b) Diagonal crack pattern of beam TR-2-5/1

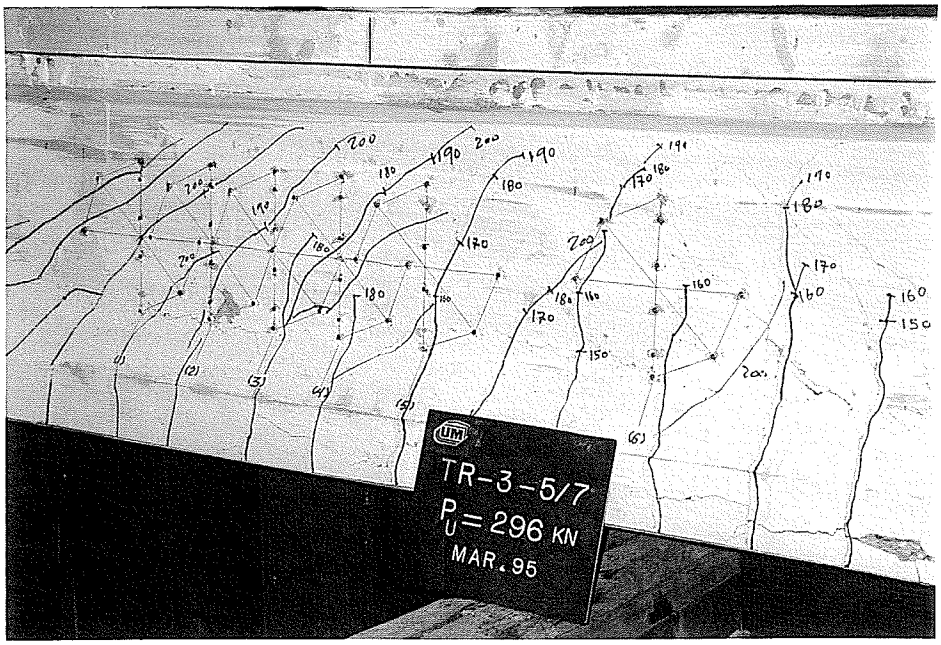

Figure 4.13 (c) Diagonal crack pattern of beam TR-3-5/7

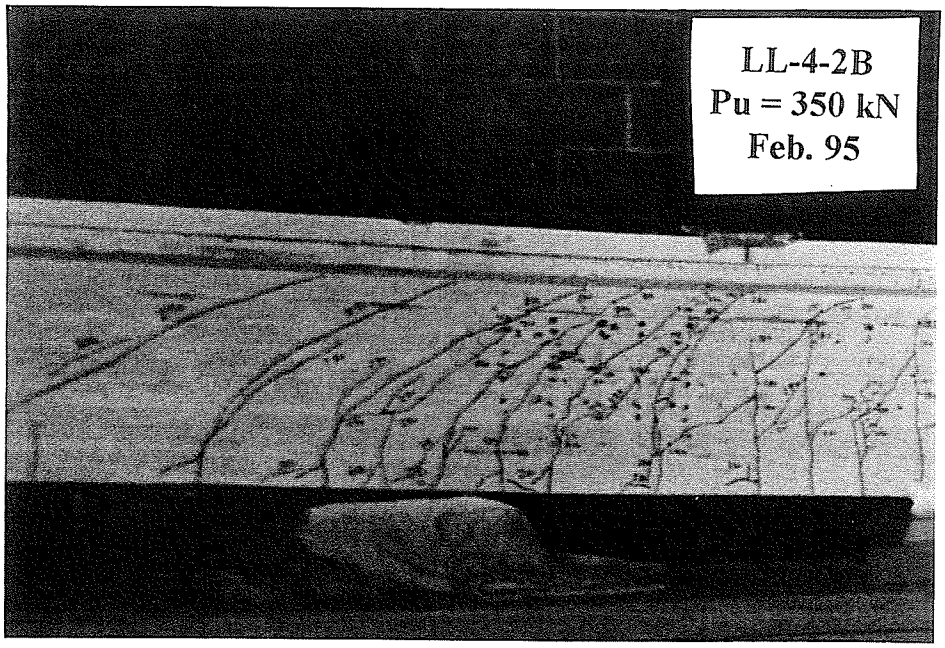

Figure 4.13 (d) Diagonal crack pattern of beam LL-4-2B

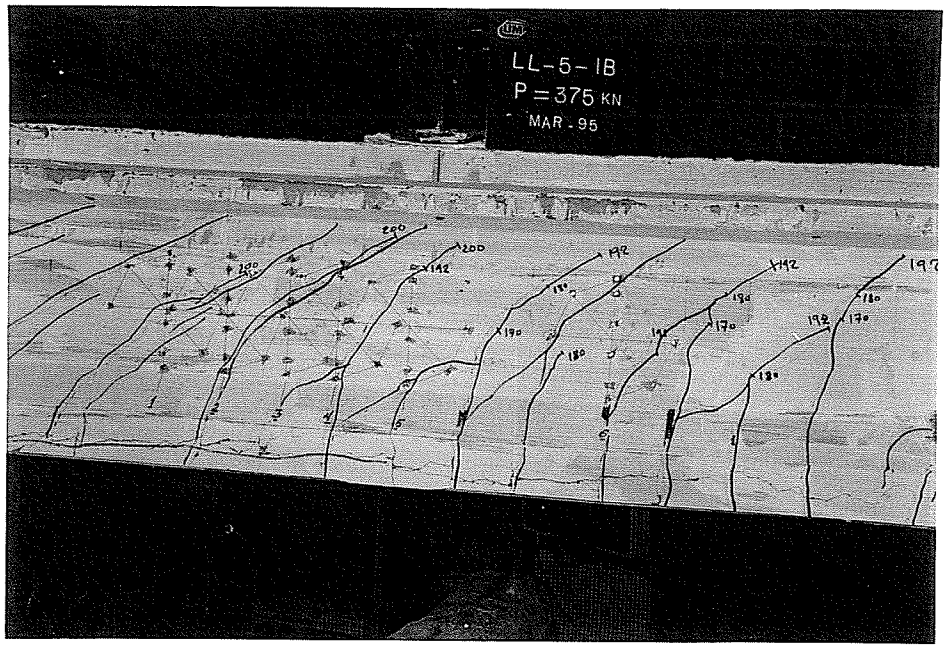

Figure 4.13 (e) Diagonal crack pattern of beam LL-5-1B

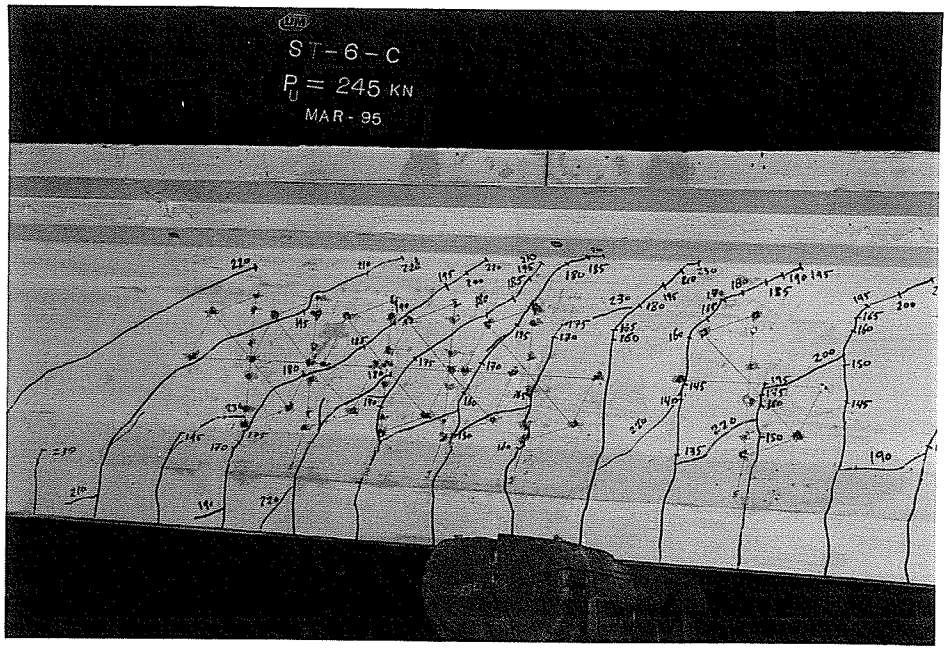

Figure 4.13 (f) Diagonal crack pattern of beam ST-6-C

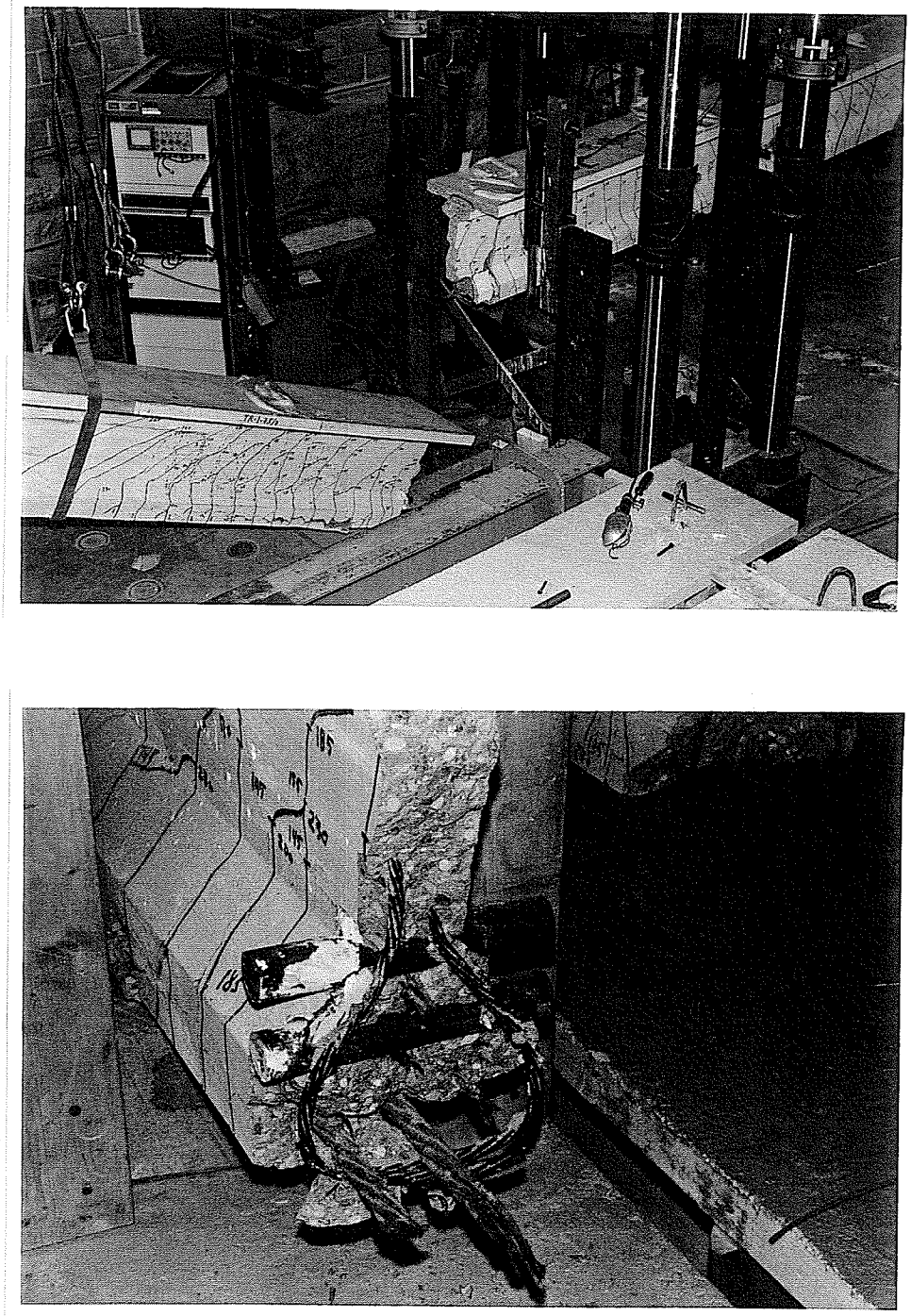

Figure 4.14 (a) Failure mode of beam TR-1-7.5/7

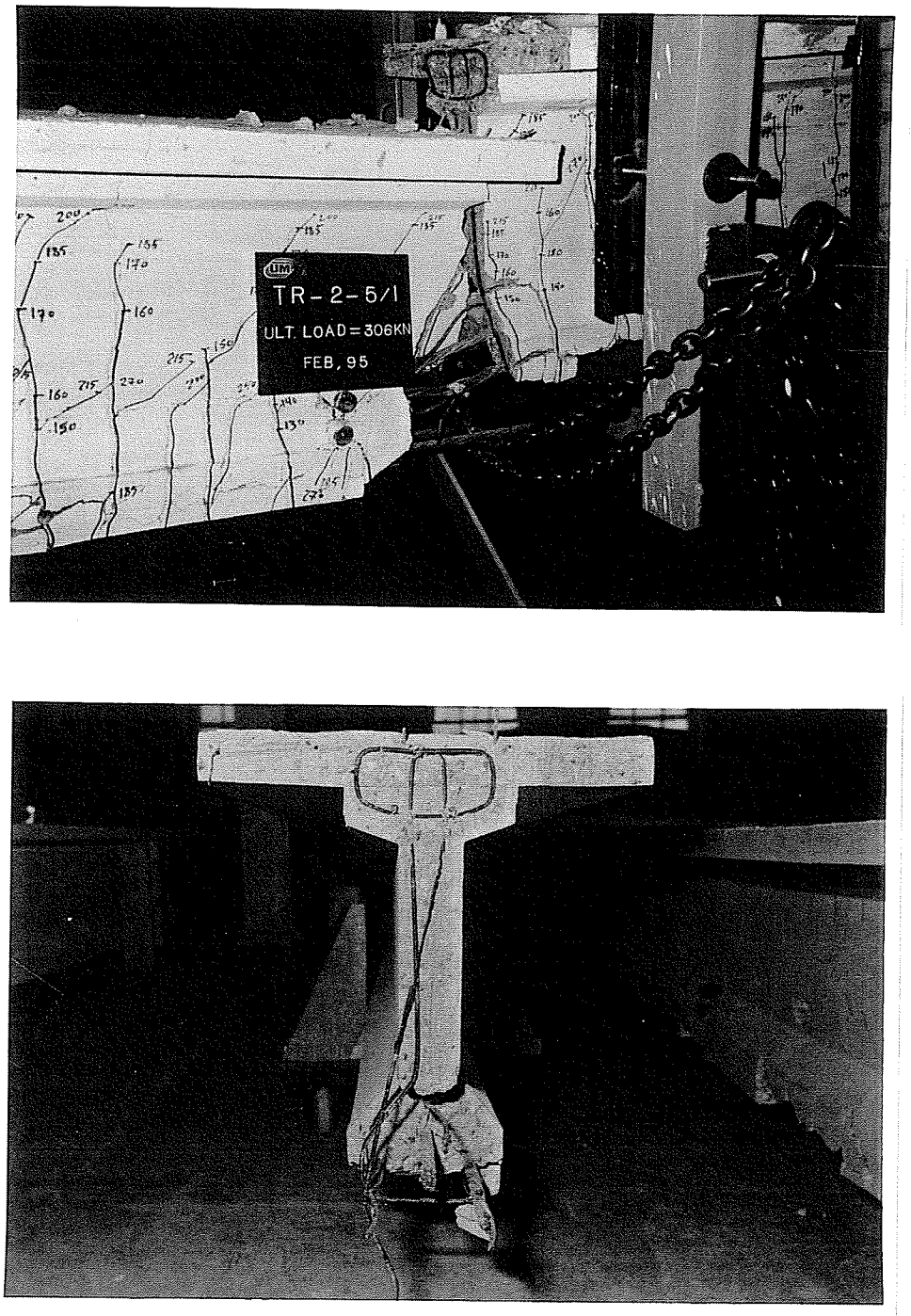

Figure 4.14 (b) Failure mode of beam TR-2-5/1

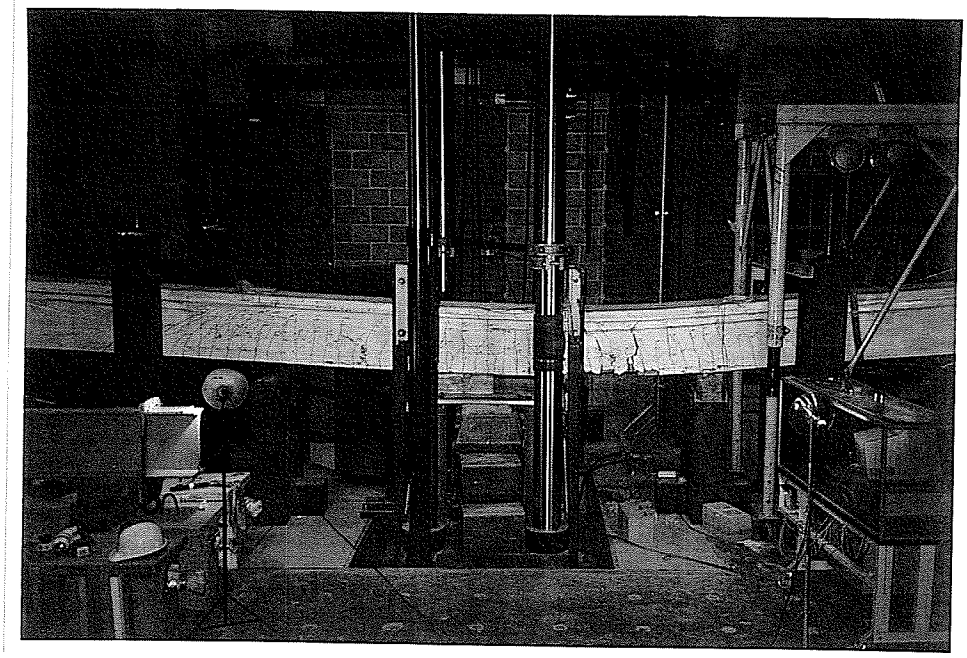

Figure 4.14 (c) Failure mode of beam TR-3-5/7

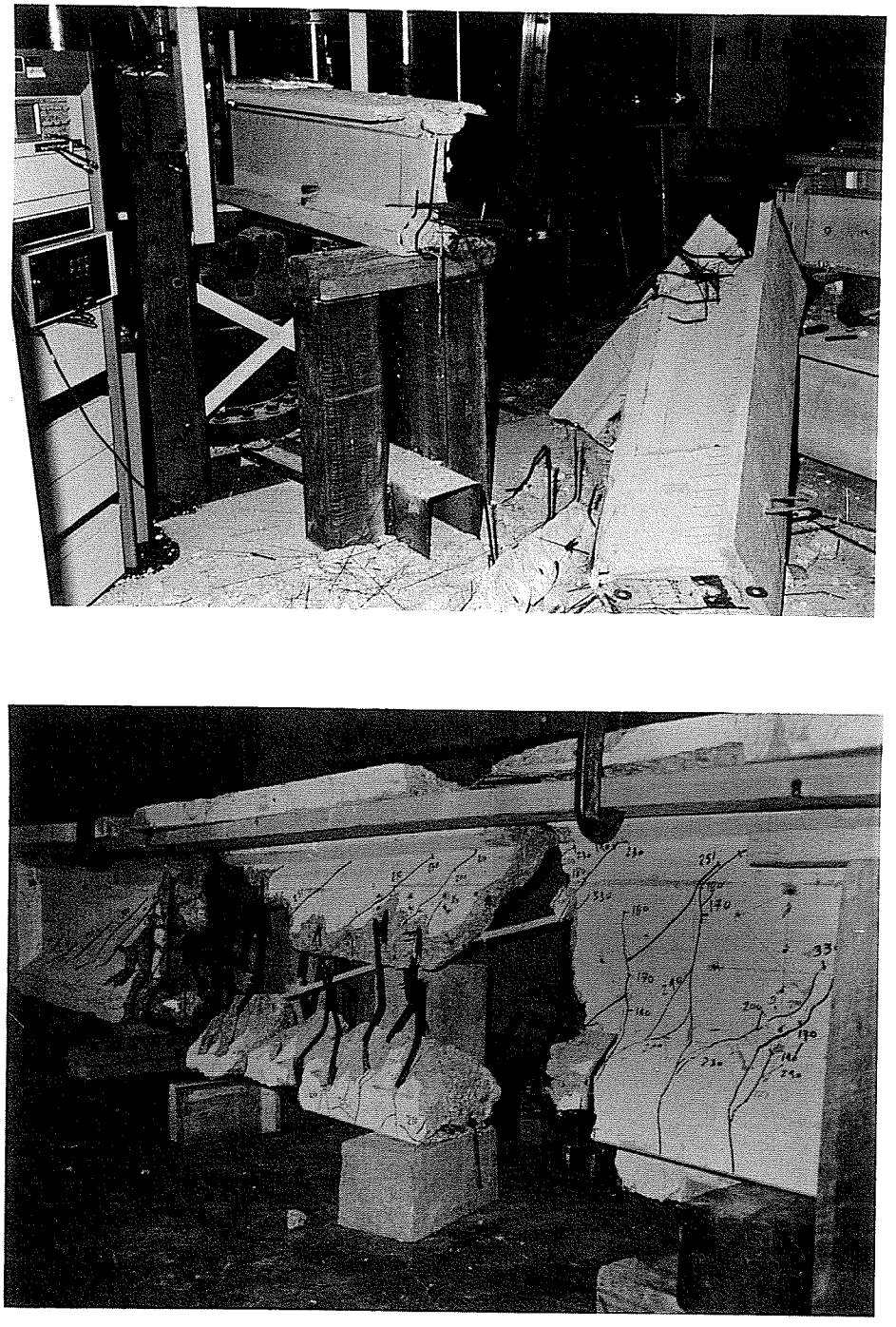

Figure 4.14 (d) Failure mode of beam LL-4-2B

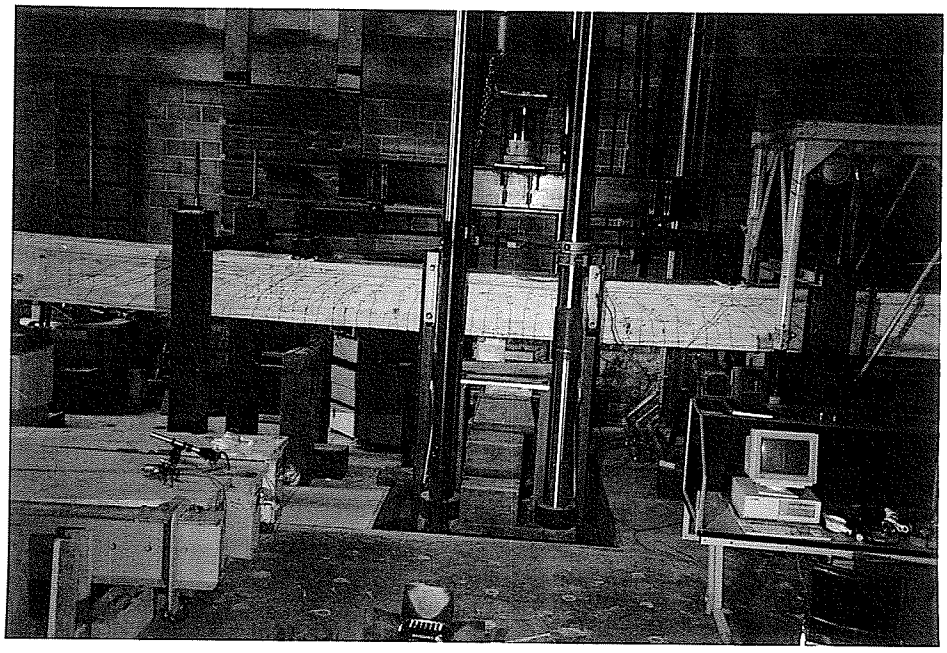

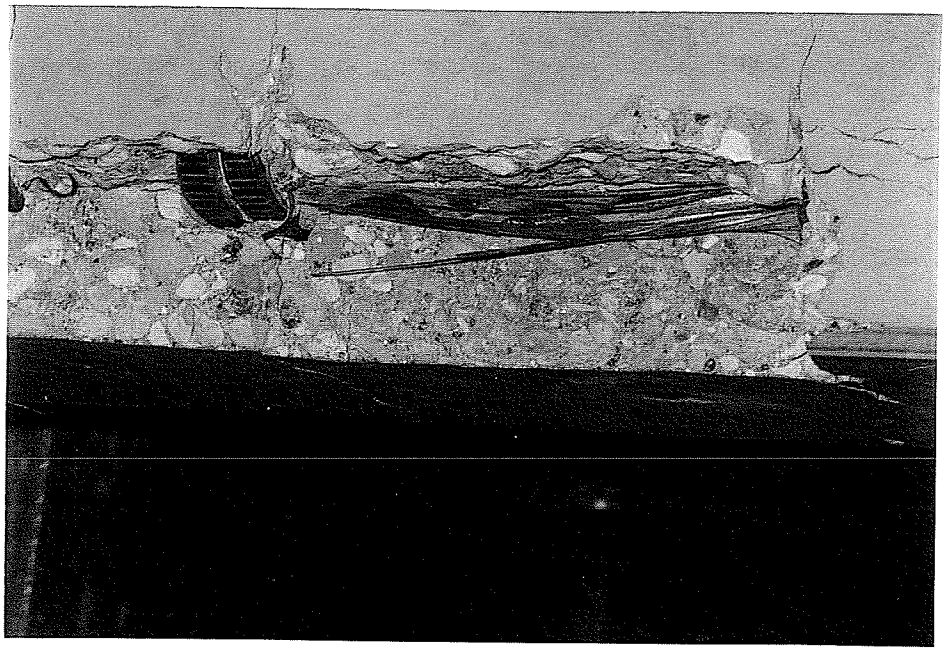

Figure 4.14 (e) Failure mode of beam LL-5-1B

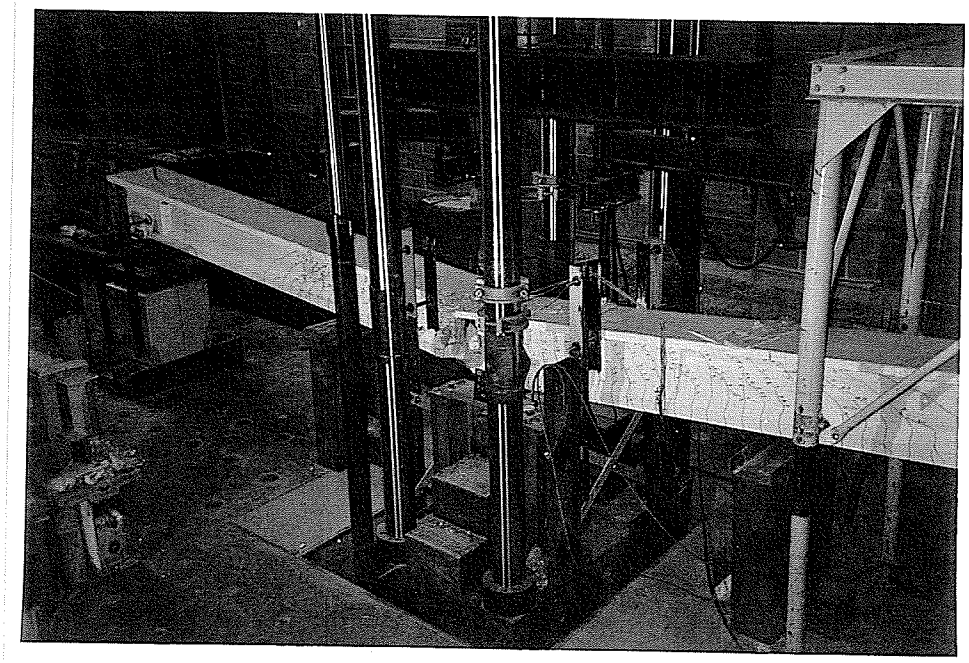

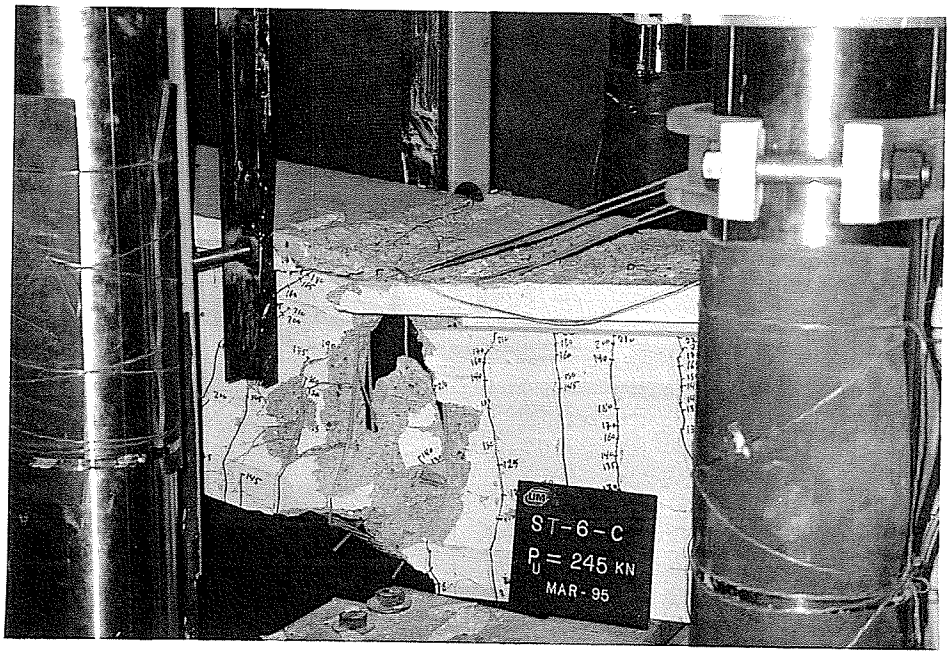

Figure 4.14 (f) Failure mode of beam ST-6-C

CHAPTER 5

DISCUSSION OF TEST RESULTS

5.1 INTRODUCTION

In this chapter, the behaviour of all tested beams in this experimental program is discussed in details. The performance of beams prestressed and reinforced for shear by CFRP reinforcements is analyzed and compared to the beam prestressed and reinforced for shear by steel reinforcements. The study is focussed on the effect of the type, percentage of shear reinforcements, stirrups configurations, draping of the tendons, and the dowel strength of the CFRP stirrups projected into the deck on both the flexural and shear behaviour respectively. The results are also used to provide assessment of the validity of the current analytical and design approaches for shear using FRP stirrups. The findings should significantly affect and contribute to the developments of future design guide lines and codes.

5.2 BEHAVIOUR OF TEST BEAMS

The entire behaviour of individual beams has been primarily divided into two categories: the flexural behaviour, and the shear behaviour.

In the section of flexural behaviour, the effect of the web reinforcement ratio and the elastic modulus on the stiffness of the beams is discussed and compared. Flexural crack patterns are compared. Flexural modes of failure are also discussed. Finally the analytical model used to predict the behaviour of the beams is introduced. In the section of shear behaviour, the effect of the web reinforcement ratio as well as the elastic modulus of the reinforcements on the stirrups strain and diagonal crack width is introduced. The shear failure

exhibited by beam LL-4-2B is also discussed.

The analytical models used to predict the behaviour of the beams in shear including the modified compression field theory, current ACI building code, and CSA simplified method of both, 1984 and 1994 codes is discussed in a separate section, section 5.5.

5.3 FLEXURAL BEHAVIOUR OF TEST BEAMS

5.3.1 Stiffness of test beams

Stiffness of different beams are computed using the measured load - mid-span deflection behaviour of test beams before and after cracking as shown in Figure 5.1. All beams behaved linearly up to flexural cracking with almost the same stiffness of about 8.4 kN/mm. Due to the relatively high elastic modulus of CFRP in comparison to other FRP reinforcements, its effect on the stiffness of the beams after flexural cracking was insignificant. All the test beams prestressed by CFRP reinforcements exhibited almost the same stiffness of the beam prestressed by steel strands before yielding of about 1.18 kN/mm showing a reduction of about 86 percent of the uncracked stiffness. The beams prestressed by CFRP reinforcements behaved linearly after cracking up to failure with the same stiffness while the beam prestressed by steel strands showed lower stiffness of 0.14 kN/mm after yielding of the prestressing strands and up to failure as shown in Figure 5.1. Table 5.1 shows the stiffness of test beams at different stages.

Comparing the post-cracking stiffness of beams prestressed by Tokyo Rope strands, TR-1-7.5/7 and TR-2-5/1, the behaviour indicates slight difference in the stiffness due to changing of the shear reinforcement ratio. The same phenomenon was observed in comparing

beams prestressed by Leadline bars, LL-4-2B and LL-5-1B, using double and single legged stirrups of the same size. Results indicate that reducing the web reinforcement ratio by 50 percent did not influence the overall deformation due to shear deformation.

5.3.2 Flexural cracks

All the beams exhibited almost identical crack patterns at the maximum moment zone as shown in Figure 4.12. Eleven cracks were developed within the 1200 mm constant moment zone almost at the location of the stirrups with an average spacing of 110 mm. Therefore it appears that number and spacing of cracks was mainly controlled by the location of the stirrups rather than the type of prestressing tendons although they have different bond characteristics. In all test beams flexural shear cracks were developed at the steel pins located 400 mm out side the constant moment zone.

Figures 4.7 and Figures A.7 show the measured maximum and average flexural crack width for the six tested beams at the bottom tendons level. The figures indicate that the values of both the average and maximum crack width are very close. Comparing beams prestressed by CFRP tendons to beam prestressed by steel strands indicates that no major difference in the crack width value. Again that is due to the fact that CFRP has higher elastic modulus compared to other FRP materials.

5.3.3 Flexural modes of failure

Test beams prestressed by Tokyo Rope strands and reinforced by 7.5 mm 7-wire, and 5 mm solid stirrups, TR-1-7.5/7 and TR-2-5/1 respectively, failed by rupture of the bottom

draped strand at the location of the steel pin, located at 400 mm out side the maximum moment zone. The initial rupture was followed by rupture of the straight bottom strands, and finally by rupture of the upper draped strand. Failure of the lower draped strand located above the bottom straight strands was mainly due to the higher jacking force for this particular strand as recorded by the strain gauge readings as shown in both, Table 4.2 and Figure 4.6 for beam TR-1-7.5/7, and Table A.2 and Figure A.6 for beam TR-2-5/1. In both beams, the initial strain of gauge G4, located on the bottom draped strand is higher than all gauges located on the bottom straight strands, G5, G6, and G7. The failure was not due to the residual stresses at the hold-down locations as evident by the failure of the third beam prestressed by Tokyo Rope and reinforced by 5 mm 7-wire stirrups where failure occurred by rupture of the bottom straight strands, two within the maximum moment zone and the third out side the constant moment zone. Referring to Table A.2 and Figure A.6 of this beam, TR-3-5/7, indicates that the initial strain recorded by gauge G4 is lower than the strain recorded by G5, G6, and G7. The failure at the pin location did not reduce the flexural capacity as the three beams failed at almost the same load level as shown in Figure 5.1.

Beam LL-5-1B prestressed by Leadline bars and reinforced by single leg Leadline stirrups, failed by rupture of the bottom straight bars at load level higher than beams prestressed by Tokyo Rope strands as shown in Figure 5.1 due to the higher tensile strength of the Leadline bars.

Beam ST-6-C prestressed by steel strands and reinforced by 6 mm steel stirrups failed by crushing of the concrete at top surface after yielding of the bottom straight strands at load level much lower than beams prestressed by CFRP tendons as shown in Figure 5.1.

The five modes of failure mentioned above were all flexural tension failures which is the typical case of bridge girders, in composite action with the deck, and having shear capacity higher than the flexural capacity. The measured concrete compressive strain on the top surface at failure was about 0.002 in case of beams prestressed by Tokyo Rope strands as shown in Figures 4.3 and A.3 and was about 0.0025 in the beam prestressed by Leadline as shown in Figure A.3 for this beam. These value were less than the ultimate strains in compression, while the measured strains in the tendons using strain gauges indicates that the CFRP tendons achieved the ultimate tensile strains as shown in Figures 4.6 and A.6. The compression strain at the top surface in the beam prestressed by steel strands was about 0.0035 when the concrete crushed as shown in Figure A.3 while the strain in the bottom strands was about 0.04 which is much more than the yielding strain but less than the ultimate strain as shown in Figure A.4.

5.3.4 Analytical model

In order to predict the load - deflection behaviour of the test beams, program "RESPONSE" version 1.o [5] was used to determine the moment - curvature response at different sections. The program was developed to determine the load - deformation response of a reinforced or prestressed concrete cross section subjected to moment, shear, and axial load. The program uses the layer - by - layer approach and material characteristics of the concrete and reinforcement to determine the moment - curvature behaviour of a given section. The program was originally developed to analyze beams prestressed by steel tendons using a modified Ramberg - Osgood function to define the steel stress - strain relation ship [3],

given in Equation 5.1 and shown graphically in Figure 5.2. The factors A, B, and C are shown in the same figure where C controls the transition part through the bi - linear curve.

$$f_p = E_p \epsilon_p \left(A + \frac{(1 - A)}{[\, 1 + (B \epsilon_p)^C \,]^{1/C}} \right) \leq f_{pu} \qquad (5.1)$$

For beams prestressed by CFRP tendons, the A, B, and C factors were selected to create the maximum linear part of the curve by minimizing the transition curve through C value. The elastic modulus of each type of CFRP, E_p shown in Figure 3.6, was used. For CFRP tendons, the maximum input value for ultimate strength, f_{pu}, used was 2000 MPa as limited by the computer program "RESPONSE" and the minimum ultimate strain value permitted by the program, ϵ_{pu}, of 0.02 was used to minimize the yielding plateau. For steel strands, the material properties including E_p, f_{pu}, and ϵ_{pu}, shown in Figure 3.6, were used with the default values of the A, B, and C factors. Figures 5.3 (a), (b), and (c) show the material stress - strain curve used in the program for the different materials using the following equations:

For CFCC strands :
$$f_p = 137000 \; \epsilon_p \left(\frac{1}{[\, 1 + (68.5 \; \epsilon_p)^{100} \,]^{0.01}} \right) \qquad (5.2)$$

For Leadline bars :
$$f_p = 147000 \; \epsilon_p \left(\frac{1}{[\, 1 + (73.5 \; \epsilon_p)^{100} \,]^{0.01}} \right) \qquad (5.3)$$

$$\textit{For steel strands} : \quad f_p = 205500\ \epsilon_p \left(0.025 + \frac{0.975}{[\ 1 + (118\ \epsilon_p)^{10}\ ]^{0.1}} \right) \qquad (5.4)$$

Since the test beams included draped tendons, while the program deals only with individual sections, each beam was divided into 47 sections as shown in Figure 5.4 and the moment - curvature relationship was determined for each section. Figure 5.5 shows the typical moment - curvature relationship as obtained from the program for beams prestressed by CFRP reinforcements including tension stiffening effect. The flat part at the end of the curve resulted from the small yielding plateau of the prestressing material, shown in Figure 5.3 (a) and (b), as a result of the limitation of the input value for the ultimate strain in the program. The flat part of the curve was ignored since it does not represent the actual linear behaviour of the material. At this stage the behaviour was not complete since the maximum used value of the strength of the tendons was only 2000 MPa. Figure 5.6 shows the moment - curvature relationship at two sections of a typical beam prestressed by CFCC strands after ignoring the flat part, one section located at mid - span before the draped strands zone which represents sections 19 to 24, shown in Figure 5.4, while the other is located at the end of the beam before the end block at the maximum elevated level of the draped strands within the I-shape portion, section 3 in the same figure. The figure shows the effect of draping the strands on the flexural behaviour of the beam. Response of the other sections lies in between those two limits shown in Figure 5.6.

Another computer program was written to perform the numerical integration of the curvatures along the span of the beam in order to compute the deflection at different load

levels, however, the obtained response at this stage does not represent the full response up to the flexural capacity of the beam. Independently, using equilibrium - strain compatibility approach, the ultimate flexural capacity of the beams were computed for a section at mid - span. The ultimate capacity was governed by rupture of the bottom tendons at tensile strength of 2150 MPa and 2950 MPa for CFCC and Leadline respectively which is the ultimate strength of the materials provided by the fabricators as shown in Figure 3.6. Based on the fact that the incomplete load - deflection response was linear after cracking due to the linearity of the prestressing materials, linear regression was used to extend the load - deflection response up to the computed ultimate flexural capacity of the beams.

For the beam prestressed by steel strands program "RESPONSE" was used to compute the full moment - curvature response up to the flexural capacity of the beam which was governed by crushing of the concrete at the top surface at 0.0035 strain after yielding of steel. The other program was used to perform the integration in order to get the complete load - deflection response. Figures 5.7 (a), (b), and (c) show the predicted load - deflection response of typical beams prestressed by CFCC strands, Leadline bars, and steel strands respectively in comparison to the measured behaviour which was in good agreement in terms of the cracking load, ultimate load, and stiffness before and after cracking.

5.4 SHEAR BEHAVIOUR OF TEST BEAMS

The test beams were designed to simulate the bridge girders typically designed to have shear capacity higher than the flexural capacity by providing sufficient shear reinforcement to avoid shear failure. All tested beams exhibited considerable number of diagonal cracks

within the maximum shear span before failure. The diagonal crack patterns were almost similar in number and spacing as shown in Figure 4.13 and covered about 50 percent of the maximum shear span before failure of the beams in flexural mode. For beams prestressed and reinforced by Leadline stirrups, The failure occurred at significantly higher load levels compared to other beams due to the higher ultimate strength of Leadline rods in comparison to Tokyo Rope and steel strands. As a result, the diagonal cracks covered the entire shear span including the end zones as shown in Figure 5.8. Similarity of crack patterns in different beams is due to same spacing of stirrups and layout of prestressing reinforcement in different beams, consequently the same geometry of the truss mechanism. Although the diagonal crack patterns were similar, the crack width and the strain level in stirrups were varied according to the different stirrups used.

In order to select the locations of the " Rosette" demec stations, shown in Figure 3.25, a beam was analyzed in shear using the ACI code. The shear resistance diagrams including both, flexural shear resistance, V_{ci}, and web shear resistance, V_{cw}, were constructed along the span of the beam and the applied shear force diagram was superimposed as shown in Figure 5.9 for a typical case. Shaded zone (1) in Figure 5.9, located next to the last loading point at the maximum shear span, was found to be the most critical zone where the concrete contribution in shear resistance is minimum while the stirrups contribution is maximum due to the high bending moment combined with the maximum shear. Demec stations # 1 to 5 were located within this zone. Shaded zone (2) was less critical due to the lower shear at this span and accommodated demec station # 6. At the end of the beam, near the support, demec station # 7 was located to measure the strains if web cracks develop. In all test beams the

strains measured by demec stations # 1 to 5 were the maximum strains along the beam. Only in beams prestressed by Leadline bars, significant strains were measured by demec station # 7, however, they were much lower than those measured by demec stations # 1 to 5 of the same beam.

The demec stations of 200 mm gauge length were used to measure the strain of the concrete of the web in the vertical, horizontal, and diagonal directions as shown in Figures 4.8, 4.10, and 4.11 for beam TR-1-7.5/7 and Figures A.8, A.10, and A.11 for the rest of the beams. The readings, combined with the measured angle of the cracks were used to calculate the average diagonal crack width. The vertical measurements in the direction of the stirrups were considered equivalent to the average strain in the stirrups at the same location. The measured vertical strains using the 50.8 mm gauge length, shown in Figures 4.9, and A.9, were not used in analysis since the debond length of the stirrups on both sides of the diagonal crack varies and might exceed the 50.8 mm gauge length and also varies in different beams according to different stirrups sizes and materials.

5.4.1 Effect of web reinforcement ratio

The effect of the web reinforcement ratio was considered for the beams reinforced by CFCC stirrups as a group, and the beams reinforced by the Leadline stirrups as another group. In each group, the beams were identical in terms of the prestressing reinforcement number, layout, and stirrups spacing. The main variable within the two groups was the web reinforcement ratio, which was controlled by the stirrups size in the first group and the stirrups configurations in the second group. The strain level in stirrups and average diagonal

crack width were affected as follows:

(a) Strain level in stirrups:

The average of the measured vertical strains in direction of stirrups at demec stations # 1 to 5 of each beam, shown in Figures 4.8 and A.8, was used to compare different beams within the same group as shown in Figure 5.10 (a) and (b) for CFCC, and Leadline respectively. The strains for beams TR-3-5/7 and LL-5-1B are in-complete as they were tested after the brittle failure observed for beam LL-4-2B due to the inappropriate configuration of the stirrups as well be discussed in section 5.4.3.

Comparison of the three beams reinforced by the three different sizes of CFCC stirrups, shown in Figure 5.10 (a), and the two beams reinforced by two different configurations of Leadline stirrups, shown in Figure 5.10 (b), indicates that reduction of the web reinforcement ratio will result in higher strain level in the stirrups. However, the increase in strain is not directly proportional to the web reinforcement ratio as evident by comparing beams TR-1-7.5/7 and TR-2-5/1.

(b) Diagonal crack width:

At different shear levels, the total crack width, within each demec station was calculated. The measured strains in two different directions combined with the average slope of the cracks located within the station were used to calculate the total crack width within the station using the concept described in Reference [17]. Three values were obtained for the total crack width within each demec station using three different combinations of strains. The

average of the three values, which was very close to the individual values, was considered to represent the total crack width within the demec station. Figure 4.13 shows the diagonal crack at failure and Appendix B includes schematic views of the diagonal crack patterns within the demec stations for different beams.

The average of the obtained values of total crack width at the five demec stations was used to compare the cracking behaviour of the different beams. Figure 5.11 (a) and (b) shows the variation of the average of the total crack width for the beams reinforced by CFCC and Leadline respectively. Crack width of beams TR-3-5/7 and LL-5-1B were not included due to the lack of readings after cracking. Comparing beams TR-1-7.5/7 and TR-2-5/1 in Figure 5.11 (a) indicates that the diagonal crack width increased by reducing the stirrups size, however, the effect is not directly proportional to the web reinforcement ratio.

5.4.2 Effect of elastic modulus

The effect of the elastic modulus was considered for the steel reinforced beam, ST-6-C, in comparison to beam TR-1-7.5/7 reinforced by Tokyo Rope. The two beams have almost identical area of stirrups and tendons. The main variable was the elastic modulus of the prestressing and shear reinforcement. The stirrups strain and the diagonal crack width were affected as follows:

(a) Strain level in stirrups:

Similar to section 5.4.1 (a), the average of the measured vertical strain in direction of stirrups at the five demec stations was considered to compare the two beams as shown in

Figure 5.12. In this figure the behaviour was considered only after diagonal cracking, at shear levels [$V-V_{cr}$], to exclude the effect of variation of the concrete strength in tension. The figure suggests that the slight increase in the strain of the beam reinforced by Tokyo Rope in comparison to the steel is not proportional to the value of the elastic modulus.

(b) Diagonal crack width:

Figure 5.13 compares the total crack width of the two beams calculated as described in section 5.4.1 (b) at different shear levels after cracking. The behaviour does not show definite differences due to the lower elastic modulus of the reinforcements. However, it should be noted that these beams were designed to fail in flexural mode.

5.4.3 Failure mode of beam LL-4-2B

Test beam LL-4-2B, prestressed by Leadline bars and reinforced by double legged Leadline stirrups, failed at higher load level compared to the others due to the high tensile strength of Leadline in comparison to CFCC. Failure occurred at the maximum shear location, 2.6 meters from the support. Before failure spalling of concrete cover was observed at the bend of the stirrup from the web to the bottom flange which suggests straightening of stirrup at this location. Increasing the applied load caused further stretching of the stirrups until they became ineffective to resist the applied shear as evident by crushing of the web and the dramatic failure shown in Figure 4.14 (d).

This behaviour was clearly related to the stirrups configuration, originally planned for the bridge, and certainly is not related to the characteristics of the CFRP reinforcements as

evident by the flexural mode of failure of beam LL-5-1B. Although the web reinforcement ratio of this beam, LL-5-1B, is 50 percent less than beam LL-4-2B it did not exhibit the same mode of failure due to the sufficient anchorage provided for the single legged stirrups through the bottom flange.

5.5 ANALYTICAL MODELS FOR SHEAR BEHAVIOUR

This section discusses the different methods and codes used to predict the behaviour of the test beams reinforced by different types and amounts of web reinforcements. Comparison between the different methods and the experimental results in terms of full response of the critical section in shear is also provided. The different methods and codes include the modified compression field theory, current ACI code, 1984 CSA simplified method, and the 1994 new CSA simplified method.

5.5.1 Modified Compression Field Theory

The analysis using this theory was performed using the "RESPONSE" program [5]. The theory is based on applying the equilibrium conditions, the compatibility conditions, and the constitutive relationships for the materials linking the stresses and strains to determine the complete load - deformation response of members subjected to shear, moment, and axial load. The back ground and fundamentals of the theory are explained in details in chapter 2.

5.5.1.1 Input file. For each beam, two sections were analyzed in shear, the first one located at "Rosette" demec station # 1, and the second one located at "Rosette" demec

station # 5, shown in Figure 3.25. Both sections are located at the critical zone of the shear span and 440 mm apart. In order to create the data file, the "New" selection was selected from the main menu, the name that was given to the section indicates the name of the beam and the demec station number, either 1 or 5, and the metric type of units was chosen. At this stage the program displays the data - editing spread sheet with default values for most parameters. The "Unfactored" option was chosen for the material properties through the "Configure" selection.

The concrete properties including compressive strength, f_c', and the corresponding strain, ϵ_c', as a weighted average for the concrete of the slab and the girder, the cracking strength of the girder, f_{cr}, was taken as $0.6\sqrt{f_c'}$. The "High - strength" concrete stress - strain model was selected, through the "Configure"selection, rather than the "Parabolic" one since it resulted in modulus of elasticity for the concrete very close to the one obtained from testing the cylinders according to ASTM specifications. The tension stiffening factor for CFCC and steel tendons was selected as 0.7 for bonded tendons, while for Leadline rods, a value of 0.6 was selected.

Two types of non-prestressed reinforcements were selected. Type (1) to represent both, the steel reinforcements used in the flange of the I-girder provided to support the stirrups, and wire mesh in the slab, while type (2) represents the material of the stirrups. For each rebar type the material is defined by the elastic modulus, E, the yield strength, f_y, strain at the end of the yielding plateau and beginning of hardening, ϵ_{sh}, ultimate strength, f_u, and its corresponding ultimate strain, ϵ_u. For CFRP stirrups, the yielding plateau was eliminated by choosing ϵ_{sh} equal to the yielding strain, ϵ_y, and in order to create a linear behaviour up to f_u,

the stiffness of the hardening part was selected the same as the pre - yielding stiffness, which is the elastic modulus of the material, shown in Figure 3.7. The strength of the reinforcements, f_u , is limited by the program to a maximum input value of 1200 MPa which is less than the actual tensile strength of the CFRP materials, presented in Figure 3.7. However, after performing the analysis using the program, it was found that the maximum computed stress in the CFRP stirrups at ultimate was less than 1200 MPa in all the beams. For steel stirrups a bi - linear stress - strain curve, with the properties given in Figure 3.7, was used as an idealization of the actual stress - strain curve, where the yielding strain of 0.2 percent offset stress was specified. Figure 5.14 shows the idealized stress - strain curves for CFCC, Leadline, and steel stirrups that were used in the input file of "RESPONSE". All information related to the prestressing tendons data in the input file were explained earlier in section 5.3.4.

The next step in the input file is to enter the hight of the section, 550 mm, and the distance from the bottom level of the section to the centre of gravity, 319 mm.

Since this analysis was focussed on shear, the shear analysis option, "Y" was selected. The following data was specified: the width of the web, b_w, the shear depth, jd, the distance from the bottom level of the section to the horizontal web strain, ϵ_x, which was selected to the centre of the "Rosette" demec stations, distance to the centre of the web, longitudinal crack spacing, s_{mx} , and maximum aggregate size. "Y" selection was also selected for the "stirrups" option, and the transverse crack spacing, s_{mv} , the area of stirrups, A_v, stirrups spacing, s, were input, and finally the stirrups reinforcement type, type (2), specified in the material section, was selected.

s_{mx} and s_{mv} are the crack spacing indicative of the crack control characteristics of the longitudinal and transverse reinforcements, respectively. The s_{mx} is the average crack spacing that would result if the member was subjected to longitudinal tension while s_{mv} is the average crack spacing that would result if the member was subjected to a transverse tension. These crack spacings can be estimated from the CEB-FIP code as described in Reference [3]:

$$s_{mx} = 2\left(c_x + \frac{s_x}{10}\right) + 0.25\ k_1 \frac{d_{px}}{\rho x} \qquad (5.5)$$

$$s_{mv} = 2\left(c_v + \frac{s}{10}\right) + 0.25\ k_1 \frac{d_{pv}}{\rho v} \qquad (5.6)$$

Where:

ρ_x = Longitudinal reinforcement ratio.

ρ_v = Web reinforcement ratio.

k1 = 0.4 for deformed bars, and 0.8 for plain bars or bonded tendons.

s_x = Horizontal spacing of tendons.

s = Stirrups spacing.

c_x = Distance from centre of the section to upper longitudinal tendon.

c_v = Half distance between two branches of stirrups.

d_{px} = Diameter of tendons.

d_{pv} = Diameter of stirrups branch.

Following the shear data, the input of the concrete cross section and the longitudinal reinforcements were specified for each layer. The input of the concrete section was six layers,

each defined by the top width, the bottom width, the hight, and the distance from the bottom of the layer to the bottom fibre level of the section. The input of the prestressing tendons was specified using three levels, the bottom straight tendons, the bottom draped tendon, and the upper draped tendon. For each level the cross sectional area and the effective prestrain were specified. The reinforcements input was specified in two levels, the wire mesh in the top slab, and the two bars in the slab of the I-girder. Finally no displaced concrete, shrinkage strains, thermal strains, or initial strains were specified since they were not required in the shear analysis.

Appendix C includes sample data file for beam TR-1-7.5/7 at demec station # 1.

5.5.1.2 Performing analysis. The "Shear - model" was selected as the Modified Compression Field Theory, "MCFT", and the "Accuracy" of calculation was specified as "Well - done" through the "Configure" selection. The "Analyze"/ "All - loads"/ "Ratio M&N&V"/ "Full - response" selections were used to perform the analysis. In the "Ratio M&N&V" option, the "Axial load at zero shear", and the "Axial load - to - shear ratio, dN/dV" were selected as zero since no externally axial load was applied during testing. The "Moment at zero shear" was input as zero since the shear and moment were acting simultaneously during testing. The "Moment - to - shear ratio, dM/dV", simply the shear span length up to that section for concentrated type of loading, were input as 2.2, and 2.64 for sections at "Rosette"demec stations # 1 and # 5 respectively. The main differences in the input file between the two sections in any beam are the "dM/dV" ratio and the level of the draped tendons.

The output of "Full - response" option includes the stirrups strain, ϵ_t, the principal strain, ϵ_1, the horizontal strain, ϵ_x, the curvature of the section, C, and the angle of the principal strain, θ, at different shear levels up to the maximum flexural or shear capacity of the section, which ever is smaller.

5.5.1.3 Refining of the output. Figure 5.15 shows a typical shear - stirrups strain curve obtained from the program, where the response is completed up to the maximum capacity of the section regardless the over all capacity of the beam which is usually less and governed by the flexural capacity of the middle portion of the beam. In this curve, the upper part with the lower stiffness resulted from the small yielding plateau at the end of the linear part of the stress - strain curve of CFCC and Leadline longitudinal tendons used in the input data, shown in Figure 5.3 (a) and (b), which is similar to the case of the moment - curvature response discussed earlier and shown in Figure 5.5. In all the beams prestressed by CFCC tendons, the flexural failure occurred at a load level, shown in Figure 5.15 as level "A", which is below the softening effect. Therefore, data above level "A" was ignored for these category of beams. In case of beams prestressed by Leadline tendons, the flexural failure took place at higher load level, shown in Figure 5.15 as level "B", than that initiated the plastic plateau of the curve. Since the inelastic behaviour is mainly due to limitation of the program input values and certainly not related to the behaviour of the stirrups, the part showing the plastic behaviour was ignored and the part of the curve representing the elastic behaviour was extrapolated up to the flexural capacity of the beam. In all beams reinforced by CFRP stirrups, both the computed and measured maximum stress level induced in stirrups at flexural

failure were less than the ultimate tensile strength specified in the program for the stirrups material which was 1200 MPa. For the beam reinforced by steel stirrups, the output response of the program was similar to the one shown in Figure 5.15, except for the fact that the plastic part of the curve was due to yielding of the stirrups rather than the tendons, however, flexural failure of this beam occurred at load level "C" less than that initiates the yielding of the stirrups, which is quite expected for long bridge girders. Same as in case of CFCC stirrups, only the part up to level "C" was considered.

5.5.1.4 Effect of draping. Since the computer program deals with a specific section, regardless the over all profile of the beam and the tendons, it does not account for the contribution of the draped tendons in shear resistance. In other words the input data for the tendons does not include any option indicating the slope of the tendons, accordingly, it is always assumed as straight tendons. As a result, the shear - stirrups strain response obtained from the program does not include the contribution of the vertical component of the effective prestressing force in the draped tendons. In order to account for the draped tendons effect, the vertical component of the effective prestressing force in the draped tendons, which was 6.25 kN in each, was added to the shear obtained from the program.

5.5.1.5 Effect of releasing post - tensioned strands. The previous analysis was performed for sections including only pretensioned tendons, however, the beam was loaded first up to a small load of about 3 kN before releasing the temporarily external post - tensioned tendons. Releasing those strands added extra load to the beam under the same

deflection. Figure 5.16 shows the structural model simulating the concrete girder, the spreader beams, and the actuator supporting the reaction, that was used to predict the effect of releasing post - tensioned tendons while the beam was held under stroke control. Releasing eccentric stressed tendons is equivalent to applying tension force plus bending moment to the centroid of the beam as shown in Figure 5.16. The support of the upper spreader beam represents the load cell fixed to the actuator of the machine used to monitor the load change. The tension force and moment used in the analysis were based on the measured effective force in the external tendons just before the test using strain gauges, which was about 51.5 kN per tendon after about 19.5 percent losses, and an eccentricity of 71 mm measured from the centroid of the composite section to the level of the external strands. The obtained load increment from this model was 5.71 kN, which was very close to the measured load increment using the load cell after release which varied between 4.5 kN and 7.25 kN in the tested beams. Half of the value of the predicted reaction was added to the shear obtained from the program to complete the simulation of the actual test conditions.

5.5.1.6 Comparison of results. The obtained test results included the applied shear versus the measured average strains on the concrete surface in the direction of stirrups. The spreader beam weight of 9 kN was significant enough to be added to the externally applied loads, while the corresponding strain in stirrups due to the 9 kN was negligible since the beam was not cracked yet at 9 kN.

Figures 5.17 (a) to (f) show the average of the measured strains on the concrete surface in direction of stirrups at the five demec stations, shown in Figure 3.25, compared to

the predicted strain of stirrups at demec stations # 1 and 5 at different shear levels using program "RESPONSE" for the six tested beams which was in good agreement with the observed response. Measurements of beams TR-3-5/7, and LL-5-1B, are incomplete as they were tested after the dramatic failure of beam LL-4-2B.

The definition of the "stirrups strain" obtained from program "RESPONSE" is: "the strain measured over base length long enough to include several cracks", which is typically comparable to the one measured with the demec gauge of 200 mm length.

5.5.2 ACI approach

In the ACI code, the applied shear at a section is resisted by a concrete component, V_c, and stirrups component, V_s, where V_c predicts the shear cracking load level. The shear strength, V_c, is considered the lesser of V_{ci} and V_{cw}, where V_{ci} refers to the flexural shear cracking, and V_{cw} refers to the web shear cracking. Code equations are given and discussed in more details in chapter 2.

5.5.2.1 Shear cracking load. It was found that for this particular design of beams, the concrete contribution is controlled by the flexural shear cracking resistance V_{ci}, given in Equation 2.1, due to the high combination of moment and shear at the critical section locations. The concrete strength of the girders, f_c', varied between 50.5 MPa, and 65.5 MPa as shown in Table 3.2. It was found that the difference in the value of V_{ci} based on the minimum and maximum values of f_c', was only about 3.9 percent. Similarly, the losses at the critical sections in shear, based on strain gauges G8, and G9, shown in Figure 3.23, in all the

beams varied between 20.91 percent and 24.44 percent, and the difference in the value of V_{ci} based on both values of losses, was only about 3.4 percent. Since V_{ci}, given by ACI, is independent of the type and amount of reinforcement and only affected by concrete properties, geometry of the section, and the prestressing losses, V_{ci} and V_{cw} were calculated for a typical beam at two sections at the "Rosette" demec stations # 1 and 5, shown in Figure 3.25, using an average values of 58 MPa and 23 percent for the f_c', and the prestressing losses respectively. The lesser of V_{ci} and V_{cw} represents the concrete contribution in shear resistance at these sections which is V_{ci}= 93.27 kN at section # 1 and 81.88 kN at section # 5, indicating that the flexural shear cracks will take place before web shear cracks at these sections, which was observed during testing due to the high combination of moment and shear at the critical section.

5.5.2.2 <u>Behaviour after diagonal cracking.</u> In order to predict the full response of the critical sections in shear in a similar fashion to program "RESPONSE", The code equations were rearranged to predict the applied shear, V, in terms of the strain in the stirrups, ϵ, as follows:

The total shear resistance at the section, $V = V_{ci} + V_s$

$$V = V_{ci} + \left(\frac{A_v \, d \, E}{s} \right) \epsilon \qquad (5.7)$$

The above relation represent a straight line with an intersect to the shear load axis at

a value of V_{ci}, which is equivalent to the shear cracking load. The slope of the line is related to effective depth, d, spacing of the stirrups, s, the cross section area of the stirrups, A_v, and elastic modulus, E. Equation 5.7 was used to predict the shear - strain response of the stirrups at sections # 1 and # 5 for each beam. The effect of releasing post-tensioned strands, discussed in details in section 5.5.1.5, was also considered. Figures 5.18 (a) to (f), show the average of the measured concrete strain in direction of stirrups at the five demec stations, shown in Figure 3.25, in comparison to the ACI predictions at sections #1 and # 5, shown at the same figure. The comparison shows good agreement in predicting the diagonal cracking shear, however, in all the beams except beam TR-2-5/1 the code under estimated the strain level in stirrups after cracking.

5.5.3 CSA simplified method of 1984, and 1994 codes

Similar to the ACI code, the simplified method of the Canadian code is based on two components of shear resistance, V_c, and V_s. V_c is the lesser of the flexural cracking shear resistance and the web cracking shear resistance. The new 1994 CSA code provides a different expression for the flexural cracking shear resistance, V_c, for prestressed beams compared to the 1984 one. The expressions for V_c, V_{cw}, and V_s of the 1984, and 1994 codes are given and discussed in details in chapter 2.

5.5.3.1 Shear cracking load The shear cracking load was governed by the flexural shear cracking, V_c. Using the 1984 code, the calculated values at sections # 1 and # 5 for V_c were 50.54 kN and 46.05 kN respectively, while the 1994 code resulted in 99.52 kN

and 86.72 kN for V_c at sections # 1 and # 5 respectively which is more realistic.

5.5.3.2 Behaviour after diagonal cracking Equation 5.7 was used in the same way discussed earlier in section 5.5.2.2. The shear versus strain in the stirrups is predicted and compared to the measured response using the 1984 and 1994 codes in Figures 5.19 (a) to (f). The 1994 code is more accurate in predicting the shear cracking load compared to the 1984 code.

5.5.4 Evaluation of the code prediction

Although the ACI code and the simplified method of the new CSA code predict well the shear cracking load, they both under estimate the strain level in stirrups after cracking. The behaviour suggests that after diagonal cracking occurs, the concrete contribution, V_{ci} or V_c, is not fully maintained and reduces gradually due to the excessive opening of the diagonal cracks. Figure 5.20 proposes reduction of the V_{ci} or V_c contribution by increasing of the applied load to provide better prediction of the test results. Due to the limited data at this stage, further work is needed to qualify the proposed reduction.

Beam	Stiffness (kN/mm)				
	Before cracking	After cracking	% Age reduction	After yielding	% Age reduction
TR-1-7.5/7	8.443	1.1398	86.5	-	-
TR-2-5/1	8.41	1.0933	87	-	-
TR-3-5/7	8.245	1.0969	86.7	-	-
LL-4-2B	8.575	1.1356	86.8	-	-
LL-5-1B	8.61	1.0994	87.2	-	-
ST-6-C	7.973	1.2881	83.8	0.141	98.2

Table 5.1 Stiffness of test beams at different stages

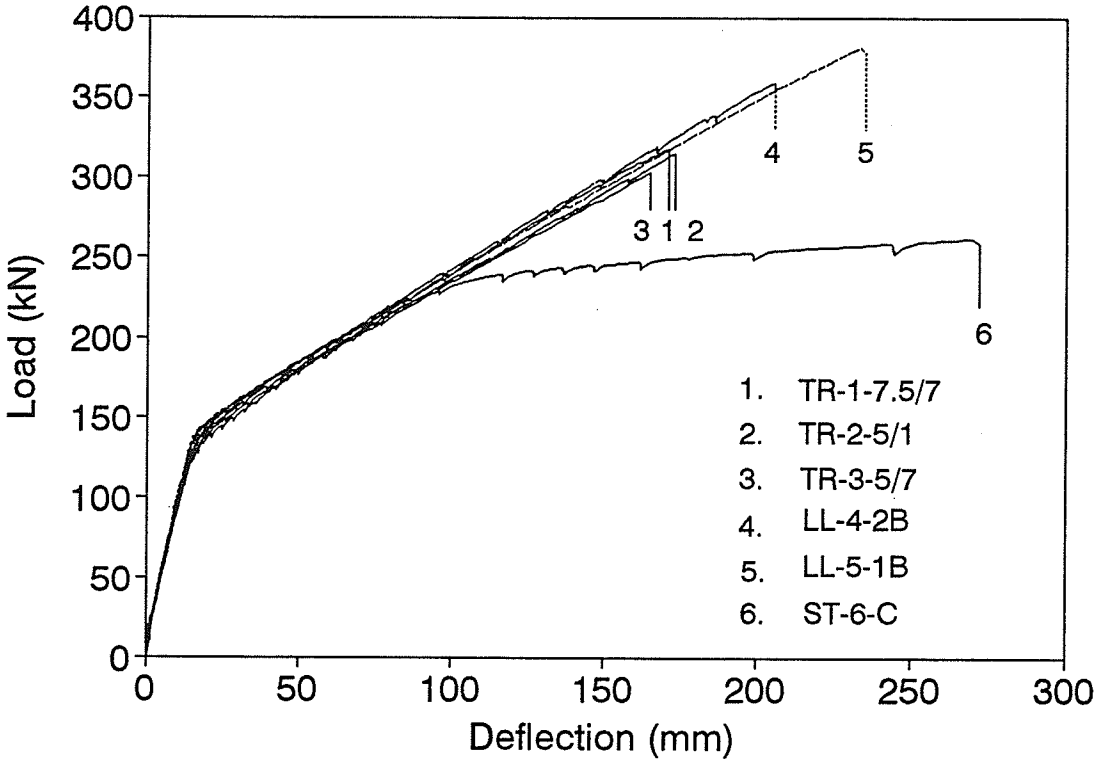

Figure 5.1 Measured load-deflection for six test beams

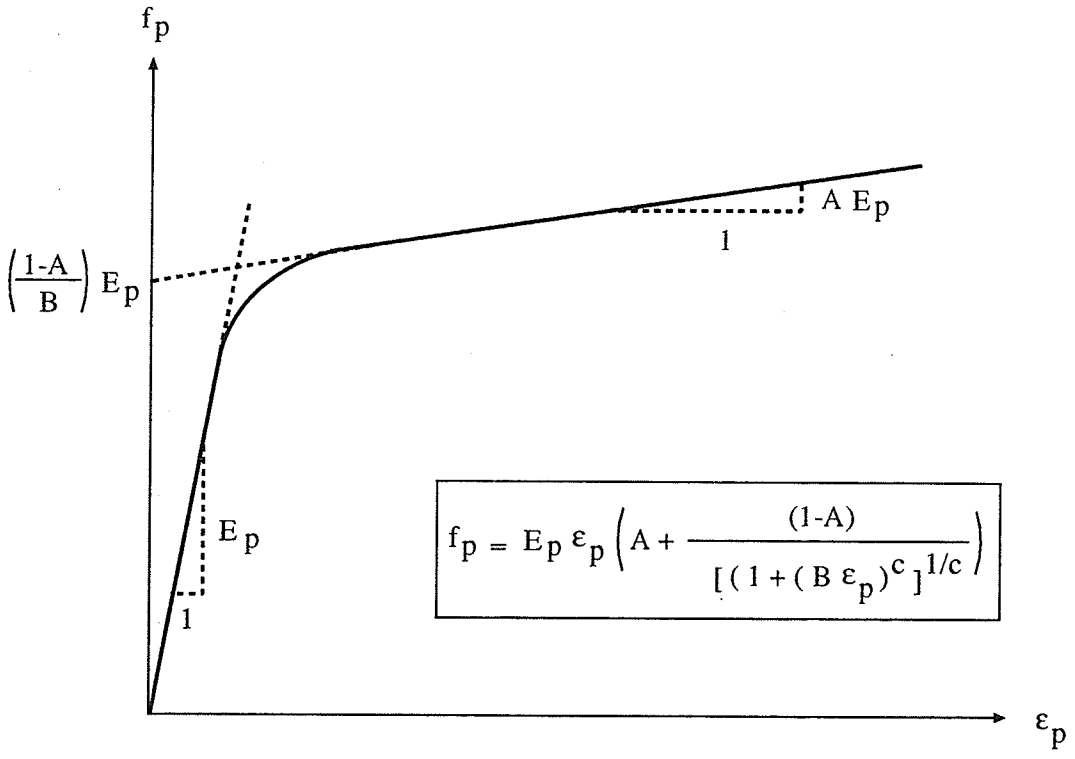

Figure 5.2 Modified Ramberg - Osgood function for the material of prestressing tendons

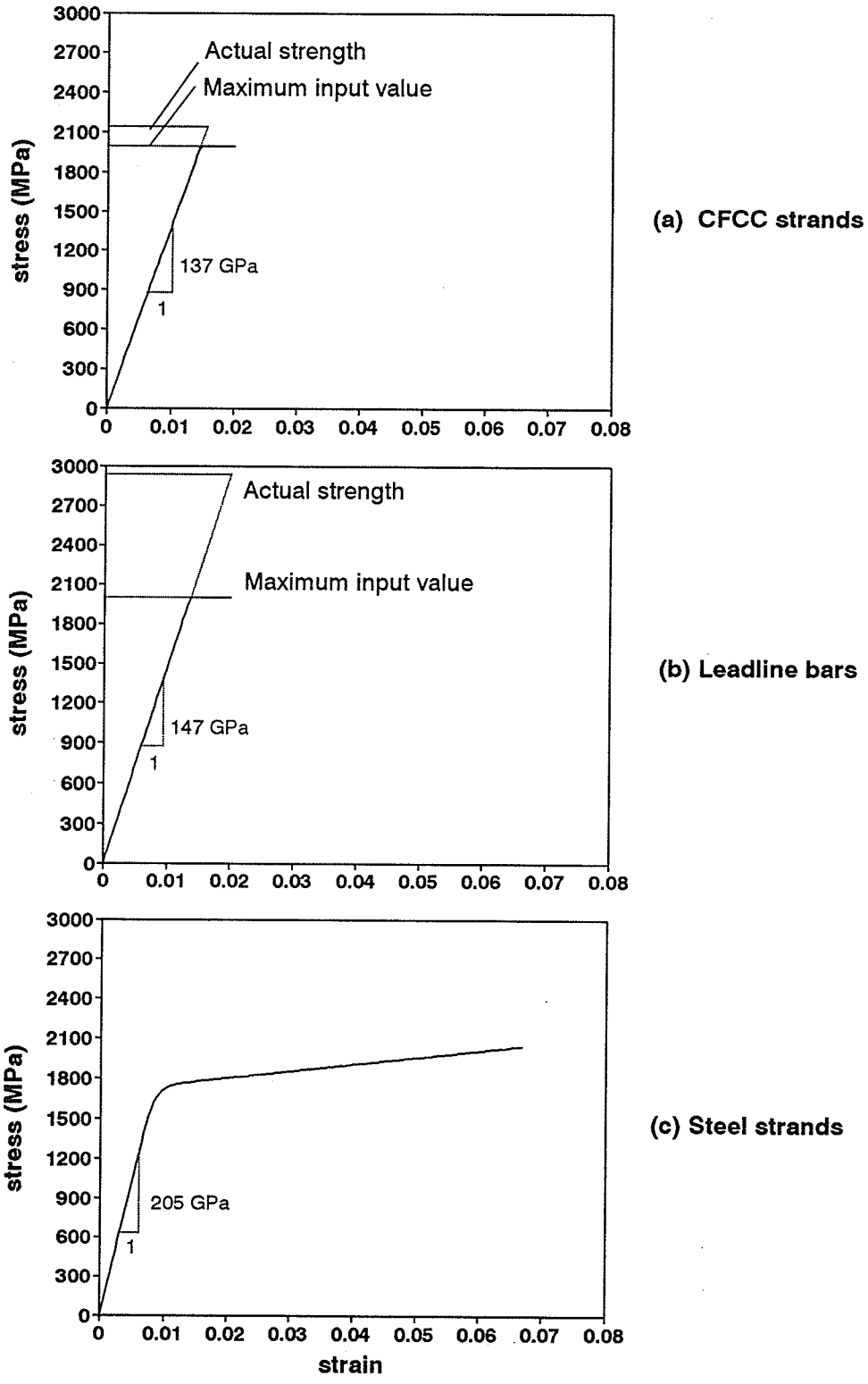

Figure 5.3 Stress-strain curves of prestressing tendons as used in program "RESPONSE"

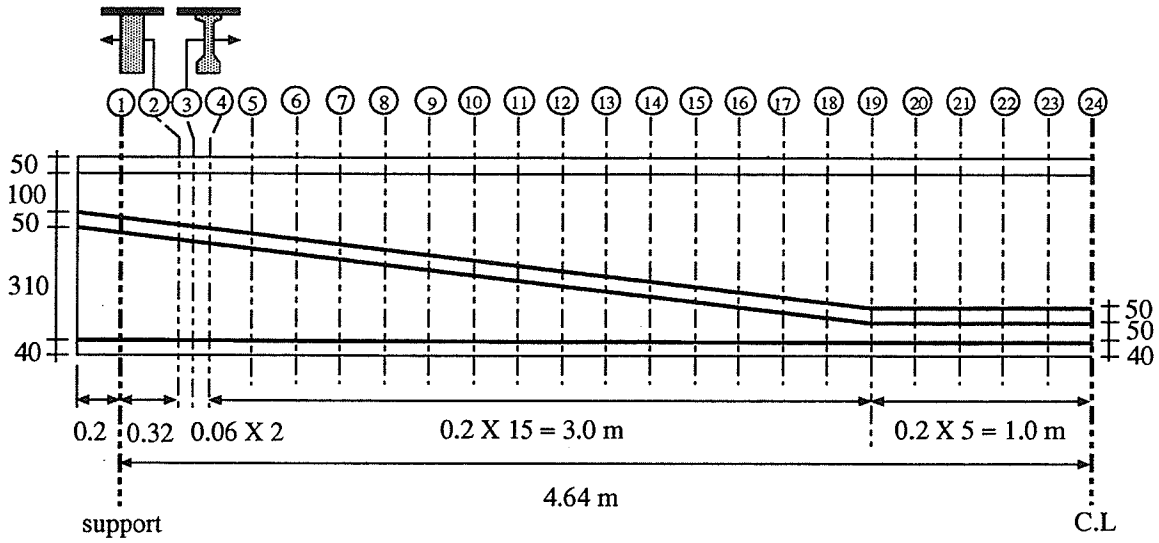

Figure 5.4 Different sections analyzed using program "RESPONSE"

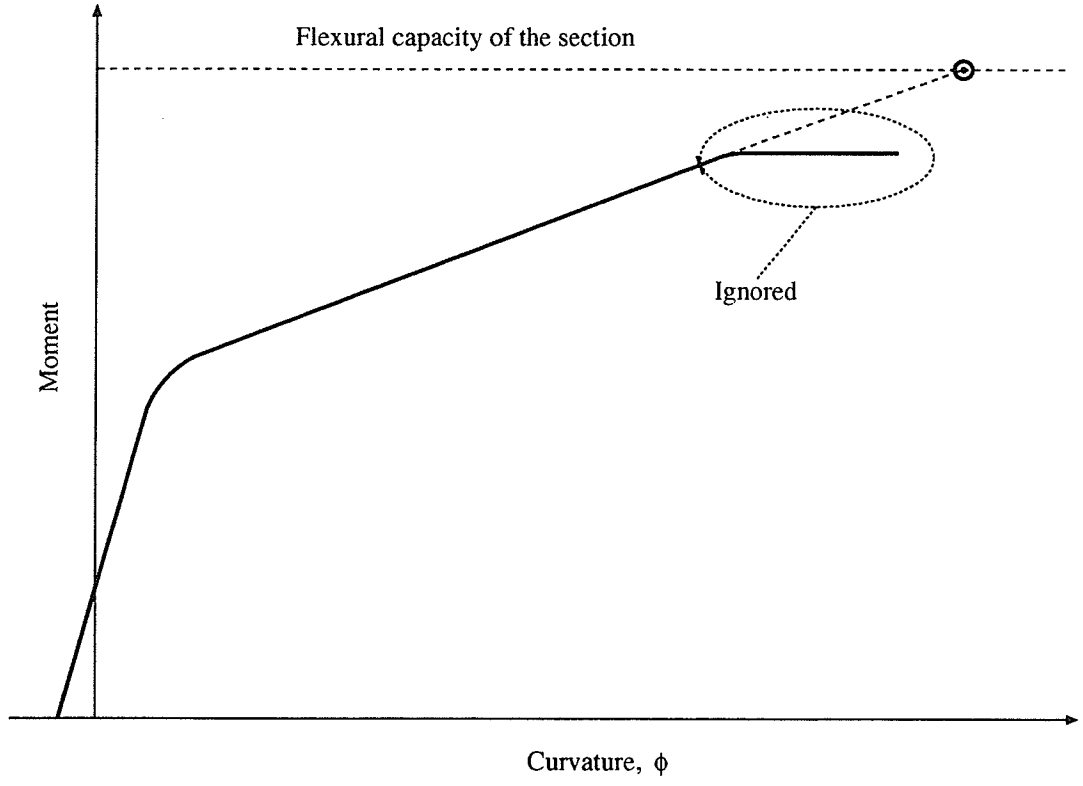

Figure 5.5 Typical moment - curvature curve as obtained from program "RESPONSE" at any section of the beams prestressed by CFRP tendons

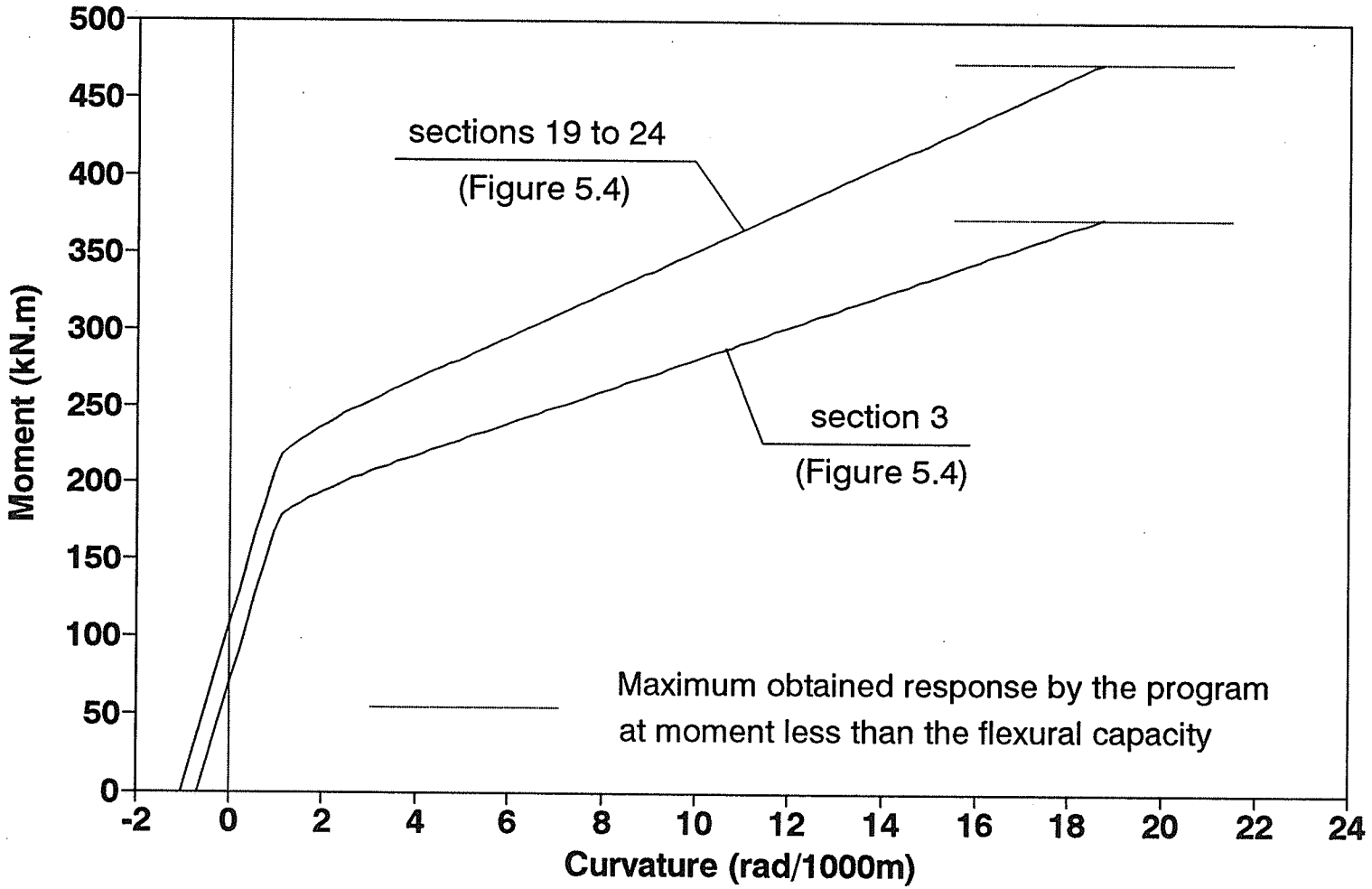

Figure 5.6 Moment - curvature response of beams prestressed by CFCC strands

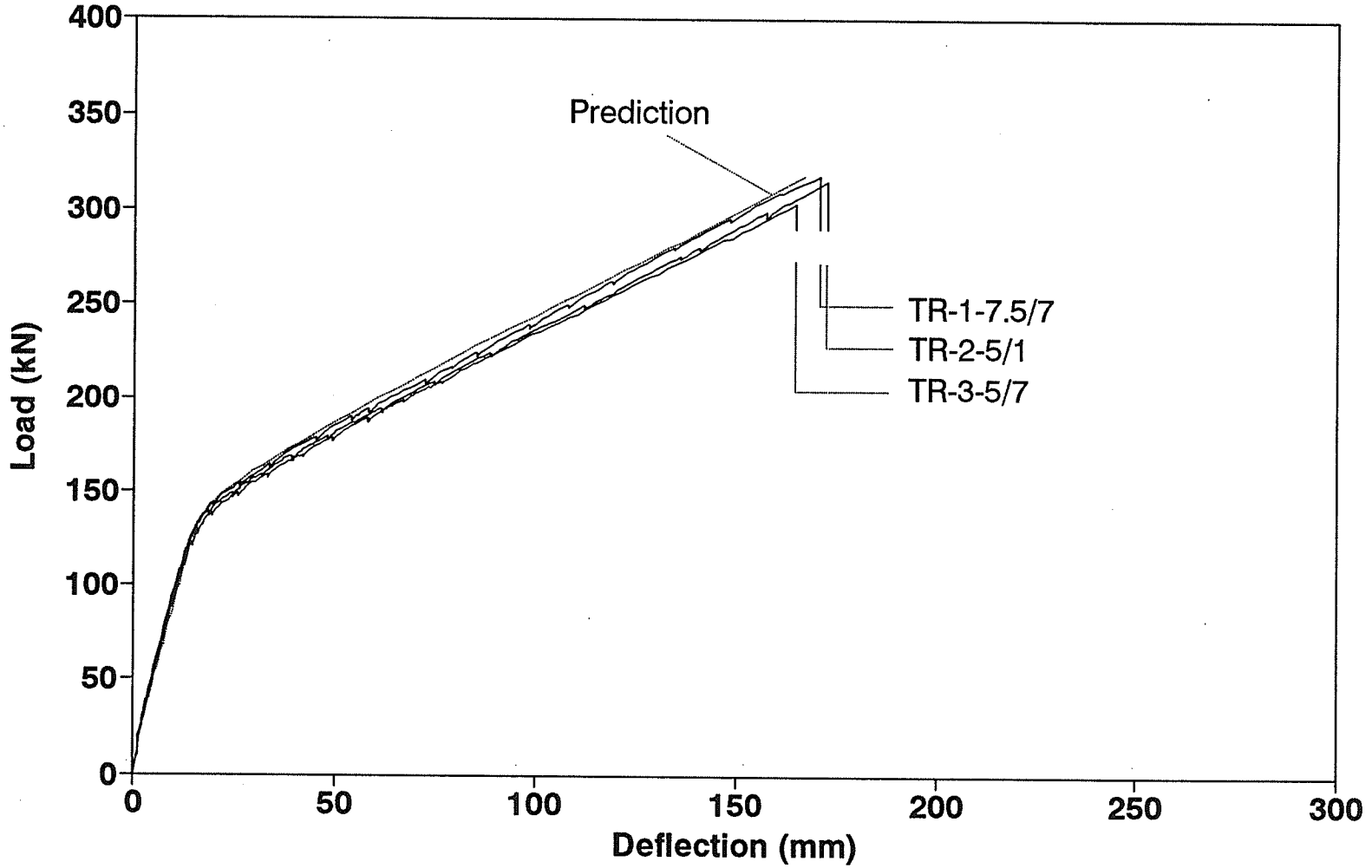

Figure 5.7 (a) Measured and predicted load - deflection diagrams for beams prestressed by CFCC strands

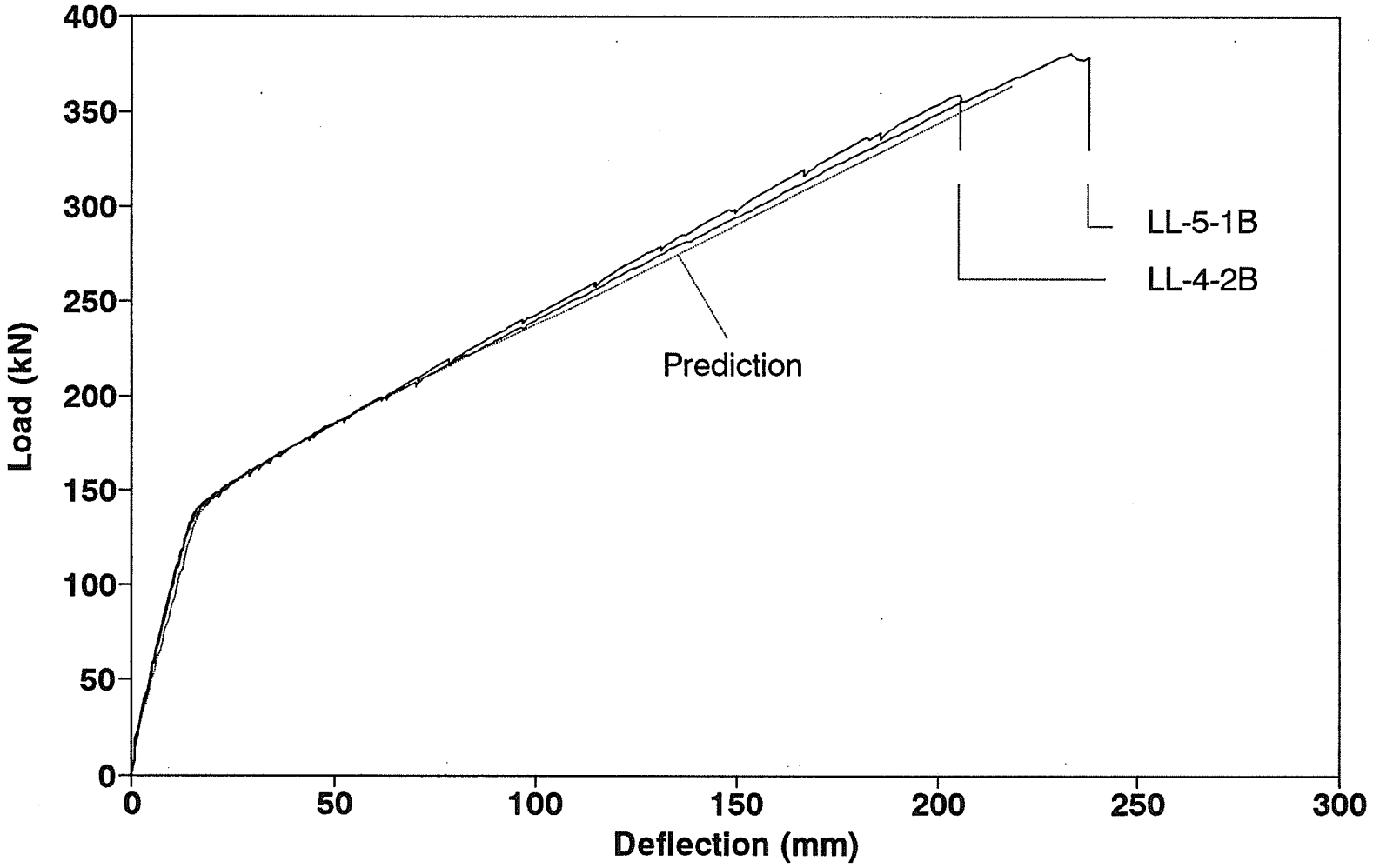

Figure 5.7 (b) Measured and predicted load - deflection diagrams for beams prestressed by Leadline bars

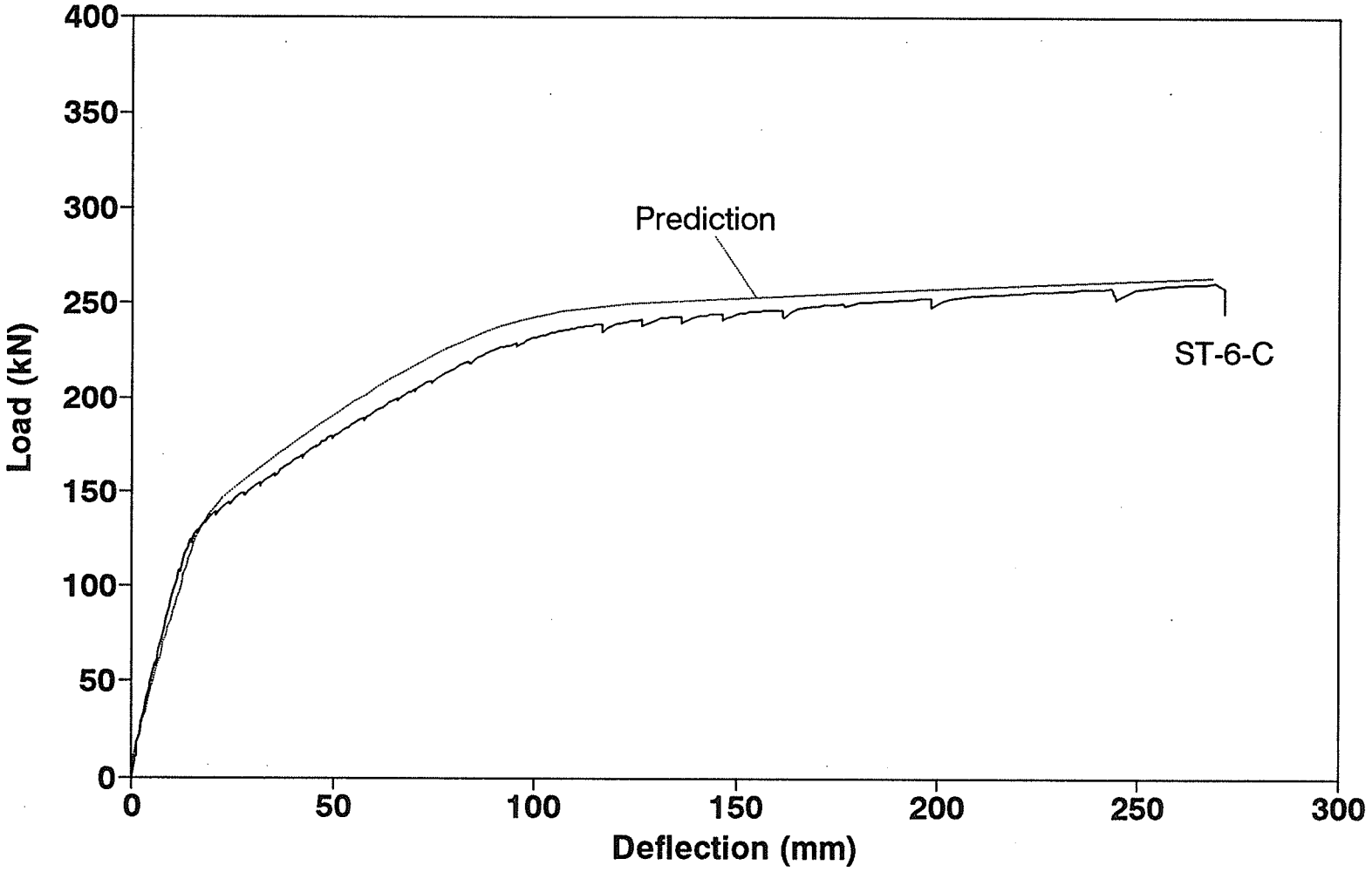

Figure 5.7 (c) Measured and predicted load - deflection diagrams for beam prestressed by steel strands

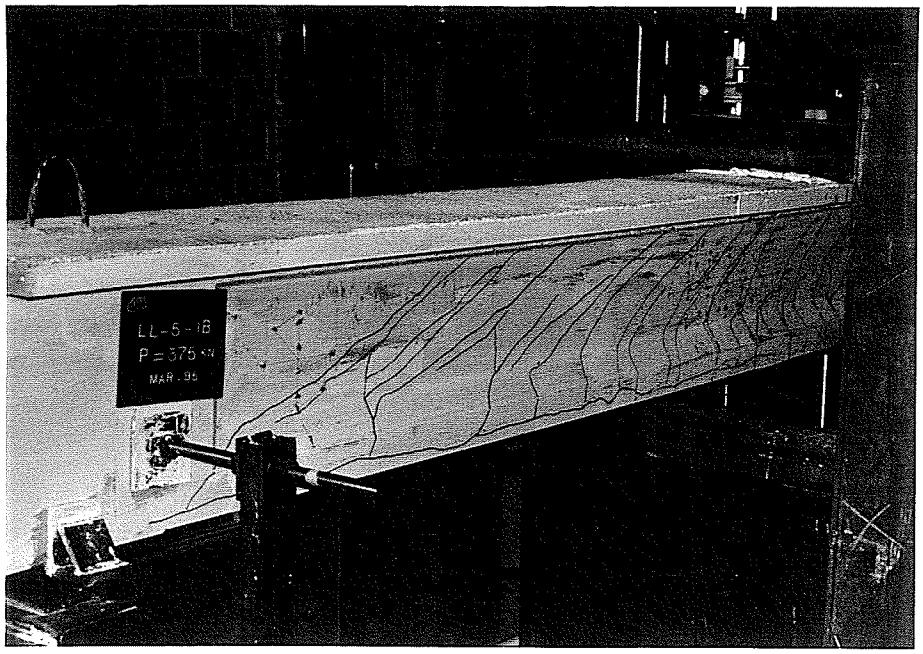

Figure 5.8 Diagonal cracks covering the entire span of beams prestressed by Leadline bars

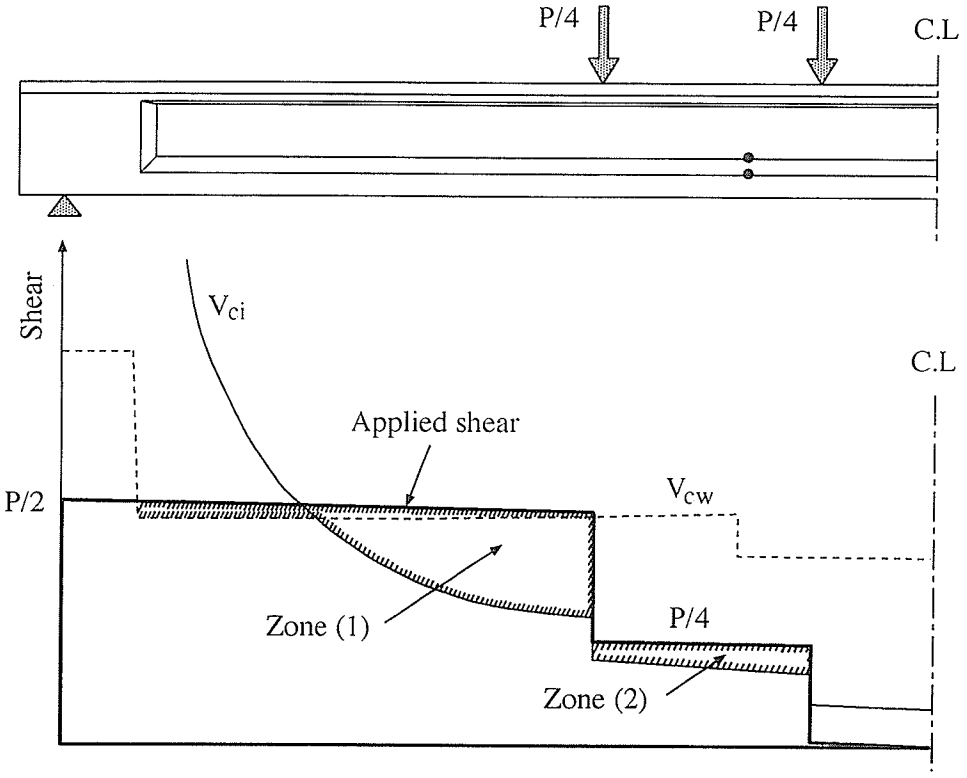

Figure 5.9 Locations of critical zones in shear

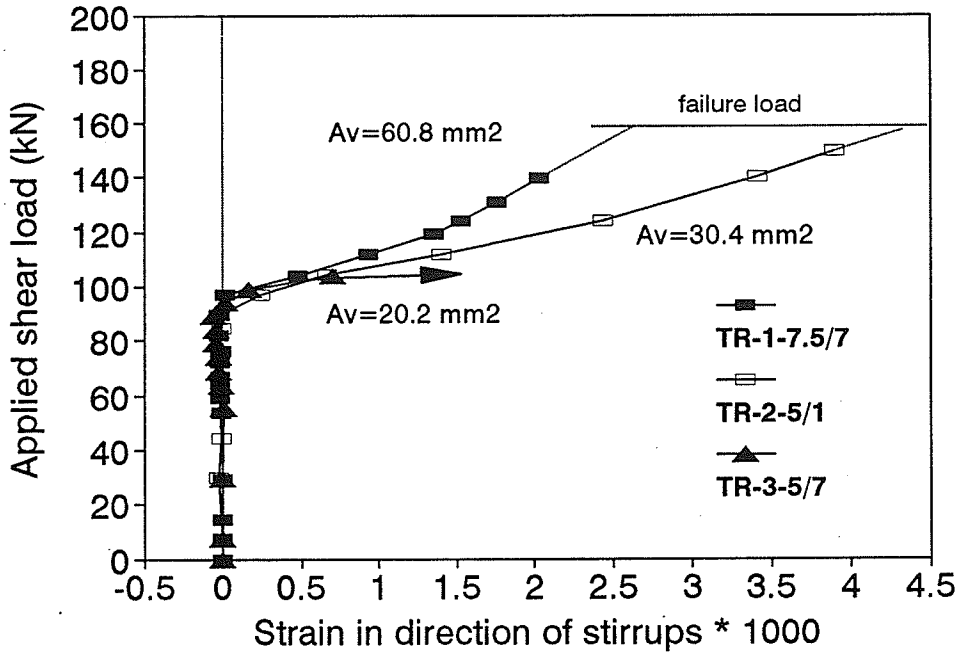

(a)

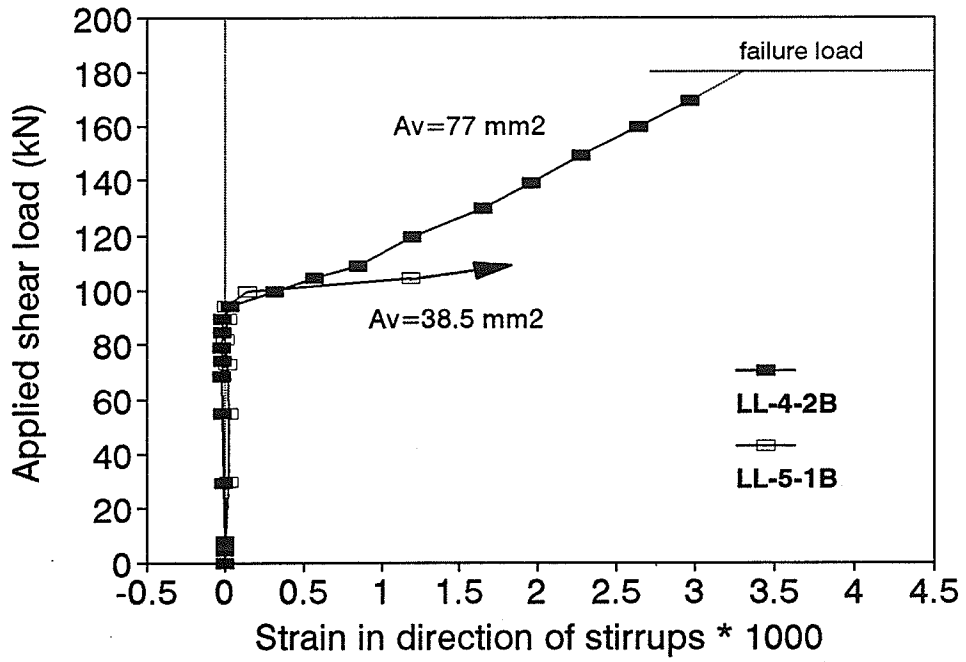

(b)

Figure 5.10 Effect of web reinforcement ratio on stirrups strain

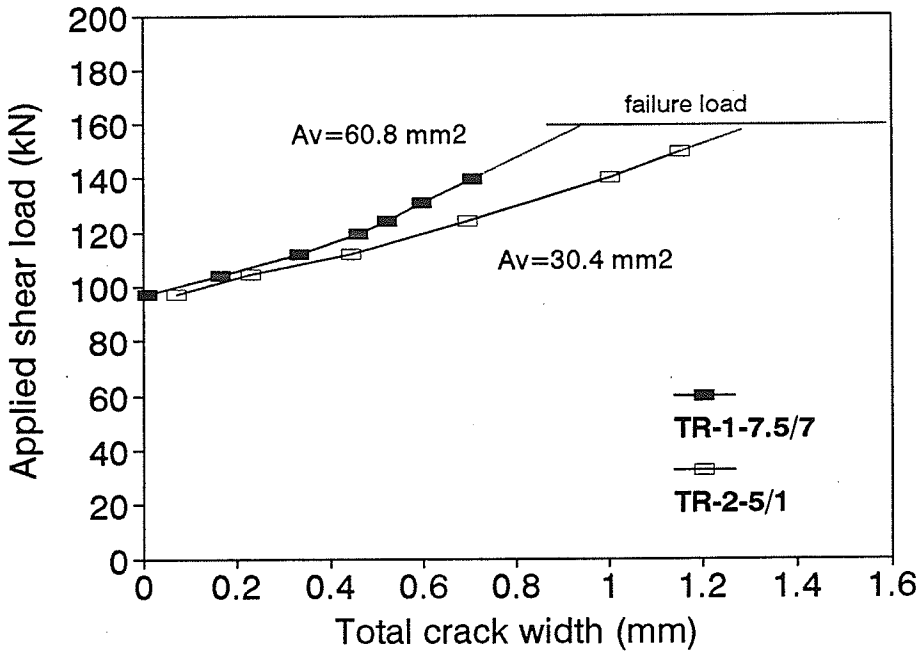

(a)

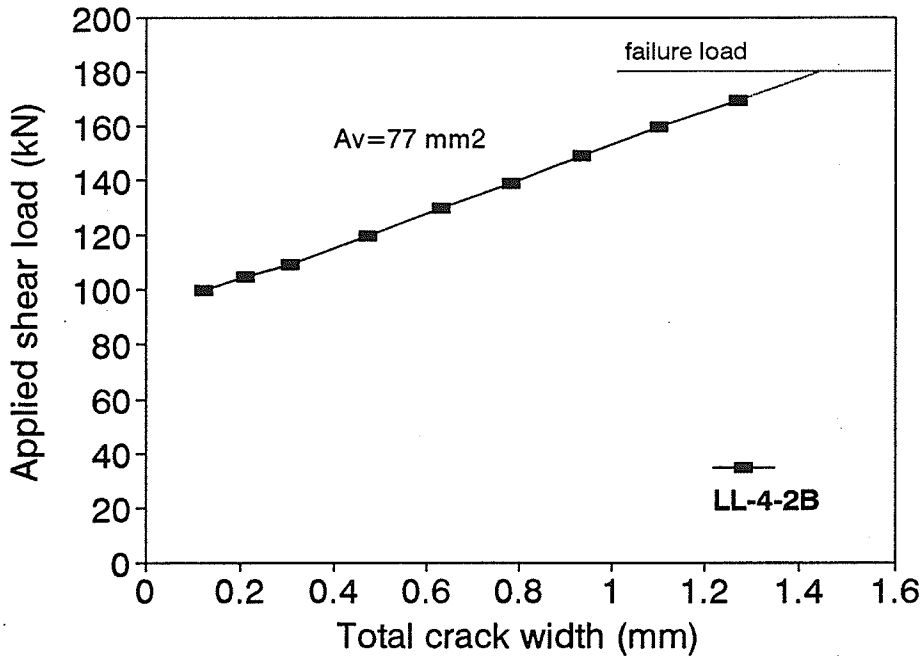

(b)

Figure 5.11 Effect of web reinforcement ratio on the diagonal crackwidth

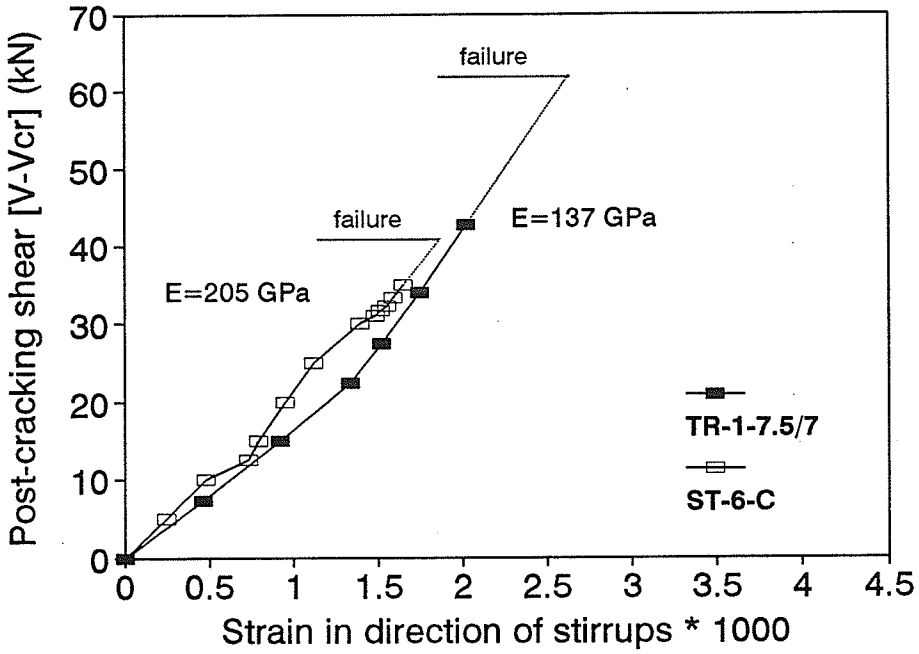

Figure 5.12 Effect of elastic modulus on the stirrups strain

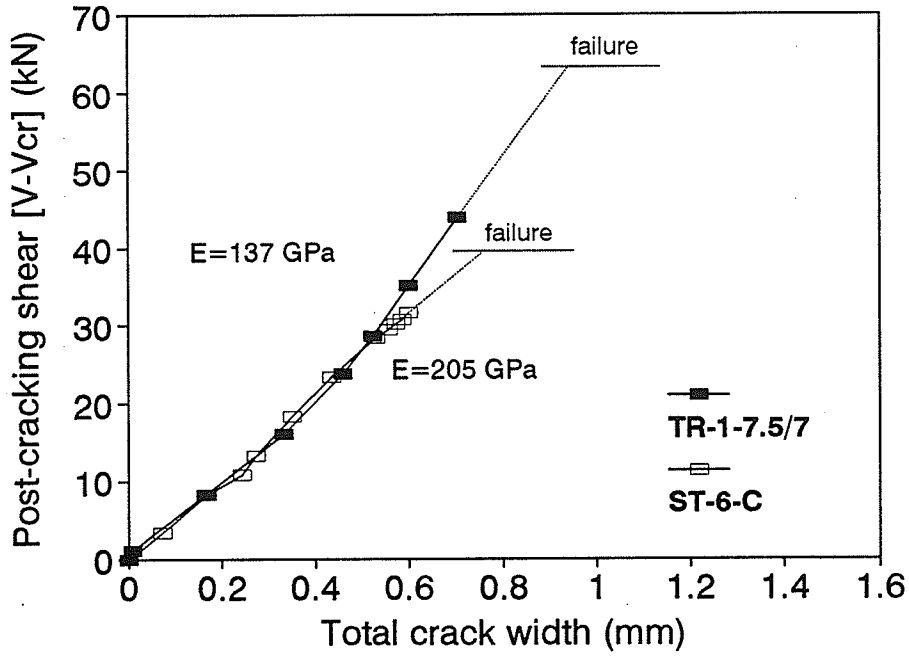

Figure 5.13 Effect of elastic modulus on the diagonal crack width

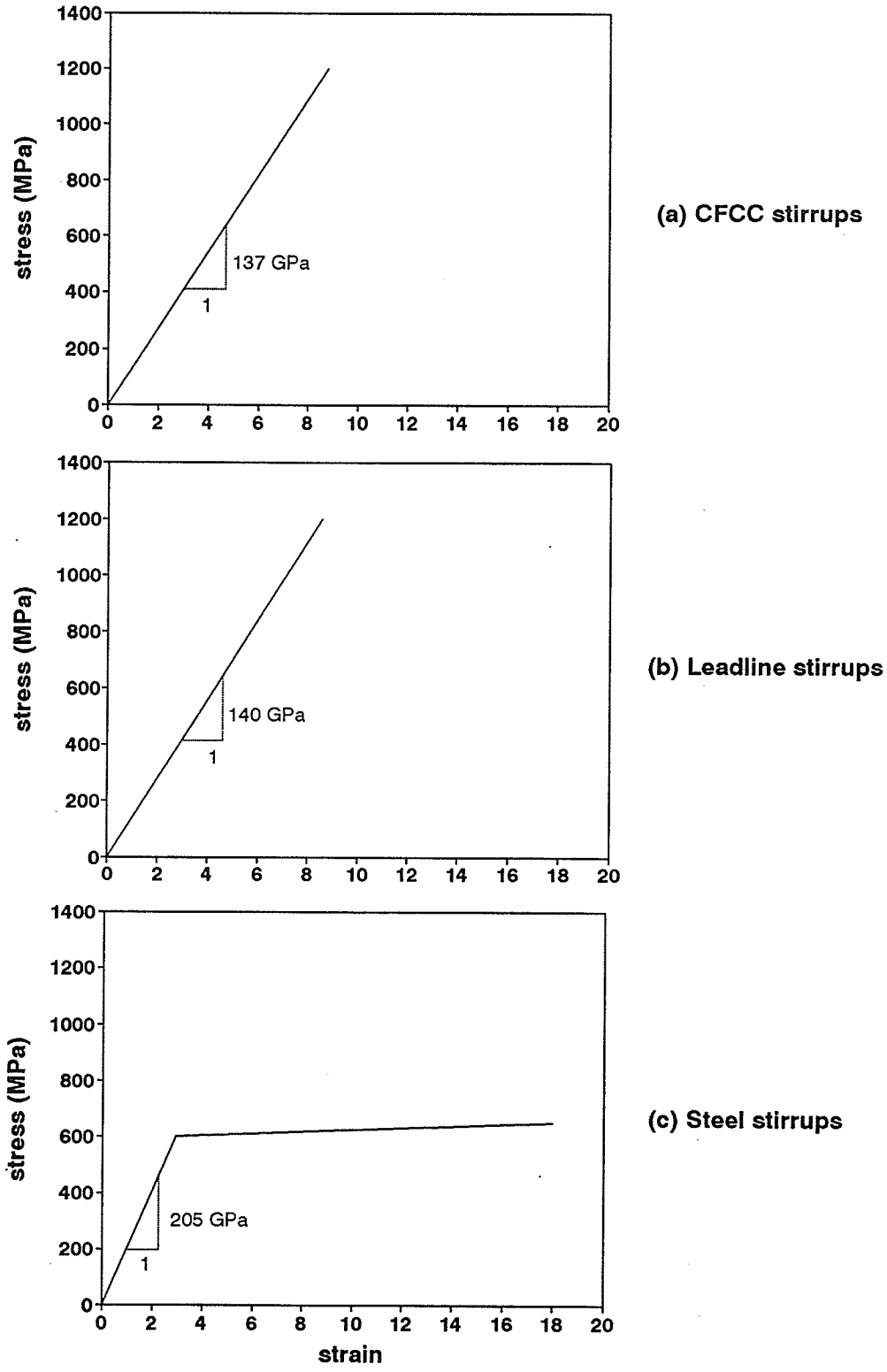

Figure 5.14 Stress-strain curves of stirrups as used in program "RESPONSE"

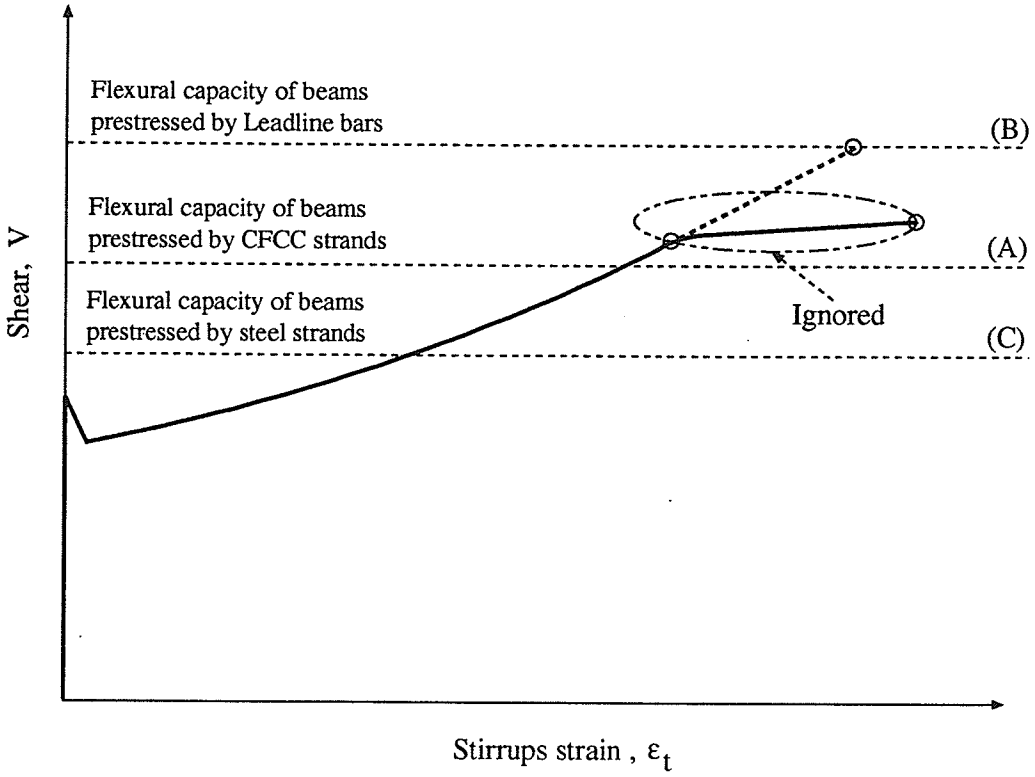

Figure 5.15 Shear - stirrups strain response as obtained from program "RESPONSE"

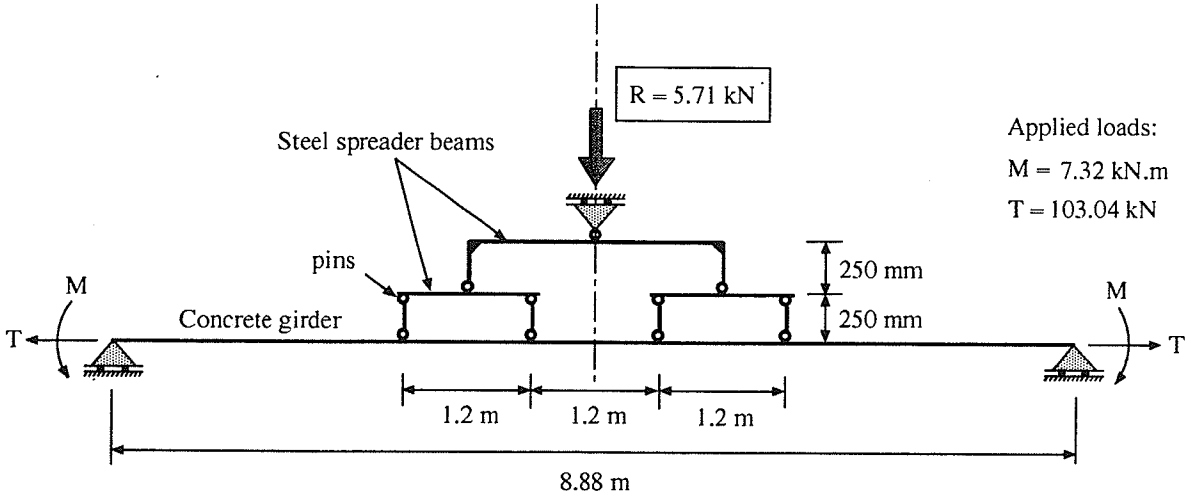

Figure 5.16 Structural model used to predict the effect of releasing post-tensioned strands

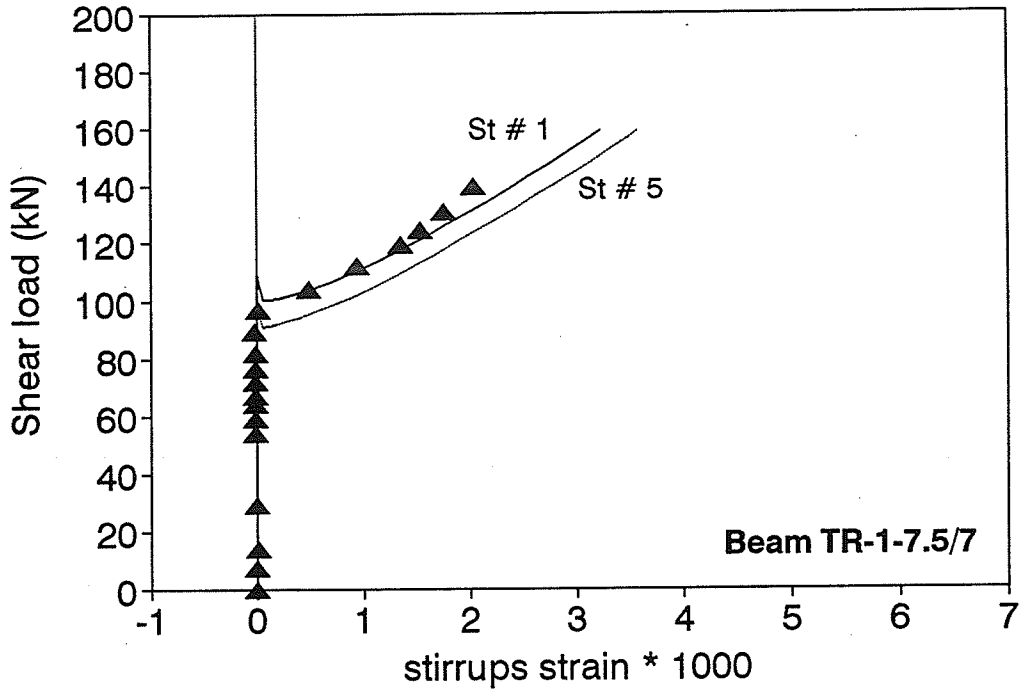

(a)

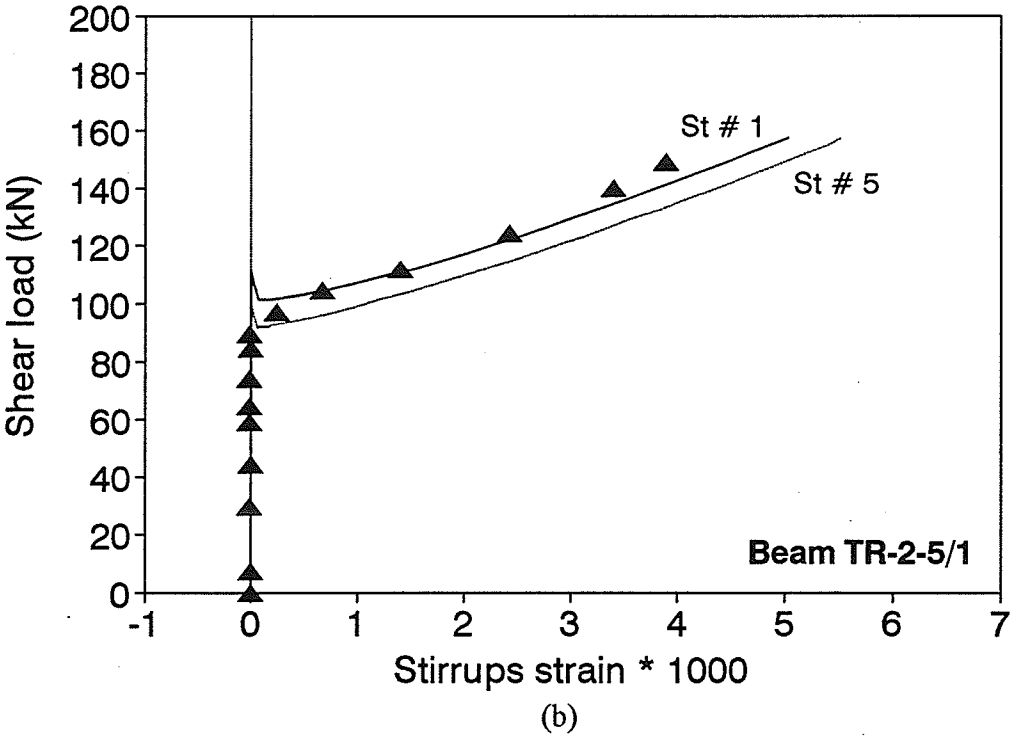

(b)

Figure 5.17 Modified compression field theory prediction

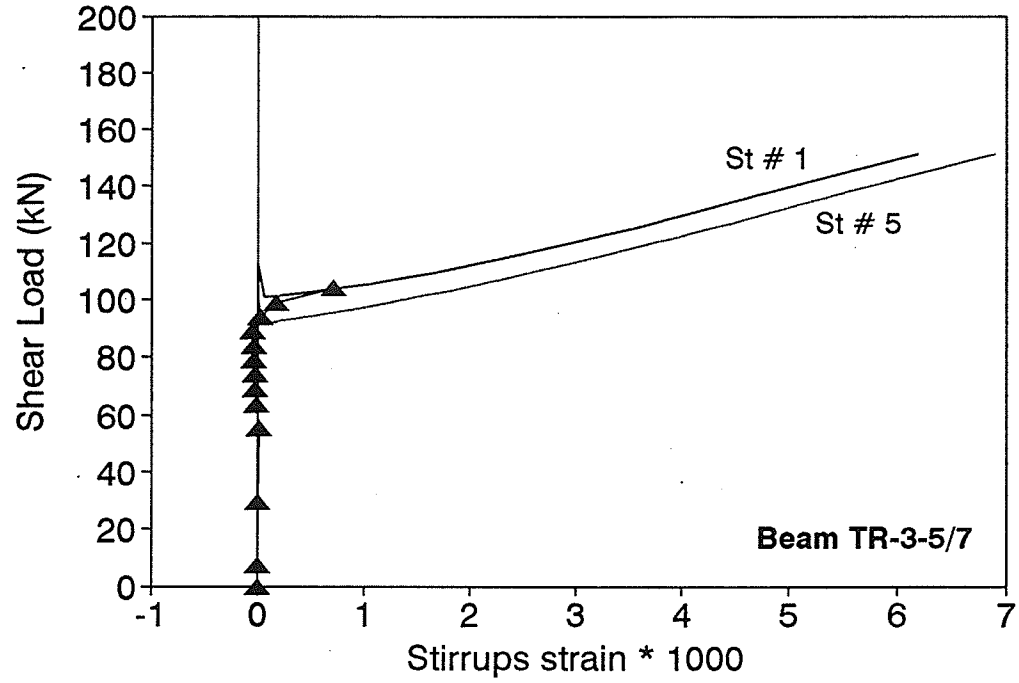

(c)

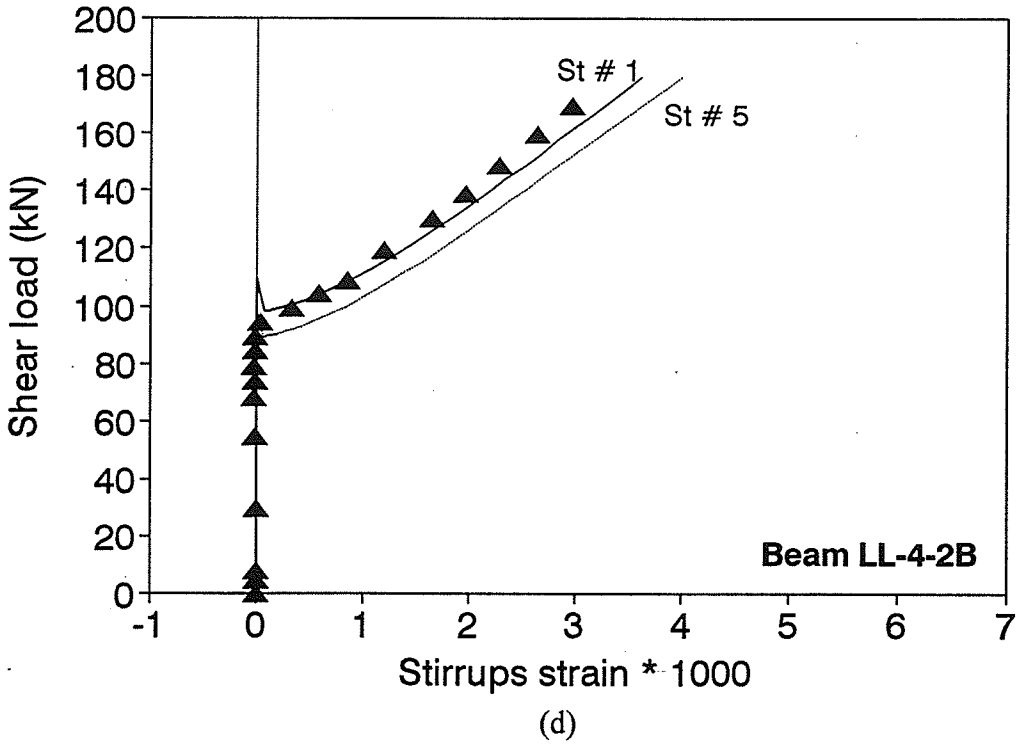

(d)

Figure 5.17 (cont.) Modified compression field theory prediction

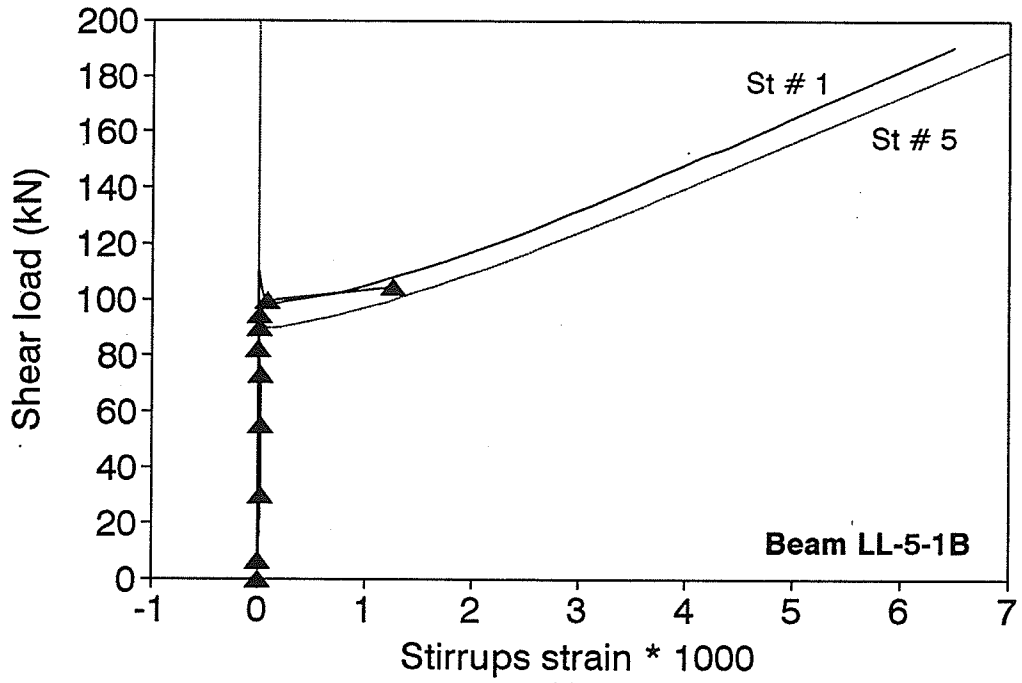

(e)

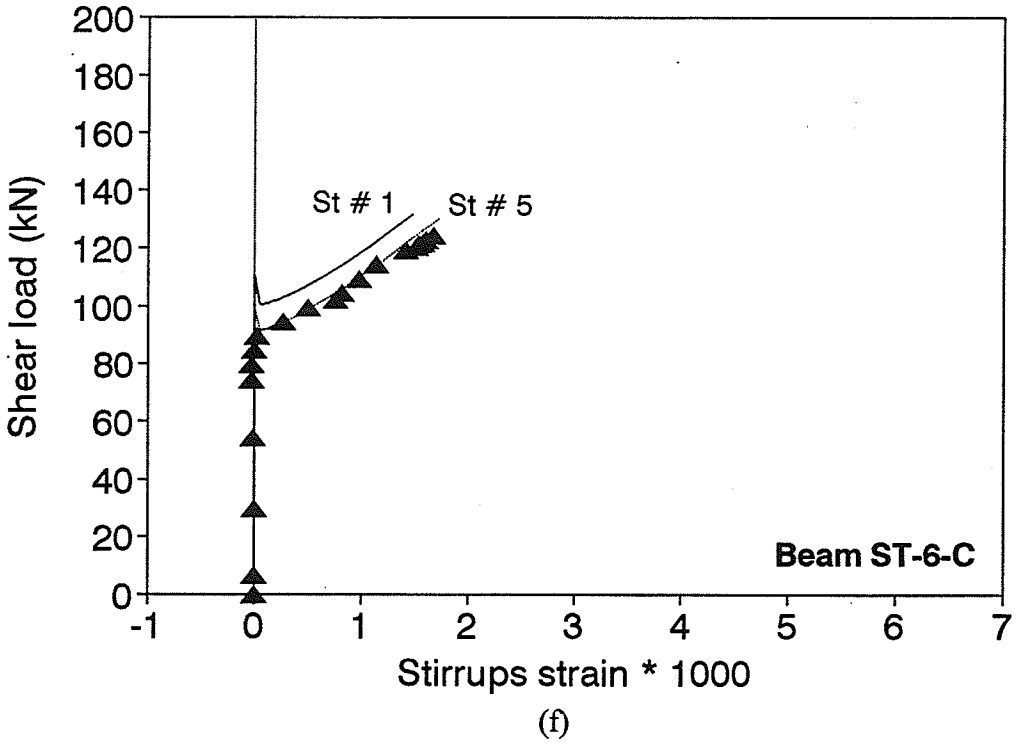

(f)

Figure 5.17 (cont.) Modified compression field theory prediction

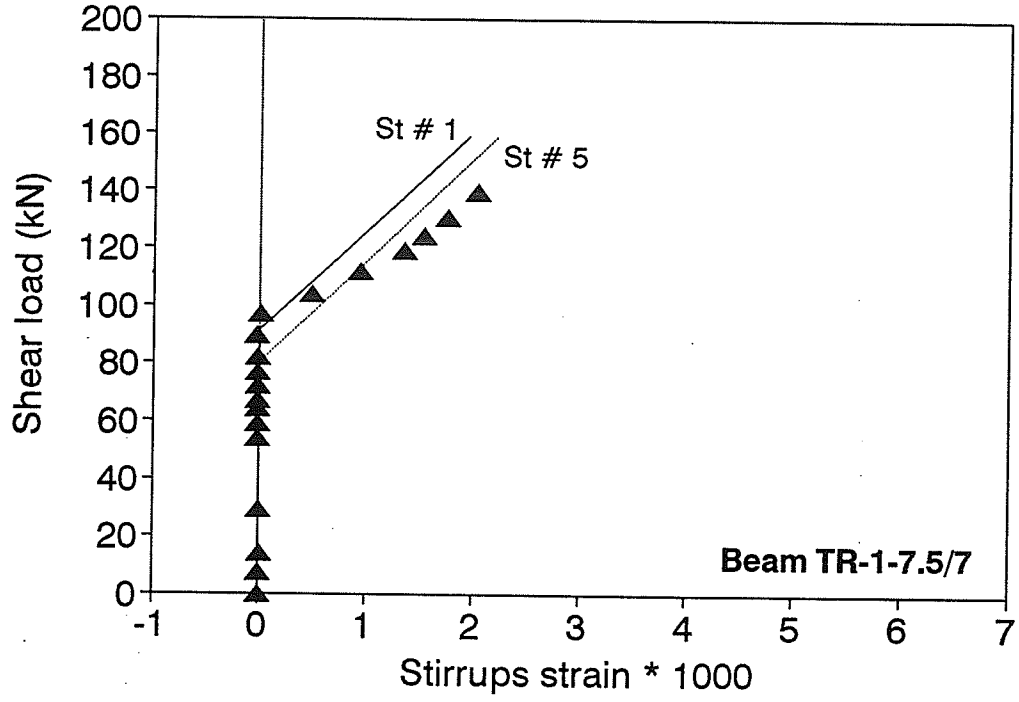

(a)

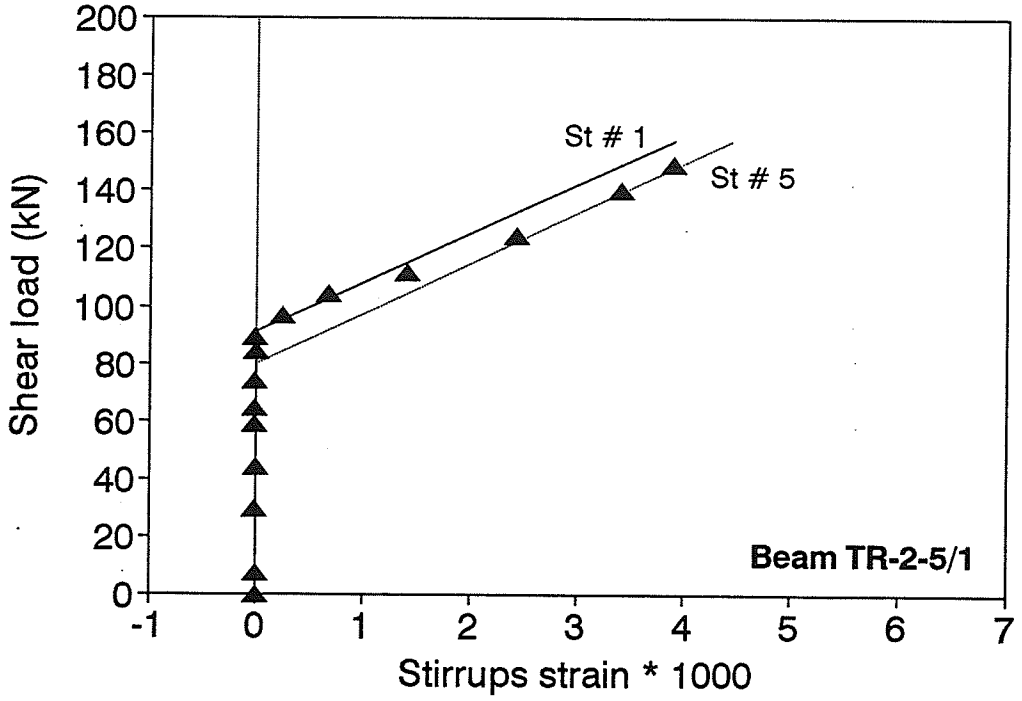

(b)

Figure 5.18 ACI code prediction

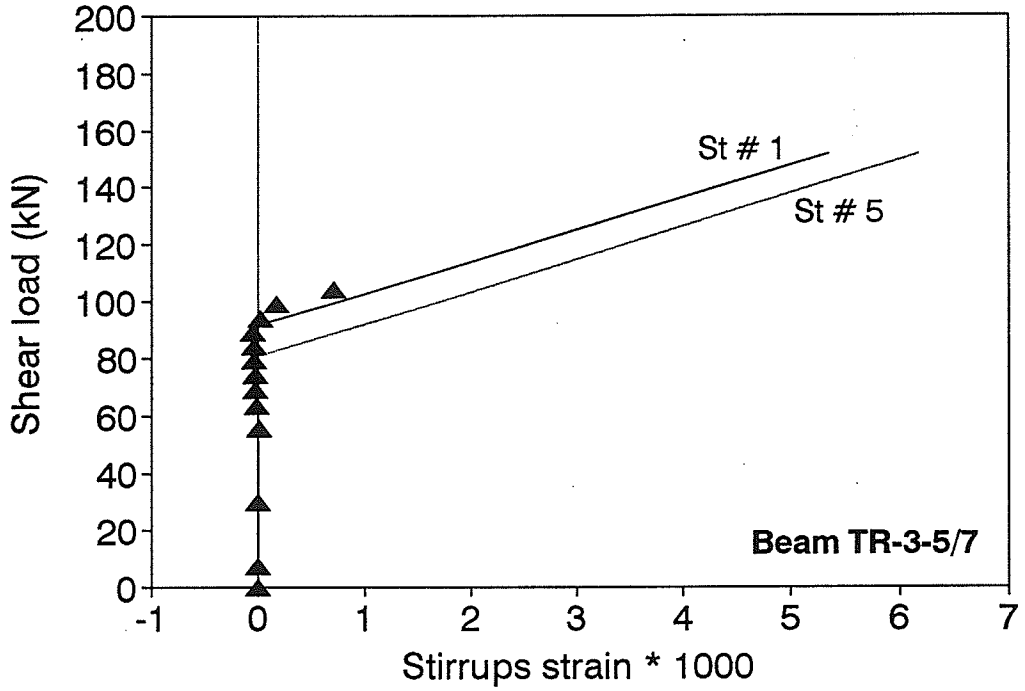

(c)

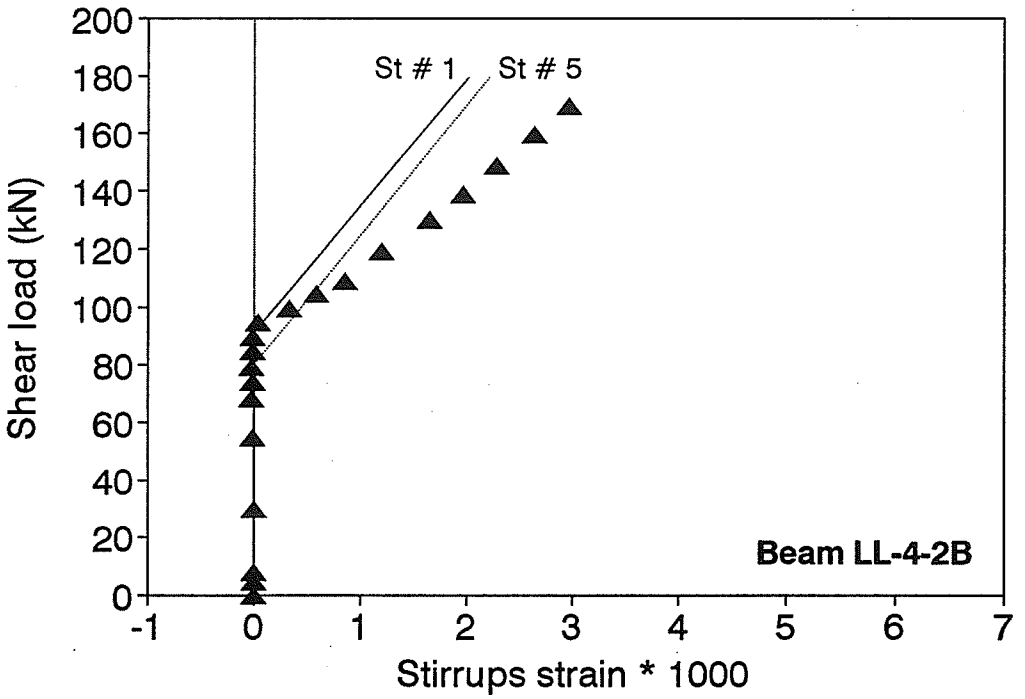

(d)

Figure 5.18 (cont.) ACI code prediction

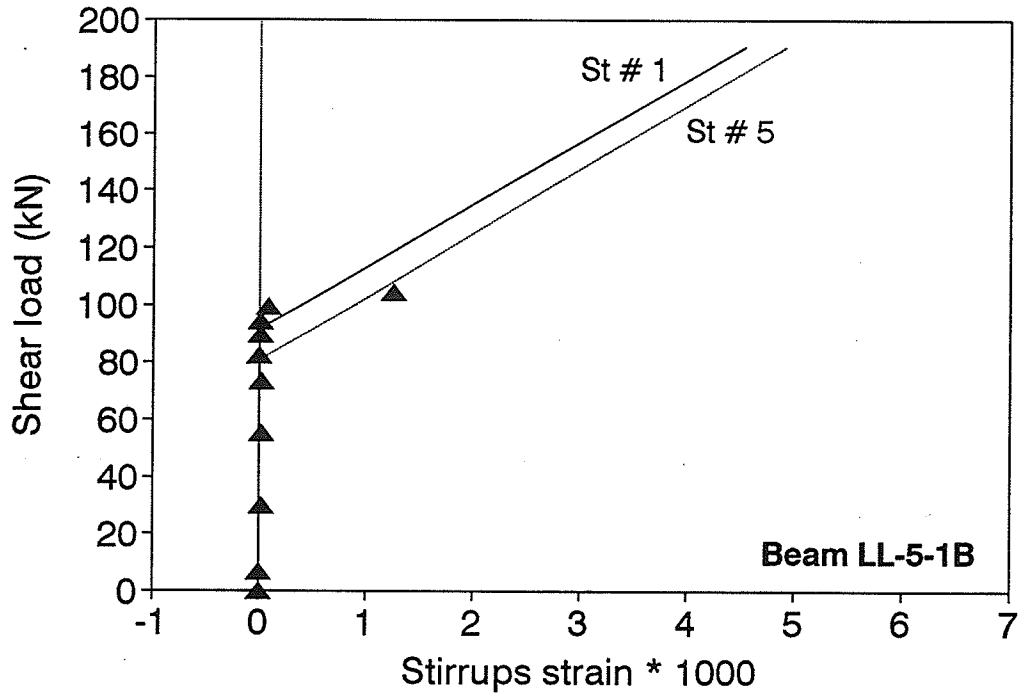

(e)

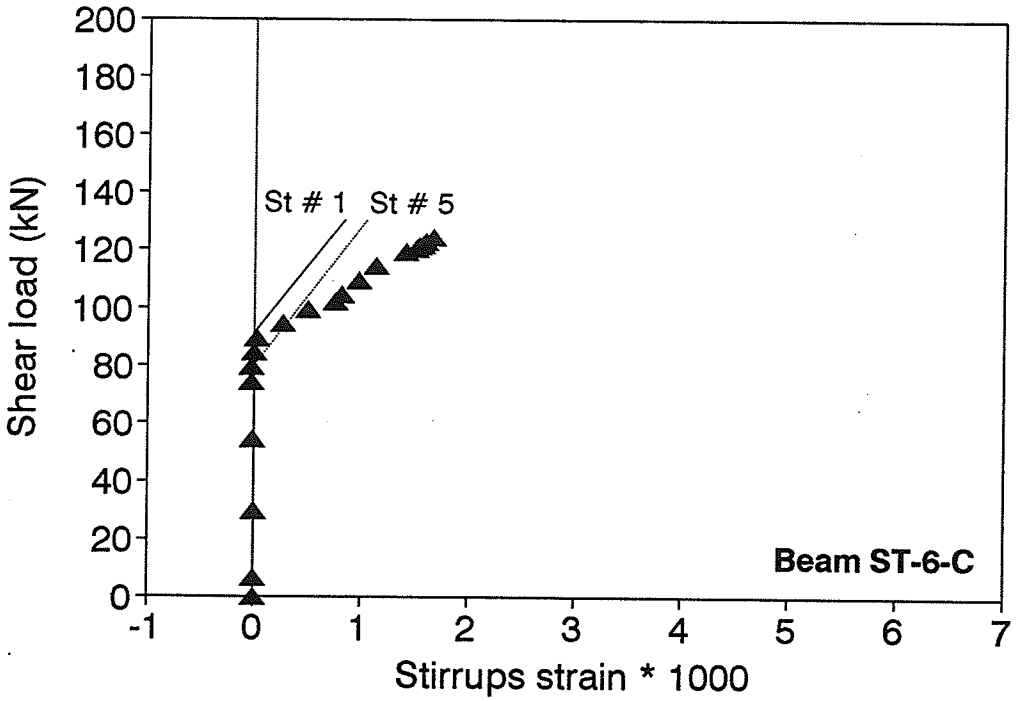

(f)

Figure 5.18 (cont.) ACI code prediction

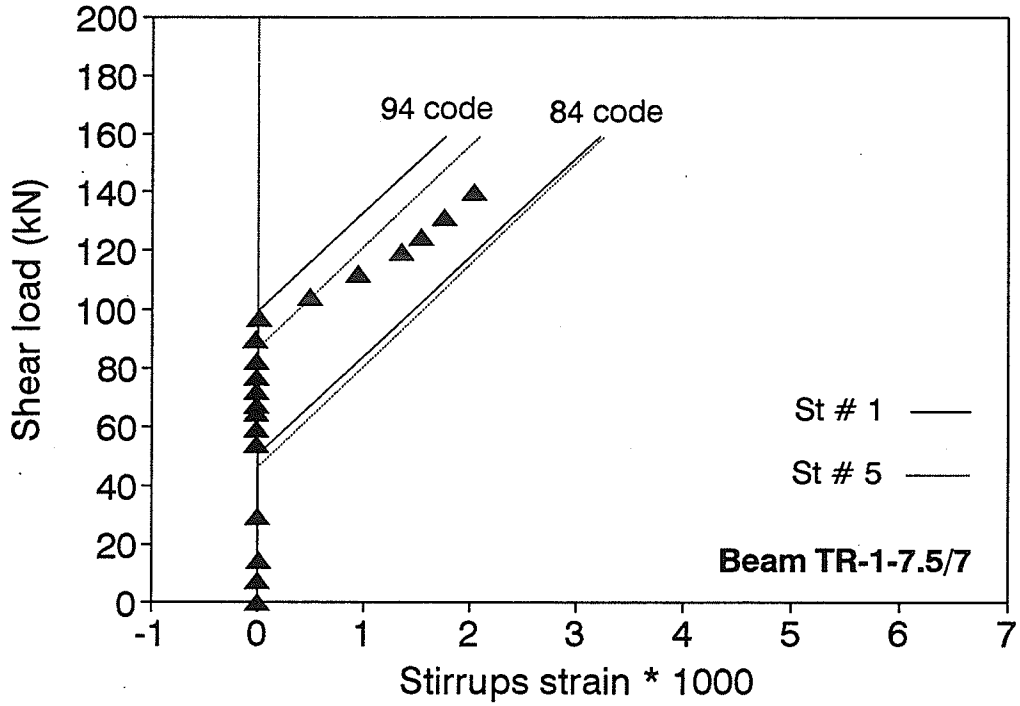

(a)

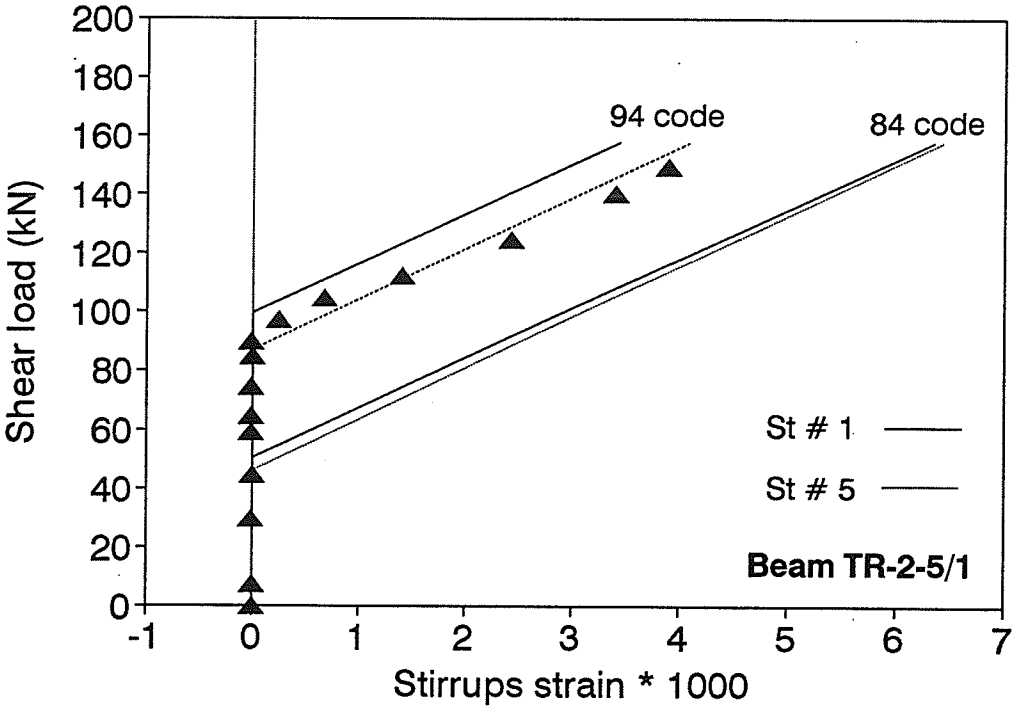

(b)

Figure 5.19 Prediction using simplified method of 84 and 94 CSA code

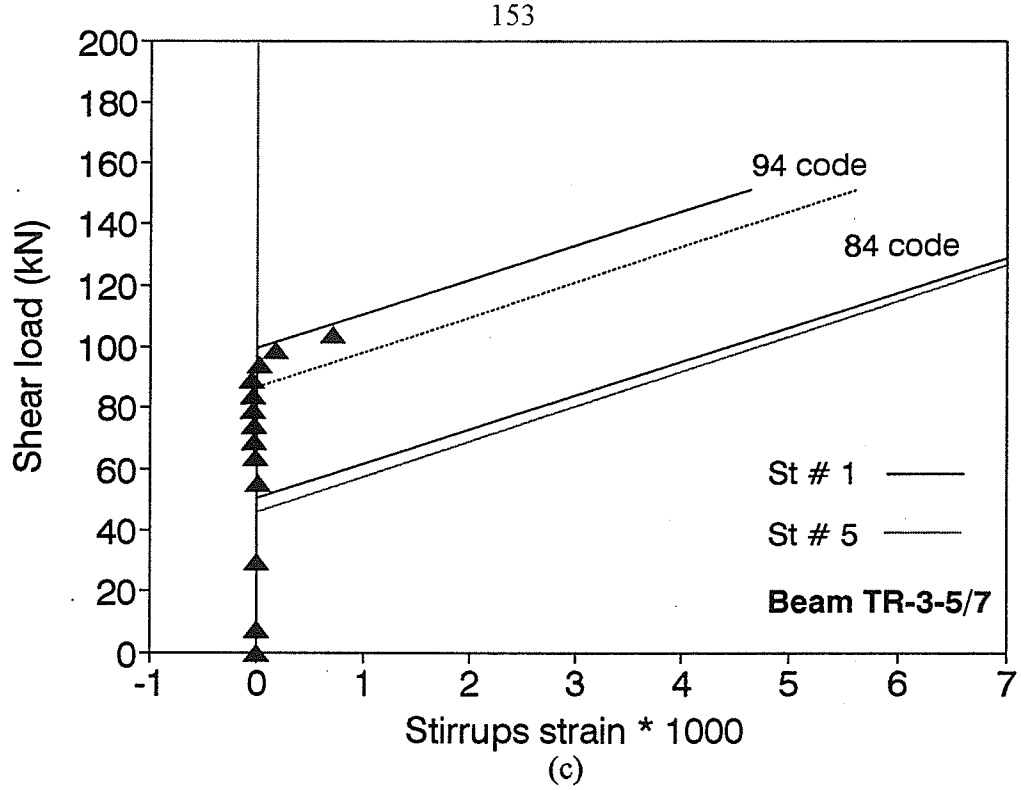

(c)

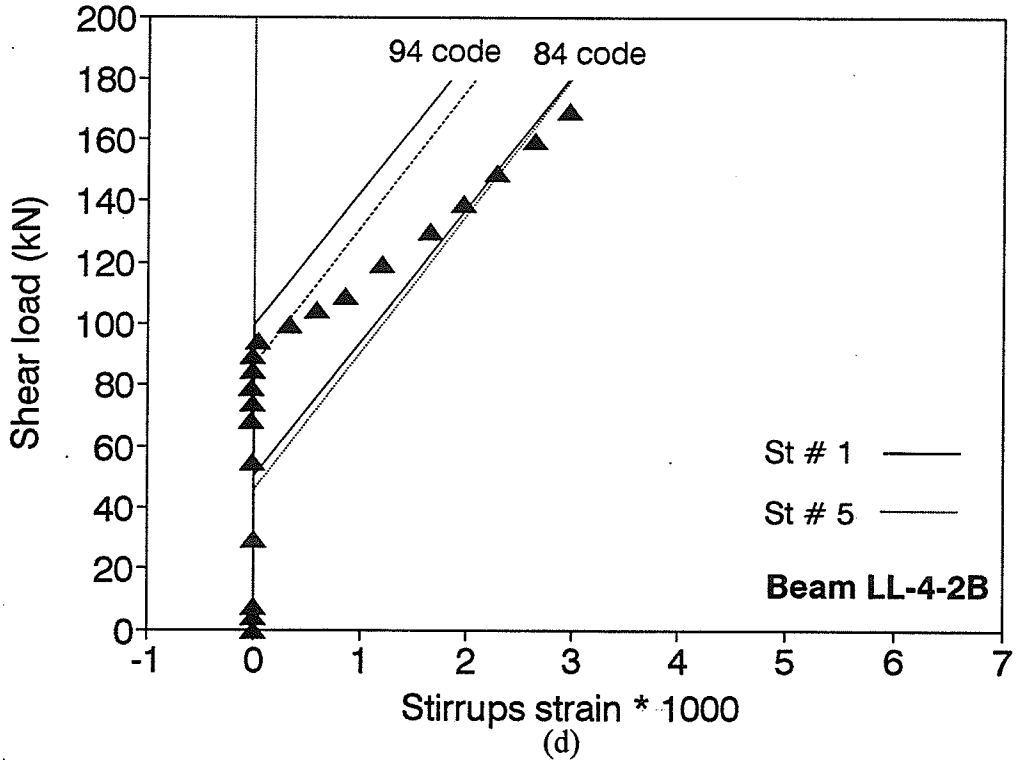

(d)

Figure 5.19 (cont.) Prediction using simplified method of 84 and 94 CSA code

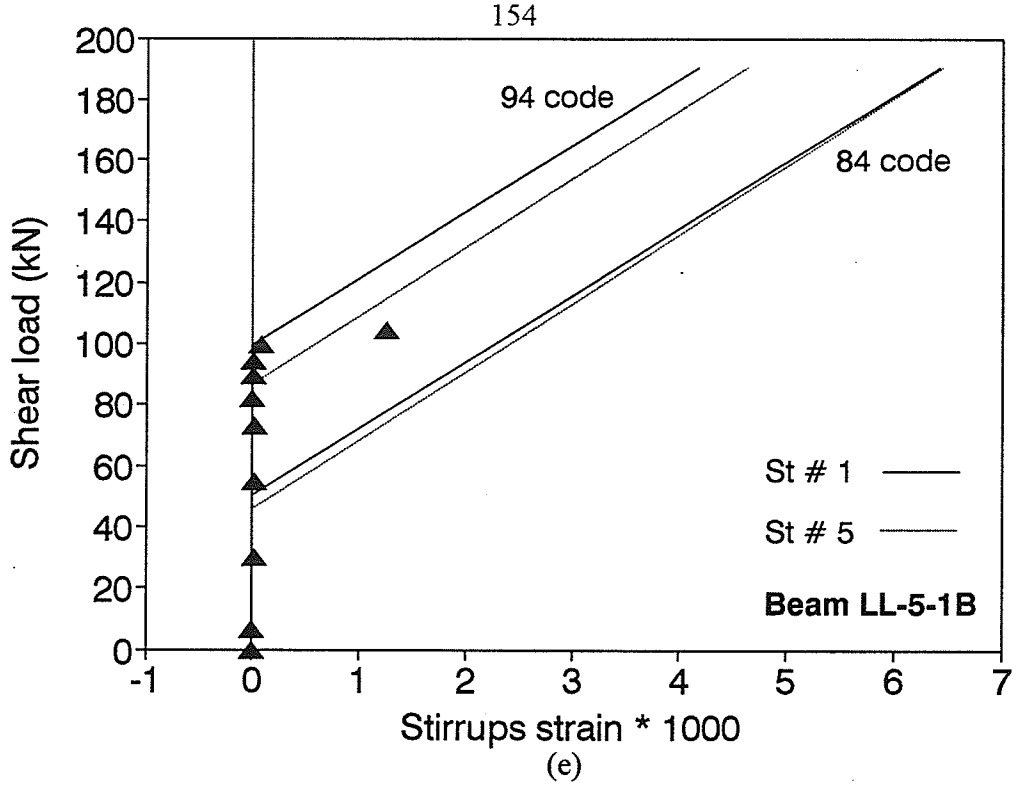

(e)

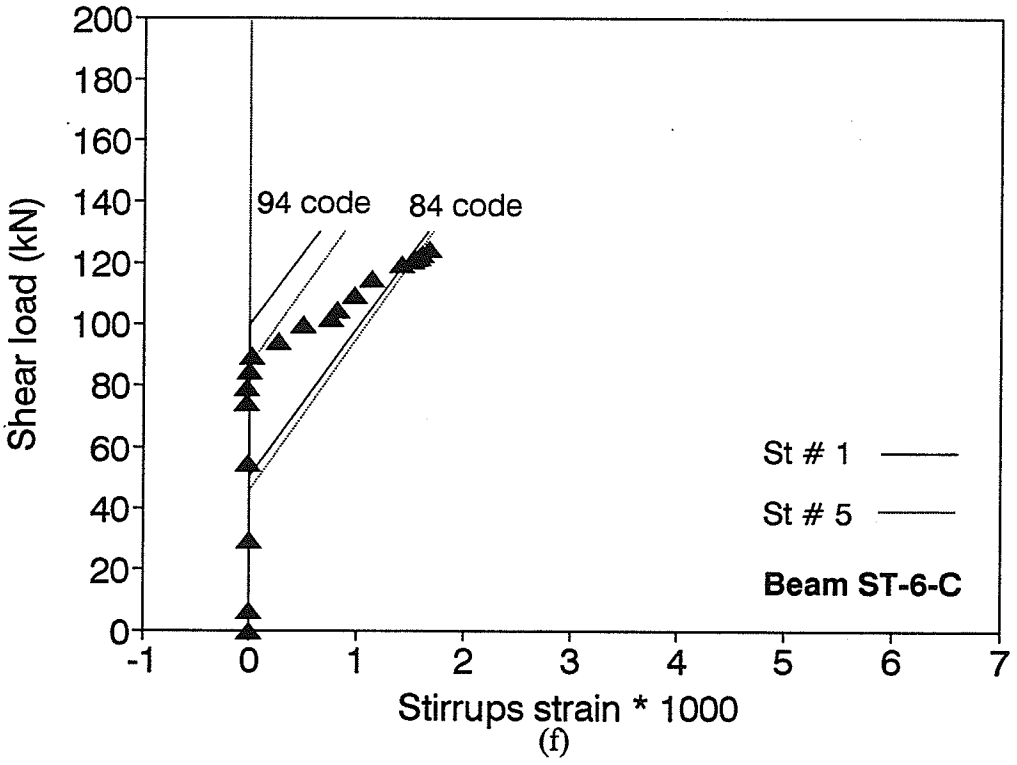

(f)

Figure 5.19 (cont.) Prediction using simplified method of 84 and 94 CSA code

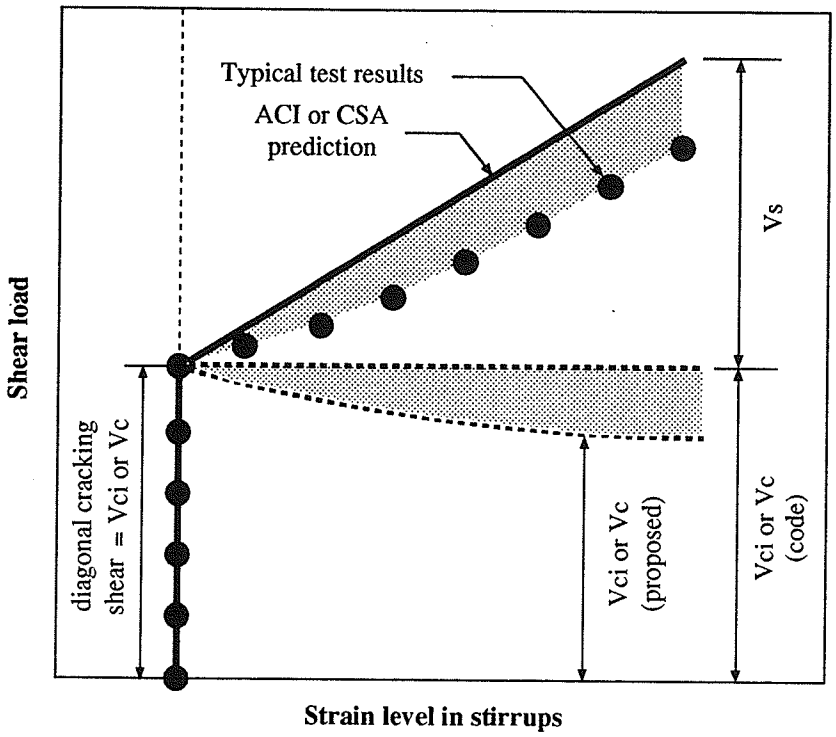

Figure 5.20 Proposed reduction in concrete contribution in shear

CHAPTER 6

SUMMARY AND CONCLUSIONS

6.1 SUMMARY

A total of six large scale prestressed concrete I-girders with top slabs in composite action with the girders were tested as model for the proposed Headingley bridge in Winnipeg, Manitoba, Canada. Five beams were totally reinforced for shear and prestressing reinforcements by CFRP and one beam by conventional steel strands and steel stirrups. The experimental program was undertaken to examine the effect of different stirrups sizes, types, and configurations on the shear behaviour and dowel action between the girder and the slab. The beams were also tested to examine the efficiency of the CFRP draped prestressing tendons. Test results provide assessment of the validity of the current analytical and design approaches for shear using FRP stirrups.

6.2 CONCLUSIONS

Based on the observed behaviour of the beams and the test results, the following conclusions could be drawn:

1. The web reinforcement ratio, controlled by stirrups size or configuration, certainly affected the induced stress level in the stirrups and the diagonal crack width. However, the effect was not directly proportional to the web reinforcement ratio.
2. Due to the relatively high elastic modulus of CFRP in comparison to other FRP reinforcements, the effect of the elastic modulus on the induced strain in the stirrups and the diagonal crack width was insignificant and was not directly proportional to

the elastic modulus ratio.

3. The flexural behaviour of beams prestressed by CFRP tendons showed similar stiffness to the beam prestressed by steel strands after flexural cracking up to yielding of the steel. Again this behaviour is attributed to the relatively high elastic modulus of CFRP tendons compared to other FRPs.

4. The modified compression field theory predicted well the entire behaviour of the critical section in shear. Both, the ACI code and the simplified method of the new 1994 CSA code predicted well the shear cracking load, however, they both under estimated the strain level in stirrups after diagonal cracking occurs. This suggests that the concrete contribution, V_{ci} of ACI or V_c of CSA is gradually reduced after diagonal cracking. The simplified method of the 1984 CSA code greatly under estimated the shear cracking load of the beams.

5. Draping of CFRP prestressing tendons is practical, feasible, and did not influence the flexural capacity, however, flexural failure could occur at the bent point location. It should be noted that an angle of four degrees was used, which is typically used for long prestressed bridge girders.

6. No slip was observed of the prestressing reinforcements nor between the top slab and the girder. This suggests that the combined resistance of both the concrete and the dowel strength of the stirrups at the interface surface is adequate to transfer the horizontal shear stress between the girder and the slab.

7. For beams controlled by the flexural capacity, variation of the web reinforcement ratio did not significantly affect the flexural behaviour of the beams.

8. Shear failure of beam LL-4-2B was very brittle and caused breaking the beam to several pieces due to the energy released from rupture of the longitudinal bars after the stirrups has stretched and broke the concrete cover due to the improper configuration of the stirrups originally planned for the bridge.

9. The beams prestressed by CFRP tendons exhibited higher flexural strength compared to the beam prestressed by conventional steel strands of almost the same prestressing level and flexural reinforcement ratio. The beams prestressed by Leadline bars and CFCC strands failed at load level, 46 and 22 percent, higher than the beam prestressed by steel strands respectively.

6.3 RECOMMENDATIONS FOR FUTURE WORK

This experimental program was mainly conducted to model the bridge girders which are typically designed for shear capacity higher than the flexural capacity to insure enough ductility before failure. However, in order to achieve full understanding of the behaviour of CFRP stirrups in shear, the research work should be extended in future to the following areas:

1. To test beams with shear capacity lower than the flexural capacity in order to utilize the full tensile strength of the CFRP stirrups and study the effect of the inclined principal stresses on the tensile strength of the stirrups, which is believed to be reduced. Another variables could also be introduced including the spacing of the stirrups and the shear span - to depth ratio of the beams.

2. To introduce a mathematical model for the proposed reduction of the concrete contribution in shear resistance after diagonal cracking, V_{ci} and V_c, given by the ACI

and the simplified method of CSA respectively.

3. To examine the dowel strength of CFRP stirrups using concrete composite beam tests.

4. To test beams with larger range of web reinforcement ratio in order to verify the nonlinear relation ship relating the stress level in stirrups to the web reinforcement ratio.

REFERENCES

1. Abdelrahman, A. A., Tadros, G., and Rizkalla, S.H., " Test Model for the First Canadian Smart Highway Bridge", ACI structural journal, V.92, No. 4, July - August 1995, pp 451- 458.

2. ACI committee 318, "Building Code Requirements for Reinforced Concrete (ACI 318M-89), " and Commentary - ACI 318 RM-89, American Concrete Institute, Detroit, 1989, 353 pp.

3. Collins, M. P., and Mitchel, D., 1991, "Prestressed Concrete Structures", PRENTICE HALL, Englewood cliffs, New jersey 07632, 766 pp.

4. Collins, M.P., and Denis, M., "Shear and Torsion Design of Prestressed and Non-prestressed Concrete Beams", PCI Journal, Sept./Oct. 1980, vol. 25, no. 5, pp.32-100.

5. Collins, M. P., Mitchel, D., Felber, A. J., and Kuchma, D. A., computer program "RESPONSE Version 1.0", 1990, for use with Prestressed Concrete Structures.

6. Collins, M. P., "The Modified Compression Field Theory and Shear Provisions of the LRFD Design Specifications", submitted to the American Concrete Institute for publication in the ACI structural Journal.

7. CPCI metric design manual "Precast and Prestressed Concrete", Copyright © 1987 by Canadian Prestressed Concrete Institute.

8. CSA STANDARD A23.3-94, "Design of Concrete Structures with Explanatory Notes", Canadian Standards Association, Toronto, Ontario, Canada, 1994, 220 pp.

9. "Current and Future Applications of advanced Composite Materials in Structural

Engineering", published by The Canadian Society for Civil Engineering, Dec. 1993, 44 pp.

10. Grant, L., Tadros, G., and Rizkalla, S., " Toward Development of Bridges in the Next Century", Proceeding of the Second International RILEM Symposium (FRPCS-2), August 1995, pp 654 - 662.

11. MacGregor, James G., 1988, "REINFORCED CONCRETE Mechanics and Design", Prentice Hall, Englewood Cliffs, New Jersey 07632, 799 pp.

12. Maruyama, T., Honma, M., and Okamura, H., " Experimental Study on the Diagonal Tensile Characteristics of Various Fibre Reinforced Plastic Rods", Transactions of the Japan Concrete Institute, Vol. 11, 1989, pp 193 - 198.

13. Mitsubishi Kasei, "Leadline Carbon Fibre Rod Technical Data", Japan, Dec. 1992, 50 pp.

14. Miyata, S., Tottori, S., Terada, T., and Sekijima, K., " Experimental Study on Tensile Strength of FRP Bent Bars", Transactions of the Japan Concrete Institute, Vol. 11, 1989, pp 193 - 198.

15. Mufti, A. A., Erki, M-A., and Jaeger, L. G., "Advanced Composite Materials in Bridges and Structures in Japan", published by The Canadian Society for Civil Engineering, August 1992, Montreal, Canada, 172 pp.

16. Mufti, A. A., Erki, M-A., and Jaeger, L. G., "Advanced Composite Materials with Applications in Bridges", published by The Canadian Society for Civil Engineering, May 1991, Montreal, Canada, 297 pp.

17. Pincheira, J. A., "Welded Wire Fabric as Shear Reinforcement in Concrete T-Beams

subjected to Cyclic Loading", M.Sc. Thesis, University of Manitoba, Manitoba, Canada, 1988.

18. "Plans of Proposed Bridge Over Assiniboine River on P.R. No. 334" by Department of Highways and Transportation, Bridges and Structures Branch, Province of Manitoba, Canada.

19. "State-Of-The-Art Report on Continuous Fibre Reinforced Materials", published by Japan Society of Civil Engineers, JSCE, 1993, 164 pp.

20. Tokyo Rope Mfg. Co., Ltd., "Technical Data on CFCC", Japan, Oct. 1993, 100 pp.

21. Vecchio, F. J. and Collins, M. P., "The Modified Compression-Field Theory for Reinforced Concrete Elements Subjected to Shear", ACI Journal, Vol. 83, No. 2, March - April 1986, pp. 219-231.

22. Vecchio, F. J. and Collins, M. P., "Predicting the Response of Reinforced Concrete Beams Subjected to Shear Using Modified Compression-Field Theory", ACI Structural Journal, Vol. 85, No. 3, May - June 1988, pp. 258-268.

23. Zia, P., White, R. N., and Vanhorn, D. A., " Principles of Model Analysis", Models for Concrete Structures, ACI special publication No. 24, 1970, pp 19 - 39.

APPENDIX A

APPENDIX A

EXPERIMENTAL RESULTS OF PRESTRESSED CONCRETE BEAMS FULLY REINFORCED BY CFRP REINFORCEMENTS

In this Appendix, the experimental results of beams TR-2-5/1, TR-3-5/7, LL-4-2B, LL-5-1B, and ST-6-C are presented in the same sequence presented in chapter 4 for beam TR-1-7.5/7. The layout of the strain gauges, demec stations for flexural and shear measurements are all shown in Figures 3.23, 3.24, and 3.25 respectively.

Beam TR-2-5/1

Beam TR-2-5/1

Time (days)	Case	Gauge number								
		1	2	3	4	5	6	7	8	9
0	Initial readings before jacking	1630	1886	710	1095	1158	342	430	400	-50
0	After jacking bottom straight tendons					7252	6358	7521	7224	
1	After jacking draped tendons			7041	9195					5558
1	After casting concrete of the girder			7036	9193	7248	6336	7475	7232	5566
	Before releasing form									
2	After releasing form			6775	9300	7380	6363	7281	7123	5643
3	After releasing draped tendons			6567	9064	7140	6139	7052	6933	5458
3	After applying post-tensioning	4954	5138	6506	9007	7088	6088	7011	6905	5398
3	After releasing bottom straight tendons	4933	5090	6185	8618	6701	5695	6574	6494	5118
125	Right before testing	4242	4403	5203	7553	5674	4680	5645	5503	4231
	Total losses (% Age)	21.4	22.6	29.0	20.3	25.9	27.9	26.5	25.2	23.7

Notes: - See Figure 3.23 for strain gauges layout.
- Strain = (reading at any stage) - (initial reading).
- All readings in micro strain.

Table A.2 Measured strains of prestressing tendons from jacking up to testing using electrical strain gauges

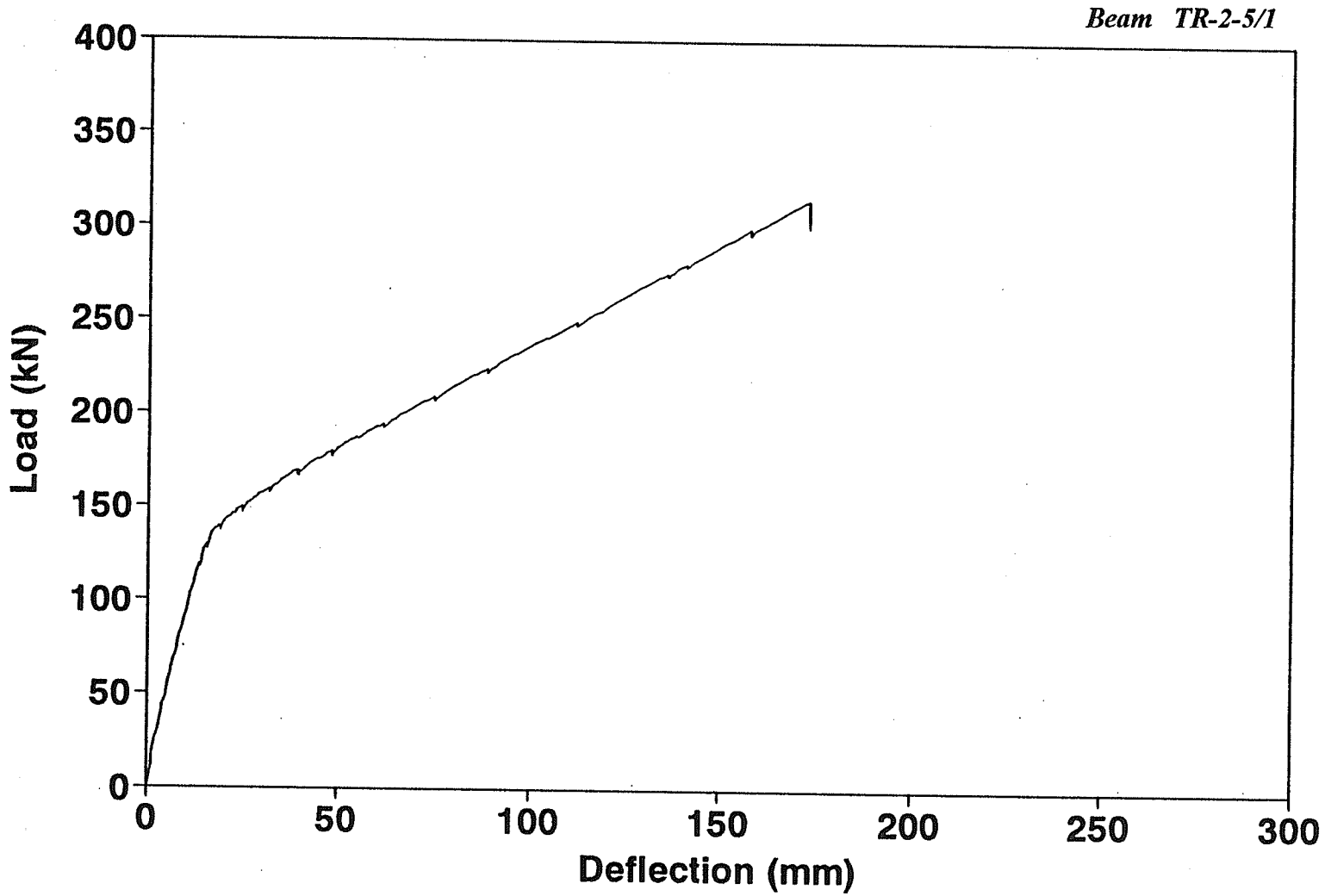

Figure A.1 Measured Load - deflection at mid span

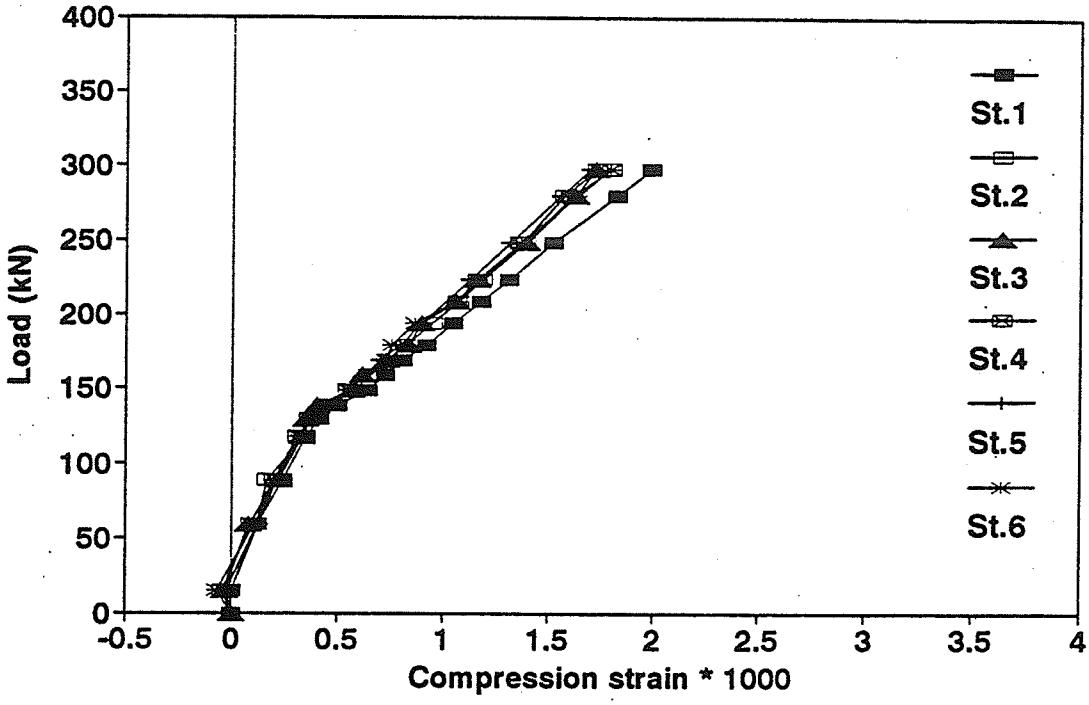

Figure A.2 Measured concrete strain at top surface at six demec stations

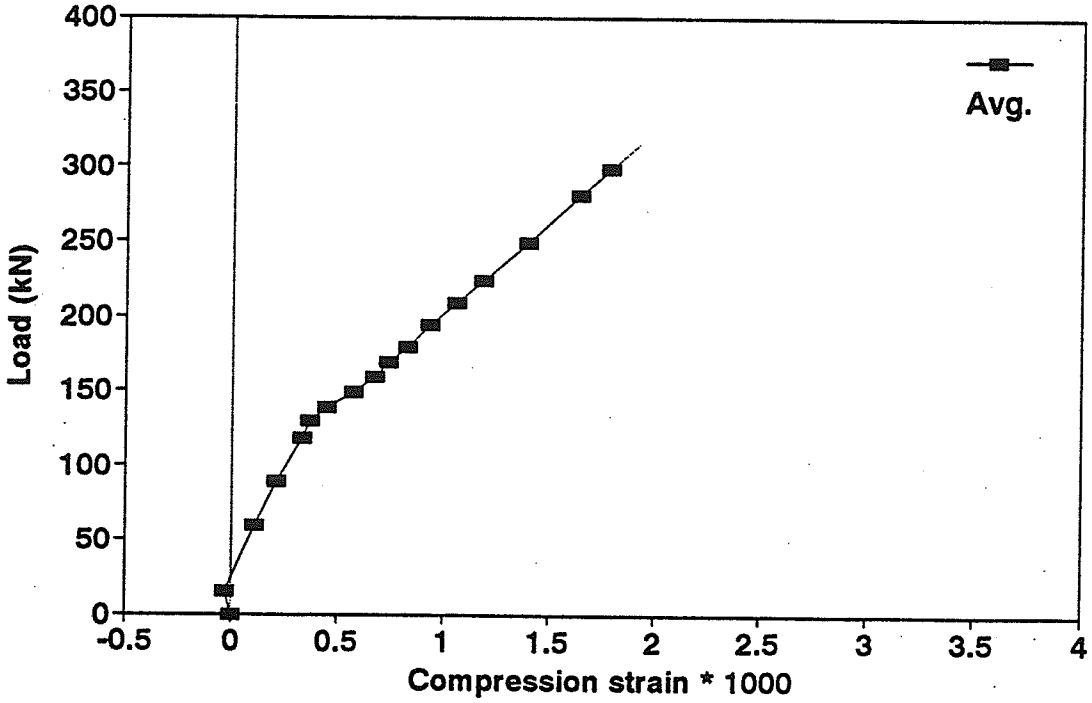

Figure A.3 Average of measured concrete strain at top surface

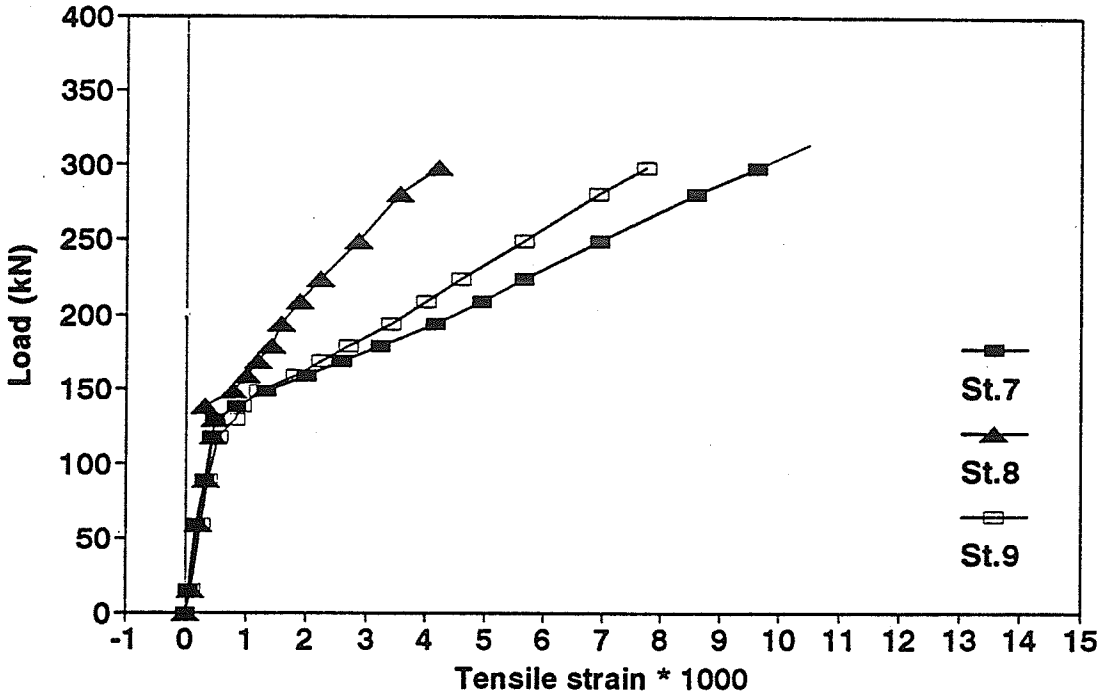

Figure A.4 Measured strains at bottom strands level at three demec stations

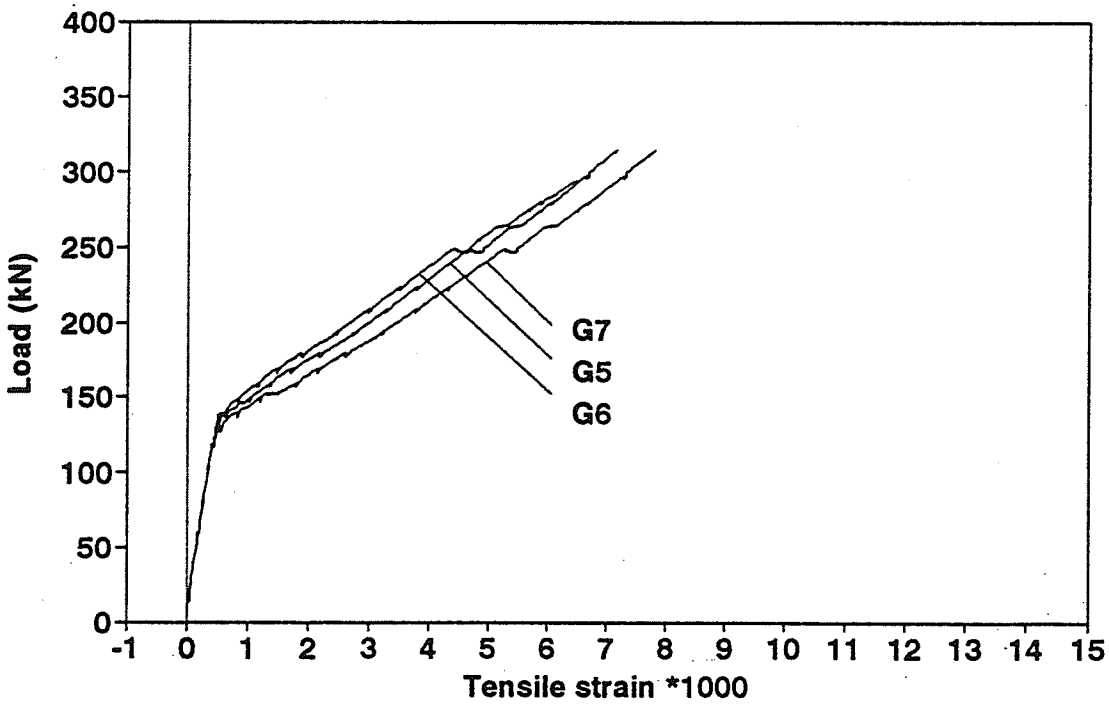

Figure A.5 Measured strains on the bottom strands during testing using strain gauges

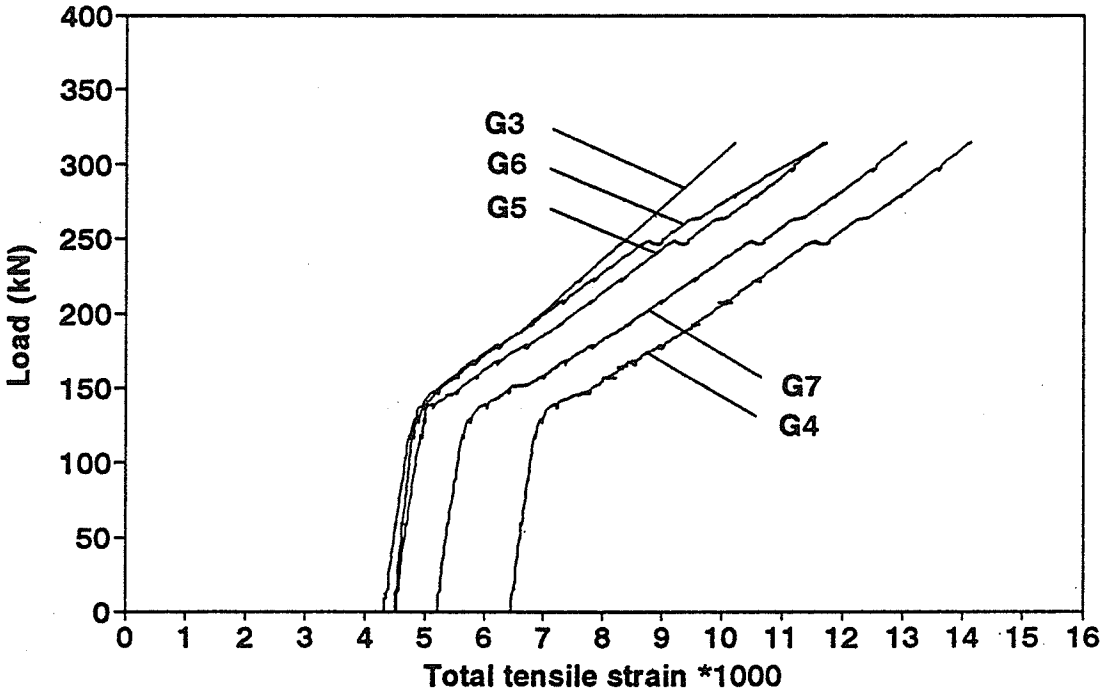

Figure A.6 Total strains strands including effective pre-strains and strains during testing

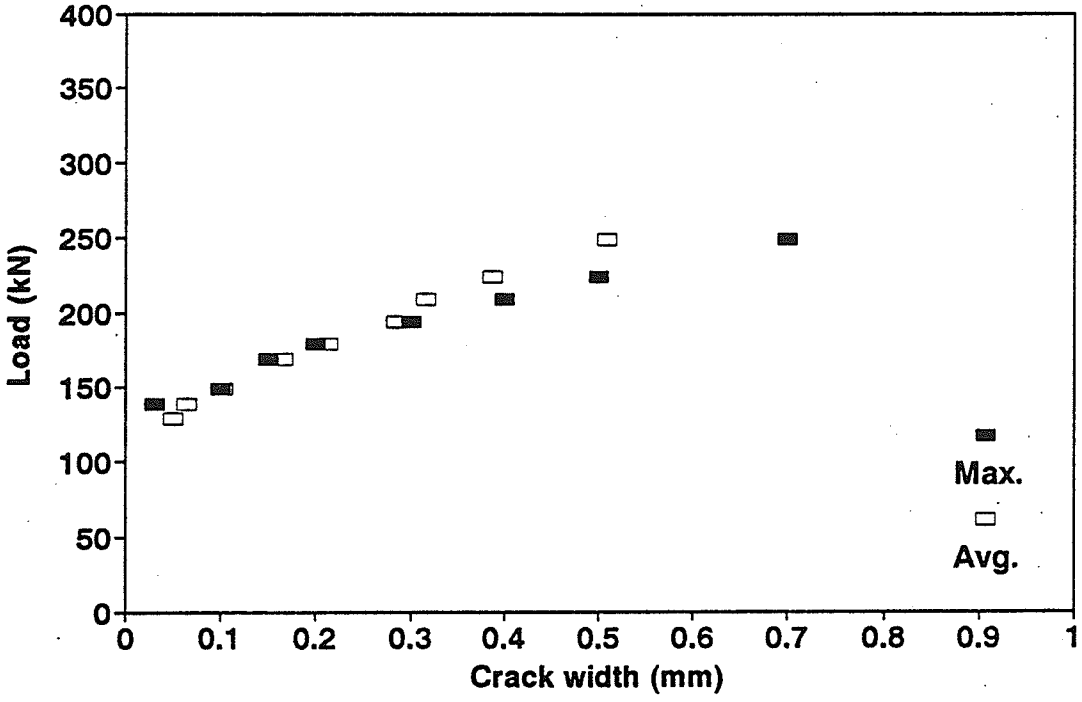

Figure A.7 Measured crack width at the maximum moment zone based on microscope readings

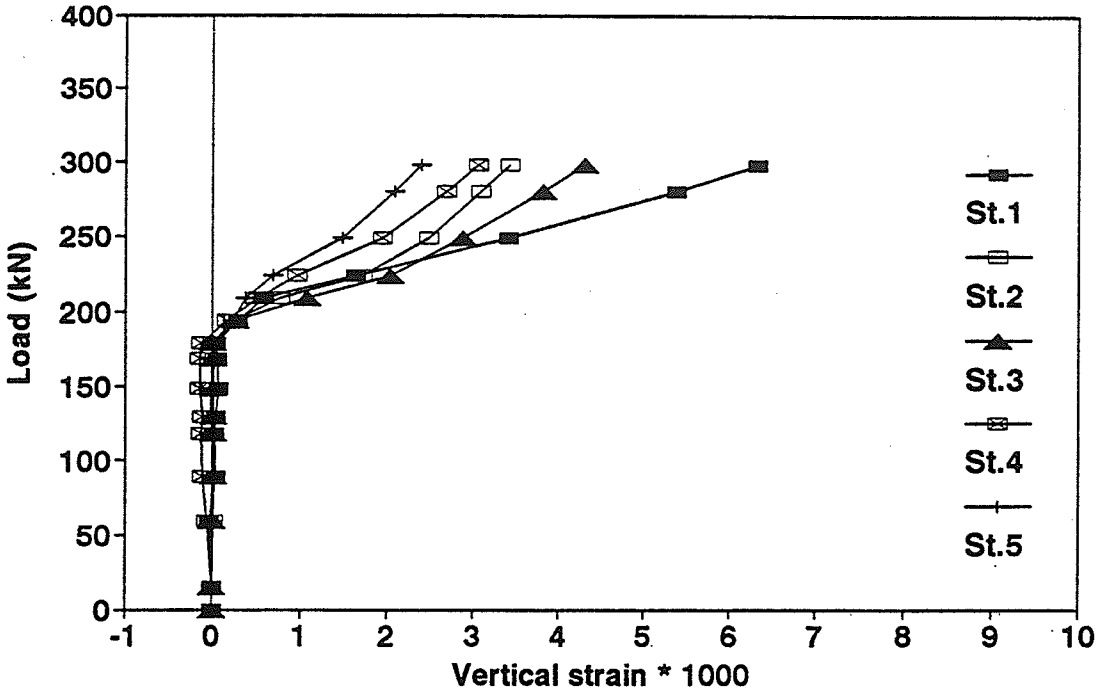

Figure A.8 Measured strain on concrete surface in direction of stirrups at five demec stations based on 200 mm gauge length

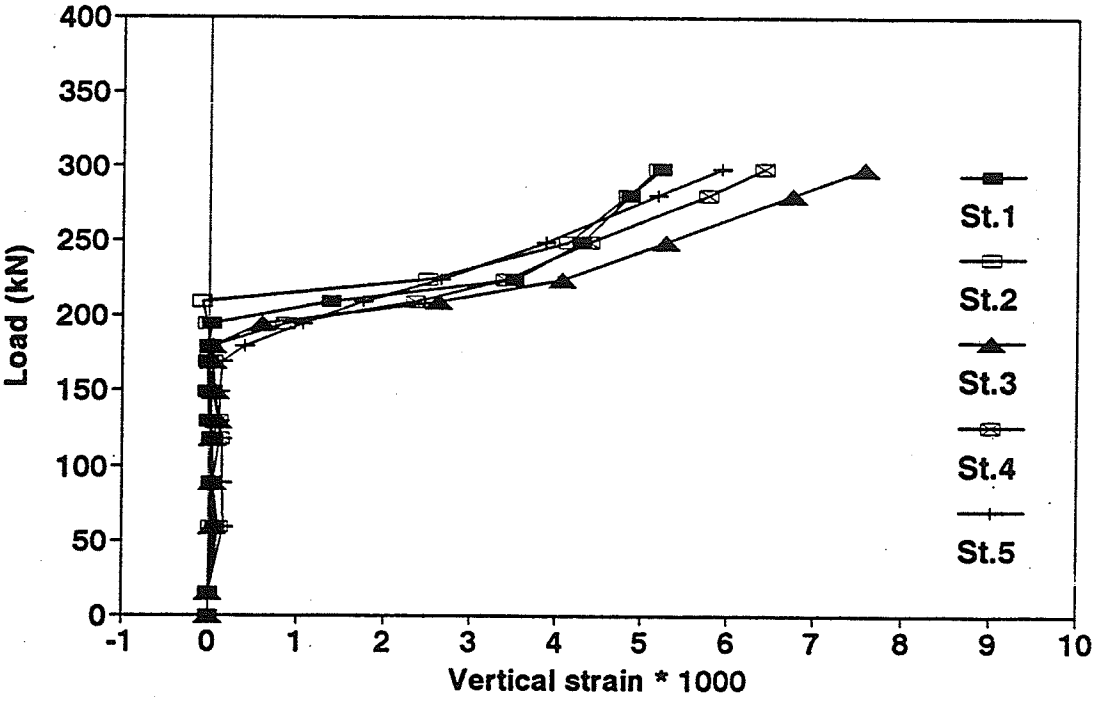

Figure A.9 Measured strain on concrete surface in direction of stirrups at five demec stations based on 50.8 mm gauge length

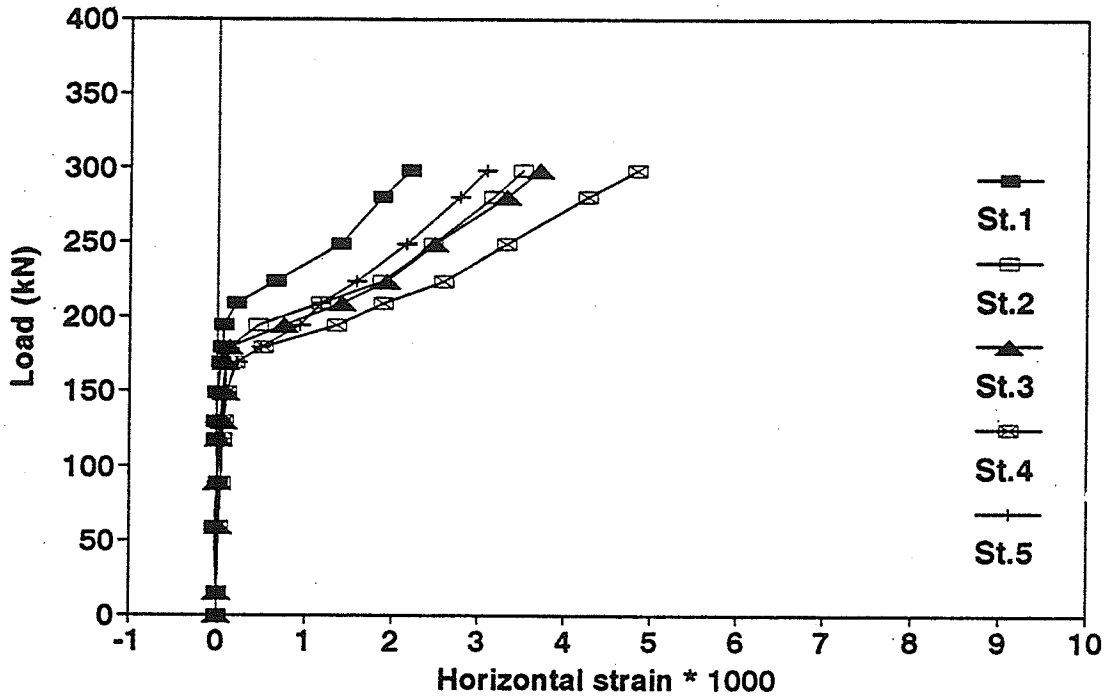

Figure A.10 Measured strain on concrete surface in the horizontal direction at five demec tations based on 200 mm gauge length

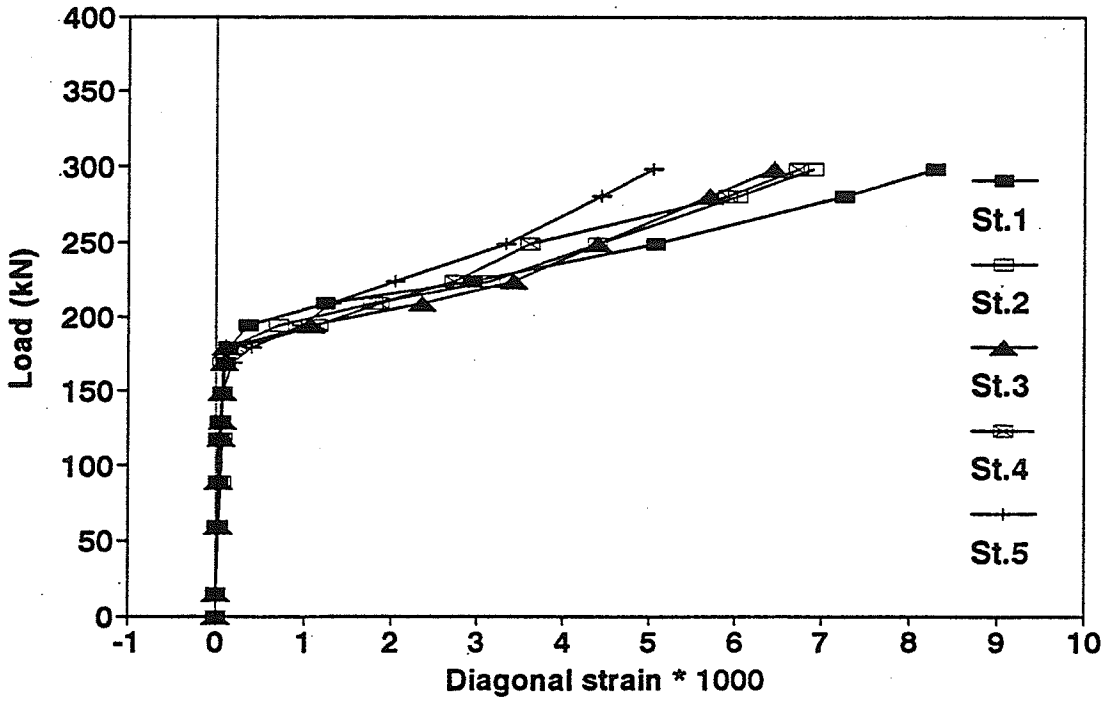

Figure A.11 Measured strain on concrete surface in the diagonal direction at five demec stations based on 200 mm gauge length

Beam TR-3-5/7

Beam TR-3-5/7

Time (days)	Case	Gauge number								
		1	2	3	4	5	6	7	8	9
0	Initial readings before jacking	3290	1440	10	-16	0	0	0	0	-58
0	After jacking bottom straight tendons					6575	7272	7727	8073	
1	After jacking draped tendons			6545	6365	6624	7247	7736	8025	7688
1	After casting concrete of the girder			6485	6348	6605	7233	7705	8013	7787
	Before releasing form									
4	After releasing form			6300	6323	6583	7111	7596	7913	8008
4	After releasing draped tendons			6152	6156	6391	6934	7425	7772	7873
4	After applying post-tensioning	6564	4808	6075	6087	6315	6864	7357	7715	7788
4	After releasing bottom straight tendons	6435	4765	5732	5652	5871	6413	6869	7203	7423
157	Right before testing	5584	3836	4798	4610	4779	5275	6359	5925	6367
	Total losses (% Age)	29.9	28.8	26.7	27.5	27.3	27.5	17.7	26.6	17

Notes: - See Figure 3.23 for strain gauges layout.
- Strain = (reading at any stage) - (initial reading).
- All readings in micro strain.

Table A.2 Measured strains of prestressing tendons from jacking up to testing using electrical strain gauges

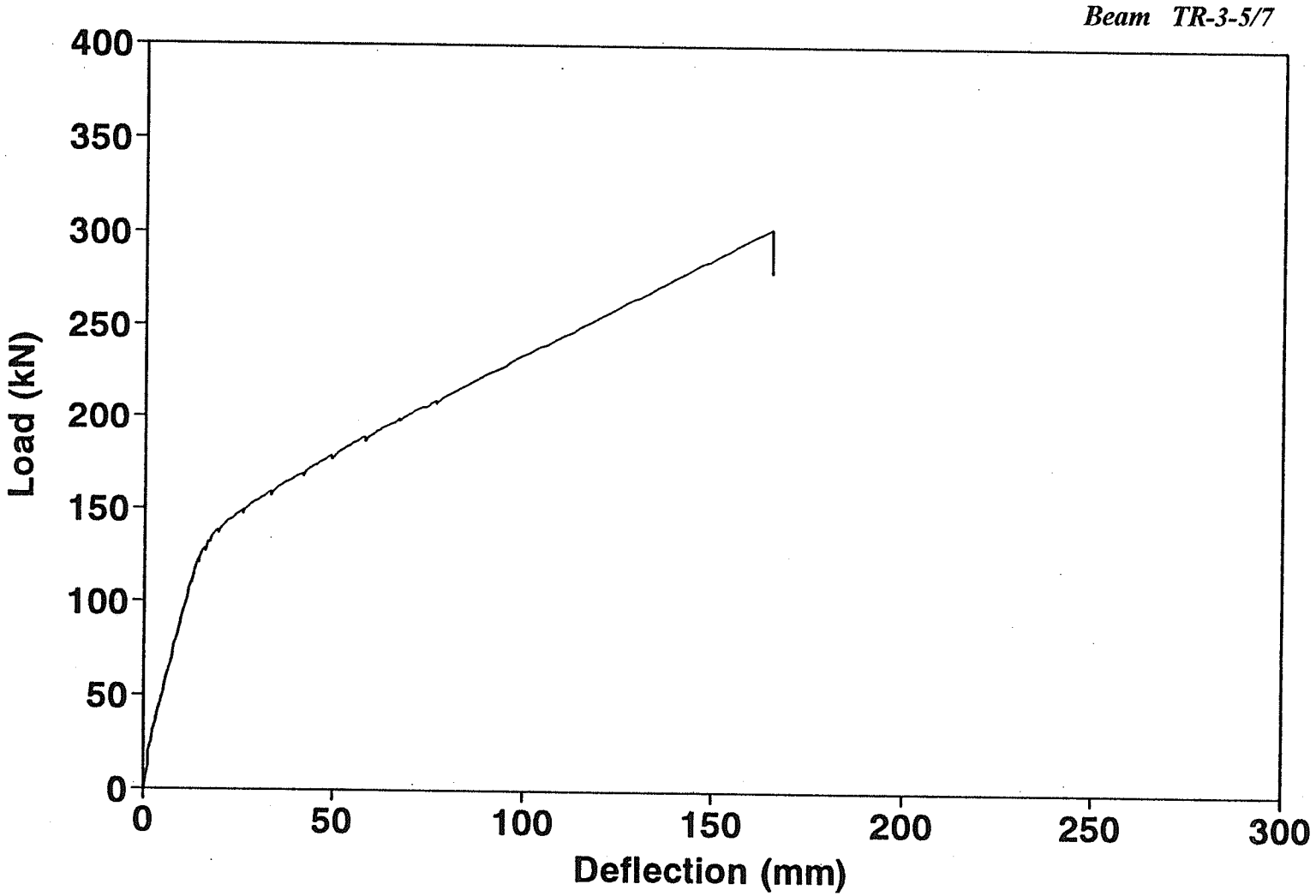

Figure A.1 Measured Load - deflection at mid span

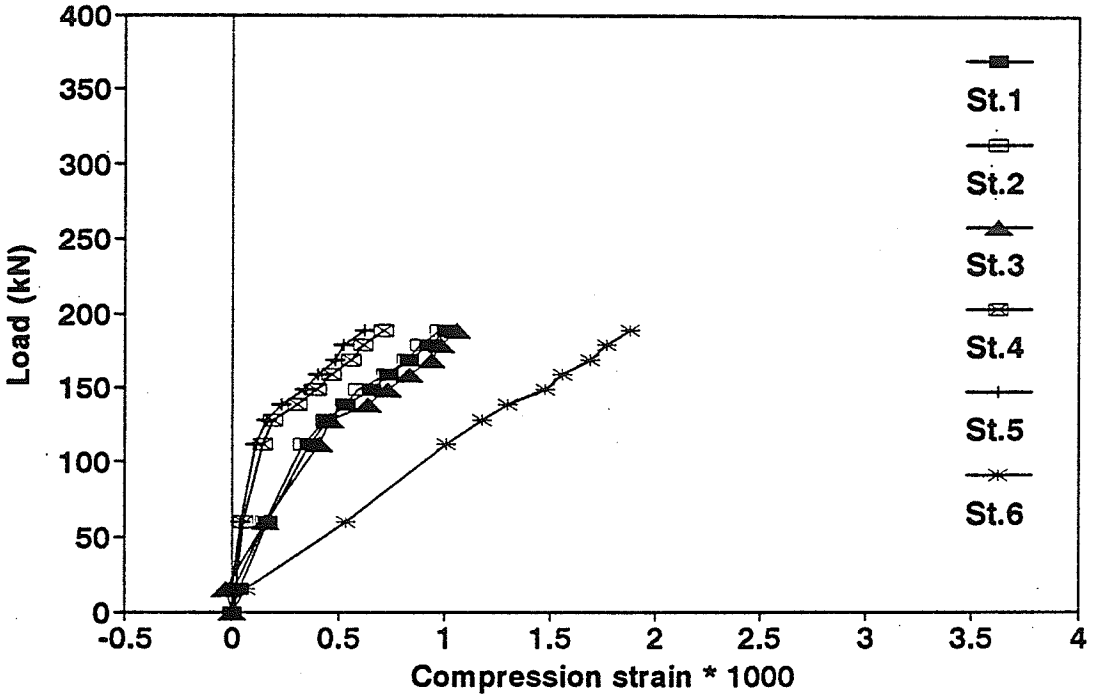

Figure A.2 Measured concrete strain at top surface at six demec stations

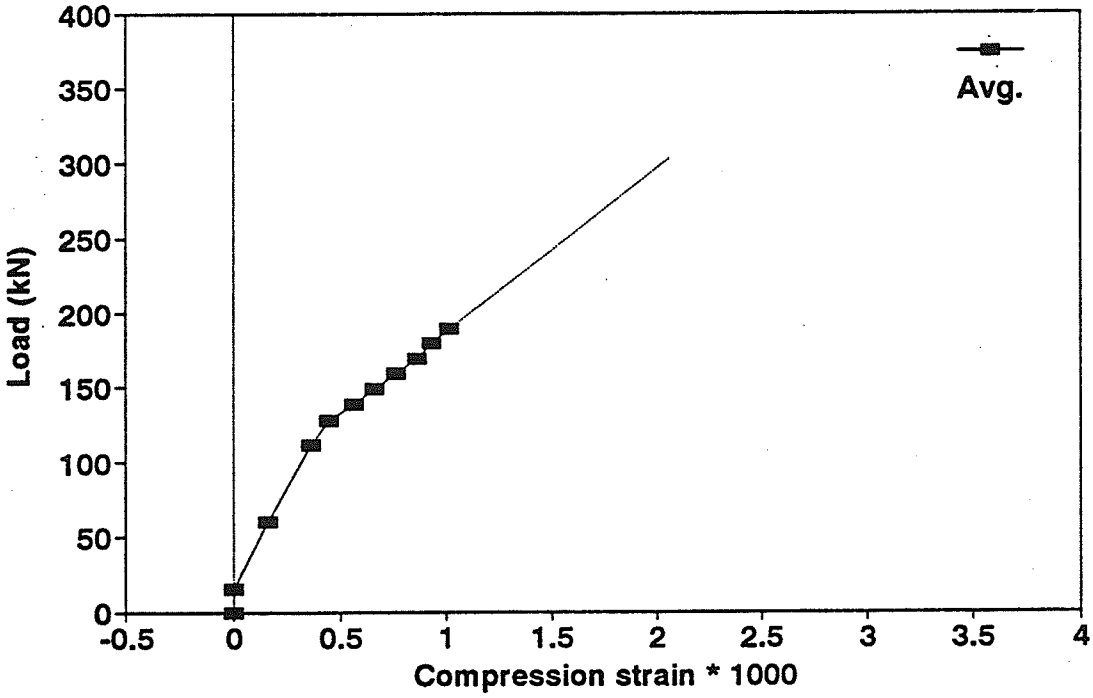

Figure A.3 Average of measured concrete strain at top surface

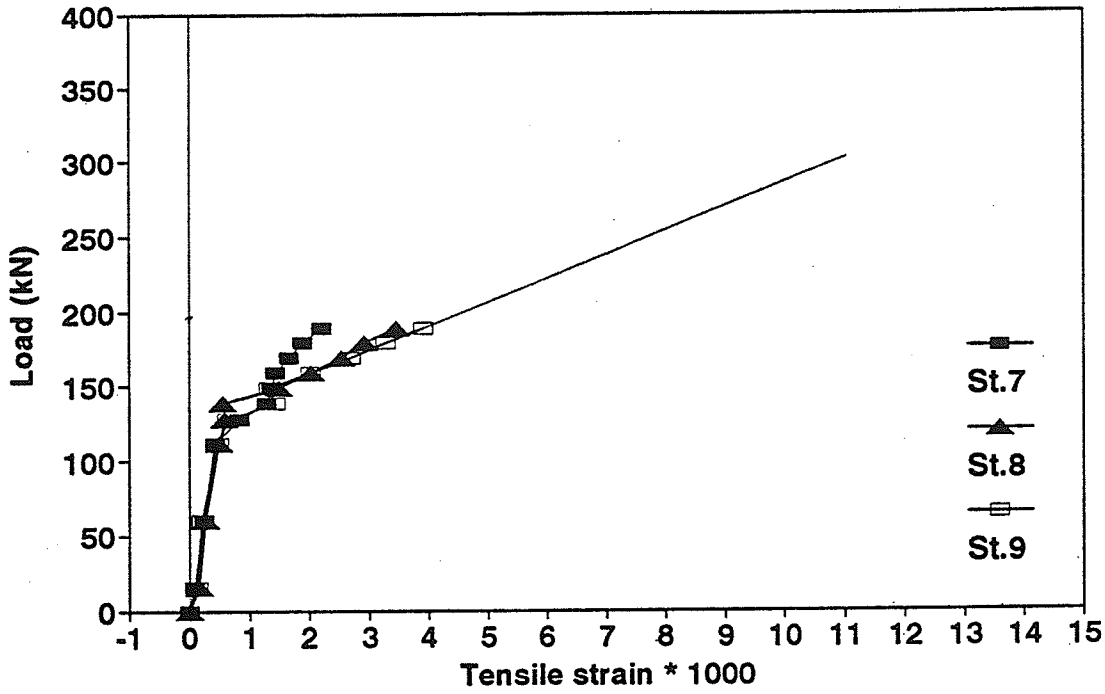

Figure A.4 Measured strains at bottom strands level at three demec stations

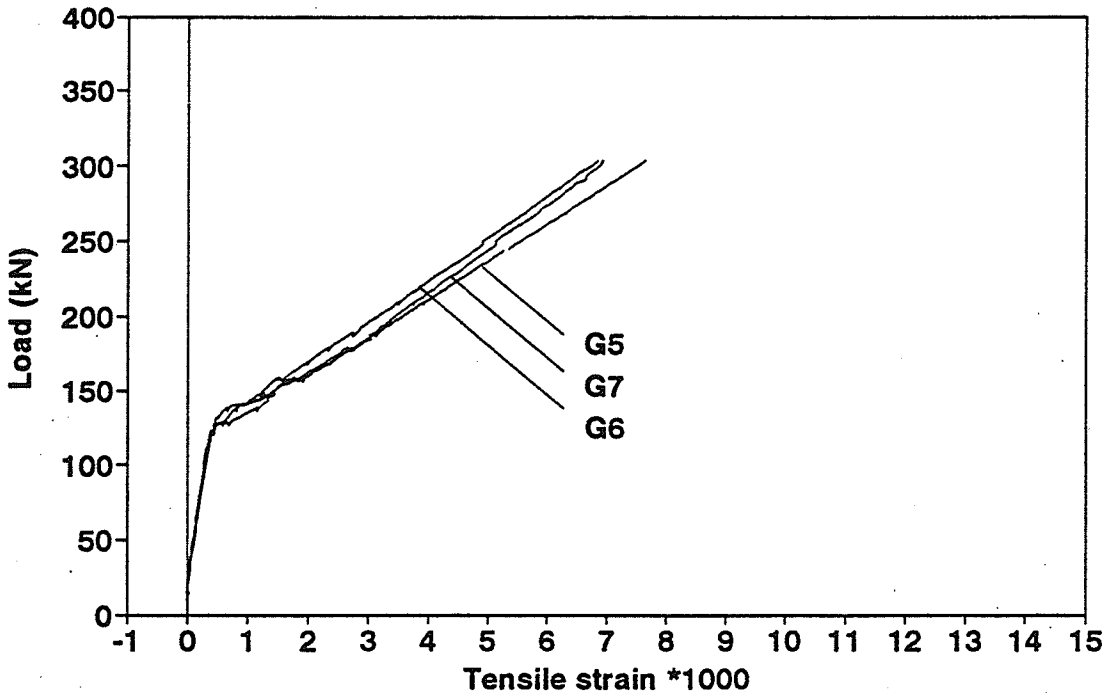

Figure A.5 Measured strains on the bottom strands during testing using strain gauges

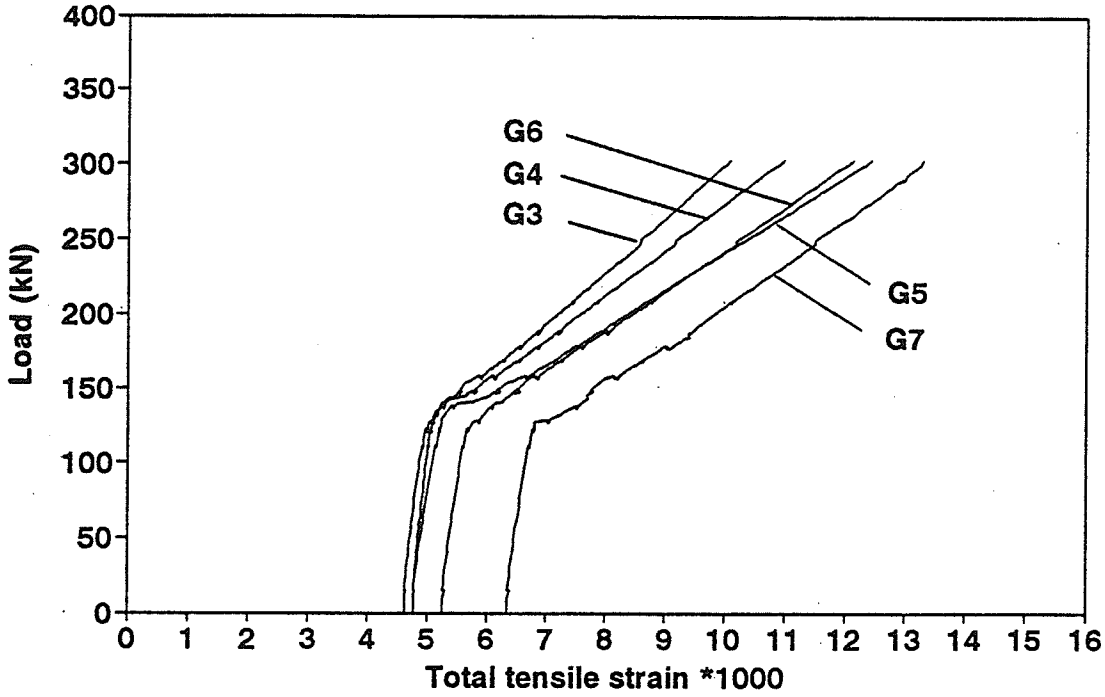

Figure A.6 Total strains strands including effective pre-strains and strains during testing

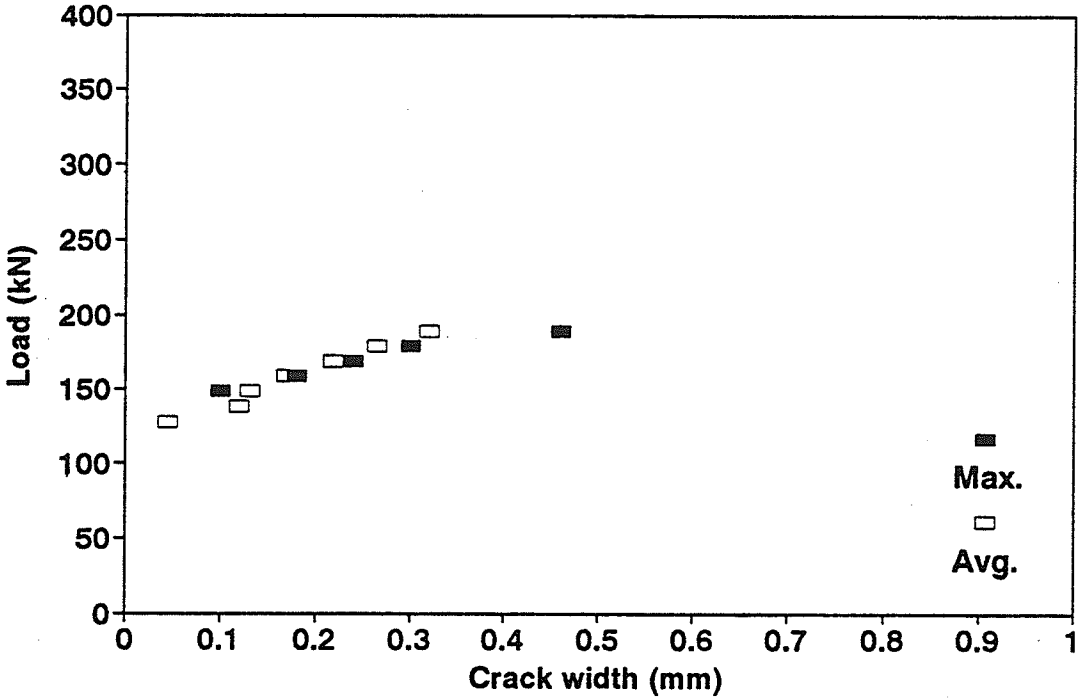

Figure A.7 Measured crack width at the maximum moment zone based on microscope readings

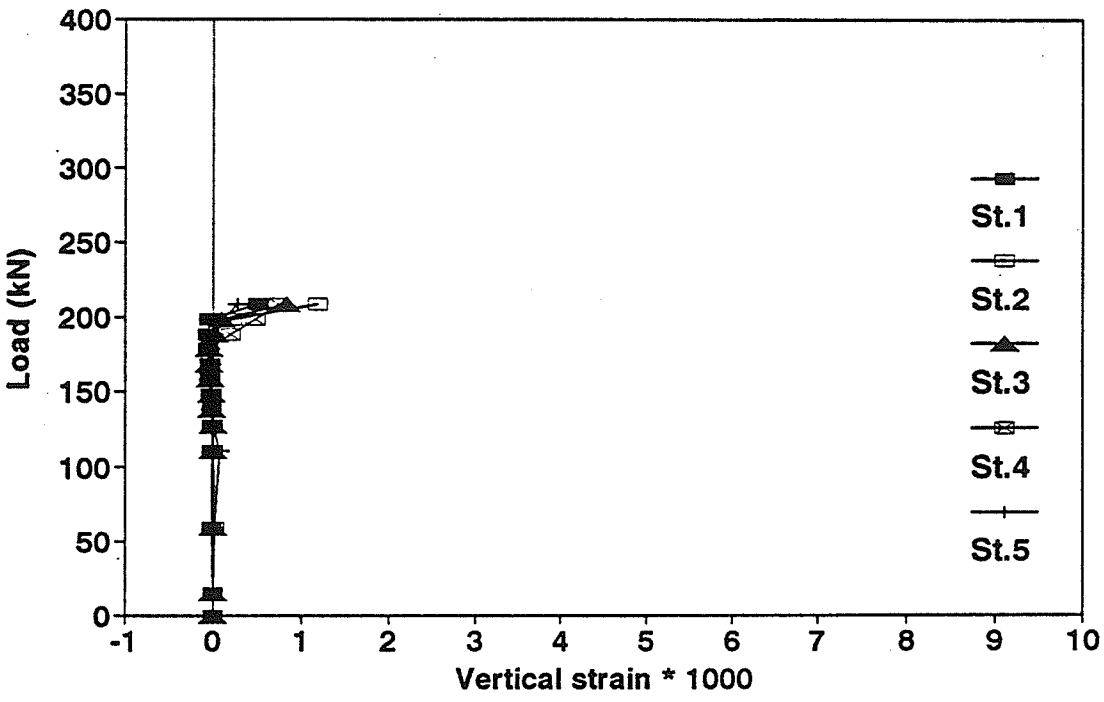

Figure A.8 Measured strain on concrete surface in direction of stirrups at five demec stations based on 200 mm gauge length

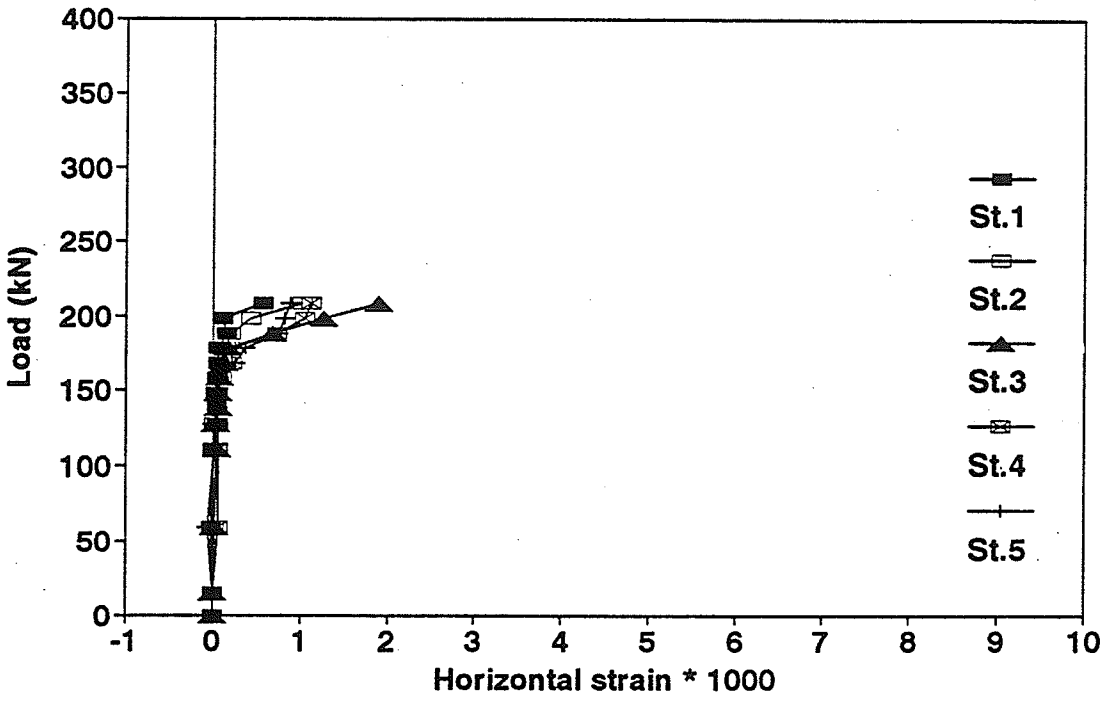

Figure A.10 Measured strain on concrete surface in the horizontal direction at five demec tations based on 200 mm gauge length

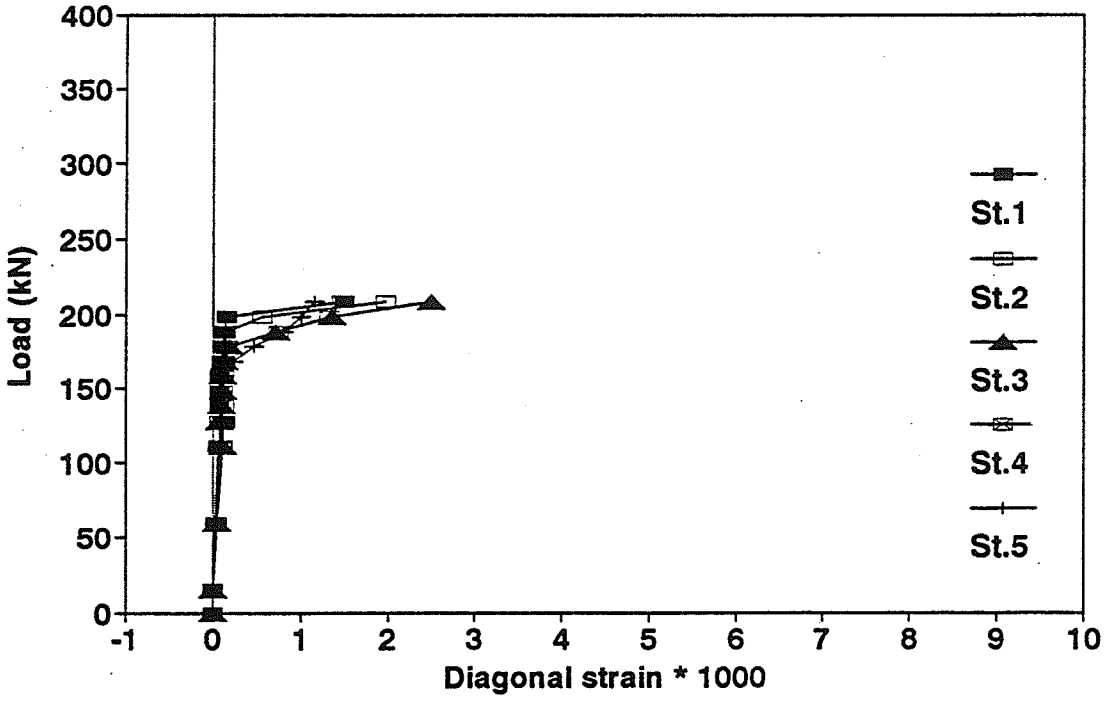

Figure A.11 Measured strain on concrete surface in the diagonal direction at five demec stations based on 200 mm gauge length

Beam LL-4-2B

Beam LL-4-2B

Time (days)	Case	Gauge number								
		1	2	3	4	5	6	7	8	9
0	Initial readings before jacking	157	-664	-675	800	41	272	1470	1567	874
6	After jacking bottom straight tendons					7918	7975	9285	9424	
8	After jacking draped tendons			7105	2810	7811	7979	9272	9445	8467
8	After casting concrete of the girder			5549	2350	7827	7994	9285	9458	8463
	Before releasing form									
	After releasing form									
12	After releasing draped tendons			3662	1336	7450	7641	8923	9172	8167
12	After applying post-tensioning	3051	2327			7438	7610	8888	9171	8133
12	After releasing bottom straight tendons	2950	2250			7018	7172	8392	8723	7812
123	Right before testing	2621	2036	3071	1538	5985	6233	7502	7802	6967
	Total losses (% Age)	14.9	9.7	51.9	63.3	24.5	25.7	24.5	22.1	19.8

Notes: - See Figure 3.23 for strain gauges layout.
- Strain = (reading at any stage) - (initial reading).
- All readings in micro strain.

Table A.2 Measured strains of prestressing tendons from jacking up to testing using electrical strain gauges

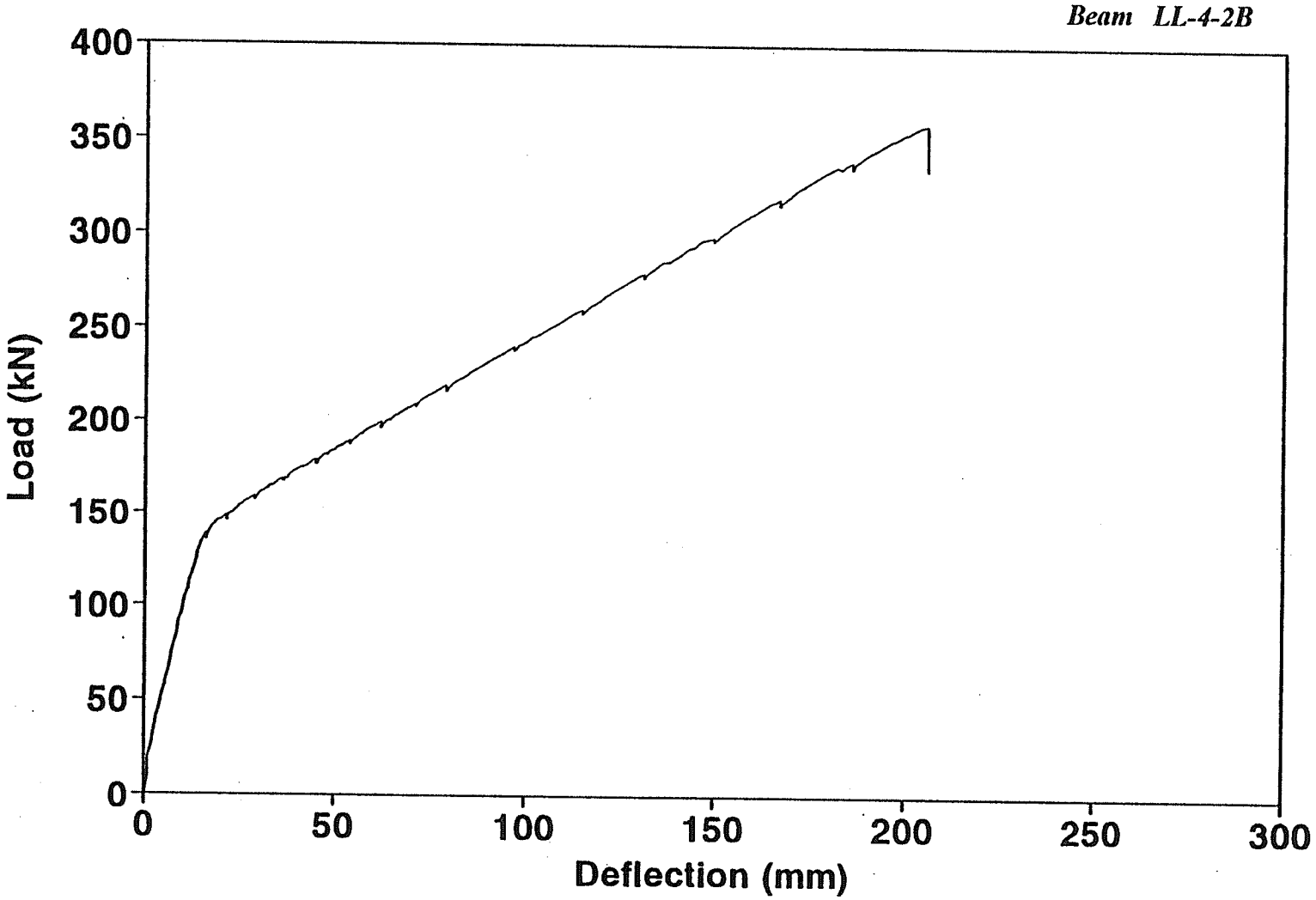

Figure A.1 Measured Load - deflection at mid span

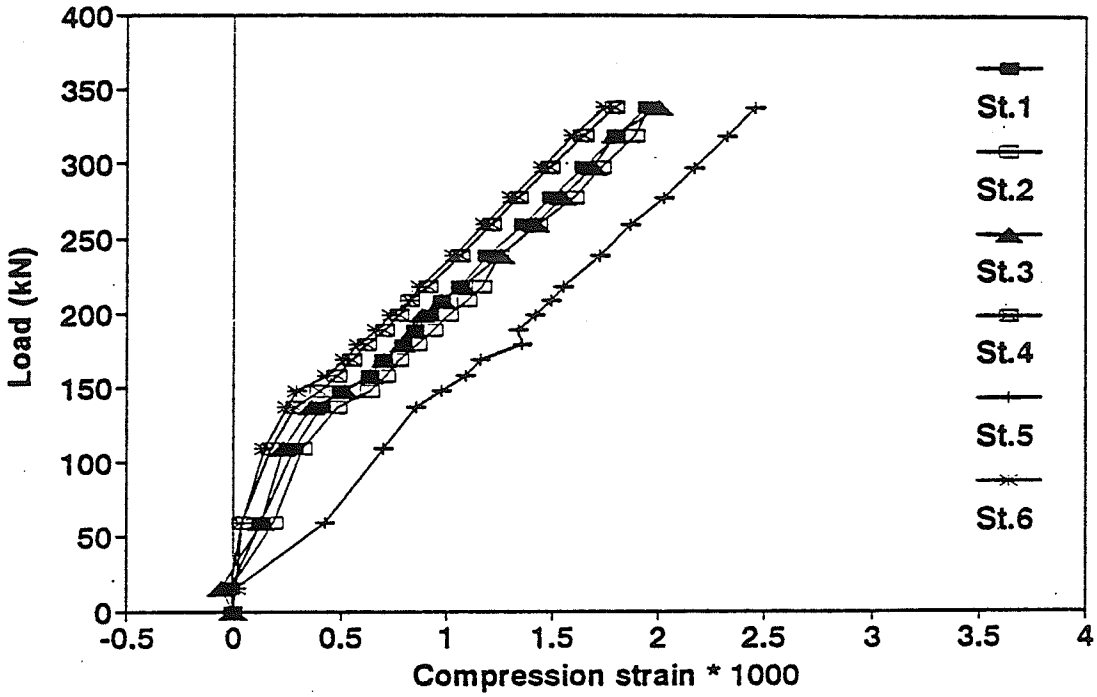

Figure A.2 Measured concrete strain at top surface at six demec stations

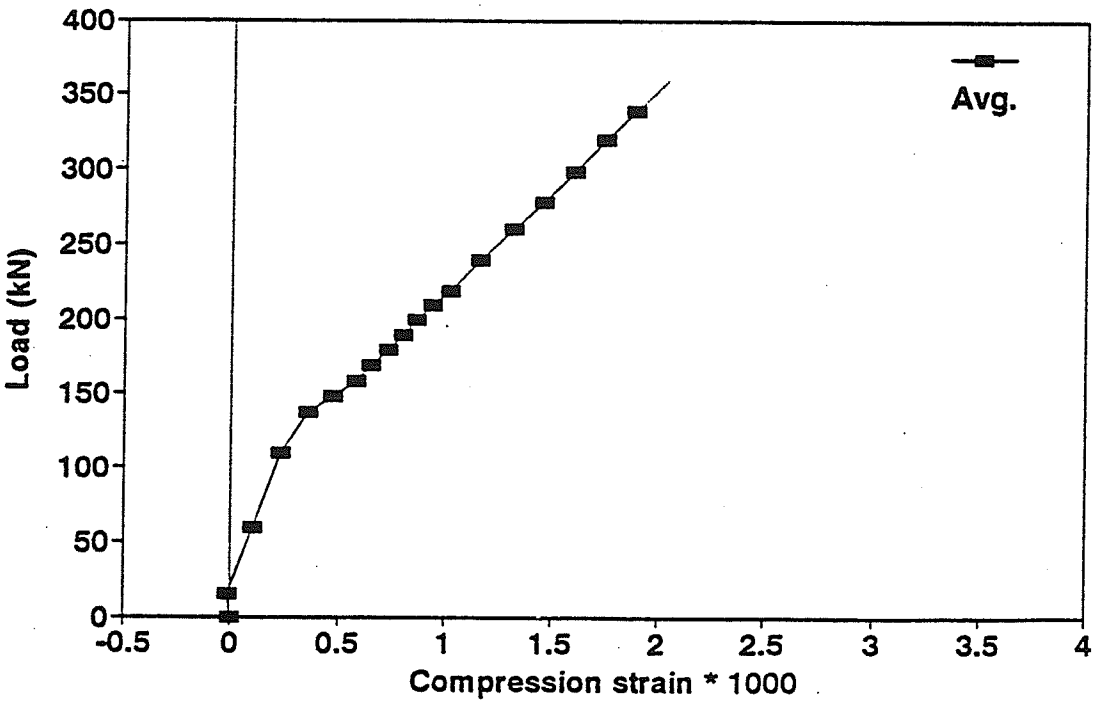

Figure A.3 Average of measured concrete strain at top surface

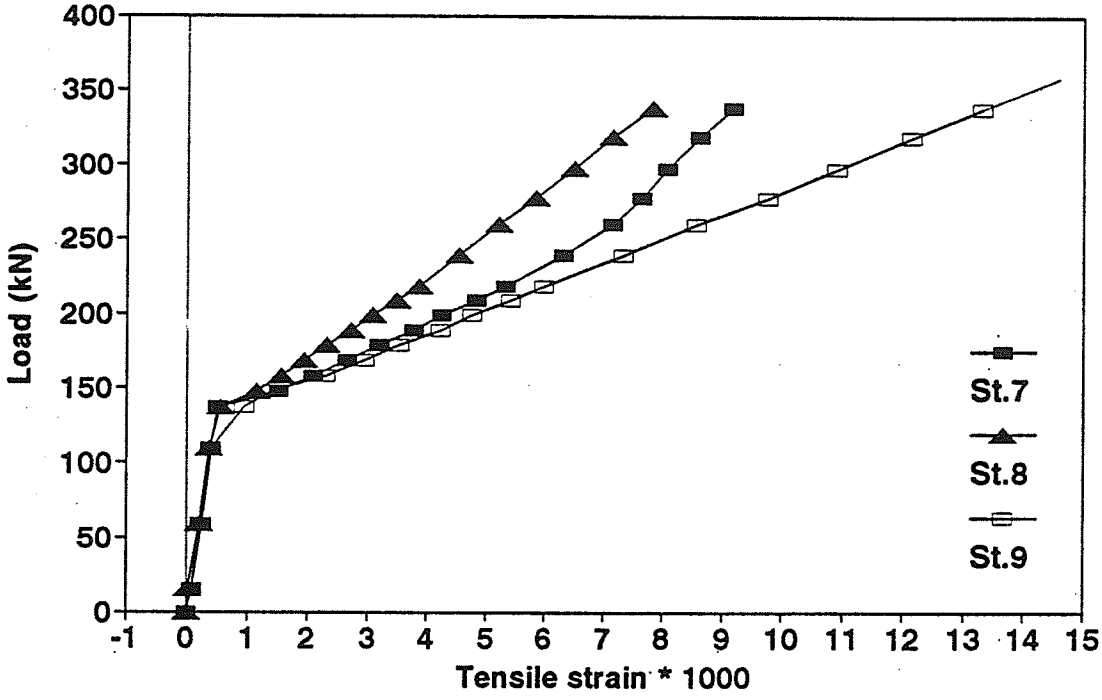

Figure A.4 Measured strains at bottom strands level at three demec stations

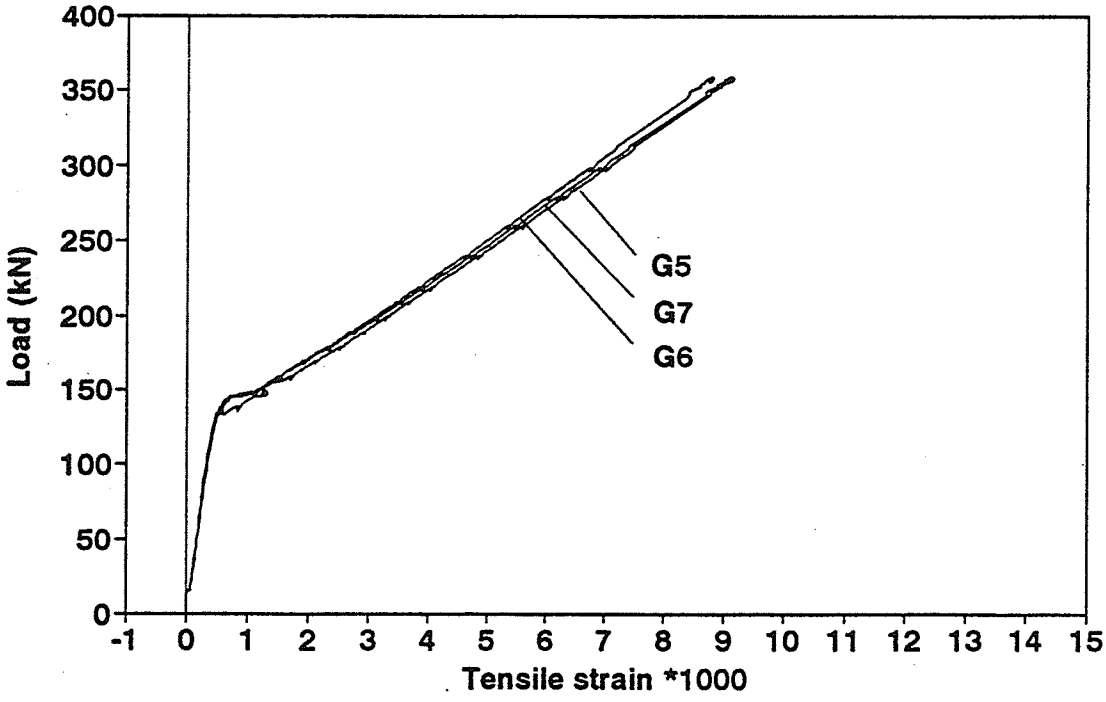

Figure A.5 Measured strains on the bottom strands during testing using strain gauges

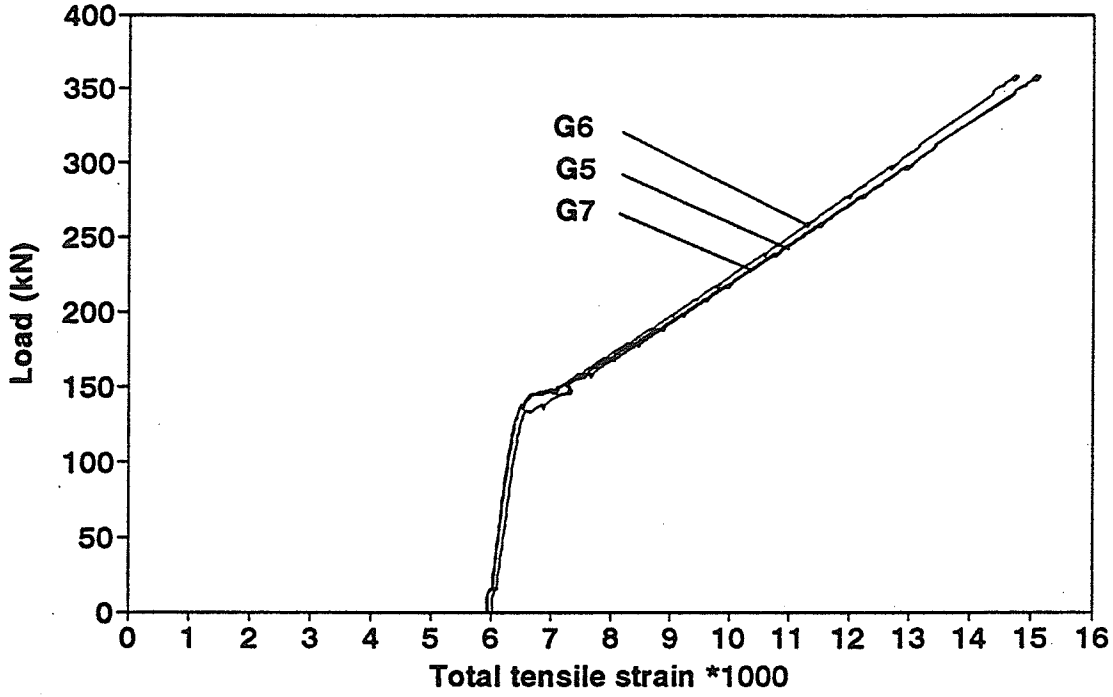

Figure A.6 Total strains strands including effective pre-strains and strains during testing

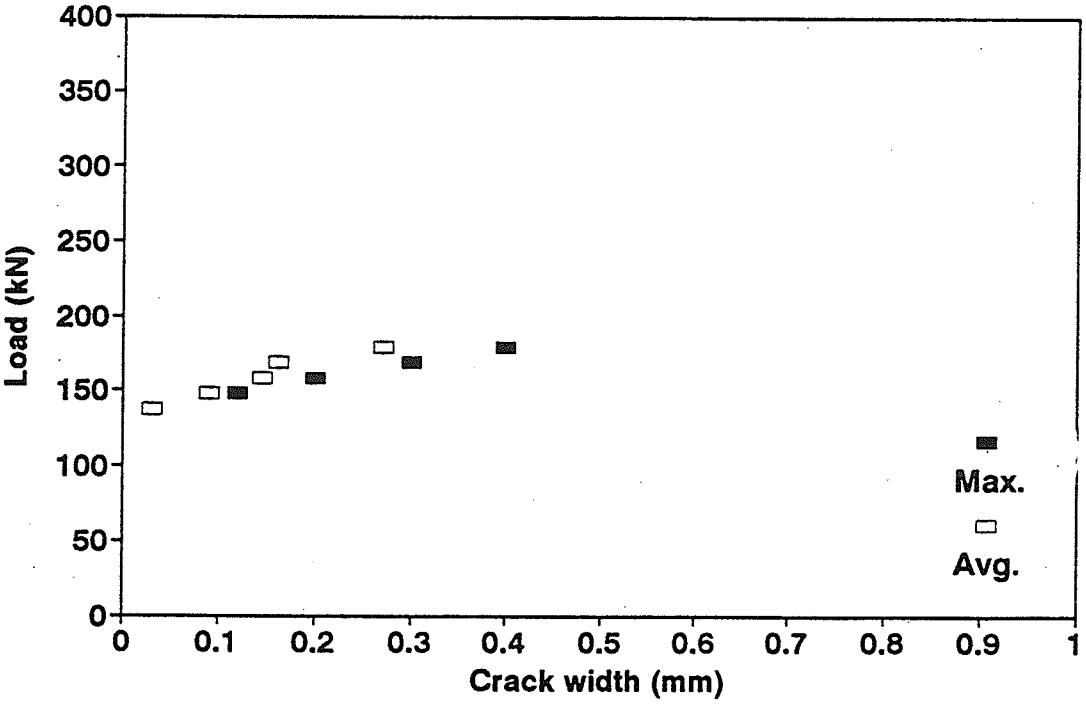

Figure A.7 Measured crack width at the maximum moment zone based on microscope readings

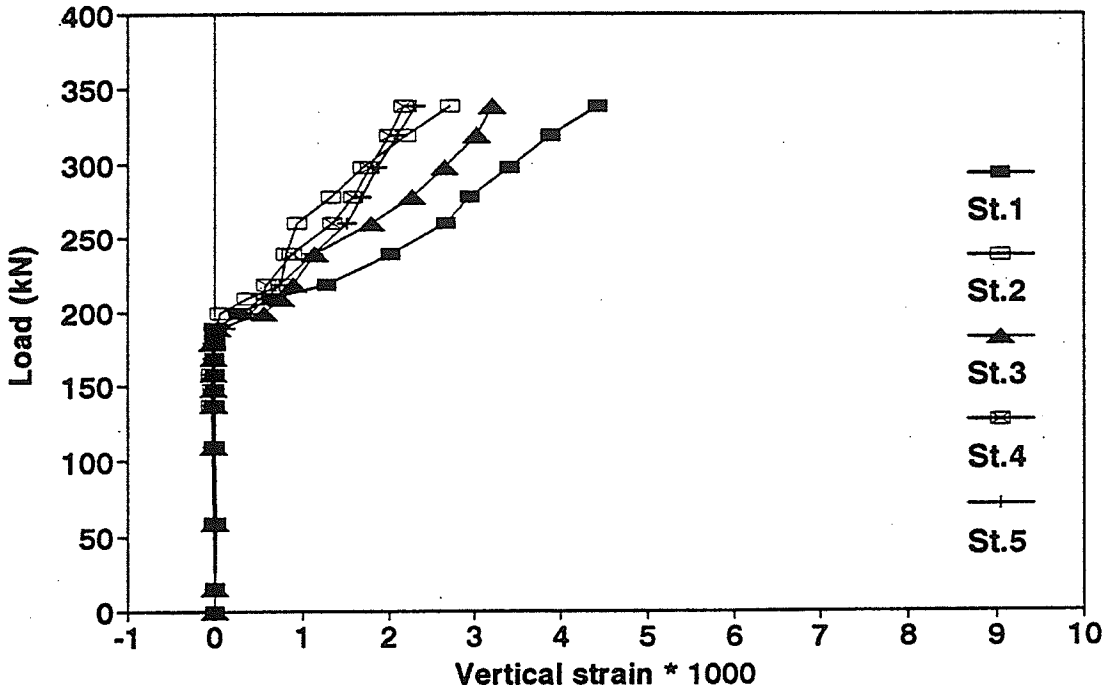

Figure A.8 Measured strain on concrete surface in direction of stirrups at five demec stations based on 200 mm gauge length

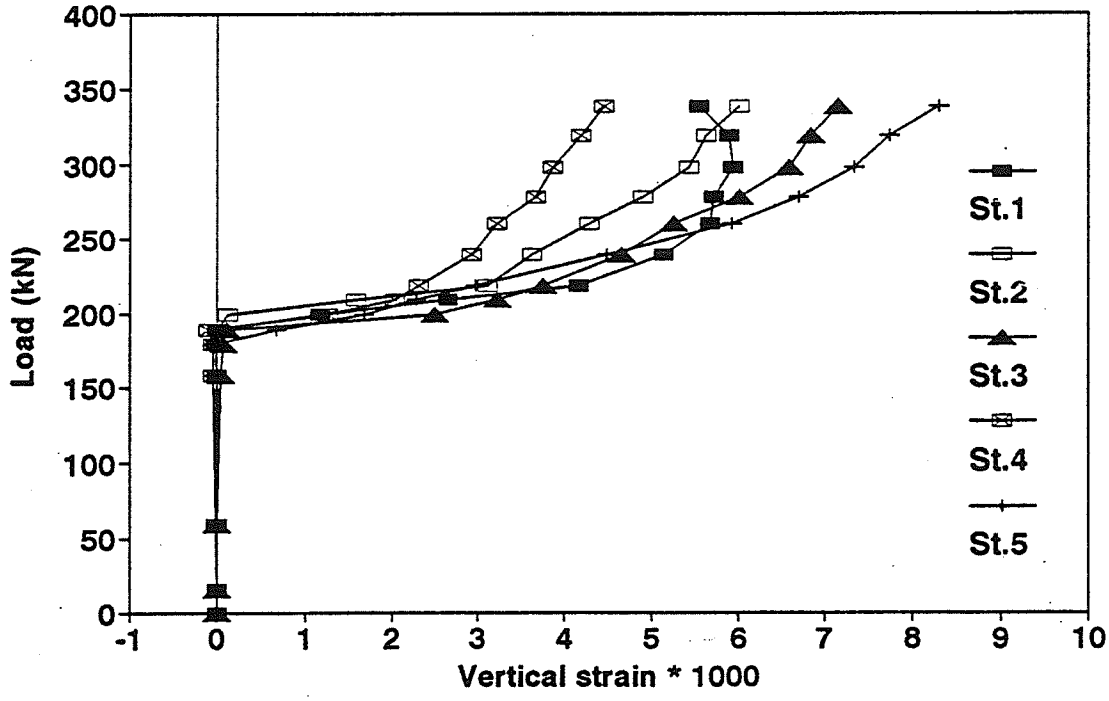

Figure A.9 Measured strain on concrete surface in direction of stirrups at five demec stations based on 50.8 mm gauge length

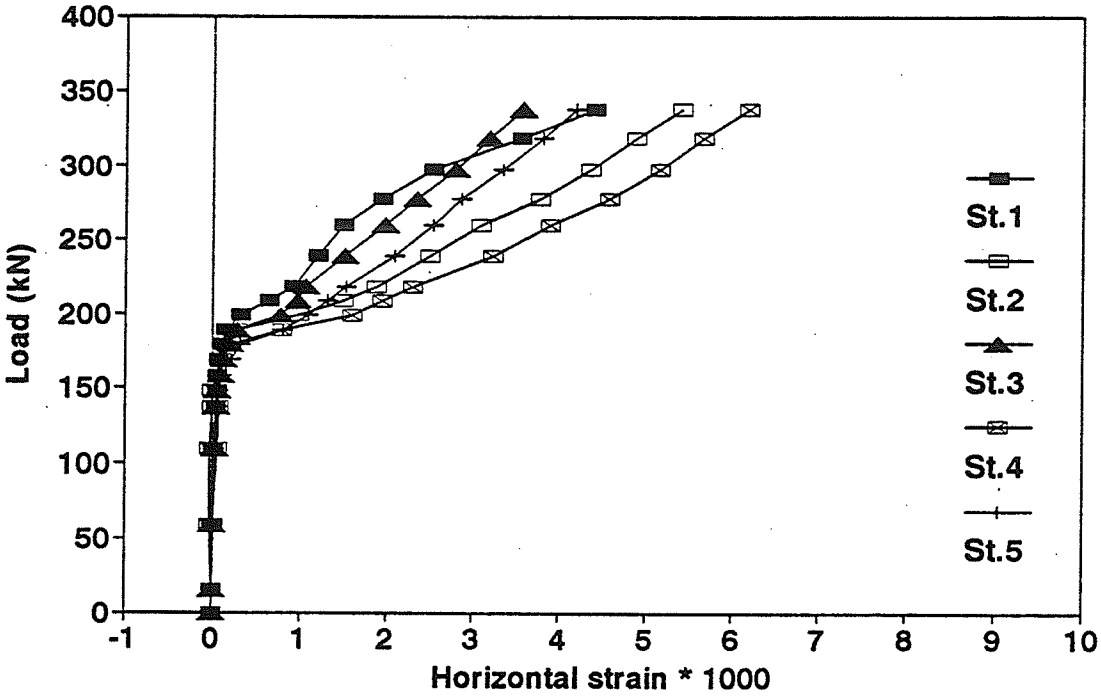

Figure A.10 Measured strain on concrete surface in the horizontal direction at five demec tations based on 200 mm gauge length

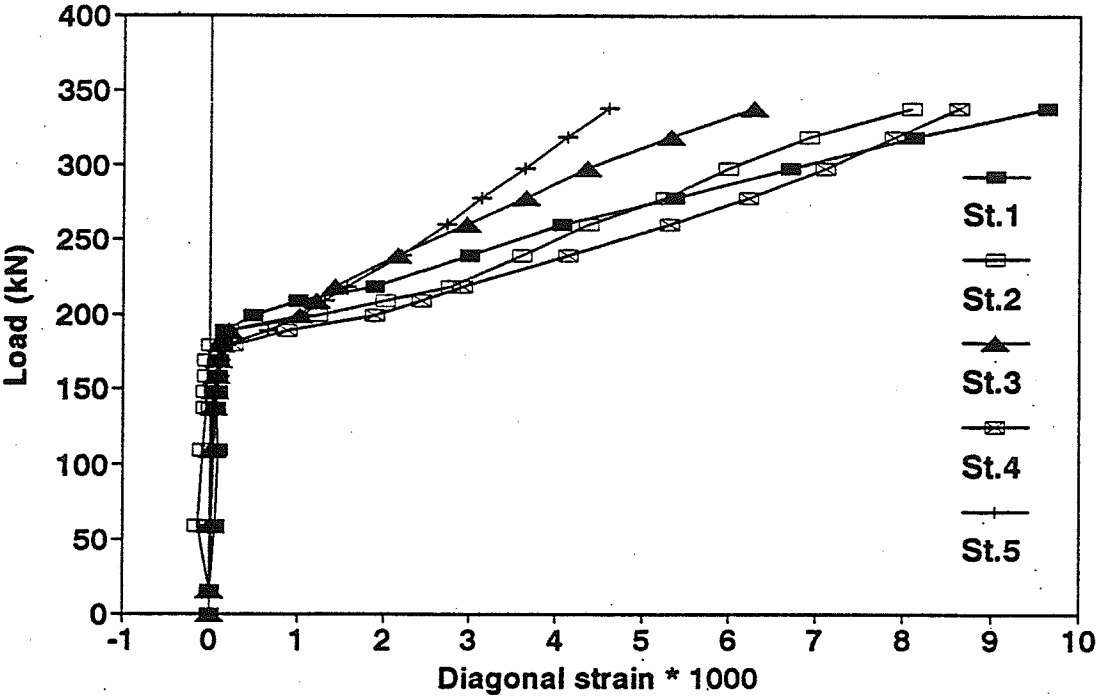

Figure A.11 Measured strain on concrete surface in the diagonal direction at five demec stations based on 200 mm gauge length

Beam LL-5-1B

Beam LL-5-1B

Time (days)	Case	Gauge number								
		1	2	3	4	5	6	7	8	9
0	Initial readings before jacking	2520	1370	872		825	1028	2963	813	861
0	After jacking bottom straight tendons					8893	8530	8530	8426	
1	After jacking draped tendons			8552		8756	8432	8418	8323	4525
1	After casting concrete of the girder			8530		8781	8463	8451	8350	4270
	Before releasing form									
5	After releasing form			8267		8593	8236	8261	8164	3215
5	After releasing draped tendons			8134		8448	8100	8125	8045	3145
5	After applying post-tensioning	5838	4647	8059		8367		8057		
5	After releasing bottom straight tendons	5740	4580	7730		7928	7636	7664	7582	2900
144	Right before testing	5115	4092	6992		6958	6733	6812	6605	2495
	Total losses (% Age)	21.8	16.9	20.3		23.9	23.9	30.9	23.9	55.4

Notes: - See Figure 3.23 for strain gauges layout.
- Strain = (reading at any stage) - (initial reading).
- All readings in micro strain.

Table A.2 Measured strains of prestressing tendons from jacking up to testing using electrical strain gauges

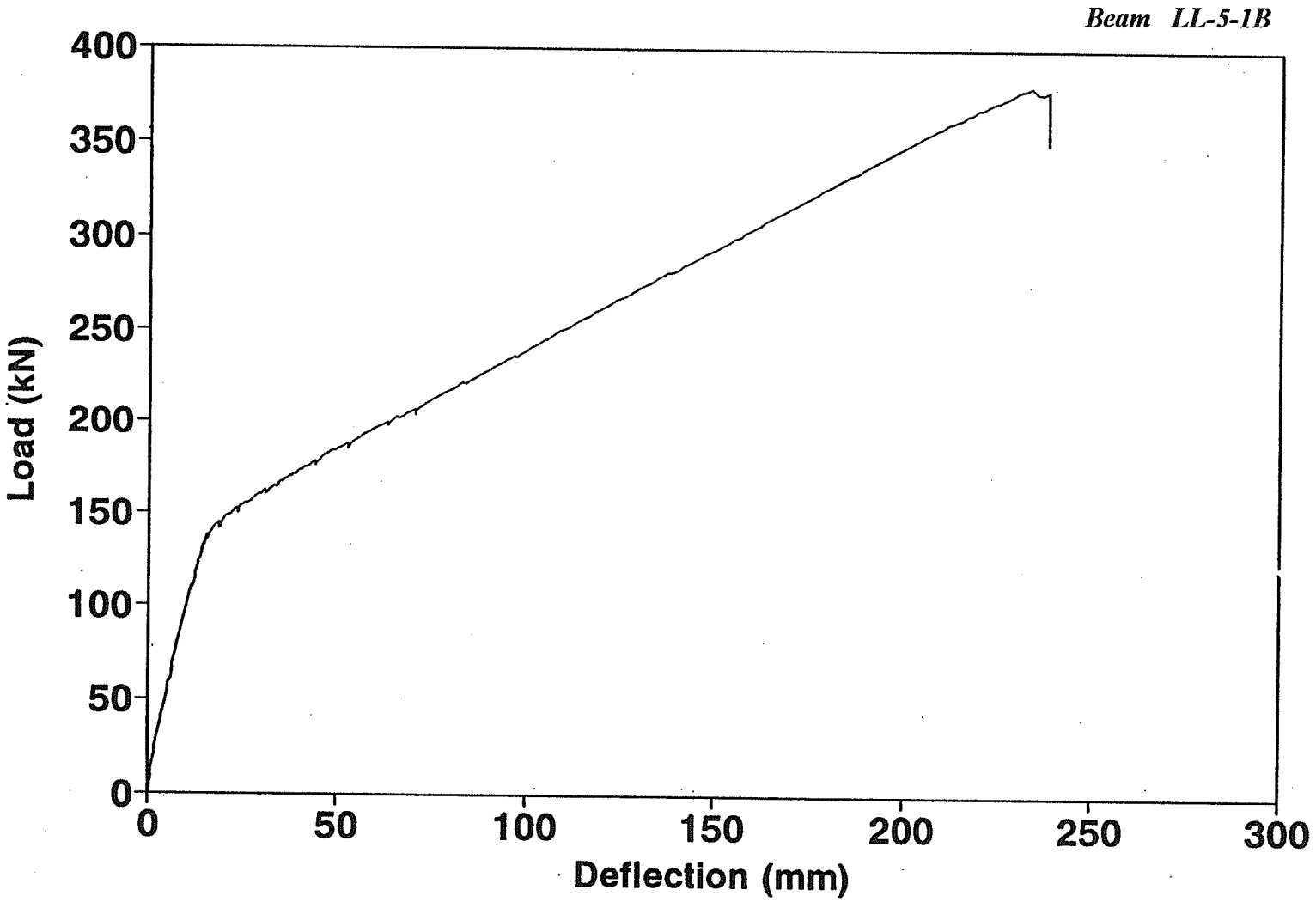

Figure A.1 Measured Load - deflection at mid span

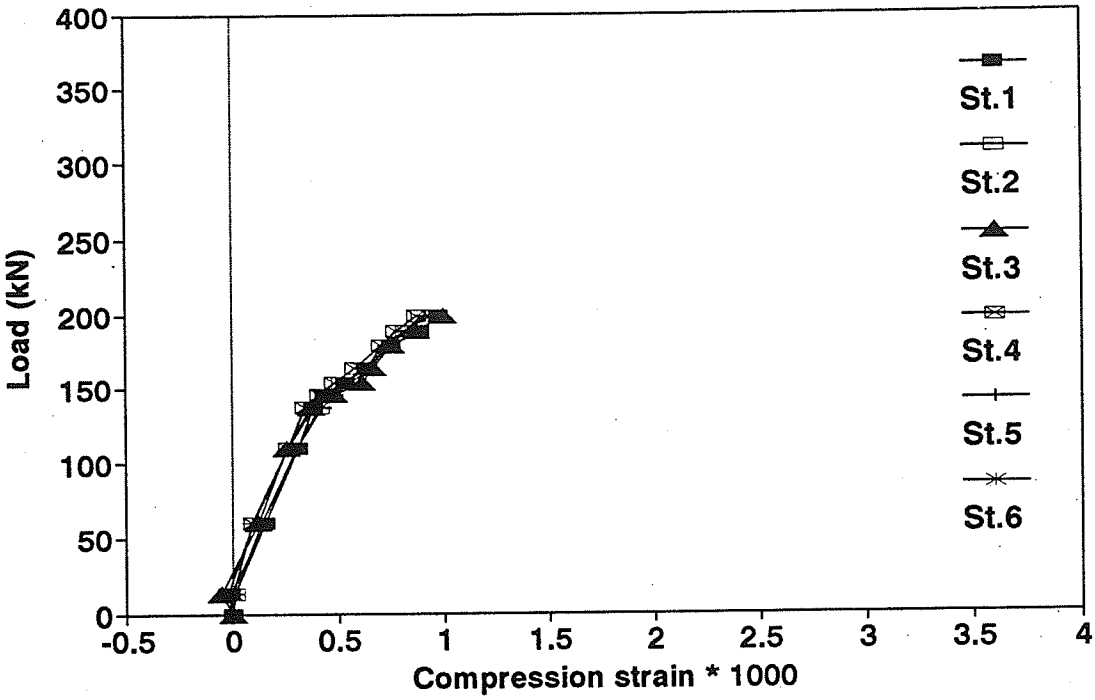

Figure A.2 Measured concrete strain at top surface at six demec stations

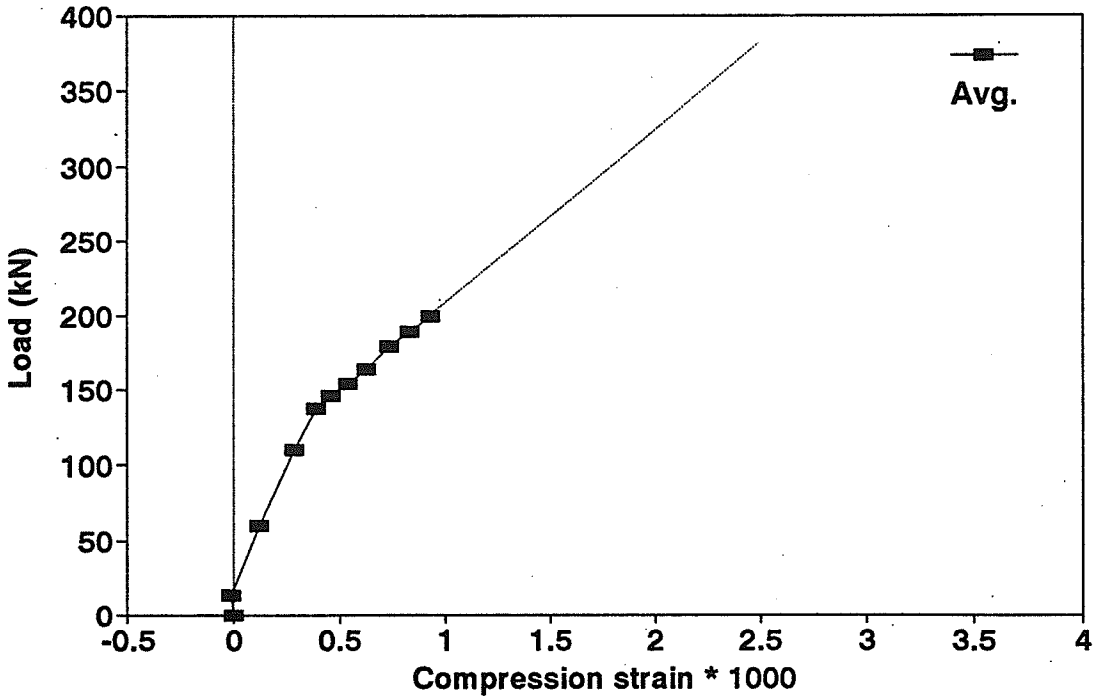

Figure A.3 Average of measured concrete strain at top surface

Beam LL-5-1B

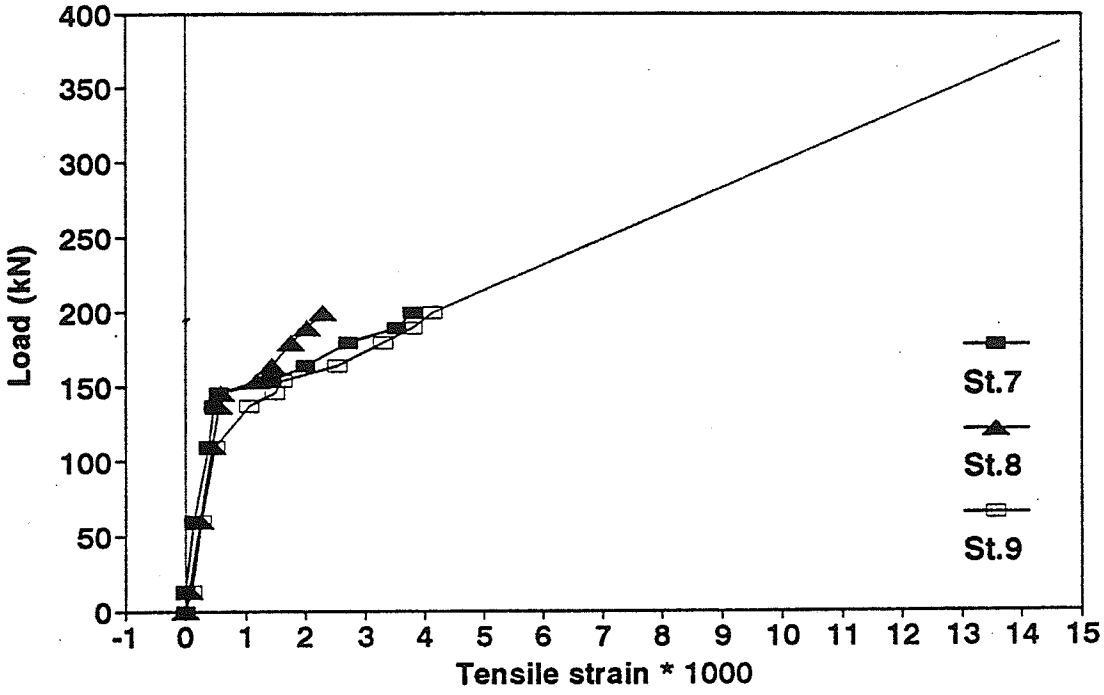

Figure A.4 Measured strains at bottom strands level at three demec stations

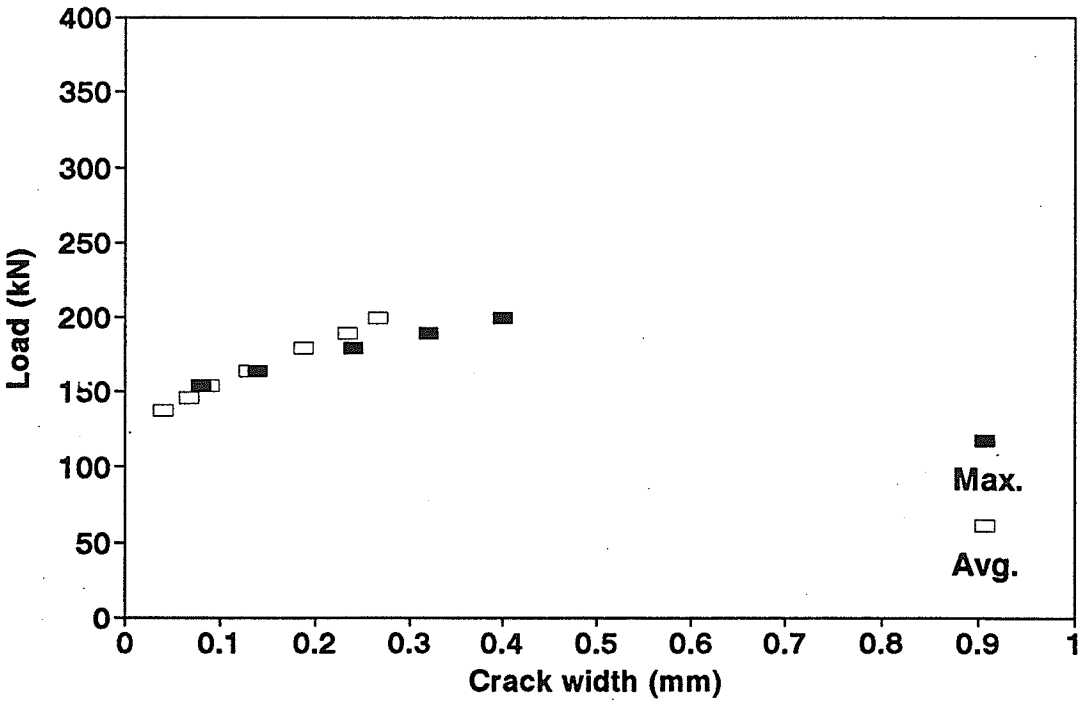

Figure A.7 Measured crack width at the maximum moment zone based on microscope readings

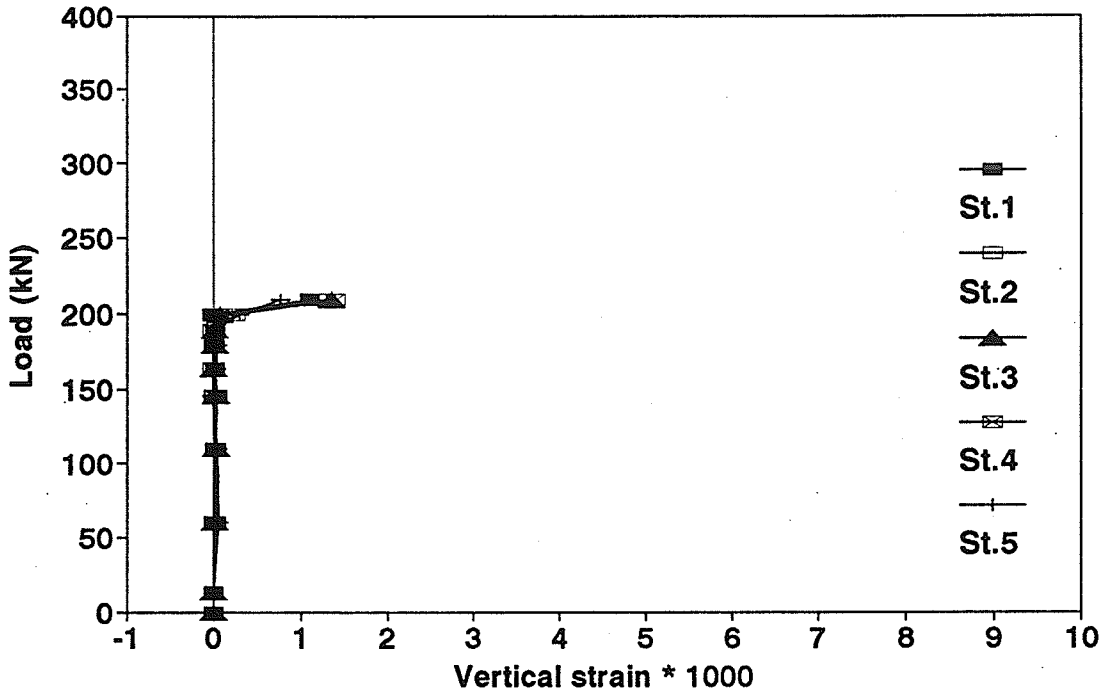

Figure A.8 Measured strain on concrete surface in direction of stirrups at five demec stations based on 200 mm gauge length

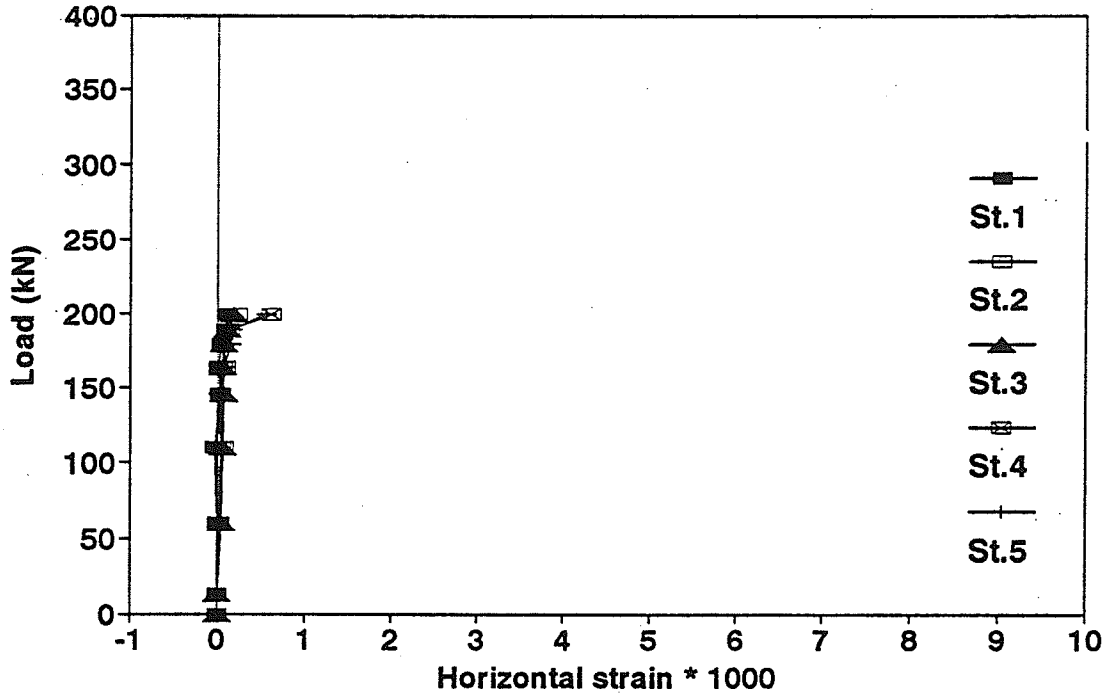

Figure A.10 Measured strain on concrete surface in the horizontal direction at five demec tations based on 200 mm gauge length

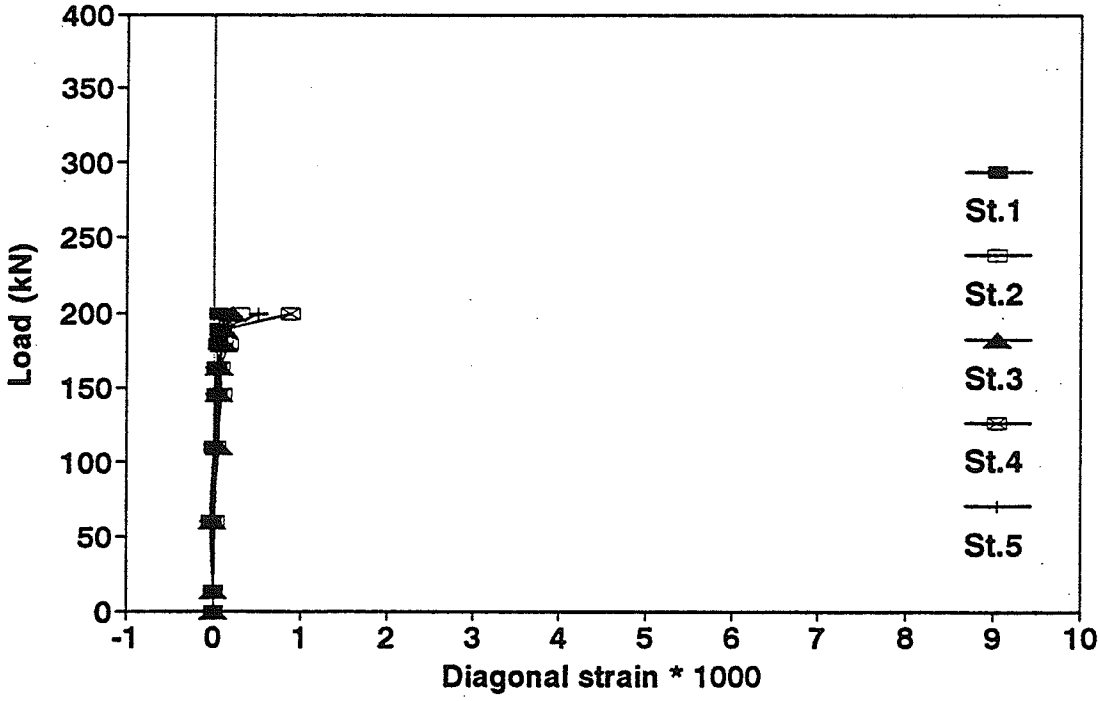

Figure A.11 Measured strain on concrete surface in the diagonal direction at five demec stations based on 200 mm gauge length

Beam ST-6-C

Beam ST-6-C

Time (days)	Case	Gauge number								
		1	2	3	4	5	6	7	8	9
0	Initial readings before jacking	1820	1553	2360	1886	2122	2327	1702	1857	1675
0	After jacking bottom straight tendons					7766	7903	7261	7458	
1	After jacking draped tendons			7997	7081	7659	7853	7169	7377	7111
1	After casting concrete of the girder			6222	3335	7000	7788	7103	7347	7050
2	Before releasing form			4306	2646	3375	7260	6481	6736	6491
3	After releasing form			4137	2205	2950	7195	6398	6674	6424
3	After releasing draped tendons						6946	6178	6504	6251
3	After applying post-tensioning	5057	4263				6881	6099	6438	6157
3	After releasing bottom straight tendons	4996	4226				6482	5640	6015	5859
191	Right before testing	4092		2752	1941	2672	3299	2230	3614	2688
	Total losses (% Age)	strain gauges were damaged during casting								

Notes: - See Figure 3.23 for strain gauges layout.
- Strain = (reading at any stage) - (initial reading).
- All readings in micro strain.

Table A.2 Measured strains of prestressing tendons from jacking up to testing using electrical strain gauges

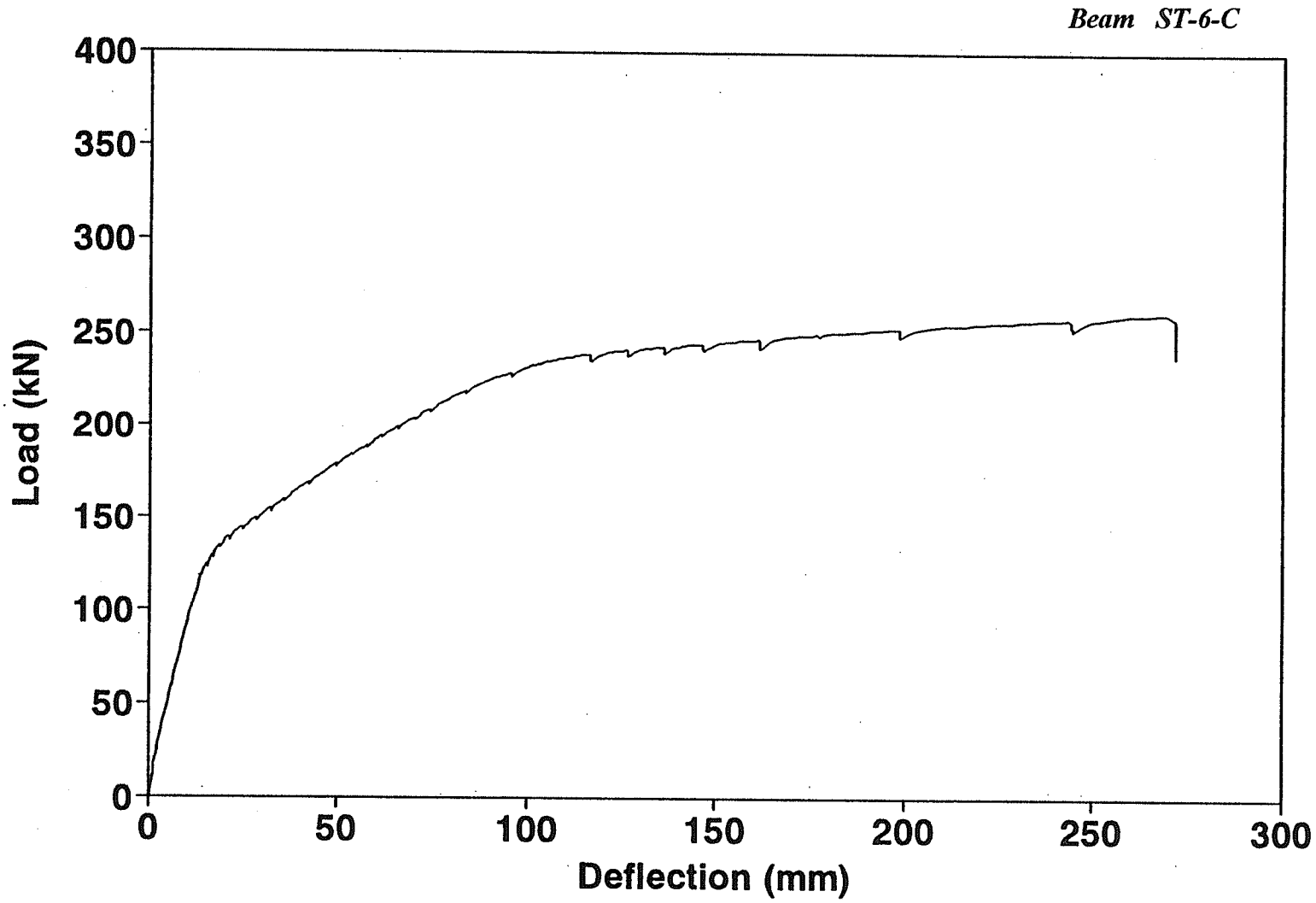

Figure A.1 Measured Load - deflection at mid span

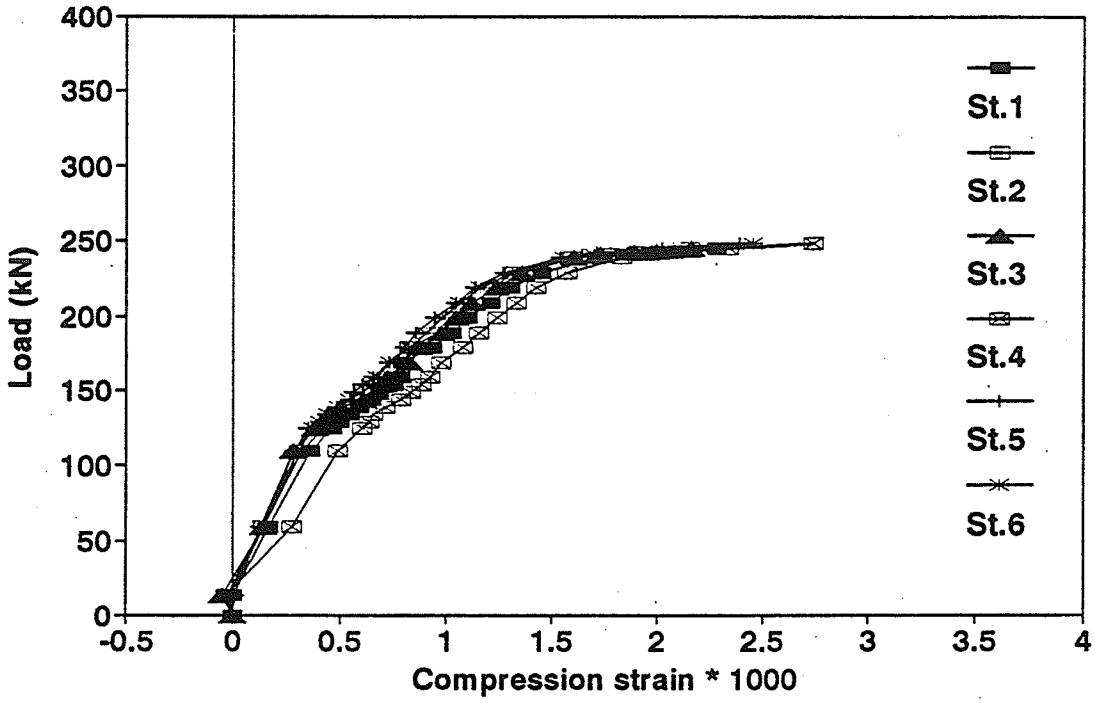

Figure A.2 Measured concrete strain at top surface at six demec stations

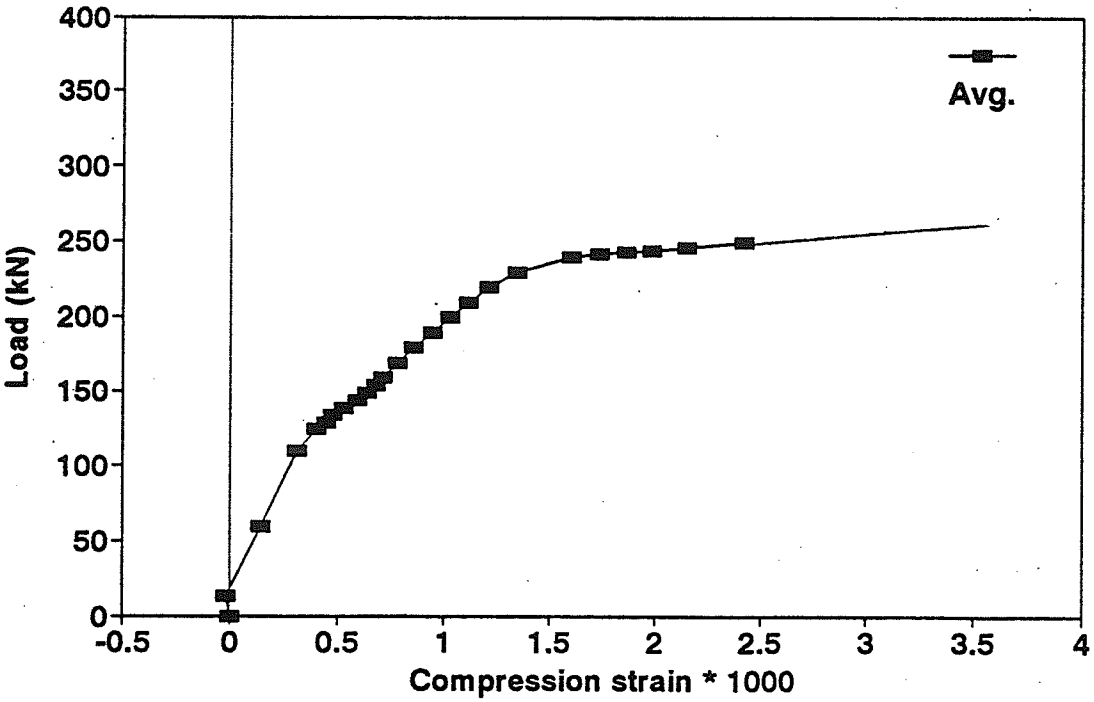

Figure A.3 Average of measured concrete strain at top surface

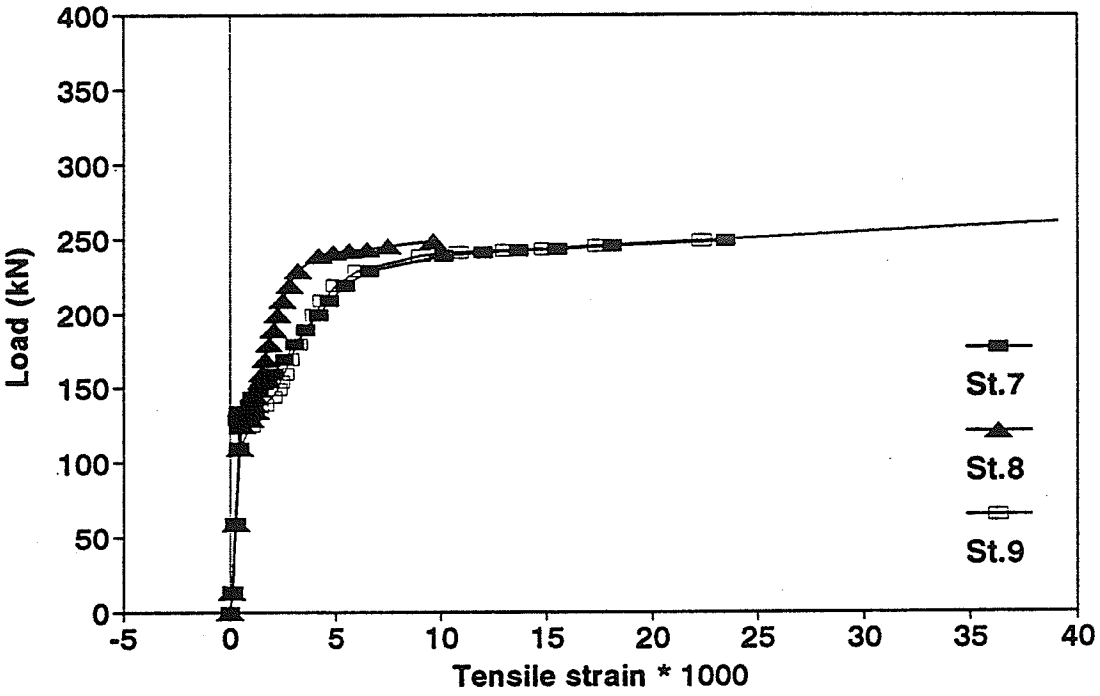

Figure A.4 Measured strains at bottom strands level at three demec stations

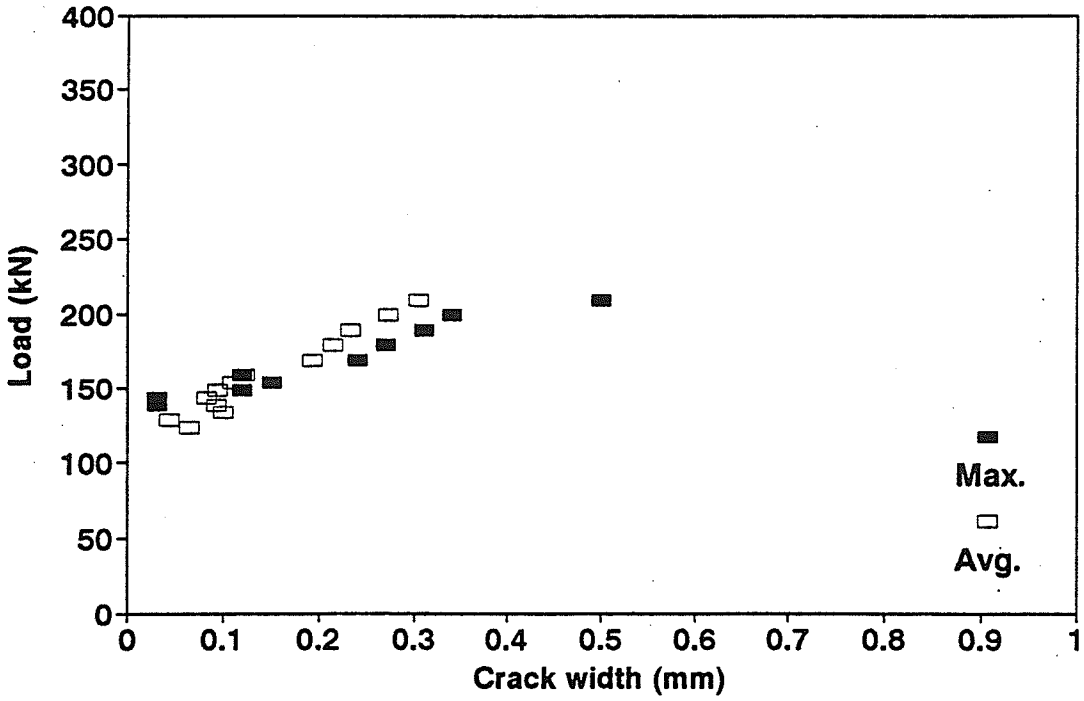

Figure A.7 Measured crack width at the maximum moment zone based on microscope readings

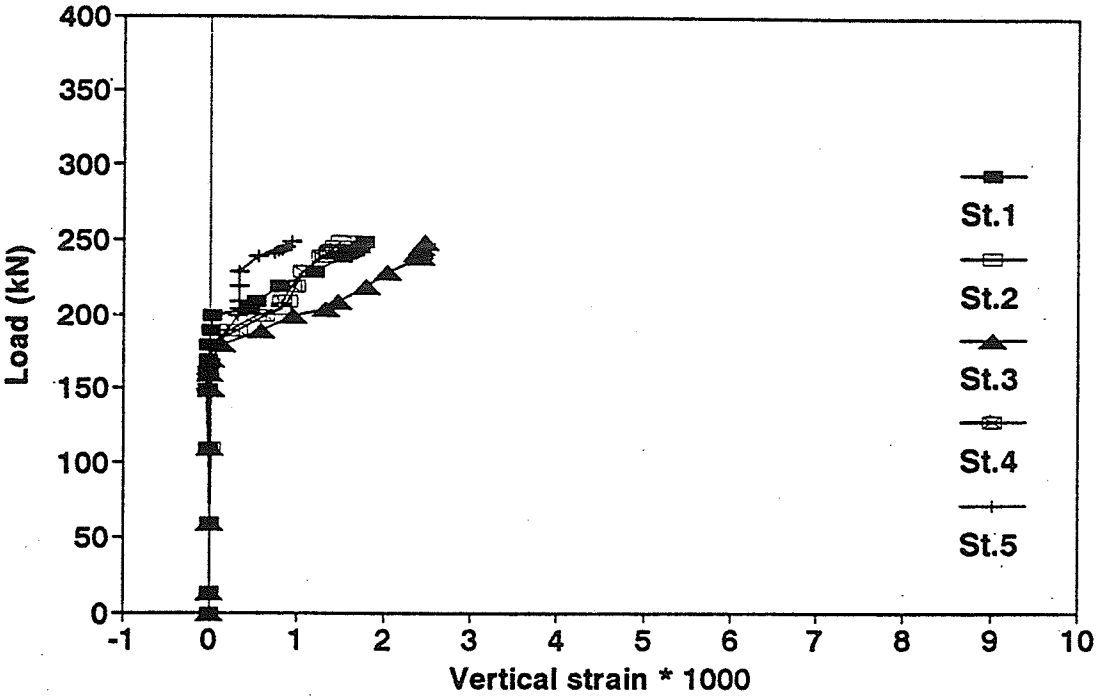

Figure A.8 Measured strain on concrete surface in direction of stirrups at five demec stations based on 200 mm gauge length

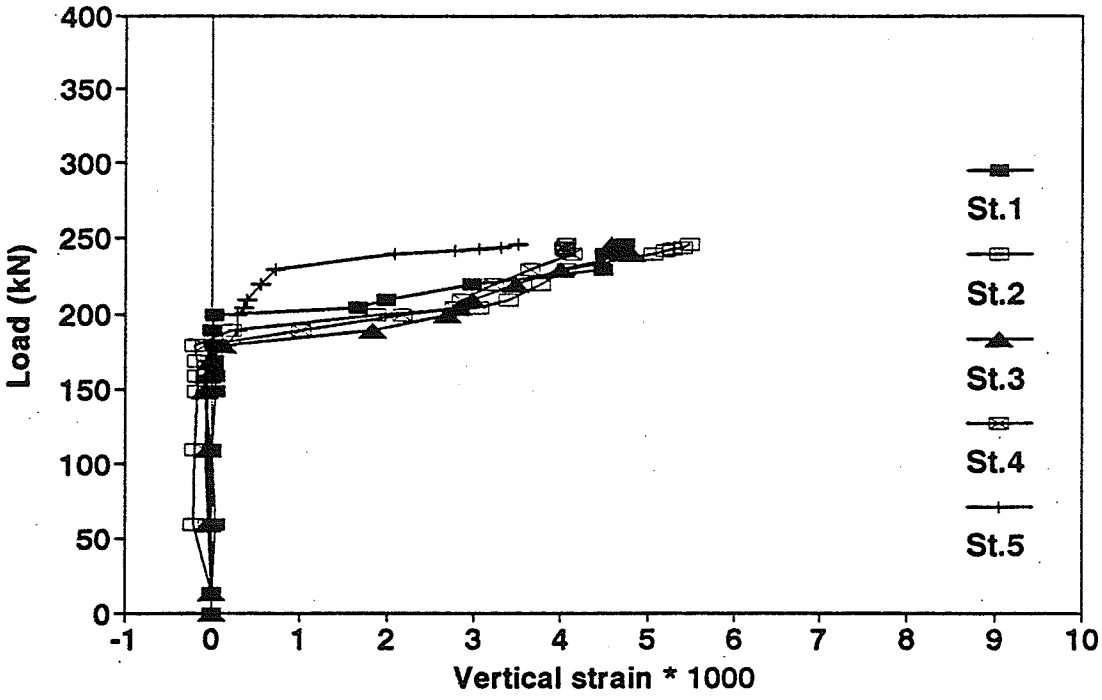

Figure A.9 Measured strain on concrete surface in direction of stirrups at five demec stations based on 50.8 mm gauge length

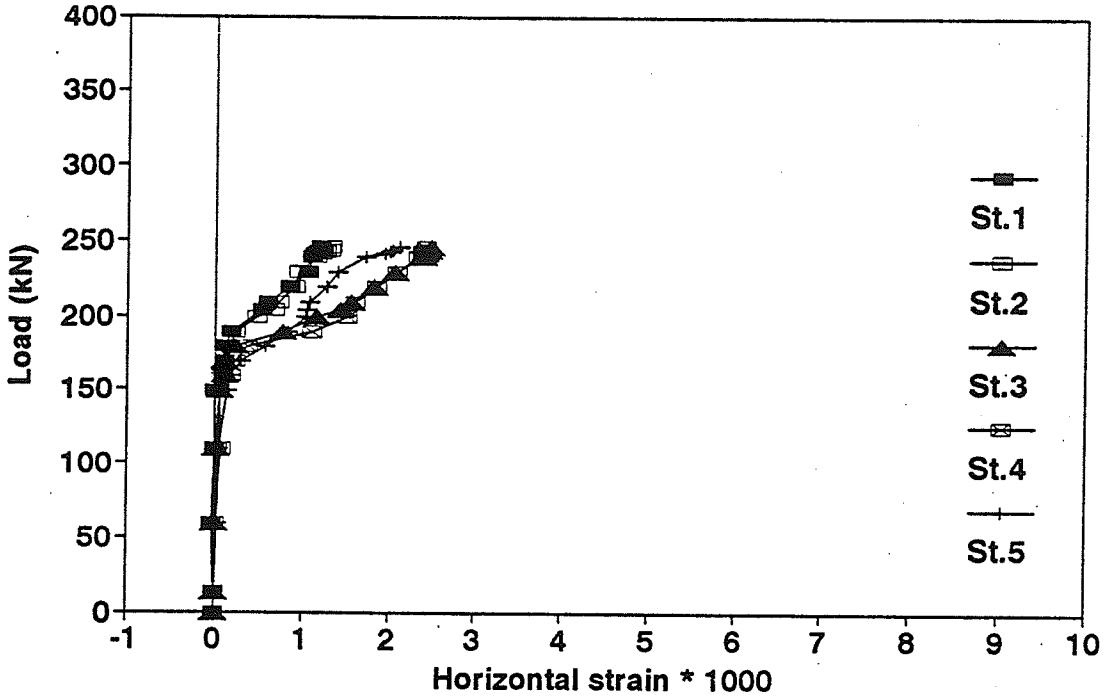

Figure A.10 Measured strain on concrete surface in the horizontal direction at five demec tations based on 200 mm gauge length

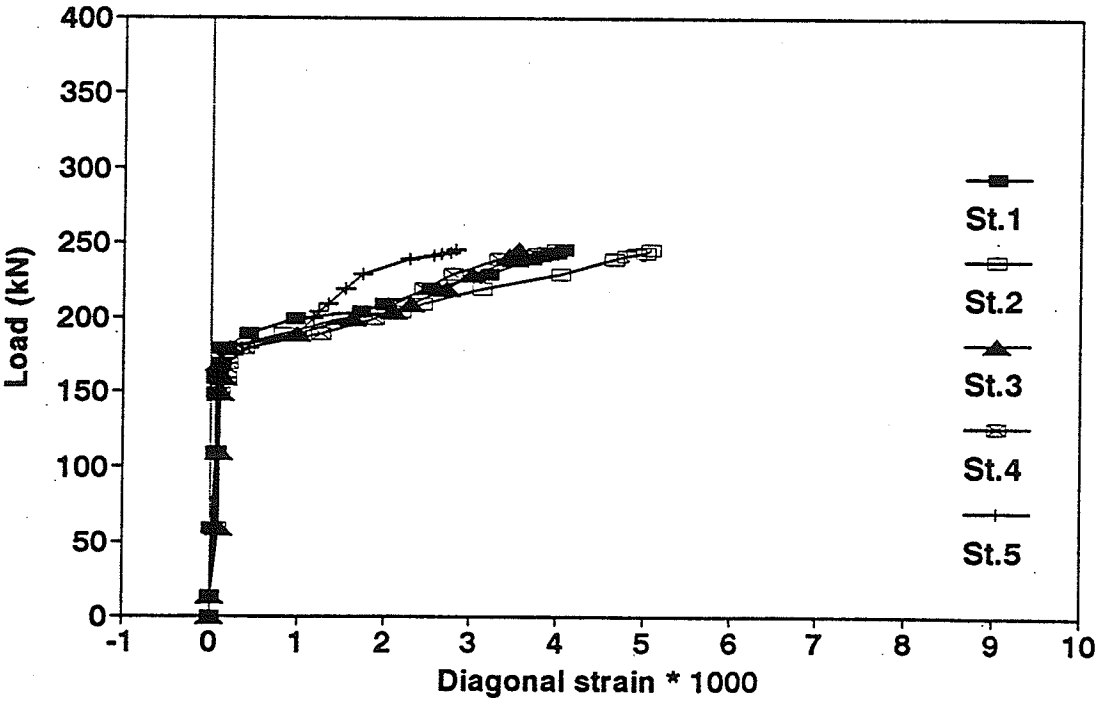

Figure A.11 Measured strain on concrete surface in the diagonal direction at five demec stations based on 200 mm gauge length

APPENDIX B

RELATIVE LOCATION OF DEMEC STATIONS WITH RESPECT TO THE CRACK PATTERN

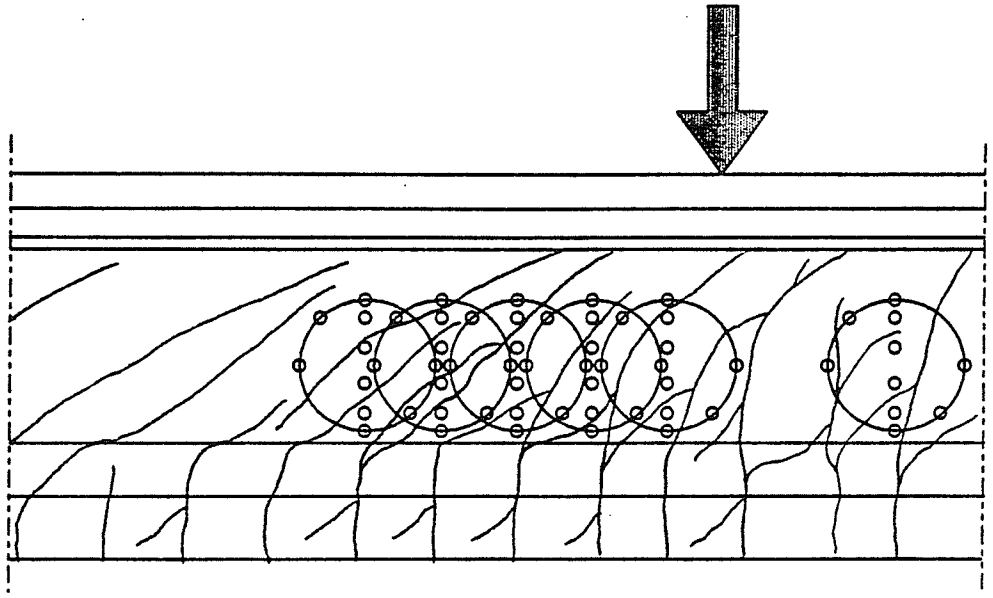

Beam TR-1-7.5/7

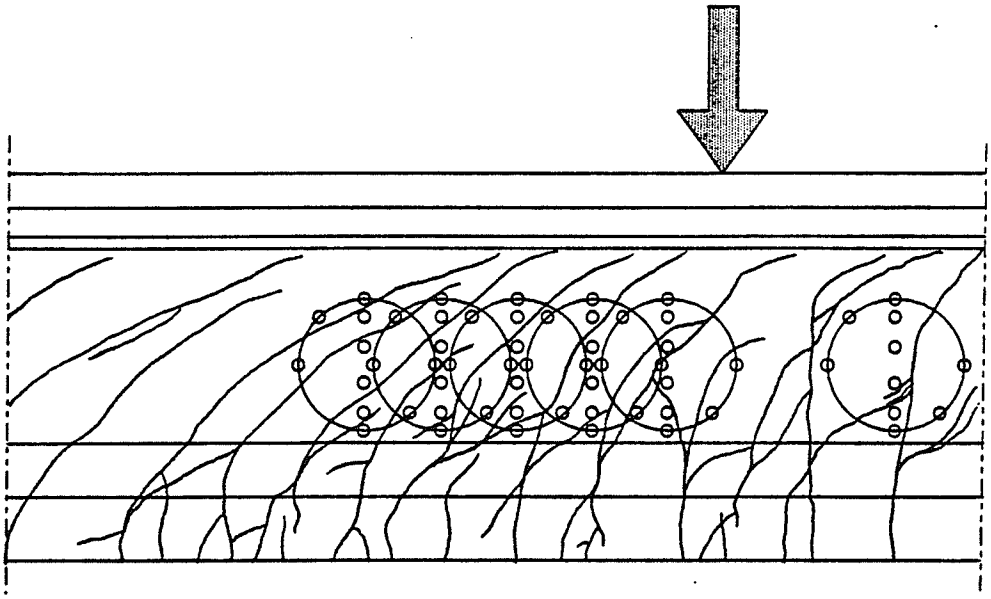

Beam TR-2-5/1

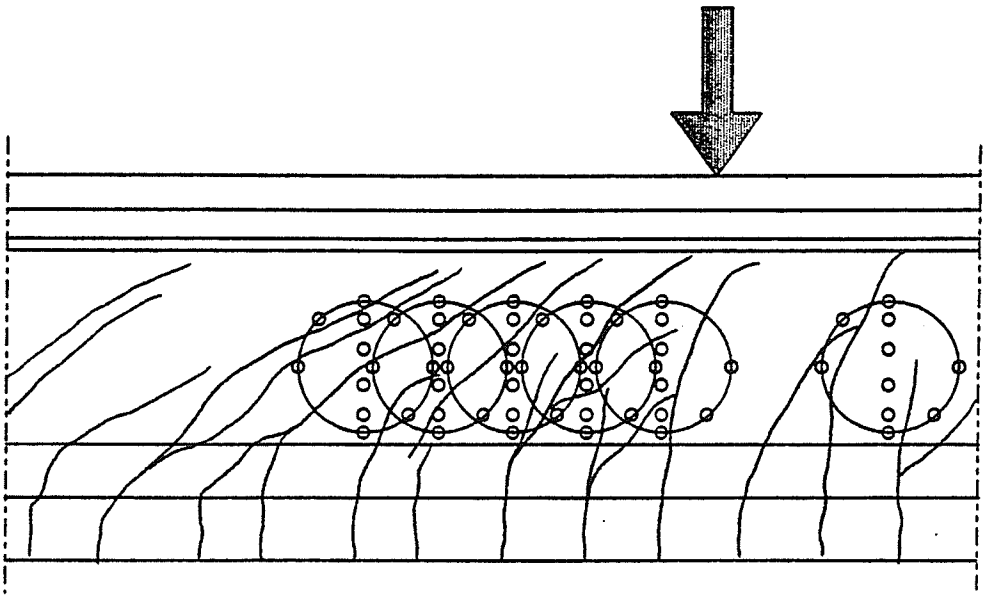

Beam TR-3-5/7

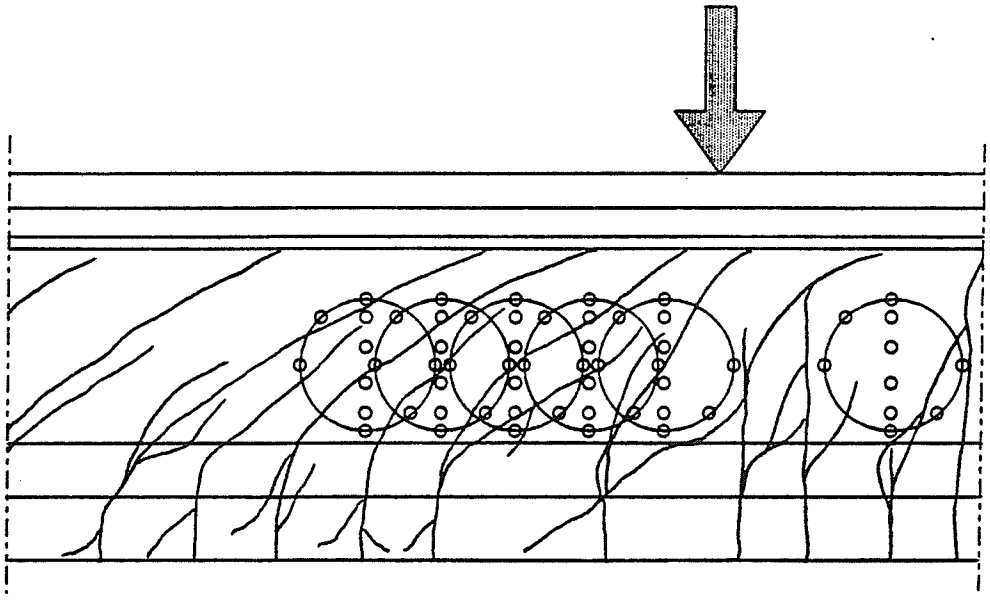

Beam LL-4-2B

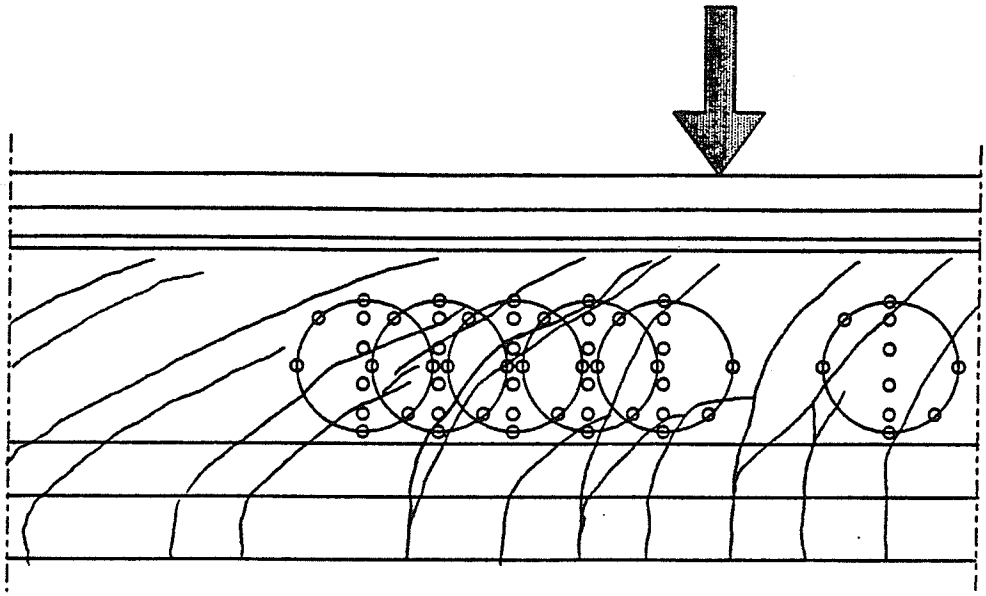

Beam LL-5-1B

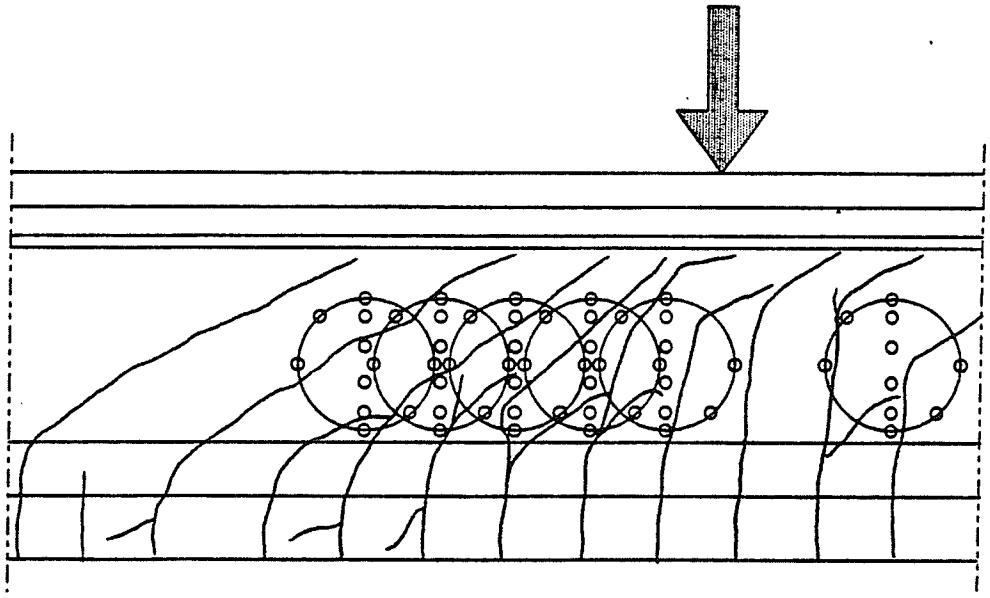

Beam ST-6-C

APPENDIX C

INPUT FILE OF PROGRAM "RESPONSE" FOR BEAM TR-1-7.5/7 AT SECTION # 1

Response Version 1 Data-File

Name of Section: TR-1 st1
Units M/U 'Metric/U.S.Customary': M
Number of Concrete Types (1-5): 1

Type Number	f'c [Mpa]	ec' [Milli-Strain]	fcr [Mpa]	Tension Stiffening Factor
1	53.80	-2.167	4.63	0.70

Number of Rebar Types (1-5): 2

Type Number	Elastic Modulus [Mpa]	fy [Mpa]	esh	esrupt [---Milli-Strain--]	fu [Mpa]
1	205000	600	2.927	18.000	650
2	137000	1000	7.300	8.759	1200

Number of Tendon Types (1-5): 1

Type Number	[Ramberg-Osgood-Factors--] A	B	C	Elastic Modulus [Mpa]	fpu [Mpa]	eprupt [Milli-Strain]
1	0.000	68.500	100.000	137000	2000	20.000

Height of Section: 550 mm
Distance to Moment Axis: 319 mm
Shear Y/N 'Yes/No': Y
Web width (bw) : 70 mm
Shear depth (jd) : 396 mm
Distance to web strain ex : 265 mm
Distance to center of web : 325 mm
Longitudinal crack spacing: 579 mm
Maximum Aggregate size : 20 mm
Stirrups Y/N 'Yes/No': Y
Transverse crack spacing : 247 mm
Area of Stirrups (Av) : 61 mm^2
Stirrup Spacing (s) : 110 mm
Stirrup (Rebar) Type : 2
Number of Concrete Layers (1-20): 6

Layer Number	y [mm]	bottom width [mm]	top width [mm]	height [mm]	Type Number
1	500	500	500	50	1
2	460	185	185	40	1
3	440	70	185	20	1
4	160	70	70	280	1
5	90	185	70	70	1
6	0	185	185	90	1

Number of Rebar Layers (0-10) : 2

Layer Number	y [mm]	Area [mm^2]	Type Number
1	540	48	1
2	483	58	1

Number of Tendon Layers (0-10) : 3

Layer Number	y [mm]	Area [mm^2]	Prestrain [Milli-Strain]	Type Number
1	234	114	5.764	1
2	184	114	5.764	1
3	40	341	5.764	1

Consider displaced Concrete Y/N: N
Thermal & Shrinkage Strains Y/N : N
Initial Strains Y/N : N